THE UNIVERSITY *of* EDINBURGH

The Importance of Grain Boundary Diffusion: An Experimental Study

Matthew Hiscock

School of GeoSciences

A dissertation submitted to the University of Edinburgh for the degree of Doctor of Philosophy

2013

Declaration

I declare that this thesis was written by me and that the work detailed herein is my own, or I have contributed substantially to such work, except where proper reference is made to the work of another author. Furthermore, I declare that no work contained herein has been submitted for any previous degree or professional qualification, except where properly referenced.

Matthew Hiscock

Contents

Figures

Tables

Equations

Abbreviations

BSE – Back-Scattered Electron (imaging)

EDS – Energy Dispersive X-ray Spectroscopy

EPMA – Electron Probe Microanalyser

FTIR – Fourier Transform Infra-Red (Spectroscopy)

GBD – Grain Boundary Diffusion

High PT – High Pressure and Temperature

MORB – Mid Ocean Ridge Basalt

MT – Magnetotelluric

NAM – Nominally Anhydrous Mineral

OIB – Ocean Island Basalt

PC – Piston Cylinder

SE – Secondary Electron (imaging)

SEM – Scanning Electron Microscope

SIMS – Secondary Ion Mass Spectrometry

Abstract

This research is concerned with the mechanisms of diffusion in the Earth and the implications of such an understanding. Specifically, this work is concerned with one particular aspect of diffusion: Grain Boundary Diffusion (GBD). An experimental investigation of GBD has been conducted by considering three specific scenarios; GBD of H in stoichiometric Mg-spinel, GBD of Ti in Quartz and GBD of Li in olivine. By considering the GBD of three very different elements it has been possible to synthesise an understanding of some of the mechanisms involved in the process.

GBD is potentially a very important process within the Earth with wide ranging implications. Grain boundaries may provide fast pathways for transportation of a range of compatible and incompatible diffusing species in the Earth's interior – potentially acting as storage locations and also as efficient pathways between different geological reservoirs [1]. It is also potentially very important in the application of a number of techniques including dating and geothermometry and geobarometry. Here, an experimental study of the GBD of H has been carried out with the overall finding that GBD appears to occur at slightly greater yet broadly similar rates to lattice diffusion. This finding is considered in terms of the mantle properties which are affected by the presence and transport of H. A follow up series of experiments was conducted looking at Li diffusion. Li was chosen due to its volatile nature and larger atomic radius as compared to H. As such, it provided a useful test of the hypothesis that the radius of a diffusant might affect its chosen method of diffusion. A third set of experiments were carried out to investigate the GBD of Ti in quartz with particular reference to the TitaniQ geothermo(baro)meter. This set of experiments provided a very useful comparison to the data which had previously been obtained from lighter elements.

This investigation has found that a combination of factors including charge, diffusant diameter and the specific mineralogical characteristics of the host phase will define the dominant diffusive mechanism and the size of the contribution made by that mechanism towards observed bulk diffusivities. A characterisation of the temperature dependency of diffusion within each setting has also been completed. As such, it also makes a useful contribution to the current dataset for GBD.

1 Introduction, Relevance & Background

1.1 Outline of Research Topic

This research is concerned with the mechanisms of diffusion: the routes taken by diffusing species as they travel between their source and sink regions. Diffusion is a process of great importance in many geological settings as it enables the transport of species across geologically/geochemically relevant distances within the available timescales of Earth's history. Diffusive processes have a controlling influence on many of the physical properties of planetary interiors and facilitate the movement of elements and compounds between regions of varying abundance. Simply put, without diffusive processes, a great deal of the chemistry which allows the functioning of our (and potentially many other) life bearing planet(s) would not be possible. In this thesis we consider and attempt to build upon and increase the current understanding of the mechanisms of diffusion and the implications of diffusive processes for the Earth. This understanding is of course applicable to other planets of a rocky nature. The work which has been conducted is experimental in nature and makes use of equipment which is capable of replicating the high temperature and pressure conditions of the Earth's interior. By using such apparatus it has been possible to subject samples to geologically relevant extreme conditions and subsequently analyse them to derive data representative of diffusion within the Earth.

The project focuses on diffusion in two specific systems: 1) Volatiles under mantle conditions and 2) Ti in quartz. Specifically it looks at Grain Boundary Diffusion (GBD) within these two regimes. By studying GBD in two systems, it has been possible to utilise theoretical and methodological parallels to aid in the development of both lines of research.

1.1.1 Grain Boundary Diffusion of Volatiles - Outline

The work on volatile diffusion along grain boundaries aims to fill a gap in our knowledge of diffusive processes in Earth's mantle: Grain boundaries have long been identified as potential fast pathways for diffusion as they are visualised as allowing diffusants to move comparatively freely along them as they are regions of long range disorder. However, to date, much of the published diffusion data for mantle minerals has been measured in single crystals. If grain boundaries do indeed provide a fast pathway for diffusion then single crystal diffusion rates are not representative of the true rate of the bulk process with strong implications for bulk diffusivity of many species within the Earth. Here we attempt to determine the contribution of grain boundary diffusion to bulk diffusion rates for volatiles in the mantle.

1.1.2 Grain Boundary Diffusion of Ti in Quartz - Outline

The work on GBD of Ti in quartz has been conducted due to the increasing use of the Titanium in Quartz geothermometer (TitaniQ [2]). TitaniQ allows Ti concentrations to be routinely used to determine the temperature of equilibration of quartz [2] (given the presence of rutile in the sample thereby fixing Ti activity at 1; if rutile is not present the activity of Ti in undersaturated systems must be quantified). In order to validate TitaniQ, the mechanisms which control the parameters it measures must be understood. As such, an understanding of the mobility of Ti is required as it is this which will determine the availability of Ti to the equilibrating quartz. TitaniQ assumes that the Ti content of quartz (which is used to calculate the temperature and pressure of equilibration of the quartz) is at complete equilibrium with the total system (i.e. the quartz contains as much Ti as it can do at the given temperature and pressure). For this to be true Ti must be available locally to be incorporated into the quartz and this Ti must have, in turn, been transported to the site of incorporation. Lattice diffusion rates of Ti in monocrystalline quartz are very slow [3], giving total diffusion distances on the order of 0.5mm per million years at temperatures characteristic of the mid crust (~500°C). This appears to be at odds with the full equilibrium of Ti in quartz observed at temperatures as low as 450°C [4] (given the likely time available for equilibration – most probably in the range of tens of thousands to a few million years at most). In this investigation, we have looked to measure GBD of Ti in quartz to determine if grain boundaries are the preferential route taken by Ti. This work will have direct implications for those using the Ti in quartz (TitaniQ) thermometer.

1.1.3 The Importance of Temperature

It is very important to consider variations in the environment in which any process is proceeding and to attempt to understand the effect of such variations on the process in question. In the case of diffusion, temperature is an exceedingly important variable with pressure having a less well constrained but generally weaker effect [5]. At high temperatures diffusion proceeds more rapidly; conversely, lower temperatures cause lower diffusion rates. This relationship is very important for the delivery of reactants to reaction sites as well as in controlling the mobility of elements such as Ti, as is being investigated in the GBD of Ti in quartz work.

A consideration of cooling quartz which is to have its thermal history determined using the TitaniQ geothermometer is useful in understanding the effects of temperature variation on diffusivity and other related parameters: Diffusion rates decrease with temperature with the implication that increasing amounts of time are needed to enable the equilibration of Ti with quartz i.e. more time is needed to deliver or remove Ti from quartz as the rate at which it is able to move is slower. This is problematic as rapidly decreasing temperatures may not allow enough time for complete re-equilibration to occur. The solubility of Ti in quartz is lower

at lower temperatures and as such some must be removed as the quartz cools. This Ti may not be able to leave the quartz quickly enough because of the decreasing diffusion rate. As such, the Ti could effectively be "frozen" into the quartz as it attempts to leave. This has the implication that when the abundance of Ti is measured to allow determination of the equilibration temperature using the TitaniQ geothermometer a falsely high reading would be obtained as both the Ti that should be in the quartz (the amount which should be there determined by the solubility of Ti in quartz at the given temperature) and that which should not be there (the Ti which has effectively been "frozen" in place as it has been slowly diffusing out of the quartz – perhaps on its way to form rutile) are measured. This high reading would then give an overestimate of the temperature of equilibration (given the previous higher concentration of Ti – this logic assumes a high abundance of Ti such that the quartz is always fully saturated by it). Conversely, a lower than actual temperature could be recorded in the case where quartz crystallises directly from a fluid which is saturated in Ti. Ti may not be able to diffuse into the quartz quickly enough to attain its maximum solubility. Whether or not a true figure for the equilibration is calculated will be dependent on how fast the Ti is able to diffuse at a given temperature. If one bases their estimate of diffusion rates on single crystal data (as is often implied) then the scenario detailed above will definitely be true as this rate for Ti diffusion in quartz is exceedingly slow. However, if, in practice, diffusion is much quicker owing to the utilisation of a faster mechanism, such as grain boundary diffusion, then the technique will still be valid. As such, temperature is the key variable in determining exactly how diffusion affects the use of TitaniQ.

This varying degree of diffusivity of Ti in quartz is indicative of an effective "closure temperature" below which diffusivity becomes so sluggish that, even over geological timescales it can be considered to be insignificant. As such, below the closure temperature, re-equilibration does not effectively occur. The precise temperature or range of temperatures at which closure occurs has not specifically been studied for Ti in quartz. In certain cases, closure temperature is a useful concept. A very high closure temperature would record the peak conditions of a system. However, in the case of a slow cooling body with a low closure temperature, peak conditions will not be recorded. In practice we are often interested in the way in which the Ti content of quartz is re-equilibrated as opposed to the more simple scenario of studying magmatic quartz. Under such conditions, closure temperature will be a very important concept. By considering grain boundary diffusion as a potential fast mechanism for diffusion – with a direct relevance to multigranular natural settings - the issue of closure temperature and how it affects natural processes can be studied.

This demonstrates an important point relevant to all aspects of diffusion in the Earth: Diffusion is only important if there is sufficient time for species to migrate through the Earth –

and as temperature has such a controlling influence on diffusion rates it is critically important that the effect of temperature is well understood.

The effect of temperature on volatile diffusion is equally important. If, as is proposed here, grain boundary diffusion of volatiles is an important process in the deep earth, temperature will surely have a significant effect on the rate at which that diffusion occurs; as is observed in the more commonly considered setting of lattice diffusion. However, there is an important difference between lattice diffusion and grain boundary diffusion and that is the mechanism by which a diffusant makes the series of jumps which forms the overall diffusive motion. If grain boundaries do indeed provide a fast route for diffusion then there may well be less variation of diffusion rates with temperature than is observed in lattice diffusion. This will have great implications for the way in which volatiles move around the earth as their bulk diffusion rates must take into account all mechanisms including lattice and grain boundary diffusion.

Thus, an understanding of diffusivity and how temperature affects it is key to understanding many geological processes and the current geochemistry of the Earth. The speed of equilibration and mechanisms of delivery of chemically and physically important species are strongly determined by the relationship between the two.

1.1.4 Statement of Research Questions

The primary research questions to be addressed in each of the two aspects of the research can be stated quite simply.

1) Which is the dominant route taken in bulk diffusion – along grain boundaries or through mineral lattices? Can the relative importance of the two different routes be quantified?

2) How do varying conditions affect diffusivities – does grain boundary diffusion dominate at a certain range of temperatures and is the effect of temperature on grain boundary diffusion rates the same as it is for lattice diffusion rates?

By looking into the mechanisms of diffusion in two geologically significant settings, this work aims to show how an understanding of the movement of and routes taken by diffusing species is of great importance to the dynamics and properties of Earth's interior as a whole.

1.2 Importance/Relevance of this Research

1.2.1 Grain Boundary Diffusion - General Case

Owing to the ubiquity of grain boundaries in the Earth, GBD has the potential to be an important process in a multitude of geological settings with far reaching implications. By quantifying the relative importance of grain boundary versus lattice diffusion, understanding will be gained on the mechanisms by which reactants are delivered to reaction sites. Hence, the geochemical reactions which take place in and define many of the properties of the deep Earth will be better understood.

Grain boundaries have already been cited as providing routes for geochemical transport under limiting geological conditions, such as the redistribution of highly siderophile elements between the core and mantle [1,6]. Hayden and Watson looked at the mobility of highly incompatible chemical species (species which are not incorporated easily within mineral structures) which are unable to move quickly through mineral grains but may still be able to diffuse through a granular medium by moving along grain boundaries. By moving along grain boundaries they may ultimately be able to move to regions of partial melting where they can easily enter the melt phase, thereby giving rise to core-like geochemical signatures. GBD may also be important in terms of the movement of compatible elements (e.g. Fe, Mg in a wide range of minerals) – particularly under conditions where bulk diffusion is impaired such as very fine grain size or low temperature (some studies from materials science have observed an increase in the importance of GBD at low temperature [7] – See section 1.3.1.2 Previous Studies on Grain Boundaries which includes a discussion of work on grain boundaries in the field of materials science.).

The movement of species along grain boundaries may, of itself, give rise to important mantle properties such as conductivity. Charged particles moving along grain boundaries may be responsible for some of the currents measured by magnetotelluric (MT) techniques. However, the most important role of GBD is likely to be in the speedy movement of species between reservoirs where lattice diffusion is either too slow or not possible. GBD probably forms a significant proportion of bulk diffusion in the Earth but to date this has not been quantified.

1.2.2 Grain Boundary Diffusion of Volatiles – Specific Case

Volatiles in the mantle are of great global importance owing to their controlling influence on many geological processes (see section 3.1.1 Background to Volatiles for a detailed discussion of the roles of volatiles in the mantle). Whilst the majority of the mantle is thought to be dry, certain nominally anhydrous minerals – (NAMs), are able to hold ppm levels of

water as interstitial H defects[8]. Whilst concentrations of H are very low, total abundances in the entire mantle are potentially vast. As such, the role of water, even in a nominally dry mantle, is potentially very significant. The mobility of this water and the mechanisms it uses to move around are thus of great importance. Diffusion of volatiles along grain boundaries is considered important as knowledge of the dynamics of volatiles, specifically H, under mantle conditions has implications for the relative volumes of water that can be held in mantle reservoirs, and on the ability of water to move between different terrestrial reservoirs (see Figure 1 which shows calculated maximum water solubility in the upper mantle). The presence and abundance of H in the deep interior may be related to that in the hydrosphere and atmosphere – if this is the case then it could be that the ability of water to move between these reservoirs (and the speed at which it can do so) acts as a buffer to the water content within them. In addition, the mobility of volatiles within the Earth has a direct influence on bulk mantle rheological properties and melting behaviour [9].

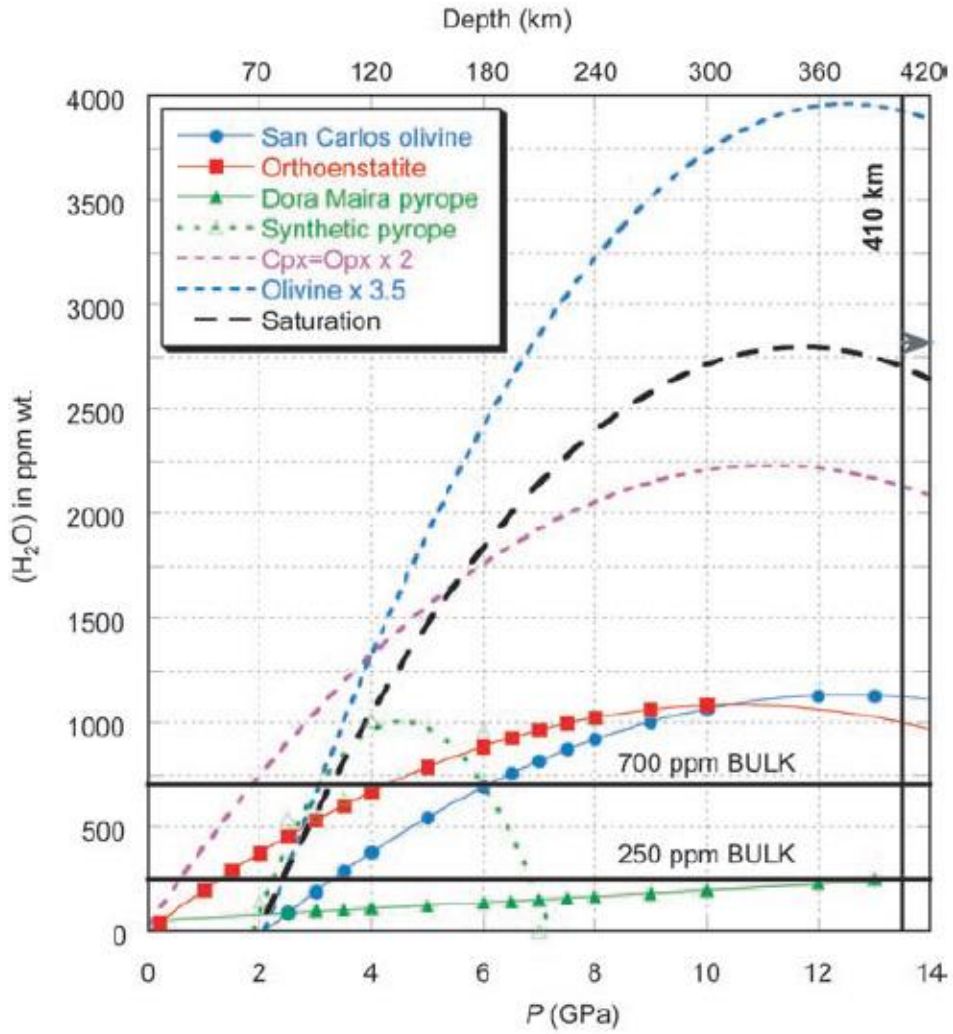

Figure 1: Calculated water content of the Upper Mantle

The black dashed line shows the calculated saturation value of water in the upper mantle. Peak concentrations of approx. 2750ppm H2O by weight are shown at a pressure of 11-12GPa equivalent to a depth of approx. 350km. See reference (from which the image is taken) for details of the calculation.

From Bolfan-Casanova, 2005 [9]

1.2.3 Titanium Diffusion in Quartz – Specific Case

The work on diffusion of Ti in quartz is significant as Ti mobility underlies the basis of the Ti in quartz thermometry technique [2,3,10] which determines crystallisation temperatures of quartz by measuring Ti concentrations within the quartz grains. The technique is enjoying a great deal of use[11–18] and is increasingly being applied to very low temperature settings (<500°C) using SIMS analysis[4,10,19–21]. Quartz at a temperature of 400°C records a Ti content of c.1ppm by weight increasing to c.24ppm at 600°C (Figure 2 shows the temperature dependence of Ti contents in quartz). Published data for Ti diffusion in single crystal quartz[3] does not support the use of the geothermometer as at temperatures of less than 600°C equilibration will require unfeasibly long timescales. The characteristic distance for diffusion of Ti in single crystal quartz (defined as $[4Dt]^{1/2}$ where D is diffusion coefficient and t is time) at this temperature is 20µm in 1Ma. Thus, lattice diffusion (i.e. that which is measured from single crystal diffusion rates) is too slow to allow Ti to get to, from and into quartz grains which are typically a few mm in size and equilibrate within the timescales implied by the geological setting (e.g. veins etc.). GBD provides a potential mechanism in defence of the technique and greatly extends the temperature range over which it can be used – which will be of great importance for constraining numerous geological processes e.g. ductile deformation of quartz veins[4]. As such, this work will be of direct relevance for workers using the TitaniQ geothermometer to determine the temperature of equilibration of quartz. Furthermore, it is a relatively simple system in which to consider GBD in the Earth in a geologically relevant setting and as such is useful for method development. Furthermore, as quartz is a good, first order, proxy for the bulk crust, information on grain boundary diffusion in quartz will be of relevance to the crust. Work to date has looked at the overall process with no consideration of the route taken by Ti as it moves through the quartz. This lack of an explanatory mechanism is troubling given the very slow rate of single crystal diffusion and this work aims to solve this issue.

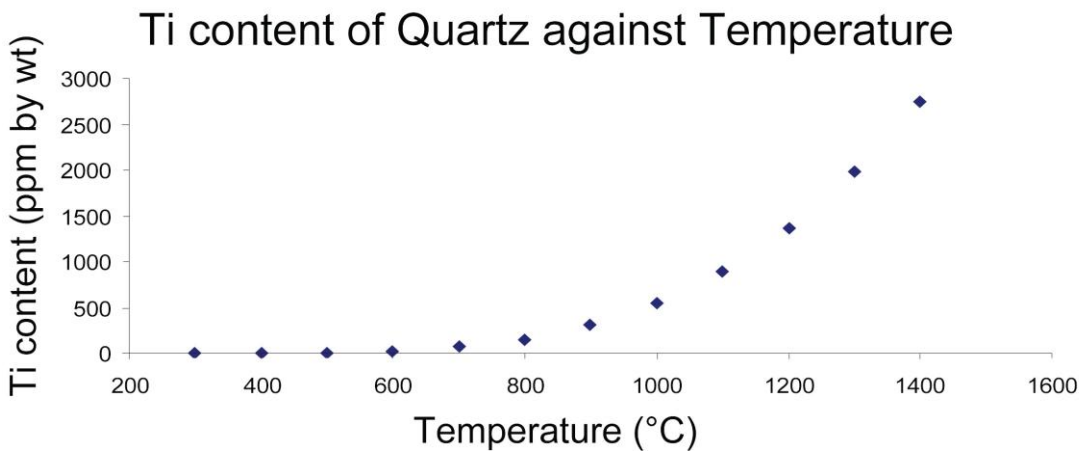

Figure 2: Ti content of Quartz plotted against Temperature

Data calculated from the relationship described in Wark & Watson 2006 [2]*. At low temperatures Ti content of quartz is very low (c.1ppm by weight at 400°C and 24ppm by weight at 600°C) but rises significantly at temperatures above 800°C.*

1.3 Background

Here we will consider the context of GBD and compare and contrast experimental techniques that have been used in related studies to date. Furthermore, we will consider the implications of data related to volatile dynamics and their effect on bulk mantle properties and indeed on the planet as a whole. By its nature the topic draws on reasoning and data from many related fields of research. Hence, this review of relevant work is necessarily broad. For this reason, we will initially discuss individual parts of the topic in isolation before moving on to discuss the specifics of this investigation. Throughout this review of background material, examples are used from different aspects of this investigation as a way of demonstrating the concepts involved. However, the ideas are equally applicable in a discussion of grain boundary diffusion in any setting; the concepts involved in a volatile molecule moving along a grain boundary will be applicable to a Ti atom/ion moving along a quartz grain boundary (or indeed any other system).

Our consideration of the context of this study is split as follows: Initially we consider the role of grain boundaries in all settings – their importance is discussed and the work that has been done on them to date is reviewed. Particular attention is paid to the behaviour of incompatible elements and their segregation to, residence at, and diffusion along grain boundaries. The mechanisms and mathematical description of diffusion are then considered.

1.3.1 Grain Boundaries

1.3.1.1 Introduction to Grain Boundaries

The Earth's crust and mantle are polycrystalline and consist of grains of numerous phases. There are a number of ways to conceptualise the granular nature of the Earth of which two are typically used in the geological sciences; either to consider the properties and behaviour of *individual phases*, or to consider the *bulk response/behaviour* of polycrystalline material. Here, in considering grain boundaries we will start by looking at them at a nanometre level - close to the atomic scale.

Where grains meet an interface is formed – either between similar grains or those of different species. The thickness of grain boundaries in the mantle is on the order of nanometres; concentration profiles of incompatible elements gathering at grain boundaries have been observed to have characteristic widths of 5nm [22] (see Figure 3). As atomic and molecular diameters are typically on the order of a few angstroms (1Å = 10^{-10}m), the width of the grain boundary region is of the order of 10 – 100 times the size of atomic or molecular species. It follows that grain boundaries could act as high capacity pathways providing a

(comparatively) fast route for the migration of chemical species (relative to lattice diffusion) as they may provide lower energy barriers than a perfect lattice.

The recognised importance of grain boundaries within the Earth is increasing with a number of recent studies citing them as having significant relevance to many geological phenomena. Work has been carried out suggesting that they may act as significant reservoirs/repositories for incompatible elements[23,24] and as a mechanism for core/mantle interaction [6]. Figure 3 shows STEM (Scanning Transmission Electron Microscopy) EDS (Energy Dispersive X-ray Spectrometry) measurements of concentrations of various compatible and incompatible elements in the region of a grain boundary - it is clear that Ca, an incompatible element, shows the greatest enrichment at the grain boundary. Indeed, grain boundary diffusion may be a dominant mechanism for diffusion between many reservoirs of a variety of species within the Earth. These studies build towards an understanding of the roles played by grain boundaries and form a useful basis for the work to be conducted here.

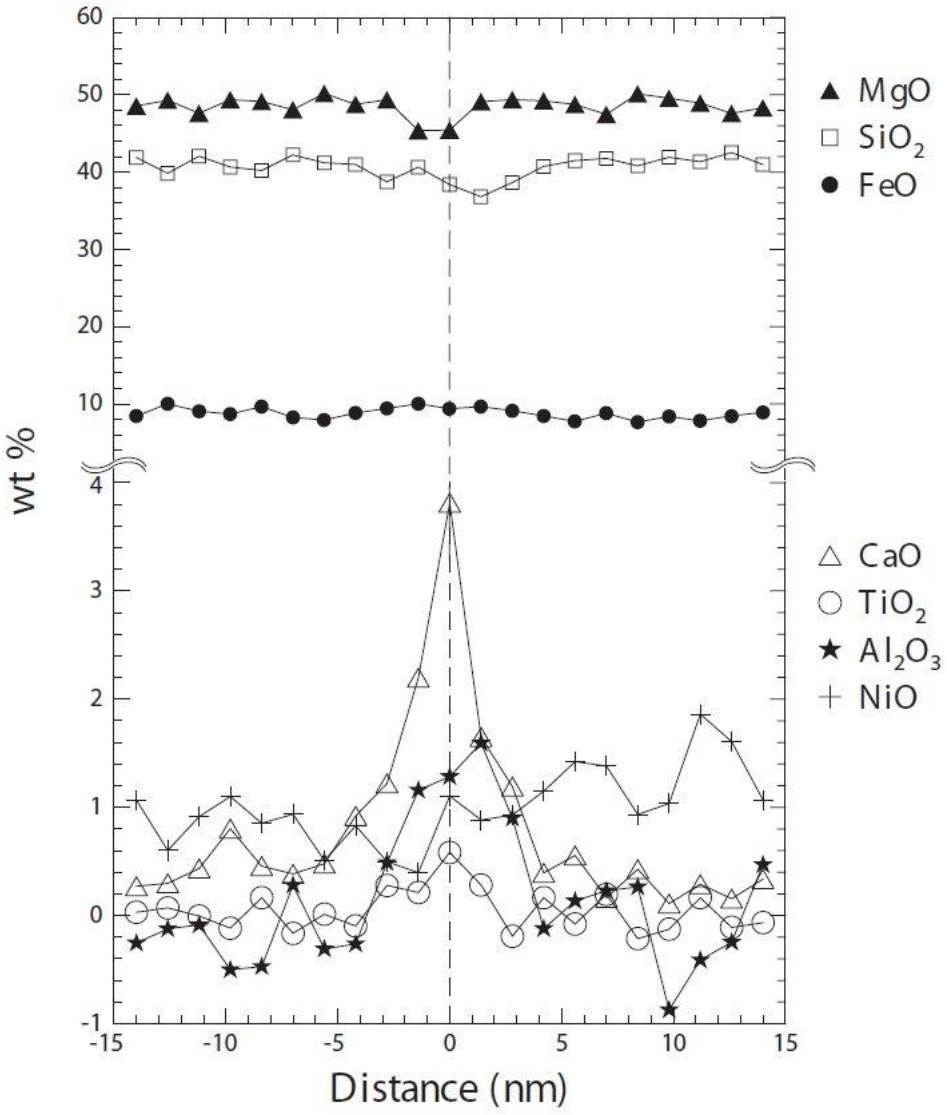

Figure 3: Enrichment of Incompatible Elements at grain boundaries

Graph showing enrichment of various oxides at grain boundary between two synthetic olivine grains. More incompatible elements (relative to the ability of the host mineral to accommodate that element e.g. Ca) show a greater segregation than those easily accommodated in the lattice (e.g. Si). Enrichments occur at distances of up to 2.5nm from the centre of the boundary, suggesting a width of approximately 5nm. Enrichment is still observable up to 3.5nm from the centre of the boundary suggesting an enriched 'crust' at the surface of the grain.

From Hiraga et al., 2003 [22]

1.3.1.2 Previous Studies on Grain Boundaries

A number of previous workers have conducted studies of grain boundaries in various scenarios. Waff & Holdren [25] (in 1981) were amongst the first to study grain boundaries in the upper mantle. By analysing dunite and lherzolite xenoliths they concluded that melt migration in the upper mantle could not be along intergranular surfaces. In 1991, Joesten [26] reviewed the state of research into the topic, importantly noting that geologists have long considered that grain boundaries could provide important routes for mass transport over the macroscopic scales needed to enable them to deliver reactants to the sites of geochemical activity.

Grain boundaries have been posited as potential storage reservoirs, particularly for incompatible elements prior to them entering the first partial melts to form. Thermodynamic modelling and experimental studies have shown that incompatible elements preferentially reside at grain boundaries instead of within mineral lattices [23,24]. This is likely due to the fact that incompatible elements have large ionic radii and may have varying charges, and that significant local distortion of crystalline structures at sites of substitutional defects are required in order to accommodate them - this being thermodynamically unfavourable. Thus, such elements are incompatible because there is a limit to the concentration of them which can be incorporated in a given mineral structure before it becomes unstable. However, structures can often contain small, ppm levels. This may be thermodynamically less stable than incorporating incompatible elements at grain boundaries thereby causing the segregation. The study of this topic is typically conducted by comparing the distribution of incompatibles observed in experiments to what is predicted by thermodynamic modelling. In this particular case [23,24], close agreement is reached between the model and experimental data.

Hayden & Watson [1,6] have suggested that grain boundaries may provide a route by which the core and mantle are able to interact. It has been suggested that a flow of siderophiles from the core into the mantle could explain upper mantle siderophile element ratios [27],although the existence of such an interaction is controversial [28]. Following the finding that self-diffusion of oxygen can occur over significant distances [29] and that incompatible elements can be preferentially stored at grain boundaries [22] Hayden and Watson chose to experimentally determine if GBD of siderophiles was viable [6,30]. Their results were consistent with grain boundaries providing a highly utilised mechanism of transport, potentially allowing diffusion over distances on the scale of km over the age of the Earth, therefore permitting element exchange between reservoirs such as the core and the mantle (which are often considered to be chemically closed systems). Their results are summarised in Figure 4. Their methods have proved useful in the design of those to be used here.

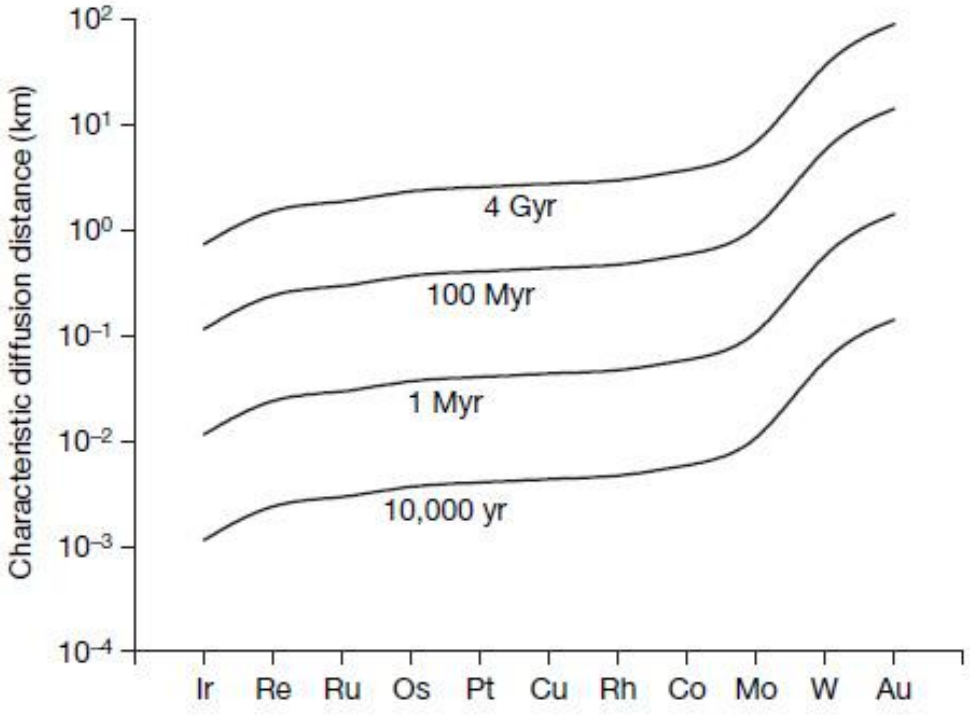

Figure 4: Siderophile Grain Boundary Diffusion Characteristic Distances

Characteristic distances of grain boundary diffusion of various siderophile elements in polycrystalline MgO. Characteristic distance is here defined as $x = (Dt)^{1/2}$ *where x is the characteristic distance, D is the diffusion coefficient and t is time. Diffusion distances of the order of 1 – 100km are possible within the age of the Earth implying that grain boundary diffusion could be a mechanism which allows siderophiles to move between the Earth's core and mantle.*

Diagram from Hayden and Watson 2007 [6].

Hayden and Watson also conducted work looking at the GBD of carbon [1]. Evidence from meteorites along with experimental data suggests that certain C compounds are stable under conditions characteristic of the core [31–33] with the implication that C could be one of the light "impurities" present therein. Their results, like studies into siderophiles, indicated that grain boundaries could provide a route by which carbon may enter the mantle from the core.

The fields of materials science, ceramics and metallurgy have long contributed to the understanding of diffusion in polycrystalline materials. Much of the theory and systematics in developed in these fields is of course of great relevance to the study of grain boundary diffusion in geological settings. It should be noted however, that geological systems may well be more complex than the artificial systems (typically monocrystalline and with simple textures) developed in the study of materials. This is due to the chemically "dirty" systems that are ubiquitous in nature and so the far greater number of chemical components that may be present. Nonetheless, the mathematical techniques developed in materials science provide a very useful starting point for the understanding of natural systems[34,35].

To date, only a limited amount of work has been conducted directly looking at the diffusion of very light volatiles such as hydrogen along grain boundaries, so it is hoped that this work will provide valuable data. As such, there is very little literature directly relating to volatile diffusion along grain boundaries under mantle conditions. Thus, work conducted in similar studies must be considered in order to make informed decisions on the design and progression of this work.

1.3.2 Diffusion

Diffusion is an exceptionally important process within the Earth owing to the breadth of geological processes in which it plays a role. Data on diffusion is frequently applied in work such as calculating the age and histories of rocks, development of chemical and isotopic heterogeneity in minerals and important near surface volcanic processes such as bubble formation and eruption mechanics [36]. As such, work on subsurface diffusion (of both volatile and non-volatile species) has been conducted considering a variety of diffusants in various geological settings [37], e.g. in silicate melts [38–40] (with important implications for the behaviour of both intrusive and extrusive rocks and their eruptive behaviour) and (of greater relevance to this study) in crystalline media under mantle conditions, primarily looking at H_2O and CO_2 e.g. [38,41]. Extensive studies of diffusion have also taken place in the research of ceramics and metals (see section 1.3.1.2 Previous Studies on Grain Boundaries). In the Earth, diffusion rates determine the mobility of species and so the interaction between different reservoirs (e.g. between core, mantle and crust, subducting slabs etc.) and can control the availability of reactants (where they are not in excess in the immediate vicinity of the reaction site) as well as the dynamics of processes such as exsolution (see footnote for a discussion

of the relevance of diffusion to volcanic phenomena[A]). Furthermore, diffusion is an important mechanism with respect to other mantle properties such as electrical conductivity.

A consideration of mechanisms and routes of transport of diffusing species on an atomic scale under mantle conditions leads to three scenarios: (1) diffusion through mineral grains, *lattice diffusion* (2) diffusion along the boundaries between grains, *grain boundary diffusion* and (3) diffusion through *grain edge fluids* (see Figure 5 for a graphical representation of these routes). As grain boundaries are ubiquitous throughout the mantle whereas grain edge fluids are likely to be of local importance only in small regions of the mantle, it is grain boundaries that are considered in this investigation.

GBD could also be an important process at shallower depths. Work by Teng et al. [45] suggests fluid assisted GBD could be responsible for Li isotope fractionation in the Tin Mountain Pegmatite, South Dakota. With the strength of the effect of pressure on diffusive processes still being a strongly debated subject [see review by Bejina (2003) [46] for a full discussion] but generally accepted to be relatively weak compared to temperature effects, it may be that data obtained at a given (high) pressure is applicable, with fairly small corrections at other (lower) pressures.

[A] Studies of Diffusion in Silicate Melts

Studies have been conducted looking at diffusion in melts with the aim of understanding variation in volatile contents through stratigraphic sequences of volcanic products [42] and also variations in the ratio of volatiles in the eruptive plume which correlate with changes in eruptive behaviour [43,44]. Furthermore, the dynamics of bubble formation and their subsequent movement are controlling factors in the mechanics of volcanic eruptions: In order for volatiles to make their way to the site of the bubble formation, they must diffuse through the melt. As such, knowledge of diffusion is essential when modelling dynamic exsolution of volatiles from melts and the subsequent effect of this process on eruptive mechanisms.

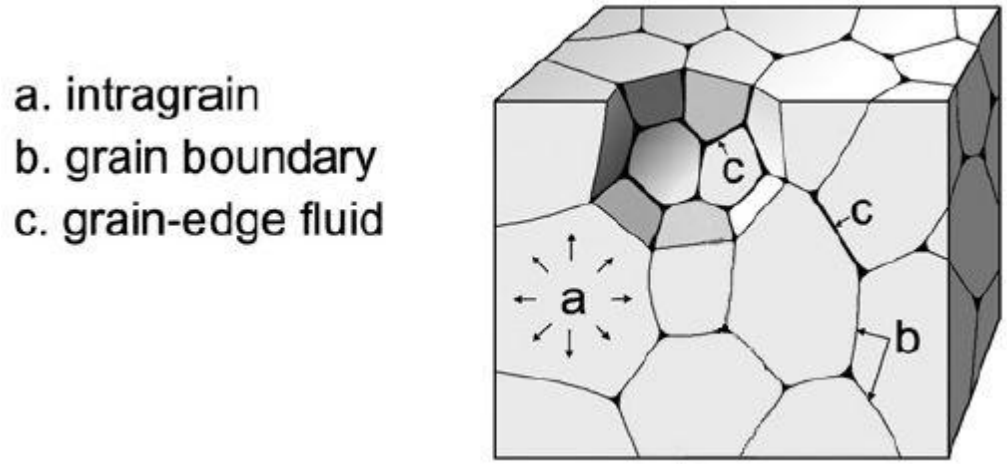

Figure 5: Diffusion routes through a multi-granular material

Route A shows diffusion through mineral grains – lattice diffusion. Routes B (grain boundary diffusion) and C (grain edge fluids) form potential fast pathways as volatiles are visualised as being unimpeded in travelling along them. Route C is not considered here as it requires the presence of fluids at grain-edges which are expected to be far less ubiquitous than grain boundaries within the Earth.

Modified from Watson & Baxter (2007) [5].

1.3.2.1 The Description and Importance of Diffusion

In order to successfully design methods for measuring diffusion in geologically relevant settings, it is important to understand both the physical and chemical processes and mathematical description of diffusion as both of these factors will inform the choice of experimental setup.

An important factor which should always be considered in the study of diffusion is the driving force behind the process. Self-diffusion is diffusion where no chemical gradient exists. As such it is the "random walk" of a particle or species through a medium. Self-diffusion is sometimes referred to as isotopic or tracer diffusion in reference to the methods which are employed in studying it (e.g. hydrogen – deuterium exchange). Chemical diffusion is the diffusion of a species in the presence of a chemical gradient [5] (the diffusing species moves from an area of high concentration to an area of low concentration). Here we are concerned with chemical diffusion as (comparatively large) sources of diffusant will be used in experiments thereby creating a chemical gradient. This is necessary to ensure that measureable diffusion is able to occur within the short timescales (compared to natural settings) which are available when running experiments. Self-diffusion coefficients are also very worthwhile knowing (especially if H is found to be stable at grain boundaries) but are considerably more difficult to measure owing to the very low concentrations of diffusants that

would exist at grain boundaries; smaller than can be currently analysed. Furthermore, chemical diffusion is more relevant to many geological processes such as the interaction between different geological reservoirs, as in these cases it is expected that large chemical gradients will be present.

1.3.2.1.1 Treatment of the Host Medium

The way in which the host medium (through which diffusion is taking place) is considered and treated is of relevance to any discussion on diffusion. The two end-member concepts describing the host phase are referred to as a *rigid lattice* and an *inviscid continuum* [5]. In a rigid lattice, atoms are considered to oscillate about a fixed position. They are, however, able to occasionally make jumps to neighbouring sites with the combined total of all jumps forming the diffusive flux. Figure 6 shows a schematic representation of the rigid lattice concept.

The frequency of site to site jumps is given by:

Equation 1: Rigid Lattice Diffusive Jump Frequency

$$\Gamma = v\exp(-E/kT)$$

(from Watson & Baxter [5])

Where Γ is the jump frequency in jumps per second, *v* represents the vibrational frequency of the atom in the site, *E* is the energy required to make the jump (i.e. an energy barrier), *k* is the Boltzmann constant and *T* is temperature in kelvin.

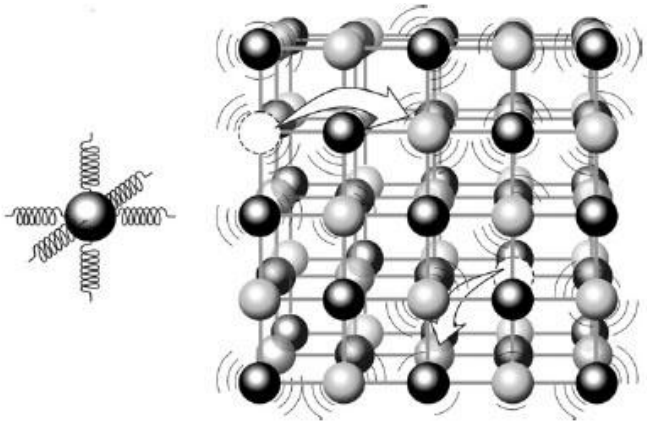

Figure 6: Schematic model of a rigid lattice

Atoms vibrate about a central point within a site here represented by an atom suspended in space by springs in orthogonal orientations. Diffusing species make jumps between sites at a frequency dependent on their vibrational frequency within a site, the energy associated with making the jump and temperature.

Modified from Watson & Baxter (2007) [5].

An inviscid continuum can be thought of as a sea of small particles through which the diffusing molecule must pass. The diffusant experiences a drag as it moves between the small particles. Hence, an inviscid continuum can be likened to a viscous liquid (see Figure 7). This model is valid as long as the molecules of the diffusant are no more than 5 times the size of the molecules of the solvent. Diffusion coefficients for this model are predicted by the Stokes-Einstein equation:

Equation 2: Stokes-Einstein Equation for Diffusion in an Inviscid Continuum

$$D = kT/(6\pi\eta R_0)$$

Where D is the diffusivity, k is the Boltzmann constant, T is temperature in kelvin, η is the fluid viscosity and R_0 is the radius of the diffusant in m.

See section 1.3.2.2 Diffusion Mechanisms for a further discussion of the mechanisms of diffusive motion in both grain boundaries and mineral lattices.

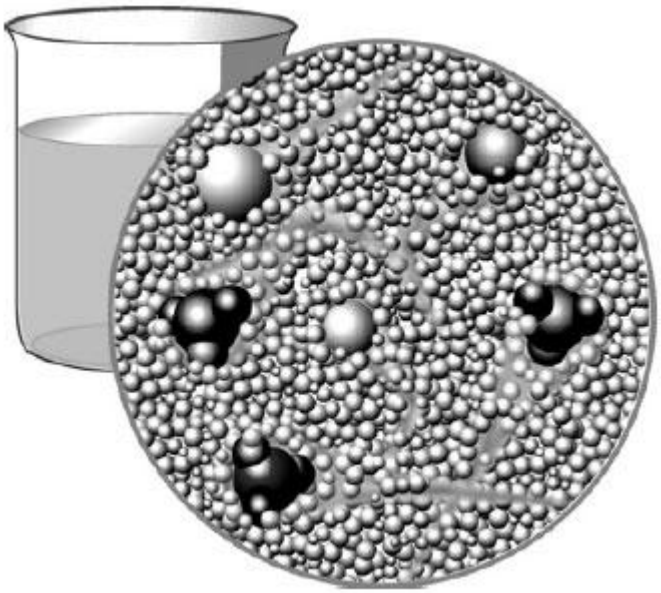

Figure 7: The Inviscid Continuum Concept of Diffusion
Here a SiO_2 solute (black) is diffusing through a supercritical aqueous fluid. The inviscid continuum model visualises the motion of a large diffusant molecule through a sea of smaller molecules which form the solvent and which cause a viscous drag.
From Watson & Baxter [5].

All geological materials which have undergone condensation fit within the spectrum between these two end-members. Silicate melts, for example, fall approximately in the middle, their exact position being defined by the degree of polymerisation (i.e. composition) of the melt [5]. Diffusants moving through mineral grains will sit much closer to the rigid lattice model. Grain boundaries may be considered as being closer to a melt in some regards as they are more amorphous regions lacking long range order.

1.3.2.1.2 Treatment of the Diffusant

Diffusion can be considered from two perspectives: At an atomic scale considering the movement of individual atoms of the diffusant through the host phase, an *atomistic* approach, or at a larger scale considering the bulk movement of large numbers of atoms, thereby looking at the *phenomenology* of diffusion. As such, a phenomenological approach utilises a statistical description of the mean motion of large numbers of diffusing atoms/molecules [5] allowing laws to be derived to describe the process.

1.3.2.1.3 The Nature of Grain Boundaries

The categorisation of GBD into one of the two categories listed above is difficult owing to our poor understanding of grain boundaries. Many factors may affect the way in which volatiles (and other non-volatile species) move along grain boundaries. In the case of H^+ diffusing along grain boundaries, an important factor will be the way in which the diffusant interacts

with the grain surfaces between which it is travelling. It is likely that H will attach itself to under bonded O ions; the ease with which H^+ can jump between them is also of great importance. Furthermore, if natural grain boundaries contain high concentrations of incompatible elements with high charges then these could affect the movement of a charged species like H+ by occupying sites that H may otherwise use as sites to make diffusive jumps between. This is due to the fact that, as already mentioned, incompatible elements have been shown to preferentially partition to grain boundaries. Thus, if they are present at a grain boundary, they may take up sites which would otherwise be utilised by diffusing H or may interact with H in some other way. As such, there could be an interesting comparison between synthetic 'clean' systems and 'dirty' natural systems with natural systems exhibiting varying deviations in behaviour as more or less cations are partitioned to grain boundaries. This would be an interesting avenue for further research. The relative widths of the grain boundary and diffusant could affect the diffusivity as could the degree of coupling of grain boundary and bulk diffusion.

1.3.2.1.4 The Mathematical Description of Diffusion

From a phenomenological point of view, chemical diffusion is mathematically described by Fick's Laws. Both Watson & Baxter (2007) [5] and Joesten (1991) [26] provide useful reviews of the reasoning behind and use of Fick's Laws. Like all such empirical laws, Fick's laws model diffusion in an idealised system – real data will almost always deviate from fits to the laws in some way. By comparing the assumptions behind the laws with proposed expectations for such deviations, further understanding can be developed. Fick formulated two laws regarding diffusion: Fick's First Law (Equation 3) describes steady state diffusion. This law is of limited use in geochemical systems primarily due to the fact that it is not explicitly time dependent [5] In contrast, Fick's second law (Equation 4) describes non-steady state diffusion where local concentration within the diffusion volume does change with time. The relative sizes of the source and sink reservoirs are important as a large difference in size may require the source or sink to be considered as an infinite reservoir or infinite sink respectively. To this end, Fick's Laws have been solved for different sets of boundary conditions. As such, the choice of experimental setup will dictate which solution should be utilised to describe the observed diffusion. If the size of the source reservoir is relatively small compared to that of the sink (as is the case in Baker & Rutherford [42], Winther et al. [47] and Freda [48]) then a solution such as Equation 5 will describe the diffusion whereas if the source is large compared to the sink, Equation 7 may be more appropriate.

Equation 3: Fick's First Law

$$J = -D\frac{\partial \varphi}{\partial x}$$

Where J is the diffusion flux (mol $m^{-2}s^{-1}$) expressed in numbers of atoms through a unit area perpendicular to direction *x* within a unit time, $\frac{\partial \varphi}{\partial x}$ is the concentration gradient in the *x* direction [φ is concentration (mol dm^{-3}) and *x* is distance (m) from the source]. *D* is a constant known as the diffusion coefficient (m^2s^{-1}) which is specific to the diffusant in question within a specific host phase. Thus *D* incorporates the mechanism of diffusion in play within the given scenario. This is a 1 dimensional diffusion equation with the implication that diffusion flux in any direction other than *x* is 0.

Equation 4: Fick's Second Law

$$\frac{\partial \varphi}{\partial t} = D\frac{\partial^2 \varphi}{\partial x^2}$$

Where symbols are as above and additionally *t* is time (s).

From the above relationships, the law can be re-stated in the following way which links concentration and distance from source to diffusivity and the initial concentration of the diffusant in the source material:

Equation 5: Concentration/Distance Solution to Fick's Second Law

$$C(x,t) = \frac{C_1 + C_2}{2} + \frac{C_1 - C_2}{2} erf\ \frac{(x - x_0)}{2\sqrt{Dt}}$$

Where *C* is the concentration of the diffusant at distance *x* along the diffusion profile and at time *t*. C_1 is the initial concentration of diffusant in the sink phase and C_2 is the concentration of diffusant in the source phase. x_0 is the position of the interface. *D* is the diffusion coefficient and *erf* is the error function. In practice, if the initial concentration of the diffusant in the sink phase is zero (as, in practice, in all aspects of this investigation it was) then the equation can be re-stated as:

Equation 6: Simplified Concentration/Distance Solution for Zero Concentration in Sink

$$C(x,t) = \frac{C_2}{2} - \frac{C_2}{2} erf \frac{(x - x_0)}{2\sqrt{Dt}}$$

Alternative solutions may be used in scenarios where alternative boundary conditions are applicable. For example, (Equation 7) is a solution which allows for a pre-existing concentration of diffusant to be present in the sink phase.

Equation 7: Concentration/Distance Solution allowing for Pre-existing Sink Phase Concentration of Diffusant

$$\frac{C(x,t) - C_0}{C_S - C_0} = 1 - erf \frac{(x - x_0)}{2\sqrt{Dt}}$$

Where C_S is the concentration of the diffusant in the source which remains constant during the run i.e. the source reservoir is very large compared to the sink phase. Here, C_0 is the concentration of diffusant in the sink phase prior to the start of a run (all other terms are as above). As such, the equation can be simplified to:

Equation 8: Simplified Concentration/Distance Solution allowing for Pre-existing Sink Phase Concentration of Diffusant

$$C(x,t) = (1 - erf \frac{(x - x_0)}{2\sqrt{Dt}}) * C_S$$

If time (i.e. run duration), concentrations and corresponding distances are known then a non-linear regression fitting method can be applied to the relationship in order to determine diffusion coefficients and initial (effective) concentrations. This is what has been done in each part of this investigation (see Data Treatment sections within each data chapter for details of processing procedures and values used).

1.3.2.2 Diffusion Mechanisms

Two of the three principle mechanisms of chemical diffusion in the mantle are considered here; *lattice diffusion* and *grain boundary diffusion* (grain edge fluids are not considered for reasons already discussed). The testing and measurement of each requires a different kind of experimental setup and careful choice of diffuser and medium. Here the mechanisms of

and methods associated with lattice diffusion will be briefly reviewed as certain aspects of the methods will be relevant in the design of experiments measuring GBD.

1.3.2.2.1 Lattice Diffusion

Lattice diffusion can be thought of as the movement of a dissolved species through a rigid lattice made of atoms coordinated with their neighbours in a specific way [5] (see section 1.3.2.1.1 Treatment of the Host Medium and Figure 8 for examples of mechanisms of lattice diffusion). An atom/ion of a diffusing species residing within the lattice, for instance in a site normally occupied by a lattice constituent, can jump into a nearby vacant site. Alternatively, atoms could reside in interstitial positions and jump to neighbouring interstitial positions. A great number of other mechanisms are of course also possible as ions exchange positions to utilise lattice or interstitial positions or utilise vacancies. This repeated "jumping" forms the diffusive movement. It should be noted that the direction of any single jump of a single atom/molecule of diffusant will be essentially random (i.e. not necessarily in the direction of the overall diffusive flux). However, as chemical diffusion progresses, the mean motion of all of the atoms/molecules of diffusant will be from a region of high concentration to a region of low concentration. There is an energy associated with making each jump as an atom diffuses through a lattice. This is due to the elastic deformation of the lattice that must occur to allow the jump to take place. Furthermore, there will be an energy associated with any other jumps or substitutions that must take place so that both mass and charge balance can be achieved. Hence, it will be the single step in the whole process with the highest activation energy which will be rate limiting. The magnitude of the activation energy can vary greatly with figures of the order of 40kJmol^{-1} recorded for CO_2-H_2O interdiffusion in fluids under supercritical conditions[49] up to many hundreds e.g. 700 kJmol^{-1} for C in diamond [50].

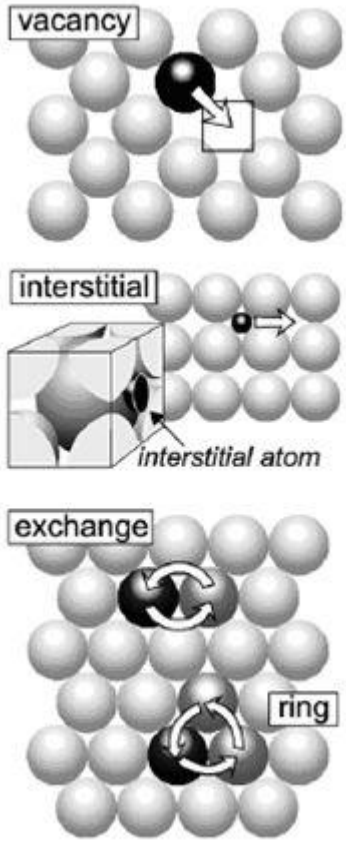

Figure 8: Intragranular diffusion mechanisms.
The top image shoes a diffusing molecule (black) moving by jumping into a vacant lattice site. The middle image shows a small diffusant (relative to the size of the surrounding lattice ions) moving through the lattice by residing at interstitial sites. The bottom exchange mechanism operates by a diffusant swapping place with a lattice ion. The vacancy and interstitial mechanisms have been well observed and documented whilst the example exchange reconfigurations are hypothetical.
From Watson & Baxter, 2007 [5].

Kröger-Vink Notation

It is useful to be able to succinctly describe and notate the reactions and exchanges which take place as changes occur within a mineral lattice. To this end a dedicated notation system was developed by Kröger & Vink [51] in 1956 to describe lattice defects and the charges (and charge balancing) associated with them. An example of particular relevance here is the incorporation of hydroxyl (OH) into the olivine structure. A likely mechanism to explain incorporation of OH into olivine (i.e. incorporation of interstitial H^+ associated with an O^{2-} ion) according to Wright & Catlow, 1994 52, is shown below in Equation 9.

Equation 9: Hydroxyl Incorporation in Olivine Mechanism

$$2Fe_{Me}^{\bullet} + 2O_O^x + H_2O_{(fl)} \rightarrow 2Fe_{Me}^x + 2(OH)_O^{\bullet} + \frac{1}{2}O_{2(fl)}$$

Where the notation system is as follows:

A site within the lattice is represented as: M_S^C

Where *M* represents the species residing in the site. This could be 1) an atom, 2) a vacancy (denoted as *V*), 3) an electron (denoted *e*) or 4) an electron hole (denoted *h*).

The subscript *S* denotes the site within the lattice which the species occupies. In Equation 4, on the left-hand-side, Fe resides in a metal site, denoted as *Me*. On the right-hand-side site of the reaction, OH resides in an O site. Often the species in question may reside in an interstitial position between sites that is not normally occupied. Interstitial sites are denoted i.

The superscript *C* is the charge of the species relative to the site that it occupies. For example, if Na^+ were to sit in a site normally occupied by Mg^{2+} there would be a net charge on the site of -1. This would be represented as `. Positive charges are denoted • and neutral charges are indicated by x.

1.3.2.2.2 Grain Boundary Diffusion

Conceptually, GBD may be visualised as follows: Where a particular mineral grain ends a discontinuity is formed. GBD is the movement of diffusant along grain boundaries as opposed to through the mineral lattice. This movement may be between grains of the same phase or between differing phases. Relative to a diffusant moving through a mineral lattice by making a series of jumps between either vacancies or interstitial sites (and potentially requiring a counter flow to charge and/or mass balance the flow of the diffusant) it is expected that the motion of a diffusant along a grain boundary will be relatively fast with discrete diffusive jumps having a lower activation energy. This is envisaged to be due to the comparatively amorphous local environment that is expected of a grain boundary as compared to a mineral lattice (the ability of large ions to reside at grain boundaries suggests at least a degree of openness in the scale of individual nm at grain boundaries). The expected fast flow along a grain boundary is hypothesised to be caused by the need for a far smaller activation enthalpy to be overcome (it is expected that a mineral lattice will need to

undergo an energetically far more expensive stretching in order to allow jumps between sites in a mineral lattice as compared to the stretches required to move along a grain boundary). By providing comparatively wide pathways along which volatiles can pass (approx. 5nm [22] width of grain boundary as compared to atomic/molecular diameters of a few angstroms within a mineral lattice – see Figure 3), grain boundaries could allow faster diffusion meaning that transport along them could be the dominant mechanism for mantle diffusion. Furthermore, as charge balancing requirements are not expected to be so strict at grain boundaries (a flow with opposing charge in the opposing direction would be expected, but as the diffusant is not sitting on specific sites within a mineral structure with an expected charge associated with it, localised one-for-one charge balancing on an atomic scale should not be required) one would also expect GBD to be quicker for this reason.

An additional point of note is that a diffusant travelling from a source to a sink region via a grain boundary would travel a greater distance than one travelling in a direct line via a mineral lattice (I.e. travelling *around* a grain instead of in a straight line *through* it). Whilst individual atomic/molecular movements of a diffusant are random, the overall flux closely follows a straight line - the shortest possible distance route from source to sink. It follows that in multi-granular material with a large grain size, the distance to be travelled along grain boundaries would be larger and so this would decrease the magnitude of a diffusion coefficient relative to a smaller grain material. It will therefore be important to consider the effect of the grain size in this work and how this relates to natural systems.

A number of studies have investigated the storage and movement of various elements on and in grain boundaries [1,6,22–24,30,53–55]. The methods used both in theoretical and experimental settings are of use to this study; this section considers the findings and implications of such research.

1.3.2.3 Factors affecting Diffusion

When considering diffusion, particularly within an experimental context, it is necessary to consider the potential effect of the specific PT conditions under which the process is occurring. As with any chemical system or parameter, diffusion does not occur as an isolated entity but instead operates under varying environmental influences. Of particular importance for diffusion are temperature, pressure, solubility and chemical gradients.

1.3.2.3.1 The Effect of Temperature – General Case

As diffusion is the motion of one species through another, one would expect to observe variations in diffusion rates based upon variations in the energy possessed by the molecules of the diffusant. As such, diffusion rates are greatly affected by temperature: Molecules of the diffusant will possess greater kinetic energy at higher temperature. The effect of

temperature is easily understood in the case of lattice diffusion: with increased kinetic energy, atoms are more easily able to overcome the activation energy of diffusion and make each successive jump to the next site [5]. The relationship between temperature and grain boundary diffusion rates is less clear. If grain boundaries do indeed provide fast, low-impedance pathways then the relative effect of increasing temperature may be diminished. Whilst an overall increase in diffusivity with temperature can be expected due to higher kinetic energy, low activation energies may mean that temperature dependence is less strong.

The relationship between the diffusion coefficient *D* and temperature *T* has been found to vary exponentially [5]. Broadly speaking, the temperature dependence of D is expressed by an Arrhenius relationship (Equation 10):

Equation 10: Arrhenius Relationship of Temperature Dependency of Diffusion Coefficients

$$D_i = D_{o,i} exp(-E_a/RT)$$

Where *D* is the diffusion coefficient of the diffusant *i*. The pre-exponential constant D_o is an amalgam of various parameters including properties of the diffusing medium including the nature of the sites available and the characteristics of the lattice. E_a is the activation energy of diffusion (as discussed above), *R* is the gas constant and *T* is temperature in kelvin. Thus, by obtaining diffusion coefficients for a specified diffusant in a specified phase at a number of different temperatures it is possible to determine the Arrhenius relationship for the system in question.

The temperature dependence of diffusion is shown on an Arrhenius plot with axes of *1/T* and *log D* (see Figure 9 for an example). The activation energy and pre-exponential factor can be obtained from a graphical analysis of diffusion data on an Arrhenius plot. The process of obtaining these parameters is detailed below:

The Arrhenius equation can be re-written as:

$$ln\ D = ln\ D_0 - (E_a/RT)$$

Which, if the axes are specified as:

$x = 1/T$ and $y = ln\ D$

Is of the form $y = mx + c$.

By graphically obtaining the gradient and y-intercept of the best fit line the parameters may be calculated as follows:

The y-intercept $c = ln\ (D_0)$ therefore, $e^c = D_0$

The term mx is equivalent to the (E_a/RT) term and is the gradient multiplied by the x value.

$mx = E_a/R * 1/T$

As x is in the form of $1/T$,

$m = E_a/R$

So,

$mR = E_a$

Using programs such as Microsoft Excel it is possible to perform the above operations without plotting the data. Functions can be created which analyse the x and y parameters to give numerical results which can then be converted into D_0 and E_a. Calculations are shown using this process in subsequent analysis, processing and results sections.

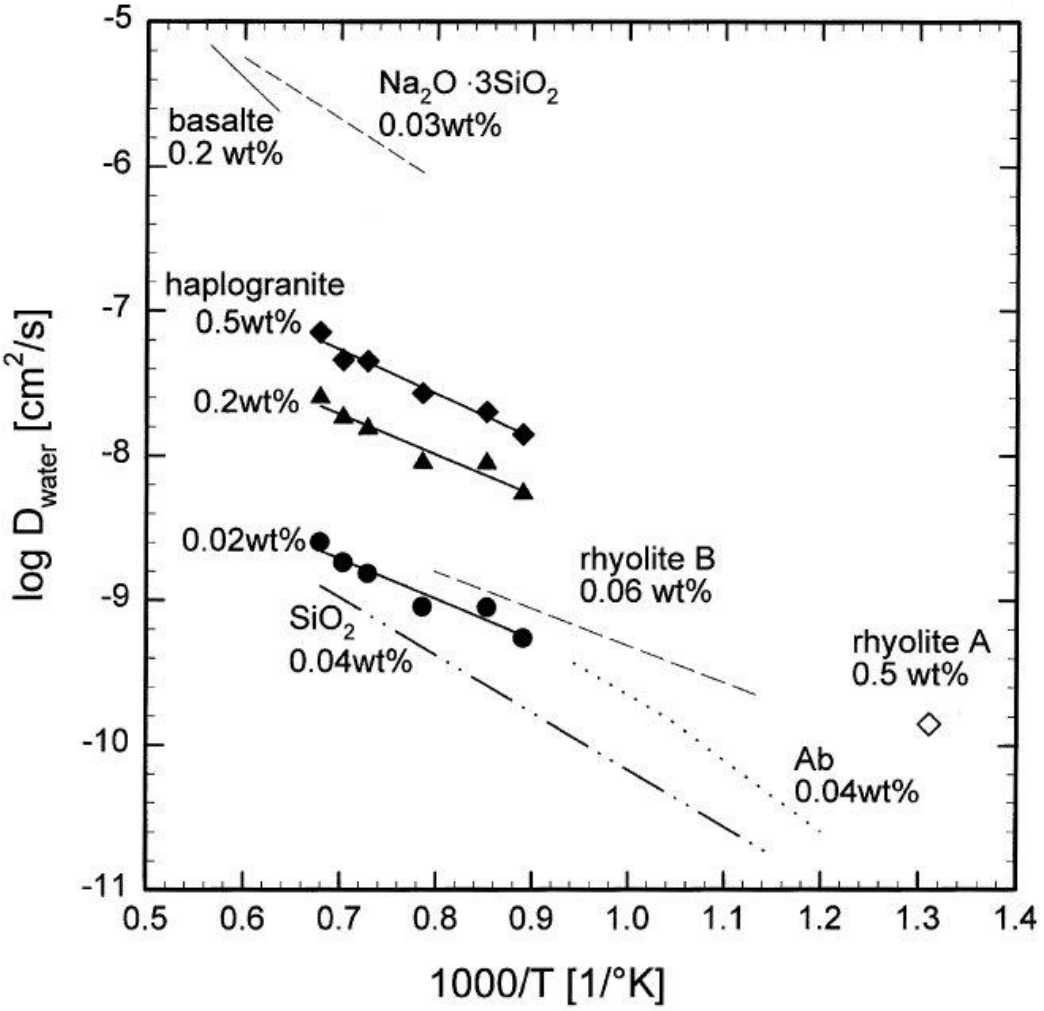

Figure 9: Example of an Arrhenius Plot

Arrhenius plot showing the relationship between temperature and diffusion coefficient, D. Temperature is typically shown as 1/T or a multiple thereof. In this example the x-axis is 1000/T where T is in K. In many cases where mantle minerals are the subject of such plots $10^4/T$ is shown on the x-axis. Diffusion coefficients D are shown as a logarithm with base 10 in either cm^2s^{-1} or m^2s^{-1}.

From Behrens, 1994 [56]

1.3.2.3.2 The Effect of Temperature on Grain Boundary Diffusion

Of particular interest here is the question of the relative strength of the effect of temperature on diffusion coefficients for grain boundaries as opposed to mineral lattices. Various studies have shown grain boundaries to allow far more frequent jumps of atoms than can occur in the mineral lattice [7]. Figure 10 shows self-diffusion of silver in mono and polycrystalline materials. Above 600ºC, values of D are essentially the same in both scenarios but below 600ºC the polycrystalline samples show significantly higher values and as such it can be inferred that it is GBD that is the dominant mechanism [7].

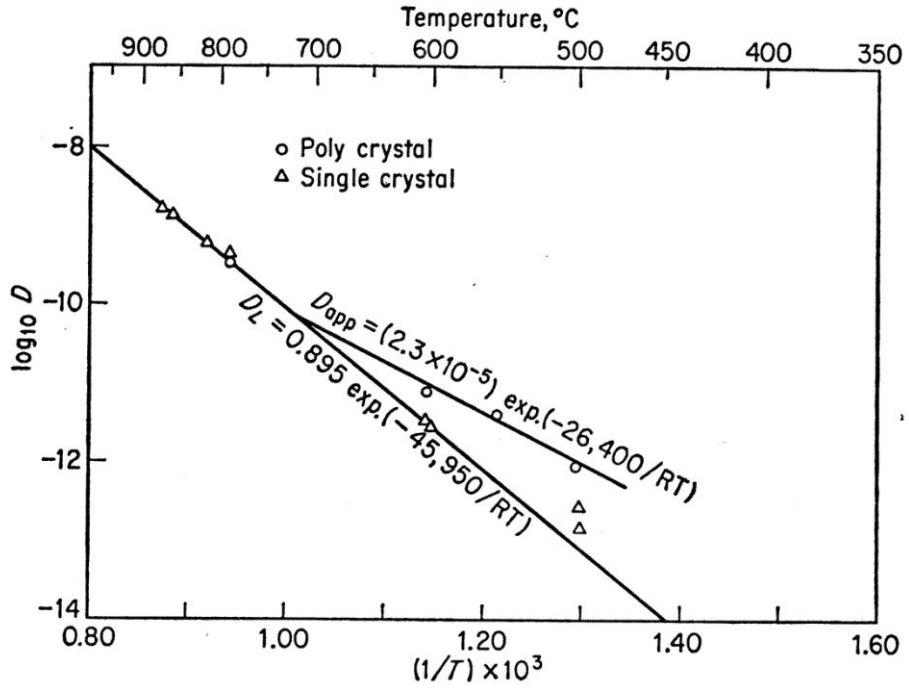

Figure 10: Self-diffusion coefficients of silver

Diffusion of silver through silver. Circles are for polycrystalline samples, triangles mono-crystalline. At lower temperatures diffusion is quicker for polycrystalline samples indicating that GBD is increasingly important as temperature decreases. Also of note is the inference that temperature dependence for each of the two types of diffusion (lattice only vs. bulk (lattice + grain boundary)) is markedly different with the polycrystalline case (lattice + grain boundary) being less influenced by temperature

From Shewmon 1963 [7].

The increasing importance of GBD with decreasing temperature is attributed to the increasing ease with which lattice diffusion can take place with increasing temperature (more thermal energy means that atoms are able to overcome the activation energy associated with jumping between lattice sites more easily) [7]. Furthermore, as grain boundary diffusion

will not have the same mechanisms requiring an activation energy to be overcome it can be expected to show a lesser temperature dependence than lattice diffusion – this will be seen as a shallower gradient on an Arrhenius plot – as seen in Figure 10. Investigation will be required to determine whether this effect is also seen in the more complex scenario of chemical diffusion of volatiles along grain boundaries and in the study of Ti diffusion in quartz.

1.3.2.3.3 The Effect of Pressure – General Case

It is important to consider the effect of pressure on diffusion coefficients as at the depths of interest in this study – equivalent to the upper mantle – pressure is not inconsiderable. Relative to temperature, little work has been done on the pressure dependence of diffusion coefficients as in general pressure is believed to have a less significant effect than temperature. Watson & Baxter [5] have stated the following relationship describing the pressure dependence of *D*:

Equation 11: Pressure Effect on Diffusion Coefficients

$$D_{t,P} = D_t \exp\left(\frac{-PV_a}{RT}\right)$$

(From Watson & Baxter [5])

Where D_t is the diffusivity at "zero pressure" at the given temperature, *T*. *R* is the gas constant. The V_a term is dependent on the diffusant and the medium in which it is diffusing, along with the mechanism of diffusion. It has been found [57,58] that in the case of large ions, V_a can take on a value closely related to the volume of the diffusing species (i.e. the diffusivity of small species such as H is likely to be less affected by pressure than that for larger species).

Care must be taken in the application of diffusion data to settings at different pressures to those at which data was obtained. Whilst in general, pressure effects are considered less important than temperature effects, this is an on-going topic of research and in the future corrections may need to be made in the light of new findings. The review by Bejina [46] provides a useful reference on the subject.

1.3.2.3.4 The Effect of Pressure on Grain Boundary Diffusion

With pressure having been observed to have a comparatively small but nonetheless significant effect on bulk diffusion coefficients, it would of course be of great interest to determine if this is reflected in cases of GBD – particularly in terms of the relative magnitude of any pressure effect compared to that observed in settings of lattice diffusion. Furthermore, the relative importance of grain boundary diffusion in different regions (i.e. at different depths and in geochemically different settings) will be of interest. Variations in geochemistry will be very important as the interaction of chemistry with pressure (and temperature) effects will be complex. As an example, the storage capacity of water in the mantle appears to be highly heterogeneous – an observation that is likely due to variations in mineralogy in response to increasing pressure with depth. Current research suggests that the mantle transition zone could contain up to several weight % water as H defects in the main mantle phases [9]. Storage capacity of the upper mantle increases significantly from a few hundred ppm near the top of the upper mantle to several thousand ppm close to the base [9]. By contrast, phases in the lower mantle might only be able to incorporate a few hundred ppm water at most. Thus, the importance of GBD of H in different regions of the Earth's interior might, as a consequence, depend on the storage capacity of mantle minerals to incorporate significant quantities of H which in turn is strongly influenced by variations in pressure. It is clear that more work on the effect of pressure variations would be exceptionally useful. Whilst this is not an aim of this investigation, it would be a very worthwhile piece of follow up work.

1.3.2.3.5 Solubility

When measuring diffusion, a parameter of great importance is the abundance of the diffusant which can be present within the host phase. The maximum amount of diffusant that can be held within the host phase is defined as the *solubility* of the diffusant in the phase of interest. The solubility of a given phase within another is, itself, affected by the parameters of the environment in which the sample exists. Temperature and pressure, along with the chemical environment will affect the solubility of a given solute within a given solvent. For example, the concentration of Ti that can exist in quartz (SiO_2) has been shown to be directly related to the temperature of equilibration of the system [2]. The relationship is defined as:

Equation 12: Ti in Quartz Solubility Expression

$$Log_{10}(X_{Ti}^{qtz}) = (5.69 \pm 0.02) - \frac{(3765 \pm 24)}{T(K)}$$

(After Wark & Watson, 2006 [2])

Where X_{Ti}^{qtz} is the Ti content of quartz in ppm by weight.

This study was conducted at a single pressure (1 GPa) thereby giving the above relationship where Ti content varies only with temperature. Further work by Thomas et al. [59] complemented the original study by extending it to pressures between 0.5 and 2 GPa. From this work, the following relationship was determined:

Equation 13: Pressure Corrected Ti in Quartz Solubility

$$RT \ln X_{TiO_2}^{quartz} = -60952 + 1.520 \cdot T(K) - 1741 \cdot P(kbar) + RT \ln a_{TiO_2}$$

(After Thomas et al., 2010 [59])

Where $X_{TiO_2}^{quartz}$ is the mole fraction of TiO_2 in quartz and a_{TiO_2} is the activity of TiO_2 which, if rutile is present within the sample will equate to 1. *R* is the gas constant, *T* is temperature in K and *P* is pressure in kbar. If rutile is not present the activity of TiO_2 must be estimated by other means.

The mechanism by which a solute is incorporated into a solvent phase (in this case a mineral) is very important as factors such as the size and charge of both sites within the mineral and of the solute become significant. Ti is able to substitute for Si in the quartz structure without the need for charge balancing due to both of the elements being tetravalent. The ionic radius of Si is 0.4Å and that of Ti is 0.605Å. Thus, a certain amount of localised structural distortion of the mineral structure is required in order to accommodate the larger Ti ion. At higher temperature the atoms making up the quartz lattice show increased thermal vibration and bond distances are longer, thus enabling larger cations (such as Ti) to be more easily incorporated. Hence, higher abundances of Ti can be accommodated at higher temperatures (See Figure 2).

1.3.2.3.6 Chemical Gradients

An important factor in diffusion is the magnitude of the chemical gradient driving the diffusion. As diffusants move from a region of high concentration to a region of low concentration, it follows that that movement will be greater when the concentration difference between the source and sink areas is greater. In many cases it is possible to treat the source region as an infinite source. This can be due to the relative size of the source and sink regions (such that the sink would reach its solubility limit for the diffusant before enough diffusant has left the source for the chemical gradient to be significantly reduced) or due to

the amount of time available for diffusion to take place (i.e. within the available time the magnitude (or “steepness”) of the chemical gradient does not significantly reduce as diffusion progresses). Depending on the design of experiments and the size of the chemical gradient, the form of Fick’s laws can be re-stated to take into account a source being effectively infinitely abundant (see section 1.3.2.1.4 The Mathematical Description of Diffusion).

1.3.2.3.7 Factors affecting Diffusion - Conclusions

Thus, there are many factors which affect the diffusivity of a species within a given medium. It should of course be noted that none of these factors act in isolation and that the interplay between them is what determines the observed diffusivity. An example of this would be the interplay of solubility, temperature and pressure on diffusion rates. In the case of titanium in quartz thermometry it was found that Ti contents of quartz increased with temperature and decreased with pressure given a constant activity of Ti. As temperature and pressure both increase with depth in the Earth it is of course the relative magnitudes of the temperature and pressure effects which will be important in determining the final solubility of Ti in quartz under given conditions. The effect of this interplay on volatile diffusion is more unpredictable and an aim of this work is to try to elucidate this. As volatiles often have a small size (at least the most common volatiles of interest here) their mobility is likely to be greater and they may be incorporated more easily into a mineral structure. By isolating different variables in different experiments it becomes possible to quantify the magnitude of each variable’s effect on the bulk process.

2 Experimental Methods, Apparatus & Analytical Techniques

This section details both the experimental methods used by previous workers and those employed in this investigation. Methods utilised by other workers were taken as a starting point for the designs of those used here. In many cases alterations were made to these methods to suit the experiments to be conducted and the equipment with which they would be run.

Methods employed by other workers are reviewed first followed by a discussion of the high temperature and pressure apparatus that makes such investigations possible. This apparatus is considered in terms of both its capabilities and limitations. The effects of these limitations on experimental design are also discussed. The methods and logic behind the determination of experimental conditions are then detailed followed by a discussion of analytical techniques. Finally, the nature and relevance of experimental research is reviewed.

2.1 Review of methods used by previous workers

Historically, a number of different techniques have been employed for studying diffusion. What follows is a brief review of the experimental set-ups and techniques used by previous workers.

2.1.1 Bulk Diffusion Experimental Methods

Studies of subsurface bulk diffusion have been carried out with regard to many settings including both the mantle (looking at bulk diffusion in minerals [5,41,60]) and to the behaviour of melts, (e.g. magmas in magma chambers [42,48]). Being studies of bulk diffusion, these examples do not differentiate between lattice and GBD (although, of course, in the case of melts there are no grains and so GBD is not an applicable concept). What is being measured is simply the flux of diffusant which has taken place over the experimental run, regardless of the route that the diffuser has taken. Many of the principles behind the experimental setups utilised are of direct relevance to those that will be used in the study of GBD.

2.1.1.1 The Source and Sink Concept

Measurements of bulk chemical diffusion (i.e. diffusion in the presence of a chemical gradient) are typically conducted using a source material either made up of, or doped with the diffusant of interest, and a sink containing none of the diffusant. The sink could be an un-doped equivalent of the source material or could be a separate phase to the source and to the medium through which diffusion is taking place (host phase). The choice of the

diffuser and the host phase is made based upon factors such as the geological relevance of the media (including, for example, structural analogues), potential reactions between sink and source materials (and the host medium if this is an additional phase), and the intended method/apparatus to be used. As an example of this final point, melting may or may not be required and different pieces of equipment are able to achieve different ranges of conditions. Thus, compositions must be chosen that will behave in the appropriate manner under the conditions that are achievable in the equipment to be used.

2.1.1.2 The Diffusion Couple Method

Winther et al. [47] and Freda et al. [48] used diffusion couples to investigate the diffusion of sulphur in albitic and basaltic melts respectively (See Figure 11 for Winther et al.'s high pressure experimental set-up). A diffusion couple is a simple setup in which two pieces of the medium through which diffusion is to take place (the host phase) are created, one doped with the diffusing species (the diffusant) and one not. The doped and un-doped discs (or cylinders) of these two glasses/minerals are then held together under the experimental conditions to allow the diffusant to move from the doped disc to the un-doped disc. By taking point readings of the concentration of the diffusant along the axis of diffusion, diffusion profiles can be obtained thereby allowing diffusion coefficients to be calculated. Winther et al.'s method was based on using albite glasses with sulphur as the diffusant. What follows is a description of Winther et al.'s method; that followed by Freda et al. is broadly similar.

The albite ($NaAlSi_3O_8$) starting compositions were made from their constituent oxides. Where it was necessary to make sulphur doped glass, the glass was made up with a sodium deficit. Sodium sulphate (Na_2SO_4) was then added to make up the sodium to the correct level and to incorporate sulphate into the glass. The compositions were then melted and ground to homogenise them. Finally the compositions were held under PT conditions similar to those to be used in the experiments, melting them again before quenching them to create glasses. The cylinders of glass were then cut and polished to form glass discs. A doped and an un-doped disc were then placed against each other in a new experimental capsule to form the diffusion couple. The diffusion couple was held at the specified PT conditions for the experimental run. As one disc was doped with sulphur and the other not, sulphur diffused from the doped disc into the un-doped disc, and by measuring the concentration of sulphur along the diffusion direction a diffusion profile could be obtained. This could then be iteratively solved using Fick's Laws to determine a diffusion coefficient.

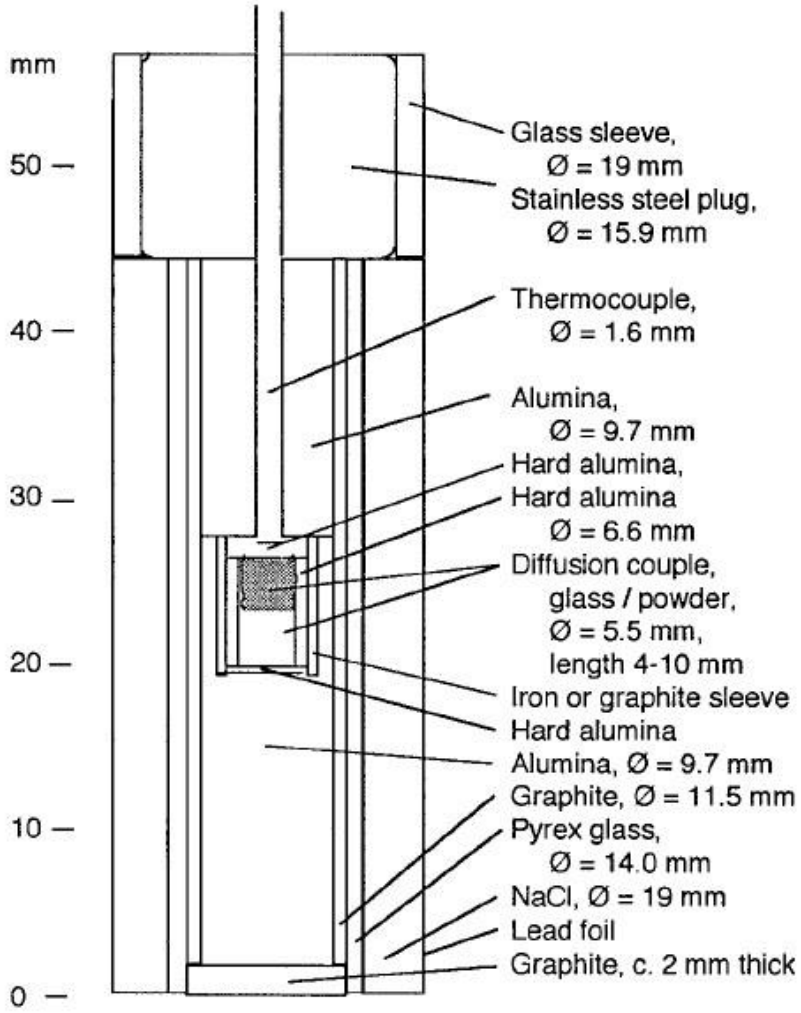

Figure 11: High-pressure diffusion couple set-up in a piston cylinder apparatus

The diffusion couple is shown at the centre of the piston cylinder apparatus (see Section 2.2 Apparatus & Techniques Used for High PT Experiments) and is encased in alumina. The sample is heated and pressure is applied to hold it at the desired conditions. The diffusant is then able to flow from the doped to the un-doped part of the couple.

From Winther et al. [47].

2.1.1.3 The Source within a Melt Method

Baker & Rutherford [42] used a different method when studying the behaviour of sulphur in rhyolite melts. Natural metaluminous rhyolite was used as the diffusion medium with a point source of sulphur (Figure 12). The rhyolite was homogenised by grinding, and equilibrated at the experimental temperature, pressure, oxygen fugacity and with water slightly in excess of that required to saturate the melt at the experimental conditions. For the majority of experiments, the glass was doped with sulphur by placing a crystal of anhydrite ($CaSO_4$) into the centre of the capsule, surrounded by the powdered glass. After the run, the diffusion data was obtained by measuring sulphur levels as one moved away from the crystal/melt interface. The melt was deemed viscous enough to hold the anhydrite crystal in place even when molten. For experiments where anhydrite was not stable (i.e. when reduced conditions were used), pyrhotite (FeS) was used as the source of sulphur. This was placed at the bottom of the capsule with the powder packed above it. When the experiment was to be conducted at a temperature below 1000°C the capsules were placed in cold seal vessels in which water was the pressure medium. For temperatures greater than 1000°C, TZM (Titanium-Zirconium-Molybdenum) vessels were used with argon as the pressure medium.

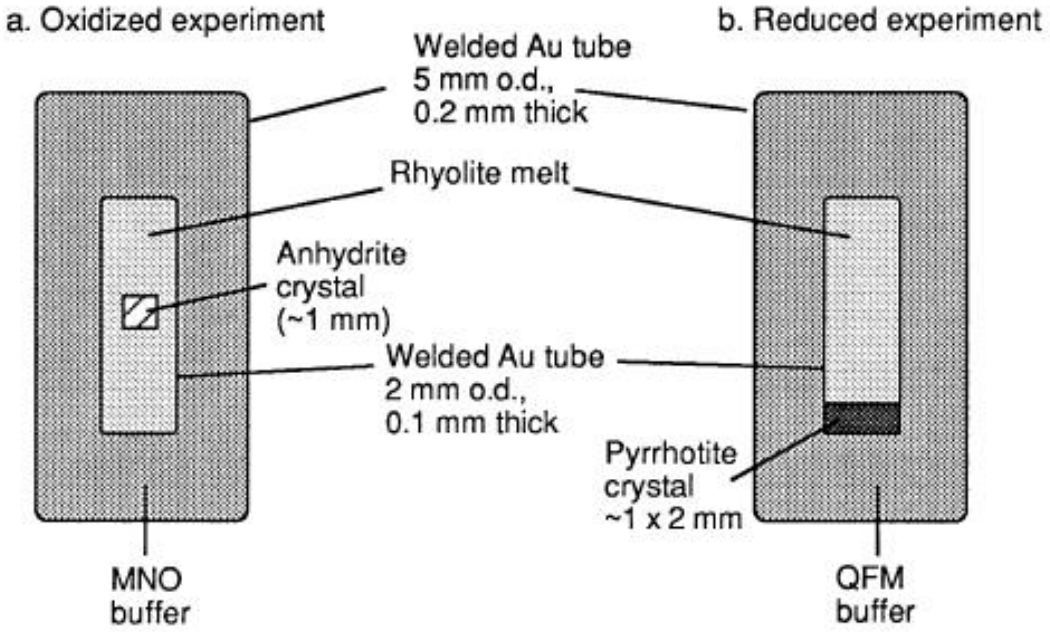

Figure 12: Experimental set-up of Baker & Rutherford

The rhyolite melt is placed in a sealed inner capsule which is then placed in a second outer capsule with buffer between them. The MNO buffer consists of a mix of Manganese/Manganese Oxide and the QFM buffer consists of Quartz, Fayalite & Magnetite.

From Baker & Rutherford, 1996 [42]

2.1.1.4 Redox Buffers

It is often desirable to control the oxidation state of the sample in order to more closely mimic natural systems. Furthermore, it is essential that oxidation conditions are kept stable through the duration of the experiment. This is done as the valency of a given species (e.g. Iron may exist in the Fe^{2+} or Fe^{3+} state) may vary due to the oxidation state/oxygen fugacity of the environment in which it finds itself. The valency of a diffusing species may well alter the mechanism by which it diffuses or the availability of other components of the diffusive mechanism (e.g. polarons). As such, it is desirable to maintain the oxygen fugacity at a known and constant value. Buffers which hold the oxidation state at a known equilibrium value are used to do this. Often these are metal/metal oxide mixes but other combinations are possible. Commonly used buffers include NNO (Nickel/Nickel oxide), QFM (Quartz, Fayalite, Magnetite) (for reducing conditions) and MNO (Manganese/Manganese Oxide) [42]. In Baker & Rutherford's experiments [42] a double capsule was used with the gap between the inner and outer capsules filled with a buffer. Electrons and protons were able to diffuse through the noble metal capsule thus keeping the sample at the oxidation state of the buffer. In all experiments conducted here, buffering is provided by the experimental assemblage, specifically the graphite furnace. Electrons and protons may diffuse through the materials making up the experimental capsules thereby maintaining the oxidation conditions within. As it is the mechanism of diffusion that is being studied here, the specific value of the oxidation state of the system is not critical as long as it remains constant between runs thereby allowing runs to be easily compared. By always using the same type of assemblage this can easily be achieved.

2.1.2 Grain Boundary Diffusion Experimental Methods

Owing to the lack of work previously conducted on this subject, there are few published methods for testing GBD. Hayden & Watson [1] created a setup to test the grain boundary mobility of carbon under mantle conditions. A diagram of their setup is shown in Figure 13. As with all diffusion experiments, the setup is based on a source/sink concept. In order to make the setup suitable for measuring GBD, careful choices need to be made in the selection of the contents of the capsule. To ensure that the diffusion which occurs is along grain boundaries, it is highly desirable to choose a polycrystalline medium through which the diffusant is unable to diffuse i.e. lattice diffusion does not occur. If this cannot be done then any potential lattice diffusion must be taken into account in the analysis and processing of diffusion data. Aside from this consideration, the rest of the design is primarily based on the geometry required in order for the diffusion laws to be solved.

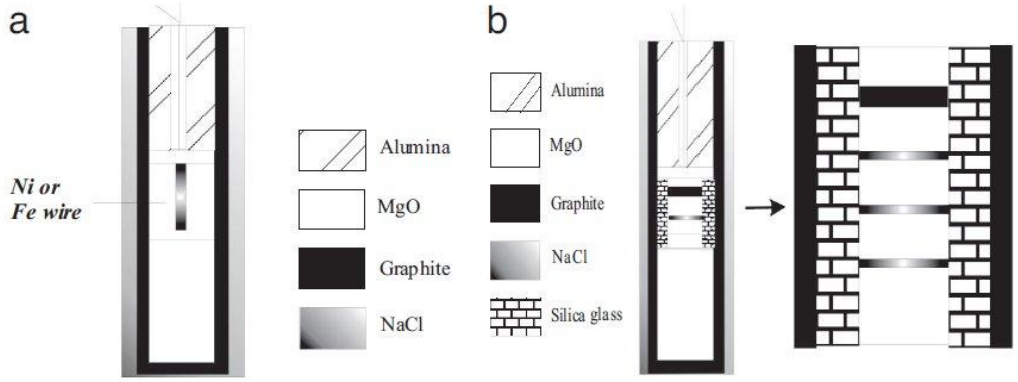

Figure 13: Experimental set-up of Hayden & Watson for studying grain boundary diffusion of carbon under mantle conditions

The method measures the degree of diffusion that has occurred by looking at the extent of carbon alloying in a sink medium. In case (a), the graphite furnace is the carbon source and the Ni or Fe wire is the sink. In case (b) the horizontal layer of carbon is the source and the lower three layers of Ni foil are sinks. The GBD of C takes place around grains of polycrystalline periclase (MgO).

From Hayden & Watson (2008) [1]

More recently Demouchy (2010) published experimental data from an investigation using very similar methods to those used here although arrived at independently [61]. Demouchy used Mg-spinel as a host phase for H diffusion and used olivine grains as sinks as we do (see Chapter 3 for a full discussion of this aspect of the research). Capsules consisted of a cylinder of polycrystalline spinel with embedded olivine grains placed against a second cylinder of talc which acted as an H source. These two cylinders were placed in a Ni capsule and runs were performed in a gas pressure vessel at a pressure of 300MPa (0.3GPa) and at temperatures between 900°C and 1250°C. An image of Demouchy's set up is shown in Figure 14. Capsules were prepared for analysis by being sectioned and the presence of H in olivine grains was tested for using FTIR spectroscopy. Diffusion coefficients were then calculated using a characteristic distance equation (see Equation 14):

Equation 14: Characteristic Distance Diffusion Equation as used by Demouchy

$$x = \sqrt{Dt}$$

Where x is the distance of the "sensor grain" (in this case a large grain of olivine – Demouchy does not make clear whether this distance is that to the centre of the olivine grain

or to the closest point of the grain) from the water source (in m). *D* is the diffusion coefficient (in m^2s^{-1}) and *t* is time (in s).

As can be seen from an examination of the above equation, the analysis method does not take into account concentrations of H in the olivine grains instead simply testing for the presence of H and equating this with distance from the H source in a given time. This method of calculating diffusion coefficients is considered potentially less reliable than fitting a dataset of multiple points with concentrations readings at a variety of distances from the water source to a solution of Fick's Laws. As such, the method utilising multiple points has been used here with the aim of producing more robust results. Furthermore, it is possible that the Demouchy results may be skewed by the presence of fluid seeping along capsule walls and not diffusing through the spinel matrix.

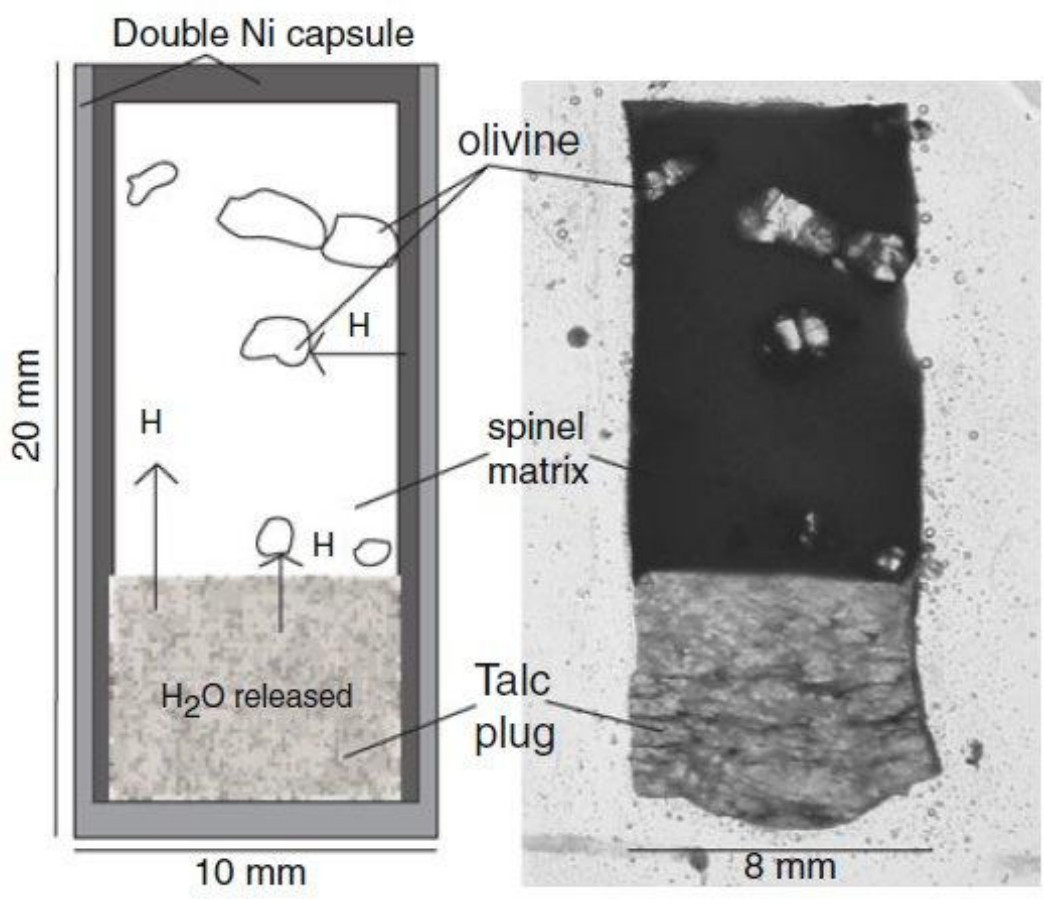

Figure 14: Setup used by Demouchy to study GBD of H in Spinel

Olivine sink grains sit within a matrix of the spinel host phase. A talc plug acts as an H/H_2O source. The presence of H in olivine grains is tested for using FTIR and diffusion coefficients are calculated using the characteristic distance equation. Whilst this method is very similar to that used here, it was arrived at independently and the data analysis used here is significantly different.

Image adapted from Demouchy, 2010 [62]

2.1.3 Conclusions Drawn from other workers' methods

The concept of utilising a source and sink is clearly important in the study of diffusion. In order for it to be successfully applied, it is essential to have the diffusant initially separate from the host phase and in a higher concentration so that a chemical gradient is imposed. Furthermore, the concept also allows experiments to be set up so that initially they are in a state of having experienced no diffusion. Thus, it is then known at the end of a run that all the measured diffusion must have occurred during the run. This is clearly demonstrated in all of the studies discussed and is implemented in many ways. Within the different sections of this investigation different approaches are utilised – in some cases the source is a separate phase, as in the majority of the work presented above, whereas in another the

capsule itself is used as a source. Previous workers' capsule designs have been of great use in designing those used here as the setup used in each part of the investigation must not only fulfil the aims of the research but also function well both mechanically and in terms of its physical properties within the apparatus to be used.

2.2 Apparatus & Techniques Used for High PT Experiments

In order to achieve the high temperature and pressure conditions required to investigate diffusion under mantle conditions it has been necessary to employ the use of specialist equipment, most importantly the piston cylinder apparatus.

2.2.1 The Piston Cylinder Apparatus

The piston cylinder apparatus is a piece of high pressure equipment utilising a solid pressure medium, meaning that high pressure is achieved by the compression of a solid but deformable material(as opposed to gas or fluid as found in other, lower pressure apparatus). Compression and deformation of a solid assemblage containing the experimental capsule creates hydrostatic sample conditions. The basic function of the apparatus (Figure 16) is to apply simultaneous high pressures and temperatures (high PT) to the experimental assemblage thus subjecting the capsule to the desired conditions. It is fundamentally a simple device making use of the principles of pressure amplification to apply force and by using a resistance furnace contained within the experimental assemblage to provide heating. The apparatus also includes a water cooling system so that heat can be effectively managed and a fused electrical system so that the current used to operate the furnace can be controlled.

The piston cylinder apparatus is able to routinely achieve temperatures of up to 2000°C and pressures of up to 4GPa – equivalent to a depth of 120km in the Earth. The apparatus works by applying a large load onto a sample which is laterally confined. A pressure of 150 tonnes (marked 'end load' in Figure 15) is initially applied to the stacked components of the apparatus, (the bridge, bomb, thermocouple plate and spacer plate along with a large aluminium spacer to fill the gap to the top of the press) (see Figure 15 and Figure 16) to provide vertical support to the stack. In the centre of the stack lies a heavy circular piece of metal called the bomb. The bomb is made up of a number of steel rings of decreasing hardness from the centre out (see Figure 17). The central cylinder is made of tungsten carbide and has a hole to accommodate an experimental capsule. The outer rings provide lateral support to the central ring, minimising lateral expansion which would otherwise shatter the carbide. The experimental capsule is placed in the hole in the middle of the central ring within an assembly of deformable material and a graphite cylinder which acts as a furnace (when a current is applied). The bridge contains a small ram which acts on a carbide piston to pressurise the sample to the desired pressure. Thus, pressure is applied in two ways, firstly by the large ram which compresses the entire stack stabilising the apparatus sufficiently to allow the second ram to directly pressurise the sample to the required

pressure. Temperature is controlled by varying power applied to the graphite furnace and is measured by recording the output voltage from a thermocouple located close to the sample.

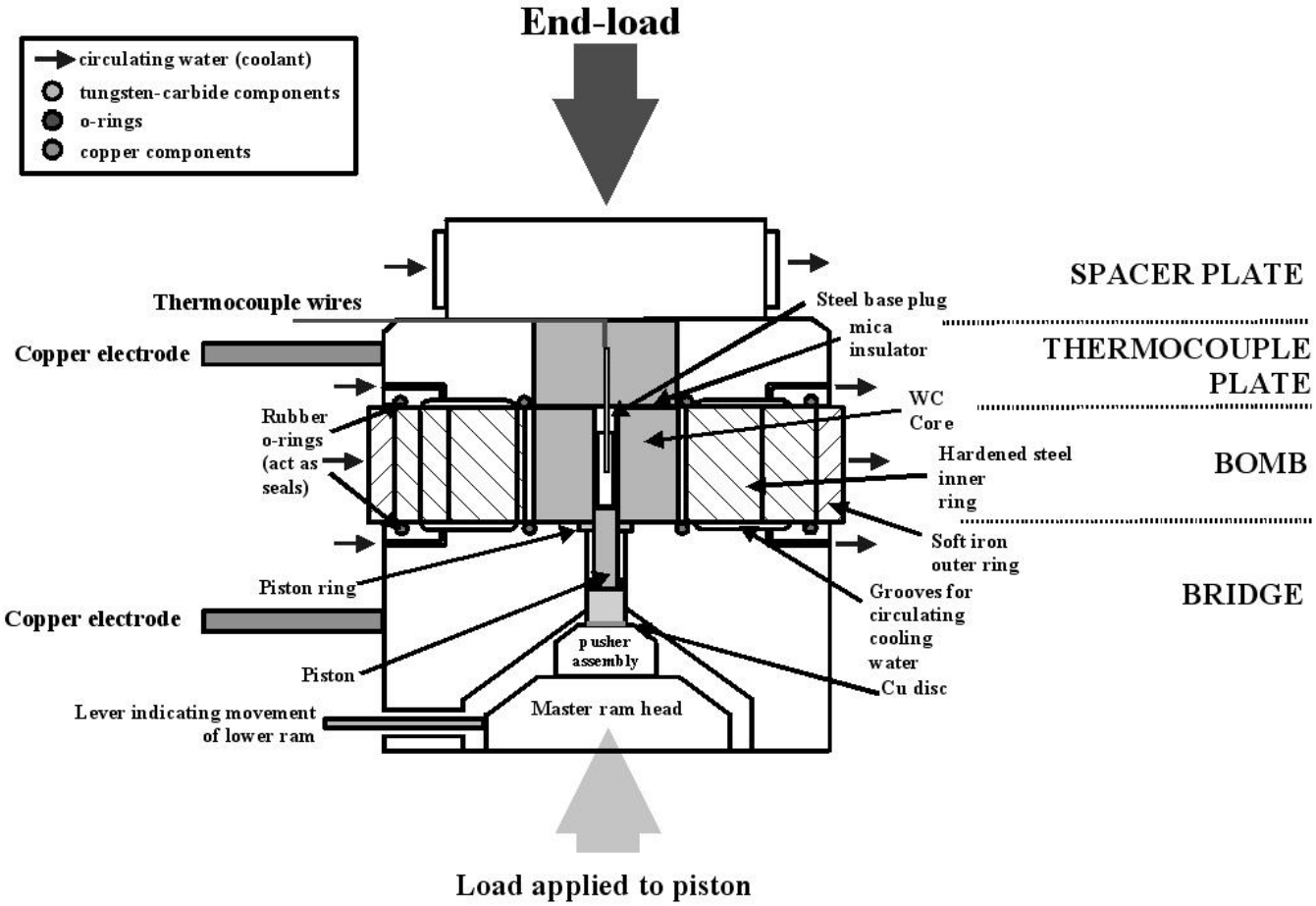

Figure 15: Cross section of piston cylinder apparatus

Showing rams and power and water connections.

Figure 16 : The Piston Cylinder Apparatus Used in this Work.

The image shows the apparatus prior to pressure being applied and also prior to the connection of heating and cooling systems. The lower ram which applies pressure to the whole stack is visible as being slightly raised from the large circular support which forms the base of the apparatus. The sample ram is located on top of the circular piece with pressure line and junction box emerging from it. The bridge with water cooling system connections (gold colour) sits above this. It also has a heating system connection on the rear. The bridge has a hole running through the middle of it enabling the piston which sits on top of the sample ram to apply pressure to the sample which sits in the middle of the bomb which itself sits on top of the bridge (larger diameter circular piece). The top plate above the bomb has water and power connections so that the circuit can be completed. Above this spacers are placed to fill the gap to the topmost plate of the apparatus so that the entire stack can be compressed.

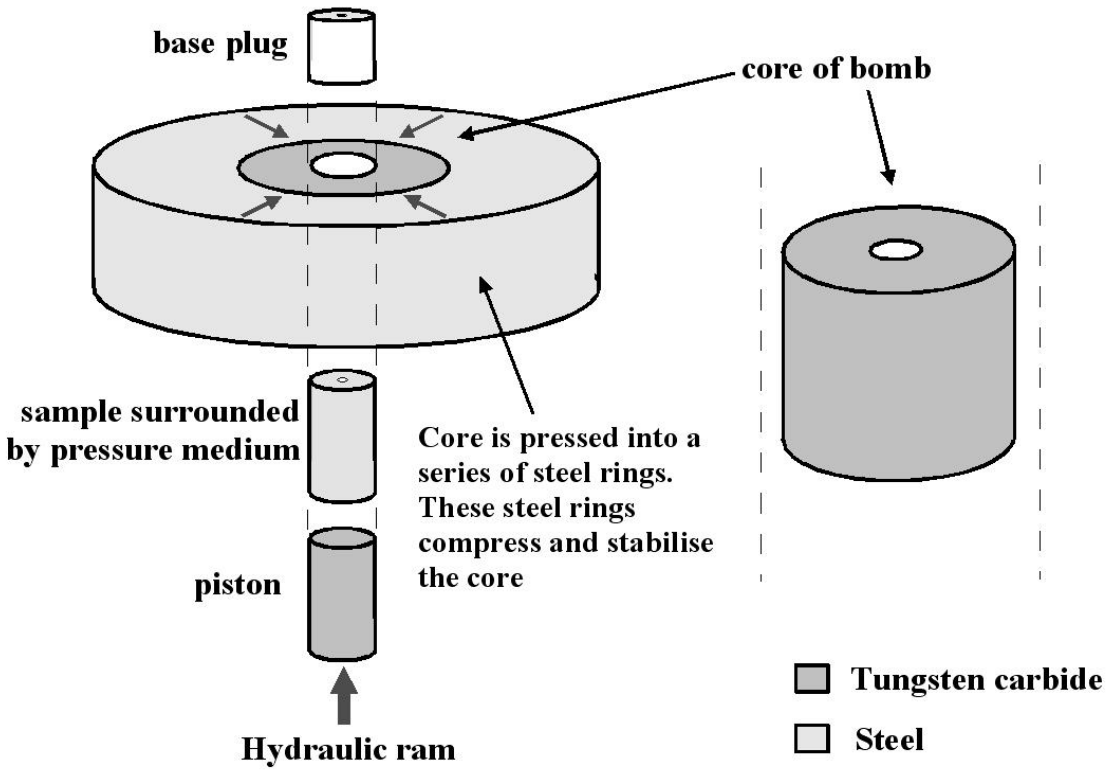

Figure 17: Bomb used in Piston Cylinder Apparatus

The bomb utilises a series of steel rings surrounding a tungsten carbide core to stabilise the pressure applied to the sample by the hydraulic sample ram.

The Experimental Assemblage

Completed capsules are placed inside an experimental assemblage (see Figure 18), the function of which is to convert the differential pressure applied by the piston cylinder apparatus to a hydrostatic pressure and also to allow the capsule to be heated (to temperatures of up to 1800°C).

Assemblages are made of: talc (a pressure medium), a Pyrex glass insulator and a graphite resistance furnace. The construction is layered with talc on the outside, the intermediate layer of Pyrex and the graphite furnace the innermost layer. When placed in the piston cylinder apparatus, use of insulation means that the only route which the current may take through between electrodes is via the carbon furnace, thus allowing heating of the sample.

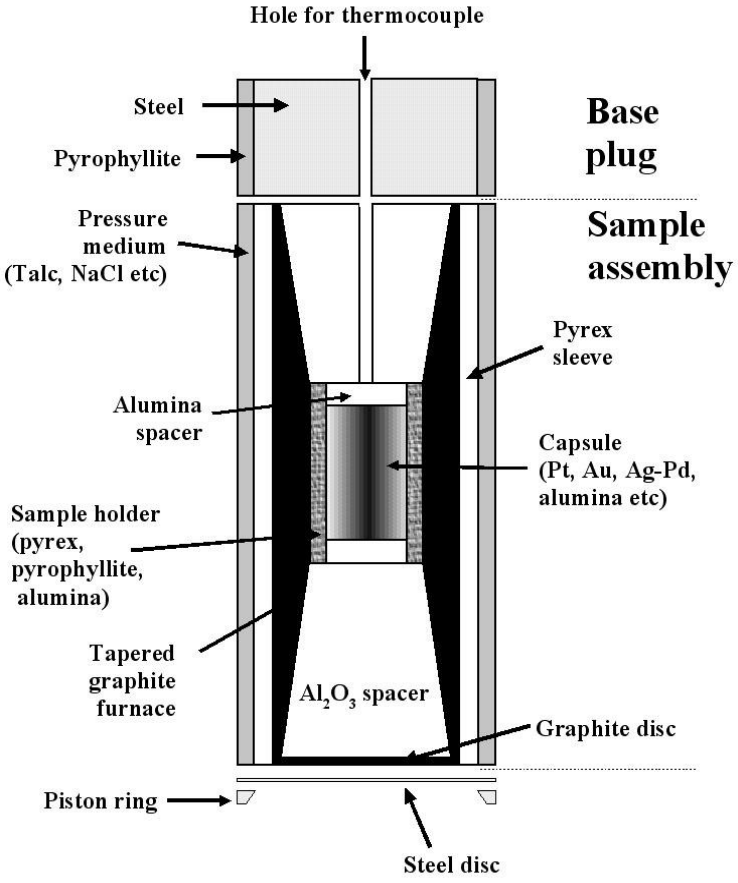

Figure 18: Experimental assemblage for piston cylinder apparatus

See text for description of the purpose and functioning of components.

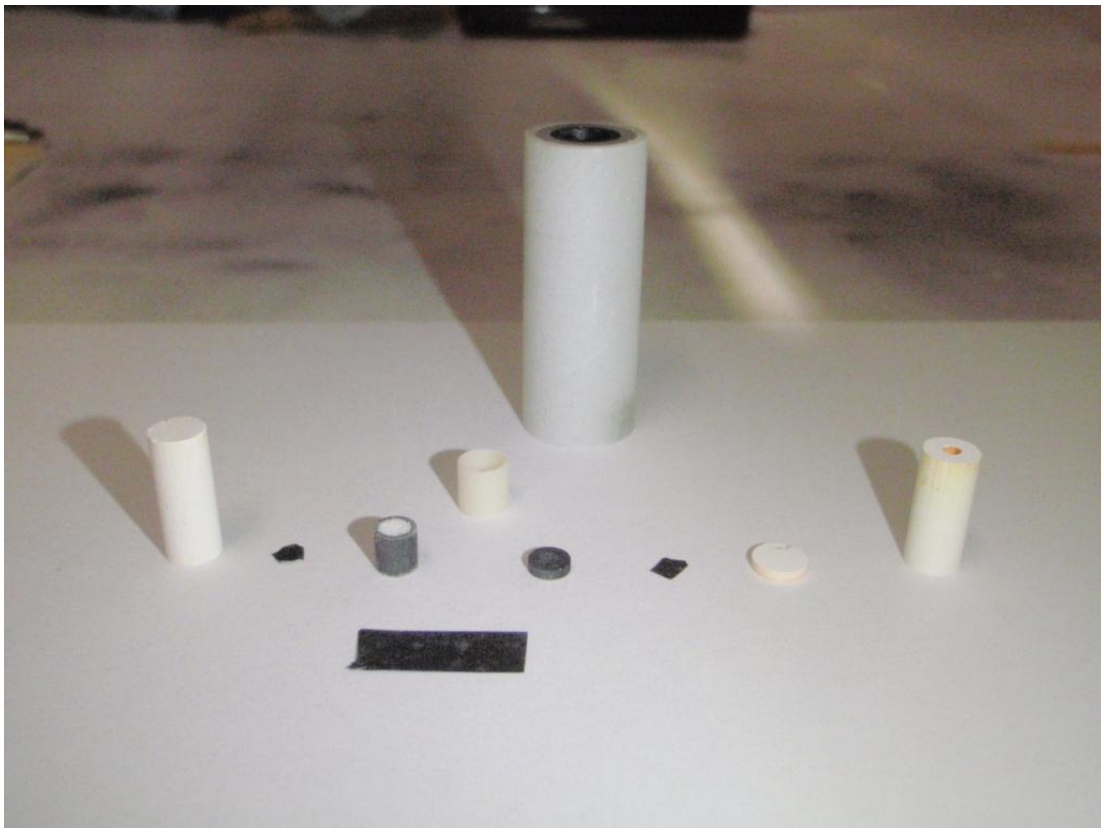

Figure 19: Photograph of an Experimental Assemblage

The large cylinder towards the rear of the photo contains each of the components towards the foreground when assembled. The talc pressure medium, Pyrex sleeve and graphite furnace which form the main body of the assemblage as seen schematically in Figure 18 are clearly visible. The lead foil which wraps around the assemblage to act as a lubricant in its insertion and removal from the bomb is not shown here. The total height of the assemblage is 32mm. The stack which sits within the cylinder is showed prior to construction with the lower components shown on the left. The photo shows components for an early Ti in quartz experiment but the majority of components are the same for all experiments. The bottom of the stack is an alumina space above which the sample sits (grey cylinder with adjacent grey lid in this case) within a small ceramic cylinder (here various foils are also shown – included to reduce the risk of capsule failure). Above the sample sits an alumina disc and above this sits a second alumina spacer with a whole drilled through the middle through which the thermocouple passes to sit against the alumina disc. Thus, the thermocouple measures the temperature within approx. 1mm of the sample location.

2.2.1.1 Sample Retrieval

At the end of each experimental run the experimental assemblage was retrieved from the piston cylinder apparatus by placing the bomb into a small hydraulic press frame and using a push rod to force the assemblage (and the piston from the piston cylinder apparatus) out of

the bomb. This typically required 2 – 3 tonnes of force to be applied. The capsule was then retrieved from the assemblage by breaking away the layers of talc, Pyrex, furnace and alumina. Typically this was done by simply crumbling the assemblage away as it had taken on a consistency which readily enabled this as a result of the high PT conditions of the experimental run.

2.3 Experimental Conditions

The choice of experimental conditions to be used in an investigation is influenced not only by the data that is required to test hypotheses but also by the capabilities and limitations of the equipment available for use. In this investigation, the use of the piston cylinder apparatus was the primary limiting factor in determining the conditions which could be achieved during experimental runs. The most extreme achievable conditions are of the order of 4GPa and 1800°C (although considerably less extreme conditions were used during this investigation so that the piston cylinder apparatus was always operated well within its performance limits). Once conditions have been decided upon it is necessary to determine run durations – calculating these is inevitably a non-trivial exercise: As the diffusion coefficients for the various scenarios being tested are not known in advance, a certain amount of guess work is required in selecting run durations which will allow enough diffusion to occur so that a diffusion profile which can yield a diffusion coefficient can be obtained but not so much that the host medium/sink phase becomes homogenous with respect to the diffusant. In practice, published data for relatively similar scenarios is used to estimate suitable durations. In many cases, the only published data describing the diffusivity of a given diffusant in a certain host medium is for single crystal (i.e. bulk/lattice) diffusion. Thus, in order to attempt to estimate suitable durations, (such that a measurable diffusion gradient will develop) an estimate must be made of how much faster than lattice diffusion GBD might be expected to be and run durations determined accordingly. Duration selection is further complicated by the effects of the run temperature and pressure as both of these parameters will affect diffusivity (to varying degrees of significance depending on the particular scenario in question). It is of course always expected that increasing temperatures will increase diffusivity and so shorter run durations will be required but the exact relationship cannot be known when the effect of temperature is one of the parameters being investigated. The effects of pressure on diffusivity are less well constrained but are typically considered to have less of an impact than temperature [5]. All experiments within this investigation were conducted at the same pressure and as such, it was not necessary to consider this parameter to a great extent. As a result, in many cases, the selection of a run duration for a given set of conditions was essentially an educated guess. In cases where experiments are run in a series of generational sets, the results from early sets may be used to determine durations for latter generations. This refinement allows increasingly higher quality and more precise data to be obtained.

2.4 Analytical Techniques

This, and all other projects of its type, rely upon the use of a number of pieces of analytical equipment to map out experimental capsules, identify phases within them and measure grains' diffusant content in order to determine the degree of GBD which had occurred.

The three principle pieces of equipment used here were a Scanning Electron Microscope (SEM), an Electron Probe Microanalyser (EPMA) and a Secondary Ion Mass Spectrometer (SIMS). Here their functionality is discussed with direct reference to their application within this project.

2.4.1 Scanning Electron Microscopy (SEM)

2.4.1.1 Introduction

The scanning electron microscope (SEM) is an instrument capable of producing images of samples down to a resolution of 3.5nm. It can also provide basic compositional analysis. It had multiple roles within this project including:

Assessing the integrity of capsules after experimental runs.

Identifying phases within capsules, particularly grains of minerals which would be subsequently analysed by Secondary Ion Mass Spectrometry (SIMS). This was done using semi-quantitative EDS analysis.

Recording images to create maps of capsules for navigation during subsequent analysis (SIMS or EPMA).

The SEM is able to create images of samples and measure their composition by recording the interaction products of the collision of an incident electron beam with the sample. Electrons are created above the sample using a thermal emission source (i.e. a filament with a high voltage passed through it) and are focussed onto the sample using a series of electromagnetic lenses (see Figure 20 for a schematic representation of an SEM). Images are created by raster scanning the sample with the electron beam which has a diameter on the order of a few microns. There are two kinds of imagery that can be recorded depending on which interaction products are measured; Backscattered electrons (BSE) or Secondary Electrons (SE).

2.4.1.2 SEM Theory & Imaging Methods

BSE imagery relies on the detection of electrons supplied by the electron beam which have been scattered upon interaction with the sample. These interactions are elastic and owing to the high energy of the incident electrons (10 - 30 keV) are able to escape from relatively deep in the sample within an interaction volume which extends to a depth of approximately 5µm. The number of electrons which are back scattered is strongly dependent on the atomic number of the elements within the sample; thus, the degree of back scattering is dependent on the electronic density of the sample and it is this dependency that allows image contrast to be determined by compositional variations in BSE imaging. As such, BSE imaging allows compositional variations to be seen and can be very useful for differentiating between elements/minerals/compounds within a sample.

An alternative imaging method is based on secondary electron (SE) emission from the sample. In this scenario, the primary electrons in the beam interact inelastically with the outer electrons of the sample causing scattering of low energy electrons which are subsequently detected by the SE detector. The much lower energy of secondary electrons (<50eV) as compared to backscattered electrons provides a method for differentiating between the two sources of electrons. The topography of the sample greatly affects the number of secondary electrons which are able to arrive at the detectors and so this method is particularly well suited to looking at the surface morphology of samples.

Identification and quantitative measurement of the composition of phases can be performed with the SEM using the attached energy dispersive X-ray spectrometer (EDS). The EDS system available on an SEM is similar to that used in an electron microprobe with a few significant differences. Due to these similarities, the main underlying theory will be dealt with in the subsequent electron microprobe section. The main difference between the two pieces of apparatus is that an SEM utilises a solid state detector which differentiates X-rays by their energies as opposed to the diffracting, tuneable crystals used in an electron probe which differentiate X-rays by their wavelengths and as a result is more precise and accurate. Thus, an SEM EDS system (and specifically the one used in this study) is not capable of achieving the detection limits that an electron probe is capable of. However, it is possible to calibrate the system for given beam conditions and working distances. Once this is done, rapid analysis is possible with a precision of 0.1wt%. The system was utilised within the project, primarily un-calibrated – its use will be discussed subsequently.

2.4.1.3 Conductive Coatings for SEM Analysis

Samples being studied in the SEM are normally given a coating to give them a surface conductive film. This allows electrons from the beam to be conducted away instead of

gathering on the sample which would result in localised surface charging and reduction in image quality. The material chosen to coat a sample will vary depending on the aims of the SEM analysis. If high quality images of surface morphology are required and compositional information is not, a gold coat will be used. If, on the other hand, the primary aim is compositional analysis (be that via BSE imaging or EDS) then a carbon coat will be used. In some cases (including at certain stages of this investigation) it is desirable not to coat the sample (see individual sections on specific SEM use in each section of the investigation) and as such it is possible to operate the SEM with uncoated samples. If no changes were made to the setup of the SEM, image quality would be poor with an uncoated sample as without the surface conductive film being present a build-up of surface electrons is a distinct possibility which can cause smears and distortions as an image is recorded. To overcome this, the SEM may be operated in a controlled pressure mode which allows a small amount of air into the chamber. The electron beam interacts with this small amount of air thereby causing ionisation. The positively charged ions are able to neutralise the electrons building up on the sample surface thereby preventing surface charging and so image degradation. BSE image quality is not substantially affected when using the SEM in controlled pressure mode, but it is not possible to obtain SE images. This is due to the fact that the very low energy electrons utilised in recording SE images by this method are not able to be detected as the higher air pressure and additional positive ions present when operating in controlled pressure mode are sufficient to prevent them reaching the SE detector.

2.4.1.4 SEM Use in this Investigation

The SEM has been an essential tool throughout all aspects of this project. Following experimental runs and preparation it was used to check capsule integrity and to ensure that capsules had not ruptured - interaction of the contents of a capsule with the environment outside could cause significant contamination and thus render an experiment useless for further analysis. The SEM was also used to produce maps of each capsule prior to analysis by SIMS. A series of images were recorded in BSE mode at a constant magnification and were later stitched together with photo editing software to create large (A3) maps of each capsule for use in navigation when using SIMS. By employing the EDS system it was possible to identify mineral grains within the capsule.

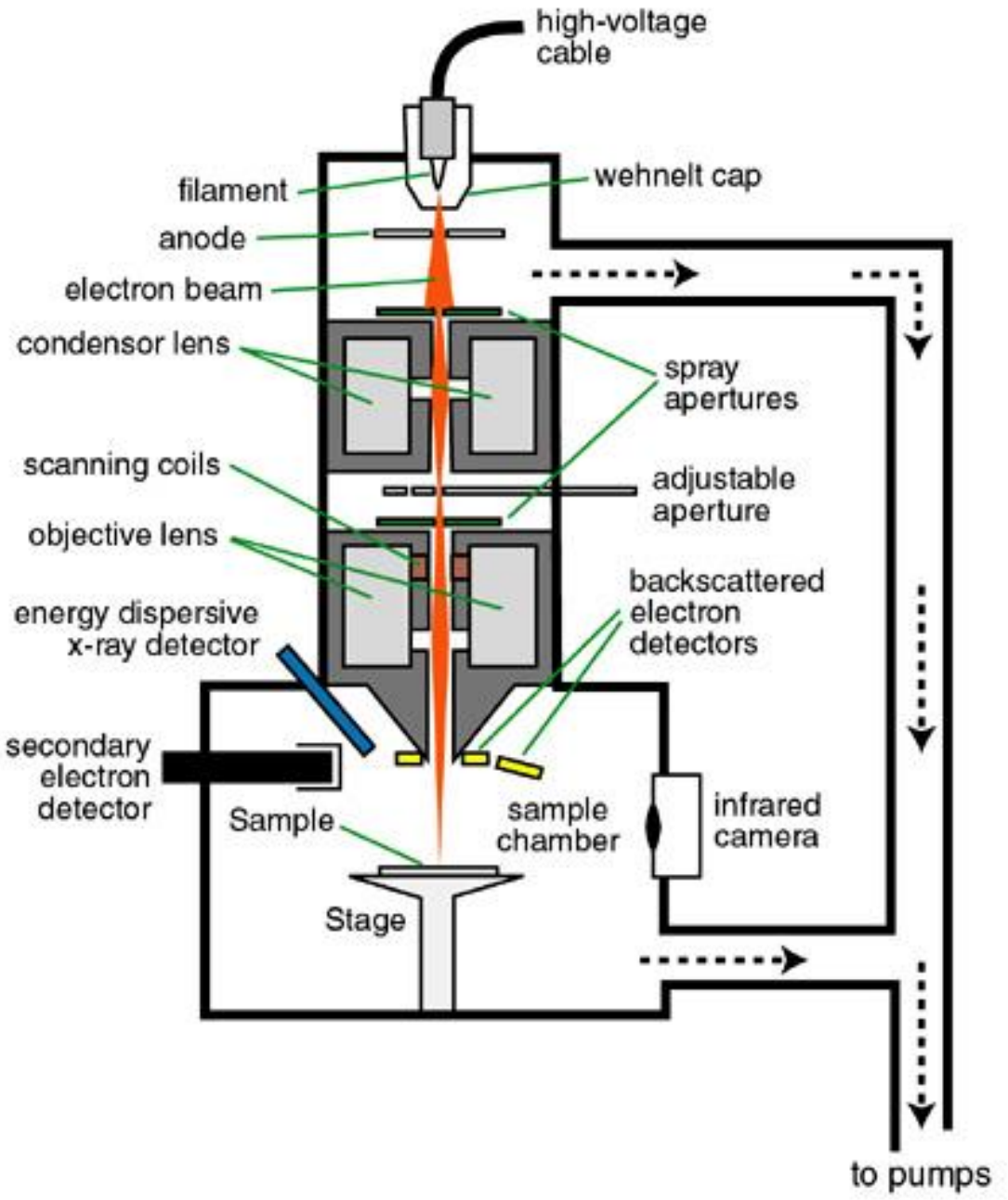

Figure 20: Schematic Representation of an SEM

An electron beam is created at the top of the column and is focussed onto a sample using a series of lenses and apertures. The electron beam interacts with the sample causing both backscattered and secondary electrons (as well as a series of other signals) to be emitted. These electrons are detected and a signal is sent to computer software to allow an image to be formed.

From http://www4.nau.edu/microanalysis/Microprobe-SEM/Instrumentation.html

2.4.2 Electron Probe Microanalysis (EPMA)

2.4.2.1 Introduction

The role of the EPMA within this project was to provide quantitative analysis of samples in situations where it was not necessary to incur the expense of SIMS analysis. The technique is easy to use and enables the measurement of concentrations of diffusants down to the ppm level depending on the particular species being analysed. It is also significantly quicker at obtaining data and has better spatial resolution than SIMS The EPMA used in this investigation enabled analysis of elements between boron (Z=5) and Uranium (Z=92). A schematic image of an electron probe is shown in Figure 21.

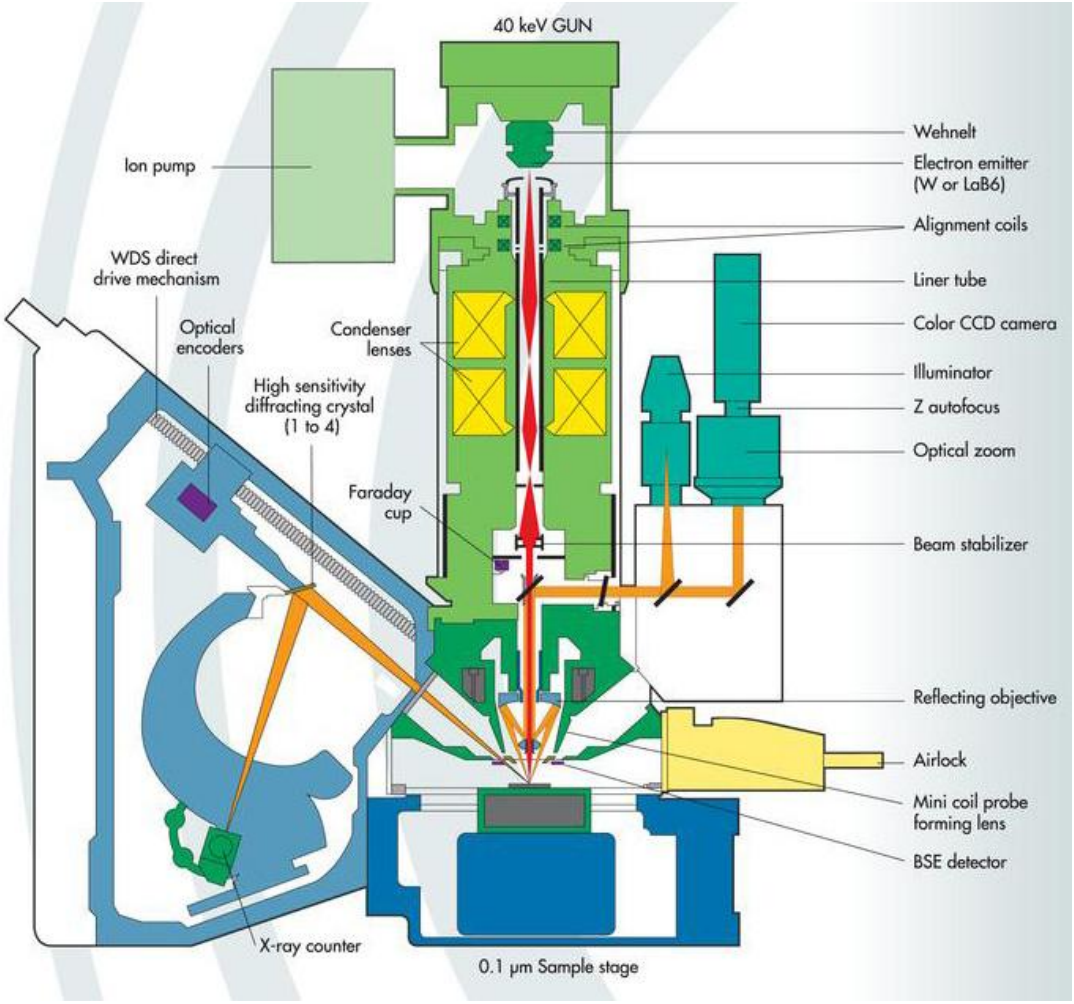

Figure 21: Schematic Diagram of a Cameca SX100 Electron Probe Micro-Analyser

As in the SEM an electron beam is generated at the top of the column and is focussed onto the sample. Unlike the SEM, high-sensitivity tuneable diffracting crystals are used in the detection system which only diffracts X-rays from the element of interest at the particular time to the detector.

Image courtesy of Cameca

2.4.2.2 EPMA Theory and Operation

The technique is based on a similar principle to the EDS system of an SEM but instead uses a system called Wavelength Dispersive Spectroscopy (WDS). (Where an SEM is designed and set up for imaging, an EPMA is set up for quantitative analysis by this method.) The fundamental concept relies on the fact that each element's atomic structure is unique and that electrons can only possess certain quantities of energy. Prior to any interactions, electrons exist in their lowest possible energy levels, sitting at discrete, quantised energy levels known as electron shells. The number of electrons that can sit within each shell is limited and increases as one travels further from the atomic nucleus. In an EPMA (or indeed, in an SEM), the primary electron beam may excite an inner shell electron causing it to be ejected from its present shell into another one at a higher energy (or altogether from the atom). This leaves an electron 'hole' in the lower energy shell. In order to fill this hole, an electron from a higher energy shell may move into the now partially vacant lower energy shell. In doing this it must lose energy in order to possess the correct quanta for the lower energy shell. It does this by emitting radiation which falls within the X-ray part of the electromagnetic spectrum (see Figure 22 for a diagrammatic representation of atomic orbitals and X-ray emission). This X-ray is then detected by one of the spectrometers that form the WDS system. The diffracting crystals which form the WDS system have specific and known lattice spacing and are set up such that they will only reflect X-rays of a certain wavelength onwards to the detector. The EPMA used in this investigation had 5 spectrometers with a choice of diffracting crystals providing flexibility and, with the use of larger diffracting crystals, greater precision. When an X-ray derived from the element of interest is passed from a diffracting crystal to the detector a chain of events is started which results in a count being registered: The incoming X-ray interacts with the atoms of a "counter" gas; when it does so a photoelectron is ejected from the absorbing atom. This photoelectron is then accelerated towards a central wire where ionisation occurs. This ionisation creates an electrical pulse which is proportional in amplitude to the original X-ray and which is then passed on to a counting device. Thus, counts of X-rays of certain energies/wavelengths are recorded allowing the concentration of the element releasing the X-ray to be calculated. As each element has a unique atomic structure, the differences in energies between electron shells are unique and so by measuring both the energy and quantity (number of counts) of emitted X-rays, both the identity and concentration of the elemental constituents of the sample can be determined.

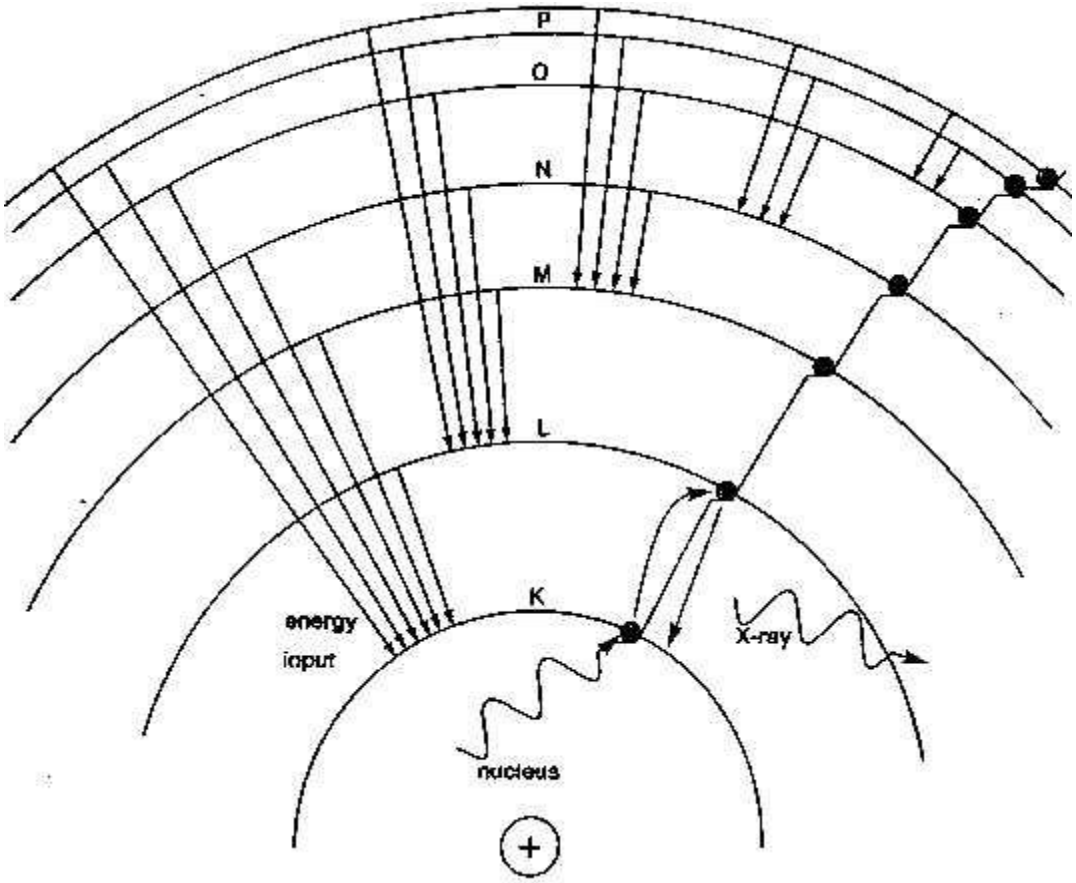

Figure 22: Atomic X-ray Emission

Representation of the mechanism of X-ray emission. As an electron moves between the discrete L and K energy shells it emits an X-ray of energy equivalent to the energy gap between the two shells.

A very small diameter electron beam may be used for analysis by EPMA enabling a very high spatial resolution. A beam size of <1µm is achievable leading to an excitation volume (the volume of sample excited by the electron beam and so which is represented within the particular analysis point) of several cubic micrometres. This resolution is particularly useful in diffusion studies as it allows for measurements to be taken very close to capsule walls so that very steep diffusion profiles at interfaces can be measured.

The EPMA is ideal for collecting large amounts of data in a relatively limited amount of time. Analyses at designated points and along lines can be programmed into the software for collection at a later stage e.g. overnight, so that data acquisition can continue when the user is not present.

2.4.2.3 EPMA Sample Requirements

Sample requirements for the EPMA are very similar to those for the BSE and EDS systems of the SEM. As such, samples must be mounted in a vacuum compatible medium (typically epoxy resin) and then polished to a fine finish with 0.25µm abrasive. Samples are then carbon coated to provide a conductive surface to conduct away the charge from the incident electron beam. In order to ensure a good contact a small strip of silver DAG may also be painted on to the surface of the polished sample block to link the very edge of the sample with the carbon coating.

2.4.3 Secondary Ion Mass Spectrometry (SIMS)

2.4.3.1 Introduction to SIMS

The Secondary Ion Mass Spectrometer (SIMS) is an instrument designed to perform quantitative analyses of samples and is capable of working to a very high resolution. SIMS is capable of measuring concentrations of naturally occurring elements from H to U with detection limits in the ppm to ppb range depending on the element in question. Relatively small spot sizes of 1 - 25µm are also possible.

2.4.3.2 SIMS Theory and Operation

The technique works by firing a finely focussed beam of charged ions (either from a duoplasmatron source where either positive or negative O or Ar ions can be produced or from a Cs^+ source) at the sample under very high vacuum conditions. As such, it is essential that samples and the medium in which they are mounted are compatible with a high vacuum. The high vacuum is essential to reduce the level of the background noise signal, particularly when highly abundant, volatile elements, such as H are being analysed. The collision of the incident ions results in the ionisation and ejection of atoms and molecules from the surface of the sample (see Figure 23) which are then known as secondary ions.

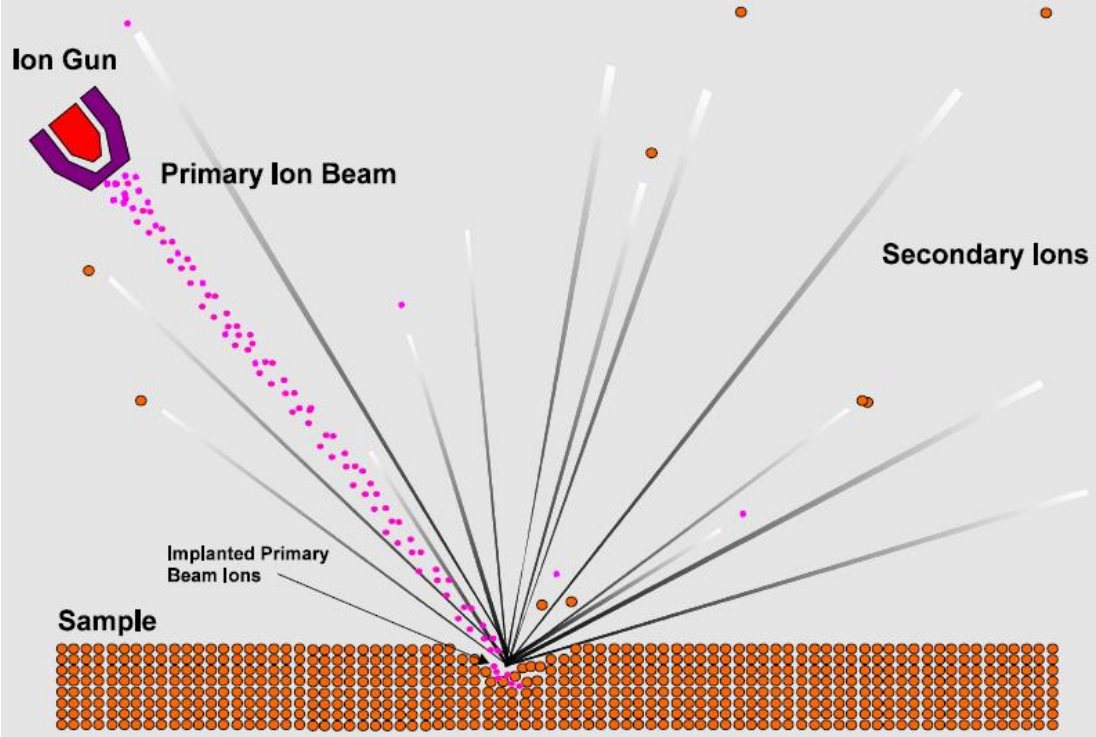

Figure 23: Ion Sputtering in the Ion Microprobe

The incident, primary ion beam interacts with the sample causing the ionisation and ejection of atoms and molecules from the sample. These are then passed on to the detection system.

Image courtesy of NERC Ion Microprobe Facility, Edinburgh

The secondary ions/molecules are ejected by the sample and focussed into a mass spectrometer by the dynamic transfer plates and transfer lenses (see Figure 24). Once in the mass spectrometer part of the apparatus the ions and charged molecules are deflected and separated by an electrostatic and a magnetic prism based on their energy and charge/mass ratio. The prisms sequentially analyse for the ions of interest by being sequentially set up for the specific masses and charges of those species. Once selected, the ions are passed onto one of the detection systems. In the case of the Cameca 4f the counts are detected by either a fluorescent screen (typically used when focussing the ion beam), an electron multiplier (which enables quantitative analysis) or a faraday cup (for use in occasions when the ion beam is on but measurements are not being made and focussing is not on-going).

The instrument is kept at an Ultra High Vacuum (UHV) of $5x10^{-10}$ Torr. This is required to minimise the chance of a secondary ion hitting a gas molecule within the instrument to an effective value of 0. An array of pressure gauges monitor the vacuum within the instrument and a further array of pumps constantly operate to maintain the vacuum.

Prior to analysis samples are loaded into an air lock chamber separate from the analysis chamber. Up to 8 mounted blocks can be accommodated within the air lock and they can be moved in and out of the analysis chamber using a remote loading mechanism so that the vacuum is maintained. It is possible to heat the air lock to encourage de-volatilisation of the samples so that degassing during analysis (for example of atmospheric volatiles which could have settled on a sample or volatiles derived from the mounting medium) does not cause excessively high background noise levels. When volatiles are the species being analysed for (as is the case in this investigation) care must be taken not to expose the samples to temperatures which could cause those volatiles to become mobile within the sample. If this were to happen, values measured at a given point within the sample might be different to those actually achieved by the geological process being investigated.

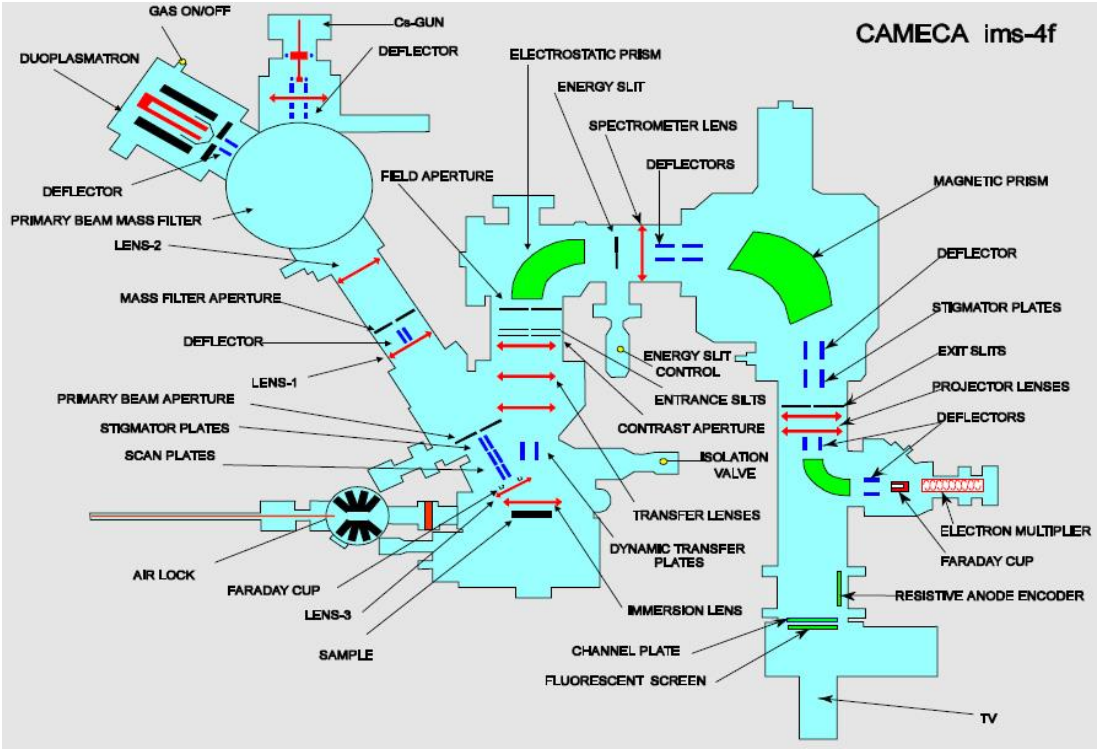

Figure 24: Schematic of Cameca 4F Ion Microprobe

The fundamentals of the ion microprobe are relatively simple in that an ion beam is generated and fired into a sample under high vacuum conditions. The collision of the beam with the sample causes the particles making up the sample to be sputtered. These particles are collected and passed into a mass spectrometer where they are sorted by electrostatic and magnetic prisms so that only particles of a given mass are detected. Each detection event is counted allowing the determination of concentrations of given elemental species within the sample.

2.4.3.3 Sample Requirements for SIMS Analysis

For SIMS analysis, samples must be mounted in a medium which is compatible with an Ultra High Vacuum (UHV) and must be polished to a flat (1µm) finish. In the case of experimental capsules (used in high pressure research), capsules must first be cut to expose the surface of interest. This surface must then be mounted face upwards in the mounting medium to allow polishing to the required degree. Once prepared samples must then be coated in a 10 – 30nm thick layer of gold. See specific sample preparation sections within each of the data chapters for details of procedures specific to each part of the investigation.

2.4.3.4 Depth Profiling Using SIMS

Typically, analyses are performed by focussing the ion beam on a single point for a designated amount of time and recording the secondary ions that are released. This was the method utilised in this investigation. As the ion beam causes the sputtering of secondary ions from the sample, the sample itself is broken down at the point where the beam hits it. As such, secondary ion release occurs at progressively deeper points within the sample. The longer that a single point is exposed to the ion beam, the deeper the secondary ions will come from. This process can be utilised to obtain information on the concentration of the species of interest with depth in the sample and is known as depth profiling.

2.5 Non-Linear Regression Analysis

Diffusion coefficients were calculated using the Datafit curve fitting software by Oakdale Engineering. The program allowed the specification of a law to which data was to be fitted and then applied a non-linear regression curve fitting technique in order to calculate values for the unknown variables. The regression method worked by iteratively improving the quality of fit of the diffusion laws to experimental data by changing the values of the two dependent variables D (the diffusion coefficient) and D_0 (the concentration of diffusant at the interface between the source and host phases)[B]. The true (mathematical) position of the interface may well change as the experiment progresses and diffusant is released from the source. As the source is slowly depleted of diffusant the interface will effectively move into the source.

Solutions to Fick's Second Law were entered into the non-linear regression software in two forms, as shown below (see section 1.3.2.1.4 The Mathematical Description of Diffusion for a discussion of the boundary conditions behind each solution). Here, Y is concentration and X is distance from the source/host interface. The unknown variables are designated as *a* and *b* where *a* is the diffusion coefficient and *b* was the pre-exponential factor – essentially a measure of the effective concentration of the diffusant at the pyrophyllite/spinel interface. This value was different for each run conducted, as it is essentially a measure of the average flux of the diffusant through the interface during the run. As such it was affected by the conditions of the run, particularly temperature. Initial values for these parameters of (in most cases) $a = 1x10^{-10}$ m^2s^{-1} and $b = 1$ were used. In a few cases solutions were not found with these initial estimates. When this occurred the estimate was changed to a value close to the value obtained for the parameter in a previous calculation. In the equations shown, the value of t is the time the run spent at the desired temperature and pressure expressed in seconds; when these equations were used in the fitting procedure, the time value was inserted here. The equations used for the fitting are shown below in both their original and re-stated forms (Equation 15).

[B] Referred to as the effective concentration – this is a mathematical requirement of the diffusion law and essentially is a measure of the flux of diffusant through the interface; as such it is not a measurement of the concentration of diffusant in the source phase. It will also vary between runs as it will be affected by the run conditions, particularly temperature.

Equation 15: Restatement of Solutions to Fick's Laws for use in Non-Linear Regression Fitting

$$C(x,t) = \frac{C_2}{2} - \frac{C_2}{2} erf \frac{(x - x_0)}{2\sqrt{Dt}}$$

Becomes:

*Y = (b)+((-b)*erf(X/(2*sqr(a*t))))*

And,

$$C(x,t) = (1 - erf \frac{(x - x_0)}{2\sqrt{Dt}}) * C_S$$

Becomes:

*Y = (1-erf(X/(2*sqr(a*t))))*b*

NB The above equations are in the exact form as entered into the datafit software. Whist the standard shorthand for a square root is *sqrt*, here *sqr* is quoted as this is what was specified.

Diffusion parameters were calculated multiple times for any given run, firstly for the raw data, again when rejected points had been removed and again when multiple analyses within a single grain had been combined. Furthermore, diffusion parameters were also calculated for each dataset (i.e. all points measured within a given capsule) with the maximum errors both added and subtracted to them. These values form the error bars in Arrhenius plots.

It was found in the vast majority of cases that both expressions of the diffusion law provided results which were indistinguishable from each other on the scale on which they were applied.

2.6 Treatment and Calculation of Errors

Errors sources were identified and quantified for each set of experiments. Details of the specific errors for each setting are detailed here with any differences for the individual experimental methods described in the respective data chapters. The full records of each experiment conducted are included within this report for review in section 10 Appendices.

2.6.1 Calculation of Errors

Absolute error values were estimated for each measured parameter. The estimations which were made and the logic by which these estimations were arrived at is detailed below. These individual sources of error were combined as detailed in section 2.6.2 Combination of Errors.

2.6.1.1 Distance Errors

The distance of an analysis point from the interface of interest (i.e. the interface between the source and host phases) was based upon accurate visual identification of the interface using an SEM (a measurement tool which formed part of the SEM software was used to determine the distance between analysis points and the visually identified interface). This identification was, in each case performed at various different magnifications to ensure that key features (discussed subsequently) were found to enable a positive identification. During capsule construction, interfaces were nominally a flat contact; however, deformation of the capsule both during preparation (prior to the experimental run – e.g. twisting of capsules/intrusion of welded portions of capsules into the main body of capsules as they were flattened in a pin press, twisting caused by the clamps used when welding) and during the run itself meant that inevitably the interfaces had a significant topography. Specific textural features within individual runs were, in certain cases advantageous in identifying interfaces. Examples of this are the presence of Ti in pyrophyllite layers and strong textures being present after a source had been depleted. Bearing in mind the inherent uncertainties in locating the interface and, in cases where the interface had a strong topography the difficulty in identifying which point on the interface was closest to the SIMS measurement point, a maximum error of +/- 20µm has been used for the measured distances.

2.6.1.2 Duration Errors

Errors in the duration of the experiment were determined by considering the method in which the experimental runs were conducted and potential sources of error. During heating, the parameters of the apparatus (percentage of total possible power output being used, current, voltage and potential difference measured by the thermocouple) were recorded along with the time (and so the time since the initiation of heating). As such, the point at which a run reached the desired temperature was known to a precision of less than 30 seconds. The quenching of a run was a significantly quicker process than heating with it taking no longer than 20 seconds for the temperature to drop from that sustained during the run to room temperature. Thus, a total of 50 seconds of potential error were possible in the timing of runs. Further allowance was made for any diffusion which would have occurred during the ramp up to temperature by allowing an additional minute of error. Diffusion below temperatures of approximately 600°C would have occurred so slowly (relative to the amount of timing taken to heat the experiment to its run temperature) as to be insignificant and so

the time taken for the heating of runs from room temperature to approx. 600°C can essentially be disregarded. The rate of heating from 600°C upwards was similar in all runs at a rate of approximately 150°C per minute.

It is of course worth noting that with greater and greater run durations the proportion of time represented by the heating period diminishes and as such errors in its longevity become less and less significant. Whilst this leads to the idea of considering errors in the duration of a run at a given temperature from a perspective of proportions, it is entirely possible to ascribe an absolute value to the error which can then be easily factored into calculations of worst case scenario diffusion parameters. This is what has been done.

In considering all potential sources of error in the measurement of the duration of experimental runs, an error representing a worst case scenario of 2 minutes has been determined.

2.6.1.3 Concentration Errors

The determination of errors in the measurement of concentration values was different for each of the aspects of the investigation, as such they are detailed in the relevant section discussing errors in each of the data chapters.

2.6.1.4 Temperature Errors

An estimation of the error associated with the measurement of temperature during an experimental run is a non-trivial task. A measure of temperature was recorded from the Pt/13%Rh vs. Pt thermocouple which was a part of the piston cylinder apparatus set up. A value in mV was recorded from this thermocouple and this could then be converted into a temperature using a series of conversion tables. The temperature recorded was the temperature at the point where the two wires which made up the thermocouple met, nominally at the end of the thermocouple ceramic although potentially higher if the ceramic broke during the experimental run thereby allowing the wires to touch at a higher point. If this were to occur, the mV value would drop quickly as the temperature being measured would now be further away from the centre of the furnace in the experimental assemblage and so would be cooler. If the thermocouple was not correctly seated within the experimental assemblage (i.e. did not reach the alumina disc which was placed above the sample capsule) then, similarly, the temperature recorded would be lower than that which the capsule was experiencing. When runs were being prepared great care was taken to ensure that the thermocouple within its ceramic tubing could smoothly pass through each of the top plate and base plug and the cylinder of alumina to sit against the alumina disc. It was also installed with great care to minimise the chance of it breaking. During heating and the initial few hours of the run the thermocouple and furnace would go through a period of

"settling" where fluctuating temperatures were recorded (typically ±15°C). This was interpreted as slight changes to the resistance (and so temperature output) of the furnace in response to pressure changes as it deformed slightly in response to the load which had been applied to it. In some cases a rapid decrease in temperature was recorded even though there was no change in the other parameters pertaining to the behaviour of the run (voltage, current, pressure). This was, in most cases a thermocouple failure and the run was terminated as there was no way of determining or controlling the temperature.

Readings of the potential difference across the thermocouple were recorded every time the experiment was checked and these values act as a temperature record for the run. Errors for the temperature parameter in the diffusion laws were estimated by taking the largest deviation in both the positive and negative directions from the nominal temperature of the run. This largest deviation was then treated as the error for the entirety of the run even though in actuality it probably only occurred for a relatively small proportion of the run duration. As such it represented a true worst case scenario.

2.6.1.5 Goodness of Fit

A measurable error was associated with the goodness of the fit calculated by the non-linear regression software. The value of this error is determined by the software and is based upon the statistical determination of solutions. This error is shown in each figure where non-linear regression has been performed. In all cases the central red line is the best fit solution to the data as determined by the regression calculation and the outer two, differently coloured lines represent the bounds of a 2-sigma deviation from the model. I.e. 95% of data with a similar deviation from the data as that used in the fitting process will fit within the bounds of these lines. In certain cases this deviation would have corresponded to a negative diffusion coefficient. Given that this scenario cannot be representative of the conditions of the experiment, a straight line, zero concentration throughout the capsule is shown in these cases. It should be noted that whilst, in many cases the bounds are fairly wide, suggesting low confidence in the calculation, this is, in most part, a consequence of the low number of measurements recorded. This, in itself is a consequence of the number of olivine grains exposed by the random section taken through the capsule when it was prepared. This is proved by the comparatively much lower deviations seen in other experiments where a far greater number of measurements were obtained. It is fully expected that if it were possible to perform a significant number of repeat experiments to obtain more data, these bounds would narrow considerably.

2.6.2 Combination of Errors

It was necessary to determine the way in which errors should be combined in order to give an estimate of the maximum possible error given the individual sources. The method by which this was determined is discussed here:

Given the errors in each of the measured parameters (as detailed in the respective data chapters), an error propagation analysis was undertaken in order to determine which combination of the potential errors gave the greatest overall error and so the maximum uncertainty in the measurements obtained. This was done by either adding or subtracting the maximum possible error in each parameter from a dataset which had previously had a diffusion law fitted to it. The calculation of the law was then performed again and the resulting pre-exponential and diffusion coefficient values were compared to the previously calculated value. The following combinations of error were tested:

+ve concentration, +ve distance, +ve time
+ve concentration, +ve distance, -ve time
+ve concentration, -ve distance, +ve time
+ve concentration, -ve distance, -ve time
-ve concentration, +ve distance, +ve time
-ve concentration, +ve distance, -ve time
-ve concentration, -ve distance, +ve time
-ve concentration, -ve distance, -ve time

It was found that the following two combinations gave the greatest positive and greatest negative deviation from the original curve fitting of the diffusion law:

Maximum positive deviation:
+ve concentration, +ve distance, -ve time

Maximum negative deviation:
-ve concentration, -ve distance, +ve time

In order to calculate the absolute error for each analysis point, new points representing the worst case scenario for both positive and negative deviations were created. The new points were calculated by taking the original values and adding or subtracting the maximum errors for each of the parameters as per the definitions above. This was done for each analysis point for a given run thereby creating a new dataset which was then processed with the curve fitting software using the same method as was used with the original data. By this process a new diffusion coefficient and pre-exponential factor were calculated representing

the maximum positive and negative errors for each analysis point. These values were then plotted alongside the original data to form the error bars on Arrhenius plots showing the temperature dependence of diffusion.

2.7 The Experimental Approach to Research

When conducting an experimental program in any discipline, one must be aware of and appreciate the limitations of information gained from experimental studies. Experiments, by their very nature, seek to replicate an isolated part of nature. It is impossible to represent all of the complex interactions and parameters that affect a natural system in an experiment and thus, experimental studies must be in some way imprecise in their representation of the natural world. Therefore, the results obtained will be in some way imprecise too. It is possible to scale up from the experimental level to the real world but as one does so one has to take into account parameters which may be insignificant on the very small scale of experiments but which may be dominant on real world scales – which may go up to the size of the solar system. Examples of this within the study of geological processes would include chemical heterogeneity (i.e. trace elements, chemically "dirty" systems) and large scale physical phenomena (e.g. rheology – convection in planetary interiors, deformation mechanisms, gravitational effects – particularly applicable on the largest scales; for instance in planetary formation). In making calculations of this nature, one must always be aware of the uncertainty which is introduced at each stage of scaling up.

It is important that one must also put aside any pre-conceptions regarding the outcomes of experimental studies before commencing them. Not doing so can lead to anomalous data being disregarded when in fact it could illuminate important processes. In certain cases it is necessary to employ techniques to overcome this innate prejudice towards unexpected data which is derived from the desire to obtain high quality results. Techniques such as blinding oneself to whether or not a data point has recorded an anomalous value when checking if there are any reasons that it should be rejected are valuable and have been utilised here to ensure that bias does not affect results.

Thus, while the experimental approach is in many ways limited and must be used with great caution, it is also invaluable and forms a large basis for many areas of science, particularly geology. Without experiments it would not be possible to confirm predictions (or aspects thereof) and test hypotheses regarding the inaccessible deep Earth. As such, it is hoped that this study will form a valuable addition to the compendium of experimental data on deep Earth diffusion studies and forms the basis for greater understanding and future works.

3 Grain Boundary Diffusion of Volatiles Experimental Program

3.1 Introduction

The perceived importance of grain boundaries is increasing as studies show that they are effective transport routes and storage sites[1,6,22,23]. They may well form fast pathways for diffusion, thereby affecting: 1) The delivery of reactants to reaction sites 2) The influence that various species have on mantle properties and processes, and 3) The degree of interconnectivity between various mantle reservoirs. Furthermore, movement of charged species such as H^+ along grain boundaries may be responsible for a significant proportion of mantle electrical conductivity. Here we seek to determine the significance of GBD as compared to lattice diffusion and understand the effects it may have on other mantle processes/properties. This research has been conducted by carrying out a series of experiments using the equipment and techniques detailed in the previous chapters.

3.1.1 Background to Volatiles

Before considering the methods used and results obtained in this aspect of the investigation, we shall first consider the roles of volatiles in the Earth. Within this review a number of aspects of volatiles are considered, including their importance to the whole Earth system, their planetary abundance and particularly their effect on bulk mantle rheological properties and on the mantle's electrical properties - information on the dynamics of volatile (particularly H) diffusion (grain boundary or otherwise) will have implications for bulk mantle conductivity, potentially allowing the use of conductivity data as a proxy for water distribution.

3.1.1.1 The Importance of Volatiles

Volatile elements and compounds – those existing in the liquid or gaseous state under ambient temperatures on the surface of the Earth – e.g. O_2, CO_2, H_2O, SO_2 etc., form many of the essential pre-requisites for life and make the Earth the habitable planet that it is. Other planets within our solar system are less suited towards hosting life primarily due to the abundances (or lack thereof) of certain volatiles both within the planets and in their atmospheres [63]. The presence (or lack) of volatiles within a planetary body has a major effect on heat dissipation within and from that body and, by consequence, the style of tectonism observed [64,65]. This in turn affects the ability of the planetary interior to degas and, therefore, the availability of volatiles at the planet's surface. As such, knowledge of the nature, abundances and methods of transport of volatiles is fundamental to the understanding of a planet as a whole, with obvious implications for phenomena observed at the surface.

The exact origin of the water in Earth's hydrosphere (atmosphere, oceans, surface water, groundwater, glaciers etc.) is not fully known. It may be present due to gradual degassing of Earth's mantle by volcanic activity or by the delivery of water to the planet by icy bodies from space when these were far more common (e.g. after the moon forming impact which could well have blown off any atmosphere present at the time). The volcanic degassing hypothesis suggests that degassing likely occurred through an initial intense phase during the first 0.5Ga of Earth history as the planet cooled followed by a slower phase that continues today [66] (permitted by the mid ocean ridge/subduction style of tectonism). It is likely that a combination of these factors lead to the abundance of water which we now see on the surface of Earth. Given that degassing continues and that water must be returned to the Earth's interior by subduction, it must be likely that there is a (or there are multiple) reservoir(s) of water within the Earth but the exact size, location, behaviour and degree of isolation of these is yet to be determined.

Work conducted over many years has confirmed the importance of the presence of volatiles to the chemistry and physical properties of the mantle [9]: The presence of water is known to have significant effects on rheology due to its interactions with the atomic structure of mineral grains, allowing and/or enhancing deformation to occur by sheer and creep mechanisms [9,67]. The viscosity of the mantle is an exceptionally important parameter as it defines the extent to which it is able to deform and flow. The ability of the mantle to flow is of great planetary importance as this parameter controls the strength and nature of convection. Convection is the primary driver of heat transport in the mantle and heat dissipation in the Earth as a whole. Thus, it exerts a controlling influence over the manifestations of heat loss at the surface: volcanism and plate tectonics. Fundamentally, the viscosity of the mantle enables the surface of the planet to be the habitable place that it is. Furthermore, the presence of water in the mantle has a strong influence on chemical as well as rheological processes, often allowing them to occur under less extreme conditions than would otherwise be required. This is particularly seen in the effect that water has on depressing the solidi of many mantle phases [68] - see Figure 25 which shows mantle solidi at a range of water contents.

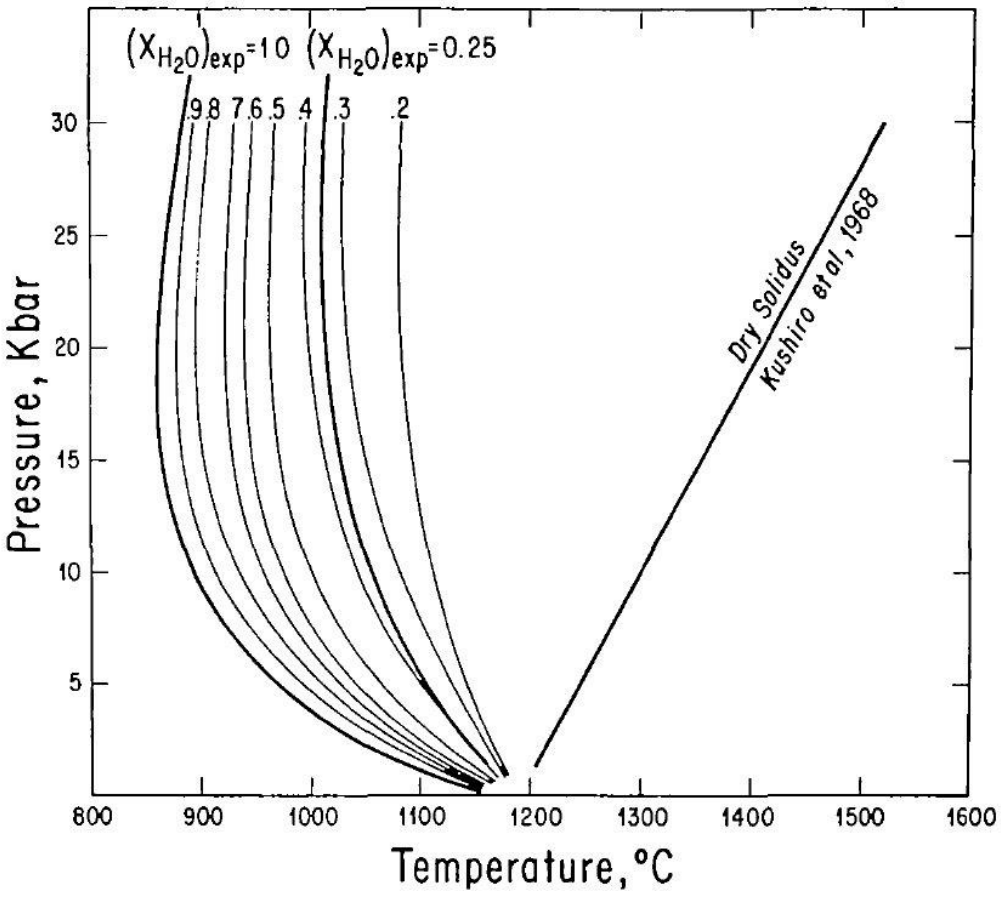

Figure 25: Melting curves for peridotite under mantle conditions

As water content is increased, the temperature of melting is depressed by greater degrees. Curves represent the mole fraction of water in the vapour with CO_2 making up the other proportion.

From Mysen & Boettcher, 1974 [68]

Whilst water is the most abundant mantle volatile, CO_2 has the second highest abundance [69]. The mantle may be the largest reservoir of C on the planet, with the possible exception of the core which may contain up to 5wt% of the element [1]. CO_2 can have a similar effect on mantle properties to water, especially in terms of melting behaviour, and owing to its abundance, is of great importance. Whilst this project does not specifically study GBD of CO_2 or C, such an investigation would be a useful follow up to this work.

3.1.1.2 Volatiles in the Mantle – Abundances & Concentration Variations

The Earth's mantle makes up 82% of its volume and constitutes 65% of its mass [70] – some 3.88×10^{24}kg. Given this vast figure, even very low absolute concentrations of volatiles in the mantle of perhaps a few hundred ppm by weight equate to huge global abundances. The concentration and distribution of volatiles in the mantle varies with the mineral phases that

host them, and also with variations in the chemistry of those phases as a function of pressure and temperature. Furthermore, at locations in the mantle where the PT conditions permit, low temperature hydrous minerals are able to hold several weight per cent of water even at very high pressure [9]. As such, the variation in abundances of mantle volatiles is dependent on the interplay between mineralogy and mantle physical properties. This balancing of factors is discussed below.

3.1.1.2.1 Water

An estimate of the water content of the Earth can be made by considering the material from which it was originally made and the processes and events that have affected it since. A calculation of this type will be fundamentally crude but can provide a reasonable order of magnitude estimate.

Following the widely held assumption that the Earth was formed from the coalescence of CI and enstatite chondrites [71] one would expect the Earth as a whole to contain approx. 2wt% H_2O [72]. The oceans are the most immediately obvious reservoir of water on the Earth and account for 0.02% of the total mass of the Earth [72]. When the entire hydrosphere is considered, this figure only increases to approx. 0.023wt%. Thus, there is a major shortfall between the amount of water which we observe on the surface of the Earth and the amount that one would expect to find in the Earth as a whole based on the assumption that it (at least originally) contained a total of 2wt% H_2O. It is quite possible that a significant amount of water may have been lost from the Earth during accretion and formation of the planet (particularly during magma ocean formation and crystallisation, the late heavy bombardment and moon-forming events) meaning that the figure of 2wt% should be considered an upper limit. If almost all of the early water in the Earth was lost during formation/bombardment then the water that we see on the surface of the Earth must have largely accreted after the planet had formed and cooled; i.e. it was delivered to the Earth from extra-terrestrial sources, comets or meteorites, and subsequently accreted. The likelihood is that the situation which actually occurred is somewhere between these two extremes; this scenario being that the Earth was initially made up of material containing approx. 2wt% water but that it lost a significant amount of this early water during the process of accretion and planetary formation. Further early water may well have been lost due to massive meteorite impacts, particularly during the late heavy bombardment. Thus, we can consider an upper limit of 2wt% water in the Earth with the implication that the water that we see in the hydrosphere (on the surface of the Earth e.g. oceans, glaciers, as groundwater; and in the atmosphere) may very well be only a small proportion of the total amount contained within the entire Earth system.

Water is stored in geological media in different ways in different parts of the planet. In the crust, water is stored in hydrous minerals and melts but owing to the low volume of the crust, the overall abundance of water in this setting is low. Hydrous minerals and melts may also be present in the mantle. Melts are limited in their extent in the mantle and their longevity may be limited; hydrous minerals may be more common but break down with temperature - they are stable only in the upper mantle and in subduction zones down to a depth where the temperature is high enough to decompose them. As such, remaining ubiquitous storage sites are at grain boundaries or within mineral grains. Virtually all nominally anhydrous minerals (NAMs) have been shown to be able to contain trace quantities of water in the form of hydrogen defects [8]. Experimental studies indicate that the storage capacity for water in the upper mantle is surprisingly high [9]; total capacities are of the order of several weight per cent and therefore, given the abundance of water in the whole Earth, the upper mantle is significantly under saturated. Thus, all water in these regions is likely to be stored within grains as hydrogen defects (interstitial, non-stoichiometric hydrogen, typically charge-balanced by other substitutional defects or vacancies). By contrast, water storage capacity in the lower mantle is low [73,74] – possibly below 100ppm. If water content in the lower mantle is higher than this then hydrogen may be present at grain boundaries and GBD will be an important mechanism for mobility. Even if hydrogen is not stored at grain boundaries, GBD could provide an efficient mechanism for its transportation. In this study we aim to characterise mobility of hydrogen as opposed to calculating how much of it is stored in the mantle (although of course knowledge of GBD of hydrogen would be critical in calculating mantle water content as well as interpreting conductivity measurements of the mantle – this is discussed subsequently).

The terminology used in discussions of water in the mantle is generally quite loose and the term 'water' is taken to include all forms of H – under the assumption that the oxidised, charge balanced form can easily be achieved when OH^- is released from the mineral lattice/storage site (e.g. during upwelling, oxidation and melting of mantle material). Thus, whilst it maybe the OH^- or H species that are measured (for instance by IR spectroscopy) it is H_2O by weight concentrations that are typically reported [75]. This terminology is common across all literature on the subject.

The form in which water is present in the mantle is of great importance. If it resides and moves around in the form of H^+, it will need to be charge balanced by a charge flux in the opposite direction e.g. a cation vacancy or polaron (particularly if moving through a mineral structure). Similarly, if it exists as OH^-, then it will need to be balance by a positive charge. The issue of charge balancing is discussed further in subsequent sections.

3.1.1.2.2 Carbon Dioxide

Carbon solubility in mantle phases is low compared to H and hence much mantle carbon is likely in the form of separate C-rich phases (e.g. carbonates, diamond, Fe-rich phases in the lower mantle). As a result of this low solubility and the presence of C-rich phases, concentrations of C/CO_2 are very low compared to H/H_2O in the mantle - on the order of 12ppm for CO2 in olivine [41] in the upper mantle as compared to several hundred ppm for water [9]. Thus, its total abundance in mantle reservoirs is very small. As it has a significantly larger ionic size than hydrogen (thereby potentially requiring more energy to make diffusive jumps) and a decreased abundance, one would expect lower mobility than H/H_2O. The lower solubility will also mean that there is less diffusant available. In this case the concentration of diffusant at any given point is likely to be so low as to be below or close to the detection limits of available detection methods thereby making analysis very difficult.

3.1.1.3 Sources of Information on Volatiles in the Mantle

Whilst it is currently impossible to directly collect in situ samples of the mantle, it is possible to derive information on the mantle and the volatiles residing within it from a number of sources. Here we consider ways of inferring the volatile content of the mantle based upon indirect samples obtained from it and remote measurement of its properties.

3.1.1.3.1 Indirect/Partially Representative Samples

Samples of the mantle can and do occur at the surface – these can take the form of tectonic fragments, inclusions in volcanic rocks [70] and inclusions within other mantle mineral phases such as diamond [76,77]. Most known mantle xenoliths are peridotites (primarily olivine with orthopyroxene and clinopyroxene along with an aluminous phase – typically garnet or spinel) but these cannot be expected to be representative of mantle composition as a whole and all evidence suggests that they are samples of the top part of the upper mantle only (see footnote for a discussion of mantle homo/heterogeneity[C]). Furthermore, the relevance of

[C] Mantle Homo/heterogeneity

The issue of the homogeneity of the mantle is a significant one with some workers suggesting that the mantle is broadly homogenous [70] (in terms of composition – changes in mineral structure are agreed to be at least in part responsible for the 410km and 660km discontinuities evident from seismic studies). Evidence derived from heat fluxes is in favour of a chemically heterogeneous mantle with the implication that upper mantle peridotites are not representative of the mantle as a whole [70].

data obtained from mantle xenoliths to the problem of diffusion of volatiles such as H and CO_2 is questionable. Volatile species typically have rapid diffusion kinetics and undergo reactions such as oxidation during their ascent. Thus, volatile contents recorded from xenoliths once they have reached the surface are unlikely to be representative of those possessed by the samples when they were at depth.

An alternative source of information on the volatile contents of the mantle can be obtained by studying primary melts, e.g. MORB (Mid Ocean Ridge Basalt) glasses [81]. However, it should be remembered that MORBs are not direct samples of the upper mantle; they are derived from partial melts that have subsequently risen to the site of emplacement before cooling and crystallising. As such, when calculating from measurements derived from this source it is of great importance that one takes into account and back-calculates for any potential changes in the volatile content caused by fractional crystallisation, alteration of the glass on the sea bed or simple volatile loss during eruption or emplacement. Thus, as direct derivatives of the upper mantle, MORB glasses are a useful source of information on this part of the Earth, but care needs to be taken in the use of data obtained from them and a full consideration of the processes involved in their formation and emplacement is required. In many cases, the necessary information on the full history of the glass may be absent meaning that a proper back-calculation cannot be made and, for this purpose, the sample may not be of significant use.

3.1.1.3.2 Rheological Properties

Estimations of the volatile content of the mantle can be made by observing rheological properties which are affected by the presence of volatiles. By considering the effects of volatile content on the properties of the mantle (e.g. seismic wave velocities, depression of phase transitions, rheology) and by combining this information with a knowledge of the spatial variations of these properties, it should be possible, at least in theory, to make at least a first order determination of volatile distributions. It should be noted that the

---

Measurements of the heat flux at the earth's surface give a figure of approx. 44TW, the vast majority of which is attributed to decay of radioactive species (K, U & Th) in the mantle [78]. The upper mantle – where Mid-Ocean Ridge Basalts (MORBs) are formed – is characterised by compositions depleted in these elements and is only responsible for 2-6 TW [70]. Thus, it follows that other (deeper) parts of the mantle must have a different composition with higher concentrations of the radioactive elements to make up the shortfall in heat flux. Furthermore, this deep region, enriched in heat-producing radioactive elements, must only occasionally be involved in the formation of rocks observed at the surface [66,79,80]. As such, evidence from heat fluxes suggests a layered, heterogeneous mantle.

uncertainties in calculations such as these are very large and, therefore, a low level of confidence is attached to them.

A good example of this is the effect of water on viscosity. The presence of water in geological settings has the effect of reducing the viscosity of the medium in which it is dissolved [67]. Water (or a derived species – H^+, OH^- etc.) is able to sit in a host phase (the position that it sits in will be determined by the structure of the phase, the species that the water is present in and the presence of other trace phases along with many other parameters) thereby affecting its surrounding environment. H can sit as a defect in a mineral structure and can be charge balanced by other defects (e.g. lower valence cation substitutions or changes in speciation of other cations such as $Fe^{2+/3+}$, cation vacancies). It is the abundance of these other defects coupled to the presence of H which can have significant effects on the bulk physical properties of the phase. A high abundance of vacancies can promote increased diffusion and in turn enhance creep of that mineral. If the presence of H is coupled to cation vacancies then a high H abundance will mean a high abundance of vacancies and so creep at lower strains [82]. By contrast, the presence of oxygen vacancies may result in the 'pinning' or immobilisation of line or planar defects, thereby inhibiting creep.

On a mantle-wide scale, variations in viscosity are important as viscosity controls whole mantle processes such as convection (and so planetary heat dissipation) and more local scale properties such as seismic wave propagation, the distribution and nature of Earthquakes, the behaviour of melts and isostasy [67] . (See footnote for an example of determining mantle viscosity from glacial isostatic adjustment [D].). The presence of water within mantle minerals affects the internal structure of minerals, lowering the viscosity [94,95]. Whilst the mechanism is far more complex than that observed in melts (where water serves to limit polymerisation thus decreasing viscosity by reducing chain length and so inter-chain forces) it is based on H allowing increased creep via diffusion of vacancies and by charge balancing diffusion of vacancies and other species. Whilst lateral variations in viscosity are (at least partly) related to lateral temperature variations (e.g. moving from the centre of a craton towards a subduction zone – as in the USA) it has been suggested that variations in water content could also be responsible for variations in viscosity [67].

[D] Inferring Mantle Viscosity from Glacial Isostatic Adjustment

The viscosity of the mantle can be inferred by measuring crustal adjustments due to the unloading associated with the retreat of ice sheets in the Late Pleistocene (the glacial isostatic adjustment – GIA) [67]. Parameters measured include changes in the earth's rotation [83,84], polar wander [85–87] and changes in surface elevations [88–93].

3.1.1.3.3 Conductivity

Measurements of the conductivity of the upper mantle give values greater than one would expect based upon a dry composition [96], and it is proposed that the presence of water enhances the conductivity of the mantle. Magnetotelluric measurements (obtained by measuring orthogonal components of the magnetic and electric fields of the Earth, thereby measuring currents in the Earth induced by lightning or solar energy), can ultimately provide a rudimentary 'map' of resistivity in the mantle. As H^+, a proton, is a charge-carrying species, its motion through the mantle can be equated with bulk conductivity (N.B. other charged species are also important in this respect, although because H is so small and mobile it is likely to be able to move faster than other species, and be responsible for a large proportion of observed conductivity). Thus, on a qualitative basis, areas of lower resistivity (higher conductivity) are likely to coincide with areas of higher H content. As an example of this, Figure 26 shows an image of resistivity/conductivity data derived from magnetotelluric (MT) data from the Turkey region. The mantle/lower crust boundary is clearly visible along with variations in conductivity at depth demonstrating upper mantle heterogeneity in conductivity and so potentially in the distribution of chemical species which affect conductivity [97]. If the relationship between conductivity and H content could be defined (GBD could be responsible for a large part of the relationship), then images such as these could be processed to effectively act as maps of water in the mantle.

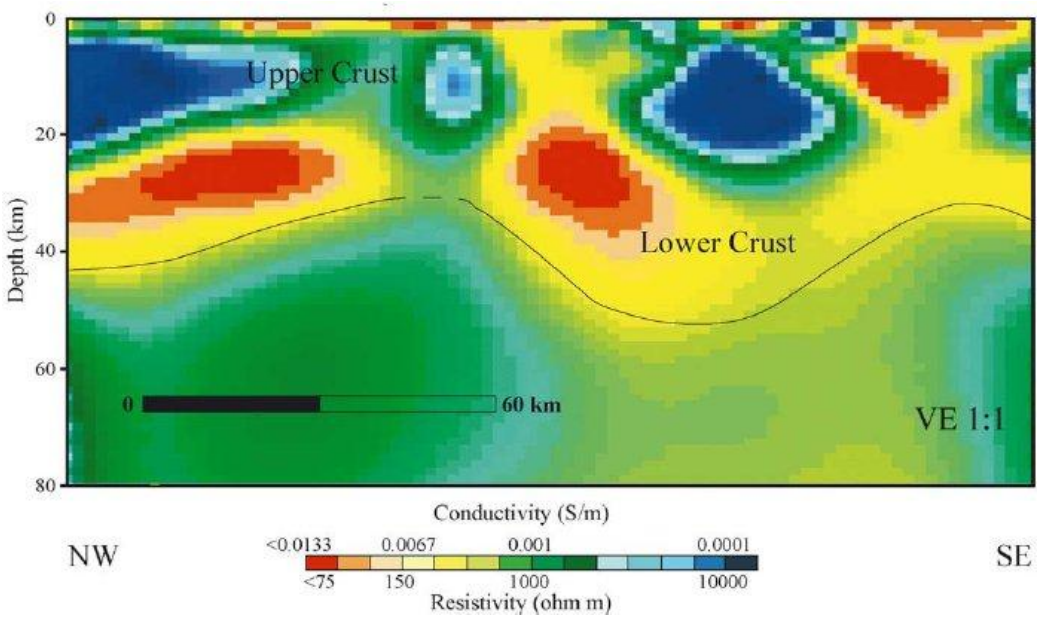

Figure 26: Example of Magnetotelluric Data

Conductivity image of the subsurface (upper and lower crust + upper mantle) derived from magnetotelluric data from south-western Taurides, Turkey. Areas of crust with greatly differing conductivities are clearly evident along with a less contrasting but still significant variability in the upper mantle. The solid black line is the inferred position of the Moho.

From Gürer et al., 2004 [97]

Anisotropy has been observed in the conductivity of the mantle as determined from MT data [98]. Furthermore, the anisotropy observed in conductivity coincides with that seen in seismic velocities. This coincidence of anisotropy in seismic wave velocities and conductivity has been observed in numerous locations around the world suggesting that there is a common link between observations. It is possible that electrical conductivity in the upper mantle may be linked to faster diffusion of H along the [100] axis in oriented crystals of olivine as both H diffusion [99,100] and seismic wave velocities are quicker along this axis [98]. Alternatively, this observed anisotropy could be due to the alignment of melt lenses and high conductivity films along grain boundaries [98]. Regardless of the mechanism governing this coincidence of anisotropy in olivine, the relationship is expected to have a significant effect on bulk mantle conductivity owing to olivine being the most abundant (and interconnected) phase of the upper mantle (to 410km depth) with the proportion of olivine being approximately 60%. Given this huge abundance of olivine, its electrical properties are expected to be largely responsible for the observed conductivity of the bulk upper mantle [101,102]. An important mechanism used by olivine to accommodate strain is dislocation creep; primarily on the [100] plane [70]. Therefore, it would be possible for a preferred crystal orientation fabric to develop potentially over distances of up to hundreds of km [103], and it may be that diffusion along preferential pathways is responsible for bulk mantle conductivity. It should be noted that with depth and water content the dominant slip system in olivine will vary with C-slip (slipping of the crystal structure in the C crystallographic direction) becoming dominant at greater depth [104].

3.1.1.3.4 The Effect of Water on Diffusivity of Other Species

The presence of water in the mantle can enhance the diffusivity of other species thereby aiding mass transport and so homogenisation. For example, interdiffusion of Fe and Mg in olivine is approximately one order of magnitude quicker under hydrous conditions compared to anhydrous conditions [105] and water has been shown to increase the diffusivity of oxygen in numerous common mantle phases [5]. This is due to the mobility of H^+ and its coupling with other defects within the mineral structure. Thus, the bulk diffusion and incorporation of H into mantle minerals is a controlling factor in the diffusivity of other mantle species.

3.1.1.3.5 Other Volatiles

Carbon Dioxide

Despite the low mantle abundance, C could still exert a significant effect on bulk mantle properties, potentially altering redox conditions (by reactions with H and O) [1] and contributing to bulk mantle conductivity [1,106,107].

Carbonates are more stable than hydrous minerals with increasing pressure [108] and therefore one would expect them to be more deeply subducted – thereby increasing the importance of carbon compounds at depth relative to water and its derived species. Furthermore, several recent studies have suggested that CO_2 may play a defining role in mantle melting at Mid Ocean Ridges whereby the combined effect of the presence of H_2O and CO_2 promotes melting far earlier than would otherwise be possible [109,110].

Thus, the roles played by carbon compounds in the mantle are varied with respect to water, occurring under different conditions and so found at varying depths. Owing to the variety of effects caused by CO_2, a study into the grain boundary diffusivity of this volatile would provide data which would be similarly useful as that obtained for water.

3.2 Methods Used & Their Development

Owing to the experimental nature of the work, preliminary results were used to refine methods as problems were encountered and overcome and opportunities for improvement were identified. Thus, at the start of the project, experimental work was carried out as much with the intention of using it to refine methods as it was for obtaining data to test hypotheses. Here we discuss the chronological development of the methods and experimental designs used. The results of some specific experiments (mainly experiments that failed for one reason or another) are discussed with regard to their use in the revision of future methods. In general the experiments which are discussed did not yield data; successful experiments from which useful data was obtained are discussed in detail in section 3.6 Results.

3.2.1 Initial Capsule Design

A number of possible designs were considered prior to settling upon that used for the investigation. Initially MgO was considered as both a source and sink material but this was rejected after initial experiments showed it to not crystallise ideally (see section 3.2.3.2 Sample Materials). This initial design which utilised MgO is shown in
Figure 27 along with the intended logic by which it would operate.

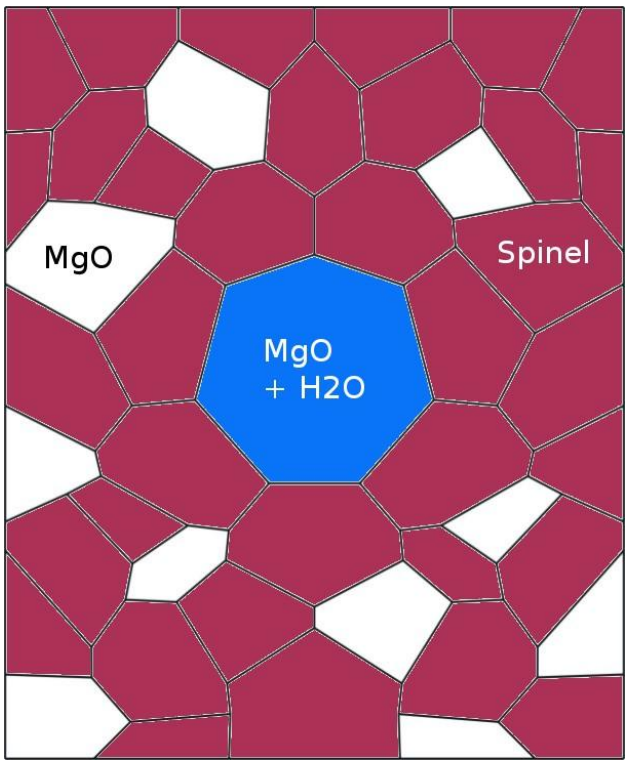

Figure 27: Initial GBD of Volatiles Capsule Design

Hydrated MgO acts as a water source with non-hydrated grains acting as a sink. The hydrated grain was to dehydrate as the experiment progressed, thereby releasing water which would flow along the spinel grain boundaries into the non-hydrated grains. These sink grains could then have their water contents measured and their distances from the central hydrated grain determined to allow calculation of a diffusion coefficient. This design was rejected owing to difficulties in crystallising suitable grains of MgO, in hydrating the central grain and to problems in making up capsules to ensure only GBD was measured (i.e. in ensuring that sink MgO grains did not touch each other which would mean that MgO lattice diffusion was being measured).

3.2.2 Second (Final) Capsule Design

Following the failure in the creation of suitable MgO crystals, a re-design of the experimental method was undertaken with the aim of using an alternative sink material. As detailed in the Materials section, olivine was selected for this purpose. It was also decided that pyrophyllite would be used as the water source phase. In order for this approach to work it was necessary to re-design the arrangement of the contents of the experimental capsule. A schematic diagram of the re-designed capsule is shown in Figure 28. In this design pyrophyllite was placed at the bottom of the capsule followed by a layer of spinel. The purpose of having a spinel only layer was to prevent pyrophyllite and olivine from coming into direct contact with each other which would lead to a very high water content in the olivine grain in question which had migrated into the grain by methods other than grain boundary diffusion. Above this layer was the largest proportion of the capsule which was filled with a mixture of olivine and spinel grains. This capsule design proved to be successful after some minor revisions (see following section) and was used for all volatile diffusion along grain boundaries experiments.

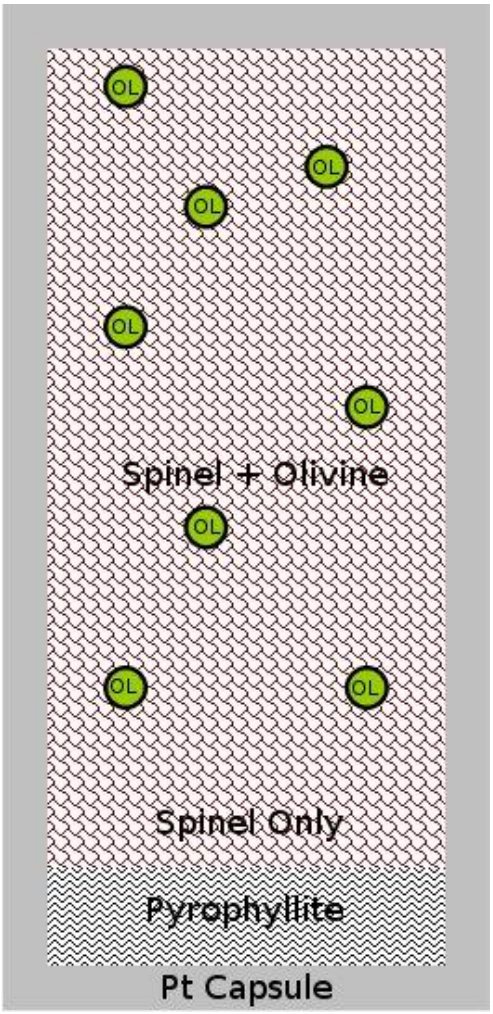

Figure 28: Schematic capsule design for Volatile Diffusion along Grain Boundaries Experiments

See text for description.

Thus, with this design it was planned that an experiment would proceed as follows. Details on each of the materials used in the experiments are discussed in section 3.2.3 Materials. It was planned that when conducting an experimental run the following would happen: As run temperatures were approached, the hydrated phase (pyrophyllite - $Al_2Si_4O_{10}(OH)_2$) would start to release various H-related species (it was possible to check that water was not transported as a fluid phase by examining capsules in the SEM after run completion). Above the pyrophyllite was a layer of stoichiometric Mg-spinel. As the spinel would not accept H into its structure, H would be forced to migrate along grain boundaries. Distributed throughout the capsule, several larger crystals of olivine (see Table 2 in section 3.2.3.2 Sample Materials for composition), would act as sinks, allowing H to enter their crystal structures. By measuring the water contents of the sink grains after the experimental run and by also measuring the distance between them and the source it would be possible to calculate the GBD coefficient of H along grain boundaries under the run conditions.

Determined diffusion coefficients for H could then be compared to lattice diffusion rates for various mantle minerals to assess the importance of GBD in the mantle.

3.2.3 Materials

Careful consideration was given to all the materials to be used in this investigation. It was important to ensure that unwanted reactions between the constituents of the experiments that might affect the diffusive processes being measured did not occur. Thus, potentially reacting minerals could not be placed in close proximity to each other. This consideration also extended to the experimental capsule where, for example, alloying between the capsule and its contents could cause a lowering of the capsule melting temperature and therefore destruction of the experiment (and potentially equipment too). Furthermore, it was necessary that the capsule's contents behaved appropriately (e.g. did not melt) under the experimental conditions to which they would be subjected. Finally, and most importantly, it was necessary that all materials, particularly those forming the experimental samples, had the right properties to enable the study of GBD. Thus, with many requirements to be fulfilled and with many potential variables, material choice was not a trivial matter.

3.2.3.1 Capsule Materials

Platinum was used as the capsule material for all GBD of volatiles experiments. Pt was ideal as it was easy to work with and weld, as well as being capable of withstanding the experimental conditions with ease. It was suitably malleable that it did not rupture when being worked and capsules did not break apart when they were removed from the assemblage. Pt also allowed diffusion of electrons through the capsule thereby allowing the oxidation fugacity to be kept constant and did not react with the contents of the capsule it being chemically inert.

3.2.3.2 Sample Materials

Fundamentally, three minerals with specific properties were required: 1) A phase capable of acting as a water source (able to hold and subsequently release a significant amount of water); 2) A host phase around which volatiles would diffuse – the phase would have to be unable to accept any of the volatile in question into its structure; 3) A sink phase into which the volatile would diffuse – this phase would have to be initially dry or able to be easily characterised such that increases in water content due to diffusion during the experimental run could be determined. The phases chosen for these roles were (respectively) pyrophyllite, natural stoichiometric spinel and olivine.

Water Source

Pyrophyllite ($Al_2Si_4O_{10}(OH)_2$) was used as the water source in the experimental runs. As pyrophyllite is heated it thermally decomposes (between 450°C and 850°C at ambient pressure) – dehydrating and thus acting as a source of water.

$Al_2Si_4O_{10}(OH)_2 \rightarrow Al_2Si_4O_{10} + H_2O + O$

The aluminium-silicate reaction product is metastable and is known as a pyrophyllite dehydroxylate [111]. The dehydration products were expected to be stable in the presence of Mg-spinel.

Given the above mineral formula, pyrophyllite contains approximately 5500ppm by weight of H or 50,000ppm by weight of water. This quantity is sufficiently high to create a large enough chemical gradient to enable sufficient diffusion to occur within the timescales available for experimental runs.

Host Phase

Stoichiometric Mg-spinel was chosen as the medium around which water would diffuse in this series of experiments (i.e. water will diffuse along Mg-spinel grain boundaries). Previous workers have shown that natural, stoichiometric spinel ($MgAl_2O_4$) is almost unique in that it is unable to accept any water in the form of H defects into its structure (down to a sub-ppm level) [112] unlike nearly all other nominally anhydrous minerals (NAMs) which have been shown to routinely be able to accommodate water concentrations of a few hundred ppm under mantle conditions[9,74]. Work conducted by Rossman and Smyth (1990) [113] using infra-red spectroscopy found no evidence of water or derived species in spinels from high-pressure eclogitic terrains despite other minerals within the same samples containing significant levels of OH. Work by Bromiley et al. [112] showed that H could only be incorporated into synthetic non-stoichiometric Al-rich spinels (which are not stable at high PT conditions) which had a significant concentration of defects present within the structure. In this case H was able to occupy an interstitial position. The detection limit for H within natural spinel in Bromiley's investigation was below 1ppm indicating that for all practical purposes stoichiometric natural Mg-spinel is anhydrous with H not even able to occupy an interstitial position.

Spinel is also stable over a wide range of pressure and temperatures, has a simple composition and is relatively chemically inert. It is the stable aluminous phase at the top of

the upper mantle and is thus geologically relevant and is ideal for determination of H GBD as it can be used in an experimental design where it is desired that lattice diffusion is prohibited.

An attempt was made to synthesise Mg-spinel (see below) so that complete control could be maintained over the composition. Unfortunately this attempt was unsuccessful as the powder did not anneal into grains of a sufficiently large size (i.e. 100μm+). As a result of this, natural spinel crystals from Magok, Burma, were used instead. These crystals were sourced from alluvial deposits, so their exact origin is unknown. Crystals had an almost perfect octahedral habit with edge lengths of approx. 4mm and had a pink colouration (due to the presence of trace amounts of Fe^{2+}).[112] These crystals were of known stoichiometric composition (see Table 1 below) having been previously used in an investigation by Bromiley et al. [112] and were of good quality (up to gem quality). Grains were checked to ensure that no inclusions were present by initial optical microscope checks, and then again after grinding – no inclusions were found.

MgO	27.88
Al_2O_3	67.43
SiO_2	0.02
CaO	0.01
TiO_2	0.09
Cr_2O_3	3.23
FeO	0.05
ZnO	0.05
Total	98.76

Mineral Formula: $MgAl_{1.94}Cr_{0.06}O_4$

Table 1: Composition of natural stoichiometric spinel from Magok, Burma
(after Bromiley et al., 2010 [112])

Sink Phase

Periclase, also known as magnesiowustite (MgO) was originally identified as a possible sink medium (see Figure 27). Attempts were made to crystallise MgO from the powdered form in which it was readily available, but these proved unsuccessful (see section below). Due to these difficulties in synthesis and the higher solubility of water in olivine, olivine replaced MgO as the chosen sink material.

Olivine, whilst being a nominally anhydrous mineral (NAM), is in actuality able to accommodate up to approximately 2500 ppm by weight of water within its structure depending on the prevalent PT conditions [9] (see Figure 1). Under experimental conditions of close to those used in the initial stage of this investigation, Kohlstedt et al. measured solubilities of 135 weight ppm H_2O (2.5GPa, 1100ºC) [114]. It is also stable alongside stoichiometric spinel under the experimental conditions to be used (as seen in natural spinel lherzolite). High quality natural samples of olivine were readily available. The olivine which was used was a natural sample from Åheim, Norway. To prevent reaction between olivine sink crystals and breakdown products from the pyrophyllite source region, the capsule design was altered so that a thin layer of olivine-free spinel matrix was placed above the pyrophyllite layer. Above this layer was spinel with olivine grains included.

MgO	49
SiO_2	41
Fe_2O_3	7
Cr_2O_3	0.3
Al_2O_3	0.5
NiO	0.3
MnO	0.1
CaO	0.05
Total:	98.25

Table 2: Composition of olivine (weight% oxides) to be used as a sink in H diffusion along grain boundaries experiments.

Attempted Synthesis of Mg-spinel and Magnesiowustite

An attempt was made to synthesise and crystallise stoichiometric spinel ($MgAl_2O_4$) and MgO. The stoichiometric composition for the spinel was essential to ensure that it would not be able to accept water into its structure [112]. Furthermore, a synthetic composition offered the advantage of ensuring purity and consistency. After grinding the component oxides (MgO + Al_2O_3) together in stoichiometric proportions, the powders were pressed to pellets, placed in Pt crucibles, and heated in an atmospheric furnace. MgO was prepared in a similar way except for the fact that no mixing of oxides was required. The initial attempt at crystallising was run over a period of 21 hours using the following program:

Furnace starting temperature 600°C
600°C ➔ 1200°C 2 hours
1200°C ➔ 1200°C 18 hours
1200°C ➔ 600°C 1 hour

Resulting spinel crystals were small but just of an acceptable size for the intended purpose (<100µm). MgO, however, retained a powdery consistency which was not appropriate for the planned experiments as crystals with a minimum smallest dimension of at least 100µm were required to facilitate effective analysis after the experimental runs had been completed.

A second attempt to crystallise sufficiently large crystals of spinel and MgO was carried out with a peak temperature of 1500°C. Heating and cooling times were extended accordingly but the period of peak temperature was kept at 18 hours. Similar results were obtained.

3.2.3.4 Preparation of Mineral Phases

Analytical requirements meant that it was planned from the outset that H contents would be measured using an ion microprobe. In order to do this, spot sizes of the order of 30µm were required. As such, the sink grains, olivine, needed to be greater than this size. Olivine grains of 100µm were considered to be ideal. This grain size was achieved by progressively grinding down larger crystals and checking grain size under the microscope on a regular basis. When the correct grain size was achieved, any finer grains were sifted out using 50µm mesh.

Spinel grains were ground finely to achieve as small a grain size as possible so that diffusion can occur along as close as possible to a straight line between source and sink. This grain sized is achieved using a similar method to the olivine but instead involves sifting with a 30µm mesh to ensure that all grains are below this size.

3.2.3.5 A Note on the Relevance of Data Obtained Using this Capsule Design

As detailed above, a capsule design was chosen which utilised a host mineral (stoichiometric Mg-spinel) which does not permit lattice diffusion. This mineral is not dominant in the Earth's mantle. Unlike stoichiometric Mg-spinel, many of the minerals which are present in this region do permit lattice diffusion to a greater or lesser degree. As such, the values obtained for GBD in our experiments must be limited to some degree in terms of applicability to natural systems. However, they are of great importance in eliciting an understanding of the mechanisms at play. By studying a simplified analogue in our experiments, an understanding can be obtained of this particular element of the more complex natural system. In utilising a host phase which is unable to accept any water into its lattice, it is clear that any diffusion which does occur must have done so along grain boundaries. Thus, the method allows the complete decoupling of lattice and GBD which would otherwise occur in natural systems. Having isolated and measured GBD it is then a relatively simple task to scale results to realistic mantle grain sizes.

3.2.4 Construction of the Experimental Capsule

Platinum tubing of 4mm outside diameter was cut to a length of 11mm. This was done by scoring the tubing with a razor blade and then snapping it. The Pt was then annealed at the top of the blue flame in a Bunsen burner for a few minutes. A three way crimp was then formed at one end of the capsule and then arc welded. This weld was flattened by hammering a pin inside the capsule with the capsule contained within a bored out cylinder of the same diameter as the experimental assemblage. Once this had been done, the capsule was cleaned by placing it in acetone in a beaker in an ultrasonic bath for 2 minutes. It was then annealed a second time in the same manner as the first to remove any trace acetone and to overcome any work hardening.

The contents were then loaded. This was done by placing a layer of pyrophyllite approximately 1mm thick at the bottom of the capsule followed by a layer of stoichiometric Mg-spinel, also approximately 1mm thick. A layer with a thickness of approximately 2.5mm of a spinel/olivine mix was then loaded into the capsule. The two phases were mixed in a volumetric ratio of between 10 and 15 to 1 (spinel to olivine). This ratio was arrived at by trial and error following SEM analysis of early experiments which were found to contain too few olivine grains when sectioned to enable accurate fitting of diffusion laws. It was found that on average this ratio meant that there were enough olivine grains within the capsule that a significant number would be sectioned and so could be analysed in any random cut through a capsule. The capsule was tapped down at frequent intervals to ensure that the powders settled. Once the capsule had been loaded, the exposed Pt on the upper inside edge was cleaned as much as possible to prevent contamination of the crimp with mineral grains. The

presence of grains within the crimp could hinder the welding of that crimp by causing the surrounding Pt to fail to melt.

The top weld was completed in exactly the same way as the lower weld with the exception that cooling spray was used to keep the capsule and its contents cool during the welding process.

Finally the completed capsule had its top flattened using a similar pin and cylinder setup as used previously.

Experiments were then run and retrieved as detailed in section 2.2.1 The Piston Cylinder Apparatus and section 2.2.1.1 Sample Retrieval.

3.2.5 Run Conditions

Experimental runs were conducted at temperatures between 650 and 1600°C. This was done to ensure that the temperature dependency of diffusion could be accurately determined. A pressure of 3GPa was used for all runs. This value was chosen as it was representative of the upper mantle and as such data obtained at this pressure would be applicable to the real world scenario of volatile diffusion in the mantle. Furthermore, the piston cylinder apparatus was known to work well at this pressure and so it was expected that this value would increase the ease of carrying out the experimental program. As previously discussed, pressure is not a variable which was investigated here but it would be very interesting to do so in any future work. Run durations were initially calculated by estimating how much more quickly grain boundary diffusion could be as compared to published lattice diffusion rates. As such, this estimate was essentially a guess. Once initial runs had been completed, diffusion coefficients were calculated and then used to estimate the next set of durations. Details of the specific conditions used for each run are detailed in section 3.6.3 Summary of All Run Results.

3.3 Methods for Preparing Samples for Analysis

Following the completion of experimental runs and the retrieval of the capsule from the assemblage, capsules were very carefully cut in half using a circular saw before being mounted in a resin which could later be removed using appropriate solvents. At each stage great care was taken to ensure that capsules were kept clean and that cracks did not take up fluids used in the preparation procedure. Once mounted in the resin block the capsules were polished on increasingly fine polishing sheets to achieve a satisfactory finish and flat surface to allow for SIMS analysis. The halved and polished capsules were then removed from the resin blocks by dissolving away the resin with a suitable solvent. Samples were then further prepared for analysis by pressing them into indium within aluminium mounting blocks. This was done instead of mounting the samples in an epoxy resin owing primarily to the resin's behaviour under high vacuum: As it dries, epoxy resin degasses, giving off significant quantities of C, H and S. This process continues and is further encouraged when the mount is exposed to a vacuum. In the case of SIMS, this degassing is enough to degrade the ultra-high vacuum used in the sample chamber, therefore affecting the quality of analysis. When analysing H, the effect is particularly significant as the degassed H from the epoxy causes a much higher background level of H which, particularly at low sample concentrations, can mask the true analytical signal therefore making data collection impossible. Once embedded in indium, capsules were imaged by SEM (uncoated, under controlled pressure – see section 2.4.1.3 Conductive Coatings for SEM Analysis) to check capsule integrity and produce maps to aid navigation in the subsequent SIMS analysis. Finally the samples were gold coated for analysis by SIMS. This was done by placing the samples into a gold sputtering coater for a period of 200 seconds. This duration of coating provided a suitably thick conductive layer to enable SIMS analysis.

3.4 Analysis of Completed Runs

3.4.1 Initial SEM Analysis

Following the completion of experimental runs and the preparation of capsules, samples were initially checked for structural integrity with an optical microscope and then in more detail with an SEM. Furthermore, SEM analysis of the capsules was used to create maps of the capsule and to identify olivine H-sink grains for later, quantitative SIMS analysis.

3.4.1.1 Creation of Capsule Map

Capsule maps were created by obtaining several images of each capsule at high resolution (width of field of view ~1mm) and then combining them digitally using Adobe Photoshop. This allowed the creation of a single highly detailed image which would not have been possible to record using the SEM alone (a single capsule would not fit into the field of view of the SEM and at the lowest magnification which was closest to fitting an entire capsule into the view a lot of detail was lost). The output images were sized to A3 so that large maps were then on hand for SIMS analysis. An example of a compiled image is shown below in Figure 29.

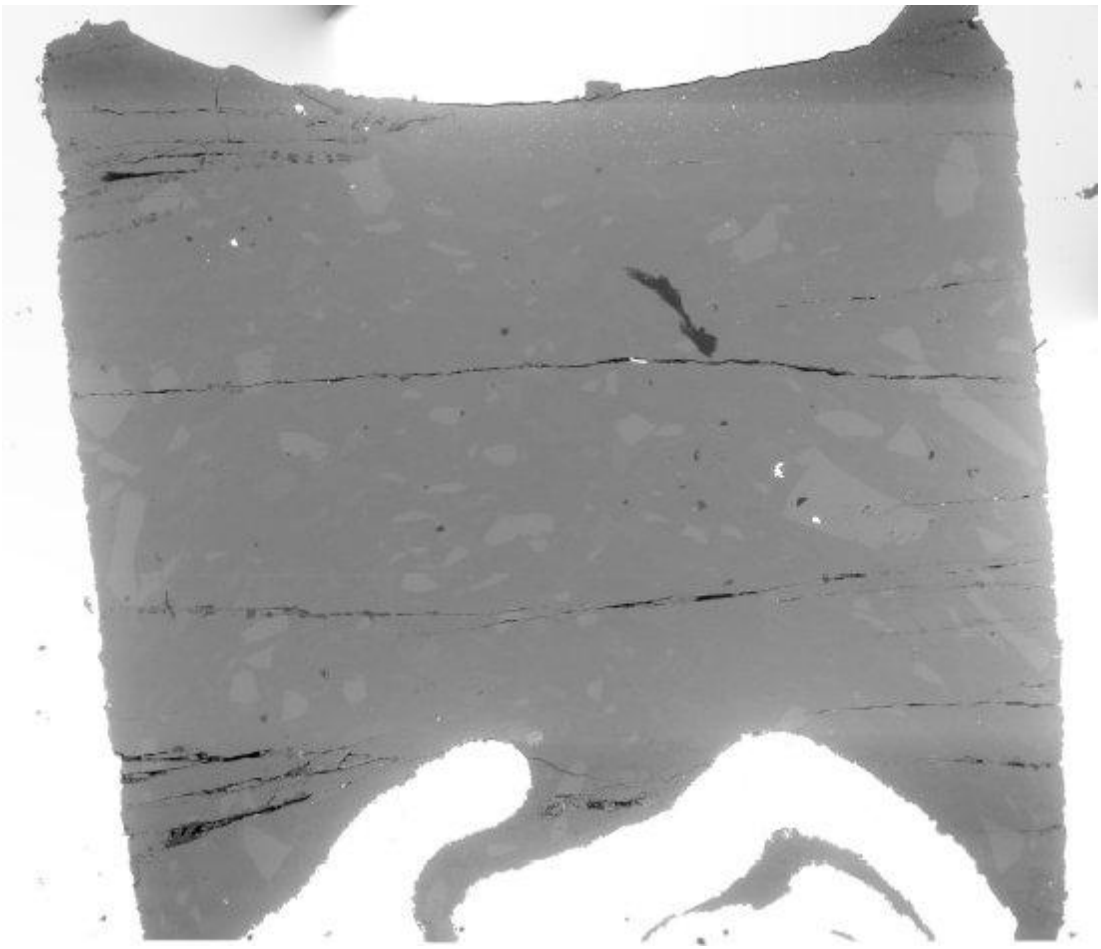

Figure 29: BSE Image of Sectioned Capsule VGB6

Example of a compiled image of a sectioned and polished capsule. Olivine grains are clearly seen as being lighter than the background spinel matrix in the body of the capsule. The image is made from the digital combination of 4 smaller images and was used at A3 size in the investigation to aid in navigating around the sample. The width of the capsule in this image is 4mm.

3.4.1.2 Mineral Phase Identification

It was very important and also non-trivial to correctly identify mineral grains within the capsule. Identification was essential as only olivine grains were to be analysed by SIMS (as they were the only grains which could take in H). They also needed to be evaluated for size and any immediately obvious defects – those of a suitably large size (ideally 50μm and above) and without major cracks running through them were selected for SIMS analysis. Both visual recognition and the EDS system on the SEM were used to identify phases. Careful tuning of BSE imagery was required in order for basic visual differentiation between mineral phases, olivine (Mg_2SiO_4) and Mg-spinel ($MgAl_2O_4$) were of a relatively similar density and so interacted with the incident electron beam in a similar way. Once a possible olivine grain had been identified by visual inspection of grains, its identity was confirmed using the EDS system of the SEM. As the grains within the capsule could only be one of two minerals, it was possible to differentiate between them based on the presence of absence of Si (as olivine contains Si and Mg-spinel does not). Olivine was clearly identified by the presence of an Si peak on an EDS spectrum whilst Mg-spinel was identified by the absence of the peak. Example spectra are shown below in Figure 30. The EDS system was not calibrated for this purpose as quantitative measurements of the composition of each grain type was not required.

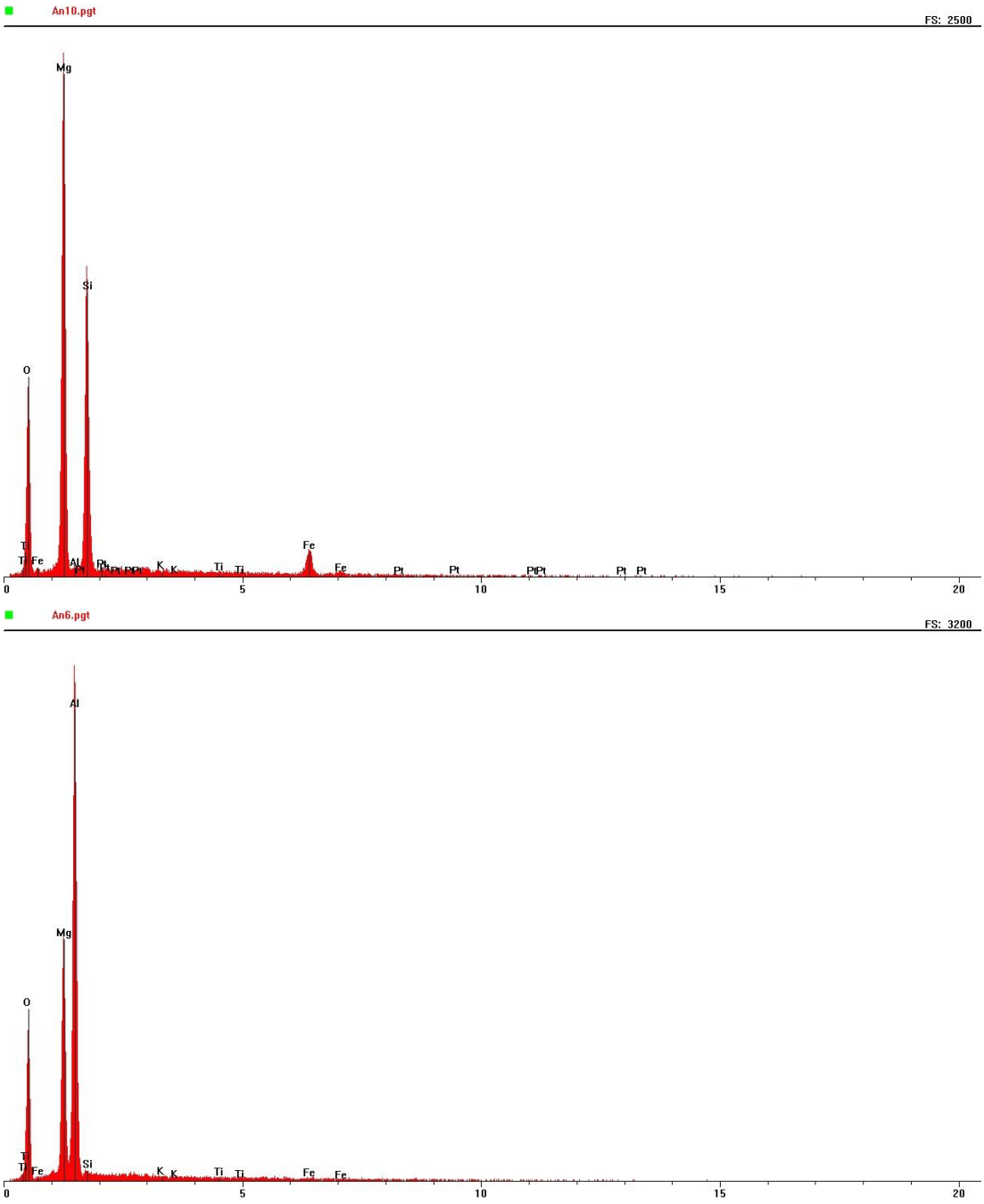

Figure 30: Un-calibrated EDS Spectra of Olivine and Mg-Spinel

Top: EDS spectrum of olivine measured in capsule VGB1. Note the prominent Mg and Si peaks. Ratios are not reliable as oxygen content is calculated by the EDS software based on assumptions regarding constituent oxides.

Bottom: EDS spectrum of Mg-spinel also measured in capsule VGB1. Mg and Al peaks are clearly visible and Si is absent. The same proviso regarding oxygen as for the top image is applicable

In almost all cases the capsules only contained pyrophyllite, Mg-spinel and olivine. However, it was essential to allow for the possibility of alternative phases forming during experimental runs (i.e. not to immediately assume that a grain must be olivine simply because it contained Si). In practice, on the rare occasion when other phases were present in the sample they were of a significantly different composition and density to olivine and Mg-spinel and so appeared very differently under BSE imaging with denser phases appearing more bright and lighter phases appearing more dark. Thus, they were immediately identified as being unexpected phases. Experiments in which these unexpected phases were found are discussed in the results section.

3.4.2 SIMS Analysis

Once samples had been analysed by SEM and target grains had been identified on capsule maps, SIMS analysis was conducted.

Samples were placed in the air lock of the SIMS apparatus two days prior to the scheduled analysis. This was done to allow any volatiles that had collected on the surface of the samples to dissipate in the vacuum of the air lock. This was an important step as these surface volatiles would otherwise be detected as significant background noise if they were to be liberated from the sample in the analysis chamber (See Section 2.4.3 Secondary Ion Mass Spectrometry (SIMS) for a full discussion).

SIMS analysis was conducted in two sessions for this aspect of the research. Runs VGB1 – 5 were prepared for SIMS analysis at a pilot session to determine if the methods used to date had been successful. The remainder of the runs, VGB6 – 20 were analysed at a later date during a week long period of analysis.

Once analysis points had been selected (using a combination of the SEM maps and the reflected light microscope which is part of the ion microprobe) they were rastered to remove gold at the surface along with any impurities such that only the sample itself would be sputtered by the ion beam. The size of the rastered area (and so the size of the area from which sample particles could be ablated) was approximately 20 x 25µm. Samples were analysed with a 5nA ^{16}O beam which had been accelerated to 10kV with an energy offset of 75V. In all cases H^+ and Si^{4+} were collected along with either Mg^{2+} or Li^{2+} (the choice of which additional ionisation products to collect was dictated by the amount of time available and the usefulness of the additional information that it provided – as with much of this investigation earlier results informed later methods – Li proved to be a very useful indicator of irregularities in certain analysis points). ^1H and ^7Li were each analysed for a total of 500s over 20 – 70 analysis cycles (depending on availability of analysis time and instrument

performance). ^{30}Si and ^{26}Mg were counted for a total of 200s across the same number of cycles. This gave a total analysis duration of approximately 20 – 25 minutes for each point collected.

During analysis the capsule maps (which had previously been made using the SEM) were extensively annotated with the locations and ID numbers of each of the analysis points. This was essential as it enabled each point to be identified later and have its measured concentration associated with a distance between the point and the pyrophyllite/spinel interface.

A grain of the olivine which was used as the sink phase was analysed to test if it had any water content prior to the commencement of diffusion runs. No water was found above the background level at which the instrument operated i.e. as compared to measurements of known "dry" standards.

3.4.3 Post-SIMS SEM Analysis

Following the completion of SIMS analysis samples were analysed in the SEM for a second time to check the SIMS analysis points for any issues that could potentially affect the quality of the data obtained and in order to obtain values for the distance of each analysis point from the H source.

3.4.3.1 Preparation of Samples

Samples were coated in gold prior to SIMS analysis and therefore already had a conductive coating. During SIMS analysis rastering and collection of data had burnt c.25µm diameter points through the gold. As no conductive layer was present at the centre of these points they allowed charge to build up which appeared as bright spots under BSE imaging. Whilst a second, very thin coating of gold was considered to prevent this charge build up, in practice this was not done as the small spots of charge build up made the analysis points easily identifiable. Furthermore they did not degrade the quality of the remainder of the image and so were considered advantageous.

3.4.3.2 Analysis Point Defect Check

Once the SIMS analysis points had been identified each one was checked for any structures or defects which might affect the quality of the data obtained from the point. This check was performed blind – points were checked without regard to the data that had been obtained during SIMS analysis. This ensured that points which had anomalous values associated

with them were not rejected based upon the values recorded. Instead, points were only rejected if a physical reason for them to be rejected was found. Examples of such defects include cracks running straight through the grain which could potentially hold trace amounts of polishing fluids and therefore provide particularly high concentrations of volatiles. This process resulted in between a half and a third of data points being rejected. Once rejected points had been removed from the dataset a further step was carried out: In the cases where there were multiple analysis points on a grain, the values for these points were averaged so that a concentration of points all at a similar distance from the water interface did not cause a weighting in the calculation of the diffusion coefficient.

3.4.3.3 Analysis Point Map Creation

Images of the capsule were collected and stitched together to provide a record of the location of analysis points. An example of such an image is shown in Figure 31.

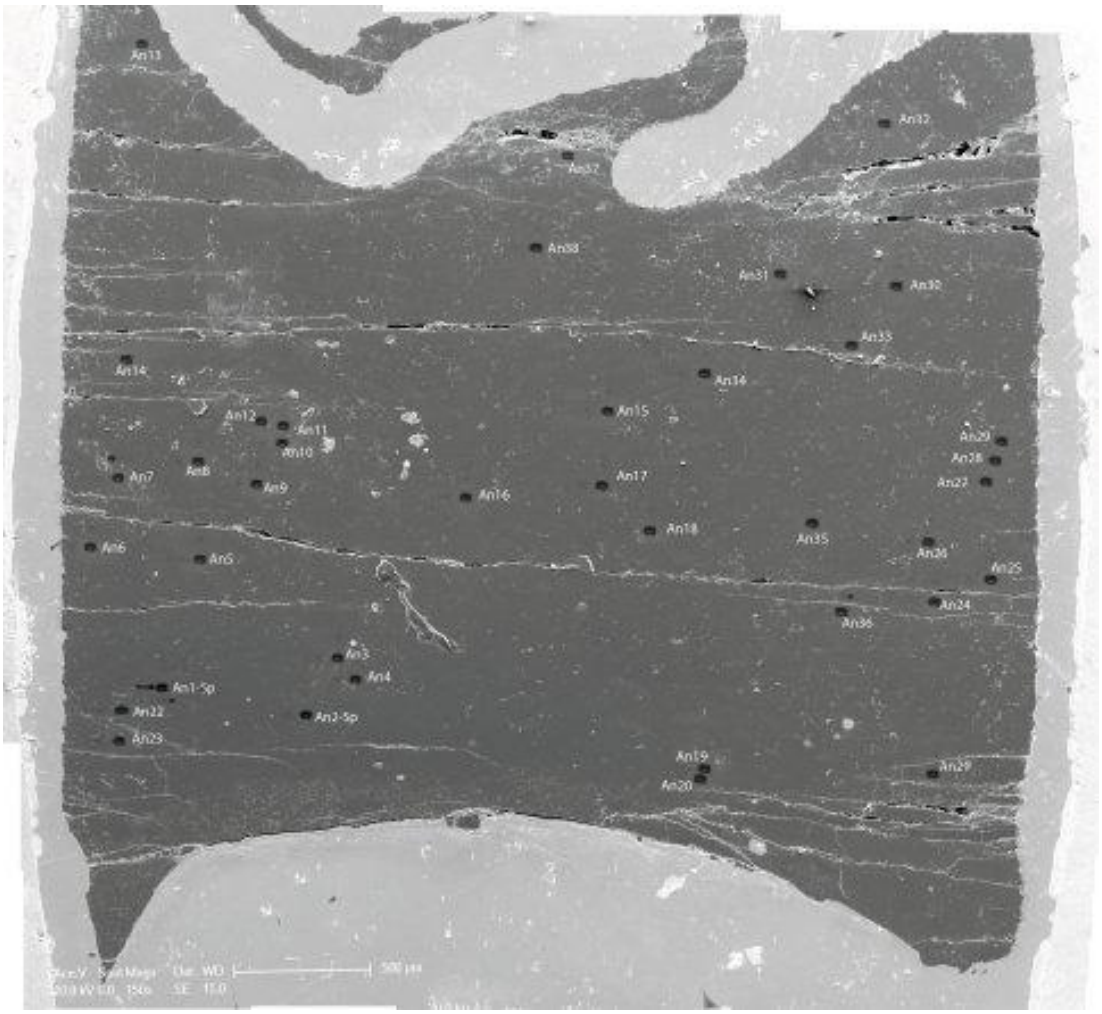

Figure 31: Capsule VGB6 after SIMS Analysis

The black spots within the body of the capsule are the analysis points and are approximately 25µm in diameter. Individual analyses are labelled The approximate width of the capsule is 4mm.

3.4.3.4 Analysis Point Distance Measurement

The most important aspect of the post-SIMS SEM analysis was the measurement of the distance of analysis points from the pyrophyllite/spinel interface. It was this distance (along with the concentrations recorded by SIMS) which would allow the calculation of diffusion coefficients.

Distances were measured between two points using the SEM software. The first point was at the centre of the analysis point and the second was at the point on the pyrophyllite/spinel interface which was nearest to the analysis point (see Figure 32 and Figure 33 which show close up SEM images of the spinel/pyrophyllite interface and the process of measuring the distances of olivine grains from the interface). By utilising capsule maps which had been annotated during SIMS analysis it was possible to attribute each distance measurement to

the particular analysis point thereby pairing up concentration and distance values. These values were recorded in a spreadsheet along with the concentration data for subsequent processing and analysis.

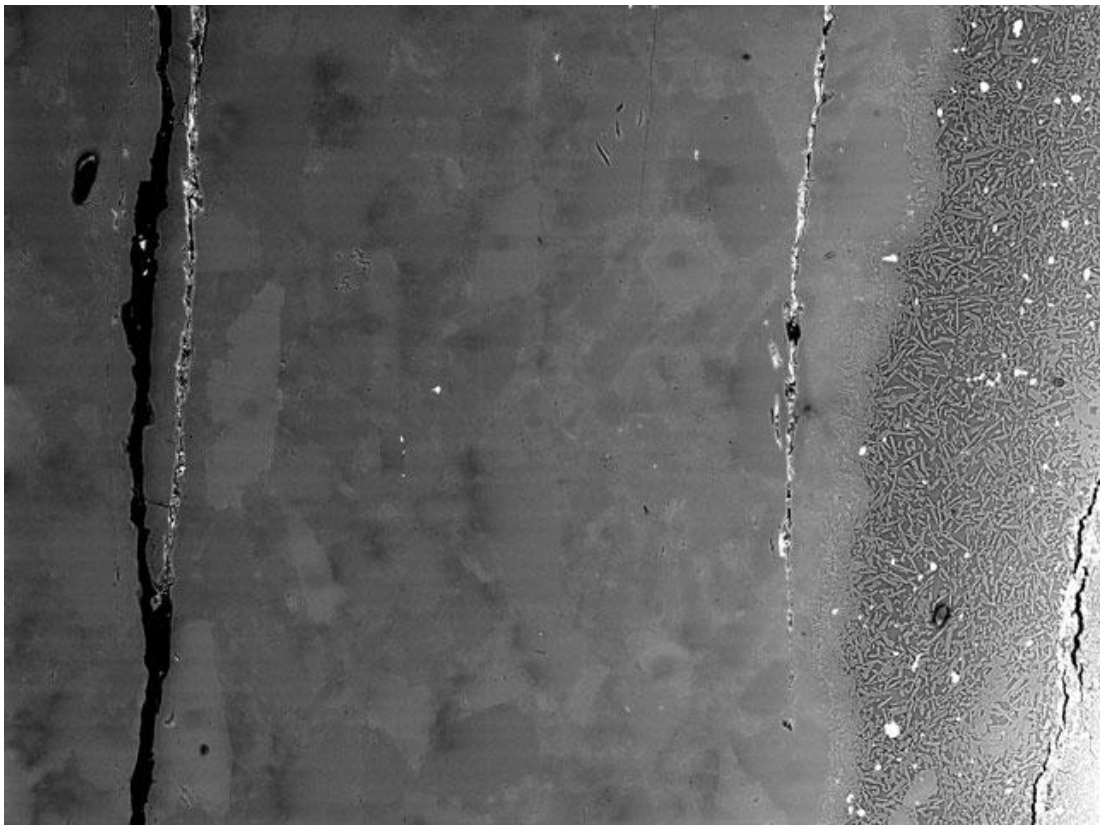

Figure 32: Close up Image of Pyrophyllite/Mg-Spinel Interface

BSE image showing the interface between pyrophyllite and Mg-spinel. The pyrophyllite shows a classic dendritic dehydration texture. It also has a number of bright white blebs which were shown by EDS analysis to be Ti. Measurements of the proximity of olivine grains to the Mg-spinel/pyrophyllite interface were taken from the centre of each analysis point to the closest point on the interface (defined as the line along which the texture above ceases). Width of field of view is approximately 1mm.

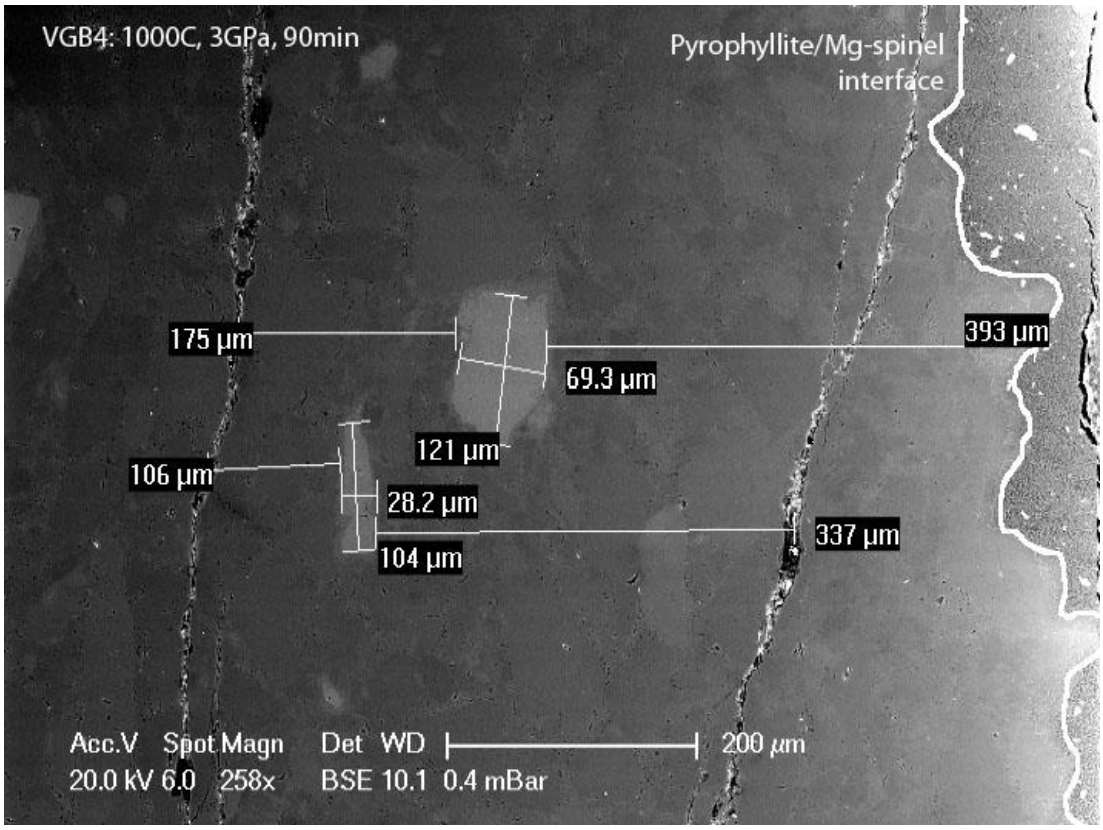

Figure 33: Run VGB4 showing Interface & Olivine Grains

Pyrophyllite/Mg-Spinel interface is shown highlighted in white. Olivine grains are clearly visible as appearing lighter than the surrounding Mg-spinel matrix. Cracks are suspected to have formed during decompression.

3.5 Treatment of SIMS Data

3.5.1 Calculation of Diffusion Parameters

The data obtained from SIMS analysis was extensively reviewed and processed to enable the extraction of diffusion coefficients and Arrhenius relationships. Errors were also carefully treated to determine the likely precision of the data obtained. The methods utilised in the determination of diffusion parameters are discussed in section 2.5 Non-Linear Regression Analysis.

3.5.2 Calculation of Errors

Absolute error values were estimated for each measured parameter. The estimations which were made and the logic by which these estimations were arrived at is detailed in section 2.6.1 Calculation of Errors. Where specific methods were required for this particular aspect of the investigation they are detailed below. These individual sources of error were combined as detailed in section 2.6.2 Combination of Errors.

3.5.2.1 Concentration Errors

There was a quantifiable error associated with the measurement of point concentrations of H content of olivine grains via SIMS. A large number (between 20 and 70) of individual analyses were recorded for each analysis point. When plotted it became clear that there was initially a large variation as the ion beam burnt through the gold coating and surface of the sample. As more and more points were collected the result obtained from them became progressively more consistent and as such are considered to be more precise. Thus, the reported value for each analysis point is a mean of the several last analysis points which were recorded (the specific number of points which were used in the calculation of this value varied as all points were checked for each analysis site and all points in the consistent “tail” of the data were used in each case – typically between 5 and 20 values). The error associated with each reported point is the standard deviation of the dataset from which that mean was calculated.

3.5.2.2 Summary of Error Magnitudes

Parameter	Value
Time	120s
Concentration	Standard deviation of all values for each analysis point
Distance from Interface	20µm
Temperature	Maximum deviation from nominal temperature

Table 3: Summary of Error Magnitudes for GBD of Volatiles Experiments

3.6 Results

3.6.1 Summary of Run Parameters

A total of 19 experiments were successfully run and analysed within this experimental program with durations of between 18 minutes and c.3 days and at temperatures ranging from 650°C to 1600°C. Run parameters are summarised in Table 4.

Run ID	Temp (°C)	Pressure (GPa)	Duration (min)	Mounting	Coating	SEM	SIMS
VGB1	1000	3	294	Epoxy	Gold	Y	N
VGB2	1000	3	1231	Epoxy	Gold	Y	N
VGB3	1000	3	1185	Indium	Gold	Y	Y
VGB4	1000	3	90	Indium	Gold	Y	Y
VGB5	1000	3	352	Indium	Gold	Y	Y
VGB6	1000	3	66	Indium	Gold	Y	Y
VGB7	1200	3	43	Indium	Gold	Y	Y
VGB8	1200	3	60	Indium	Gold	Y	Y
VGB9	1200	3	30	Indium	Gold	Y	Y
VGB10	1600	3	19	Indium	Gold	Y	Y
VGB11	1600	3	18	Indium	Gold	Y	N
VGB12	1600	3	20	Indium	Gold	Y	Y
VGB13	800	3	392	Indium	Gold	Y	Y
VGB14	800	3	394	Indium	Gold	Y	Y
VGB15	800	3	402	Indium	Gold	Y	Y
VGB17	1400	3	20	Indium	Gold	Y	Y
VGB18	1400	3	20	Indium	Gold	Y	Y
VGB19	650	3	4269	Indium	Gold	Y	N
VGB20	650	3	4217	Indium	Gold	Y	N
Aborted Runs							
VGB16	650	3	N/A	N/A	N/A	N/A	N/A

Table 4: Summary of GBD of Volatiles Experiment Parameters

The table shows run parameters for each of the volatile diffusion along grain boundary experiments conducted. Mounting mediums and coating materials are shown as are the analytical steps which were completed. One run, VGB16, was aborted and as such no durations or post experimental processes are recorded.

As can be seen from Table 4, not all of the samples which were successfully run were analysed by SIMS. In all cases this was due to the sample having features which made it very difficult if not impossible to determine which grains were the Mg-spinel host medium and which were the olivine sink grains.

3.6.2 Specific Run Observations

3.6.2.1 VGB1 & 2

The initial runs of this experimental series were run as much for the purposes of method development as with the aim of obtaining data. As such, at this early stage it was not known what the ideal proportion and grain size for the olivine sink grains would be. Examination of runs VGB1 & 2 by SEM indicated that there were two few grains of a large enough size to enable meaningful data to be obtained (i.e. smaller than 100µm diameter). Any grains which were present and which were large enough were typically gathered in one part of the capsule meaning that it would not be possible to subsequently fit a diffusion law to any concentration data obtained from them (see Figure 34). As such, SIMS analysis was not carried out on these capsules.

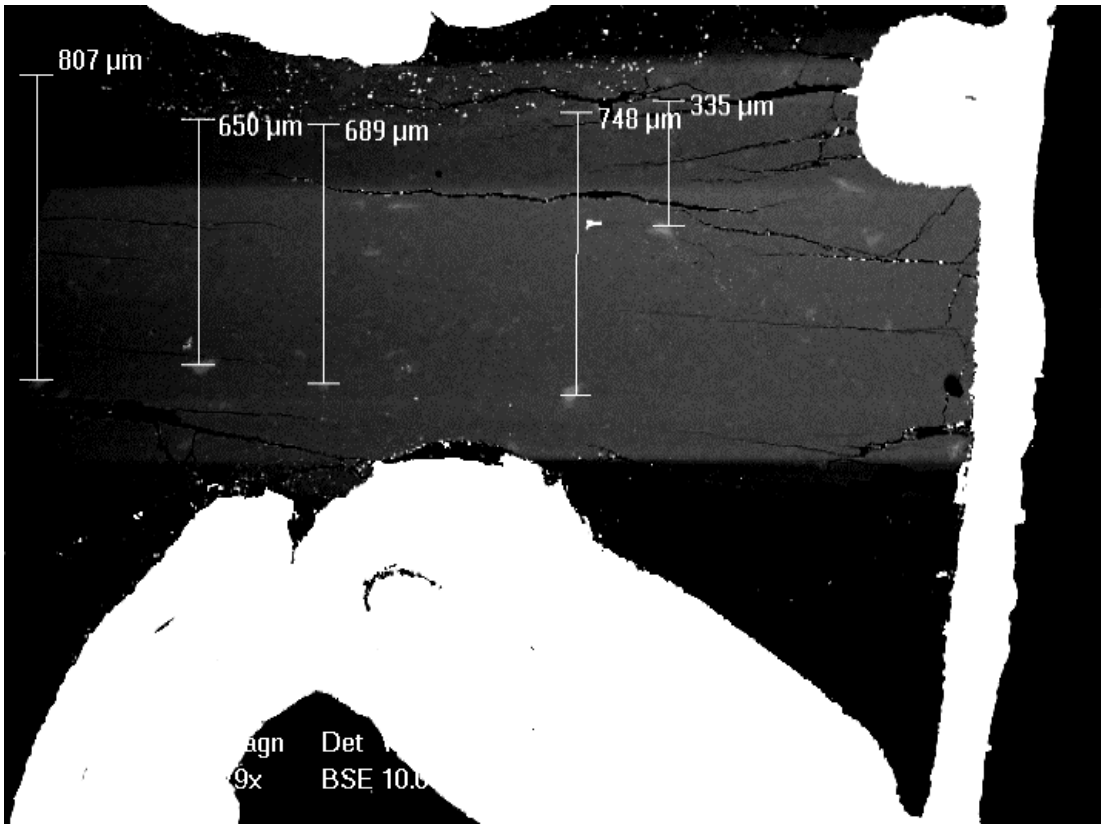

Figure 34: Run VGB1 showing Olivine Grains

There are very few olivine grains in the sample shown and those which are present are all at similar distances from the pyrophyllite interface. As such, if H concentrations were measured from the grains along with distances, all grains would bunch together on a graph of distance versus concentration and so not define a diffusion profile to which a law could be fitted. This was the case in runs VGB1&2. As such, neither run was analysed by SIMS. The approximate width of the field of view here is 3mm.

Figure 35 shows a BSE SEM image of a single olivine grain recorded from run VGB1. As can be seen from the measurements recorded on the image, the grain has a width of approximately 28µm. This grain size is typical of runs VGB1 & 2 and is problematic as it is very close to the size of the ablation pits that are created during SIMS analysis. As such, there is a great likelihood that an analysis pit may sample both a grain boundary and the olivine sink grain. This could potentially lead to anomalously high readings being recorded as the grain boundary may contain large amounts of H which, within the duration of the experiment, has not had time to diffuse into the olivine grain. It is very important, that only H within olivine grains is measured as the many olivine grains both within a sample and between runs were all derived from the same original crystal and so were of a consistent composition, thus, readings of H content from them are directly comparable. The extent and degree of networking of grain boundaries that surround them however is unknown and so they are not comparable. As such, it was important that grains were of a sufficient size that

an analysis point could be placed upon them without the point breaking the boundaries of the grain. As a result of the small grains found in these early runs, the preparation method for later runs was revised to ensure that larger olivine grains were used which would ensure that a suitable analysis surface would be available.

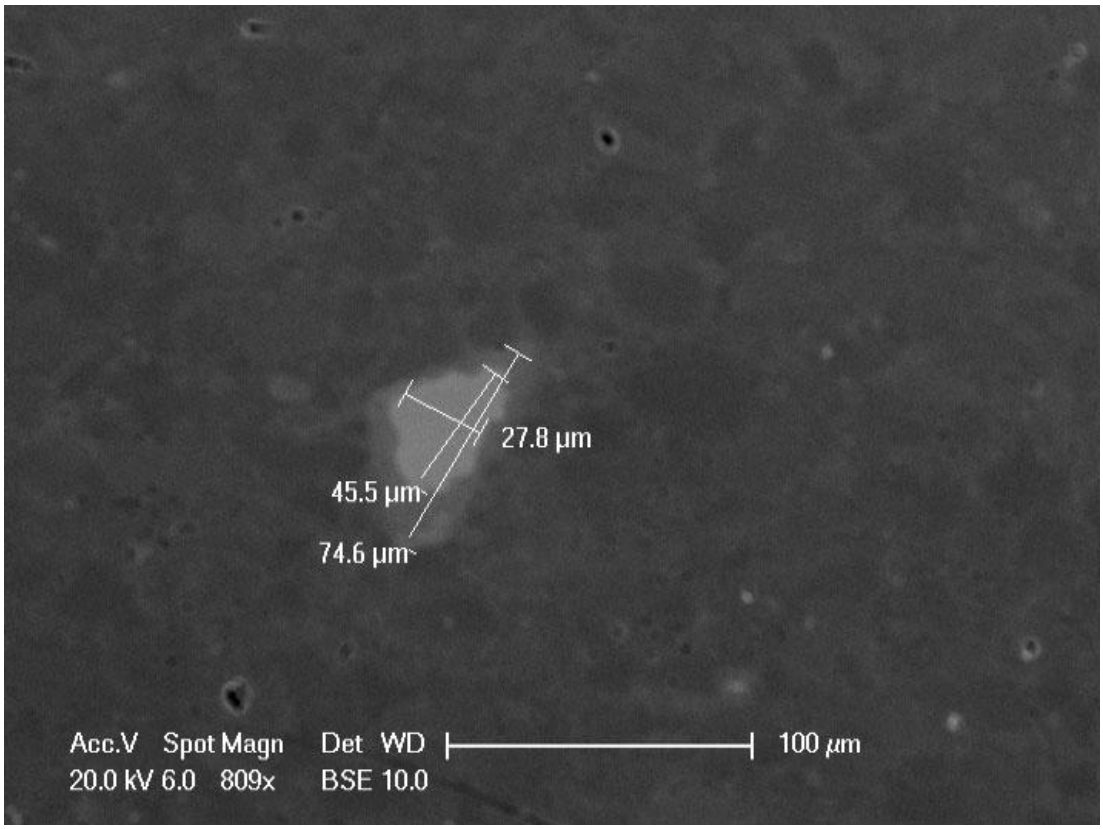

Figure 35: Single Olivine Crystal from Run VGB1

The figure shows a BSE image of an olivine grain from run VGB1 with measurements showing the size of the grain. The brighter, central part of the grain is exposed at the surface of the sample whereas the slightly darker, shadowed halo around it is interpreted to be just below the surface of the sample but still within the excitation volume created by the electron beam (as such the material immediately above the halo is likely to be Mg-spinel which typically appears darker than olivine due to a slightly lower density).

It was very difficult to accurately know the size of olivine grains that were being used in experiments. In practice the desired grain size (50 - 100µm) was achieved by trial and error. Fragments of a single large olivine crystal were ground up in a pestle and mortar and were regularly checked under an optical microscope during the grinding process to ascertain what size they had been ground too. When grinding was performed slowly the resulting grains were often of a wide range of sizes. When the selection of grains with a greater size than a given value was attempted with a gauze of known mesh size (e.g. 50µm) the finest fraction of grains tended to quickly block the mesh (quite possibly due to a build-up of static

electricity on the grain surfaces during grinding) meaning that no further material could be passed through. As such, the filtering of grains of a particular size was not a viable process. Instead large fragments of olivine were ground quickly with a large amount of pressure applied to the pestle. This resulted in the majority of grains being of a similar size which, after a series of checks under the microscope and continued grinding, were of a suitable size for future experimental runs.

3.6.2.2 VGB3 & 5

Runs VGB3 & 5 contained olivine grains which were positioned more widely although there were relatively few grains exposed in each sectioned capsule. These two capsules were analysed by SIMS with 2 readings being taken in VGB3 and 5 being recorded in VGB5. Some of these readings were rejected for various reasons (as detailed previously) meaning that it was not possible to accurately fit a diffusion law to the data, As such, these runs did not contribute useful data to the testing of the hypotheses.

3.6.2.3 VGB4

Run VGB4 was the first which yielded useful data towards the investigation. Whilst only 5 analyses were made, these were evenly spaced meaning that it was possible to fit a diffusion law to the data. Figure 36 shows a BSE image of the section capsule. The olivine grains are clearly visible and are annotated with measurements of their distances from the pyrophyllite interface.

Whilst a total of 5 analysis points were recorded for capsule VGB4, only 4 were used in the calculation of the diffusion coefficient as can be seen in Figure 37. This was due to a crack passing through one of the analysis points. Whilst this crack may well have formed during decompression of the sample it is also possible that it was extant during the run meaning that it would provide a potential fast route for H to reach the interior of the olivine grain. As such, this particular grain cannot be directly compared with other grains and so was rejected. As previously detailed, this rejection was made without any knowledge of the value of the reading which had been recorded from this analysis point. With hindsight, the reading was anomalous and may well have been caused by the presence of the crack.

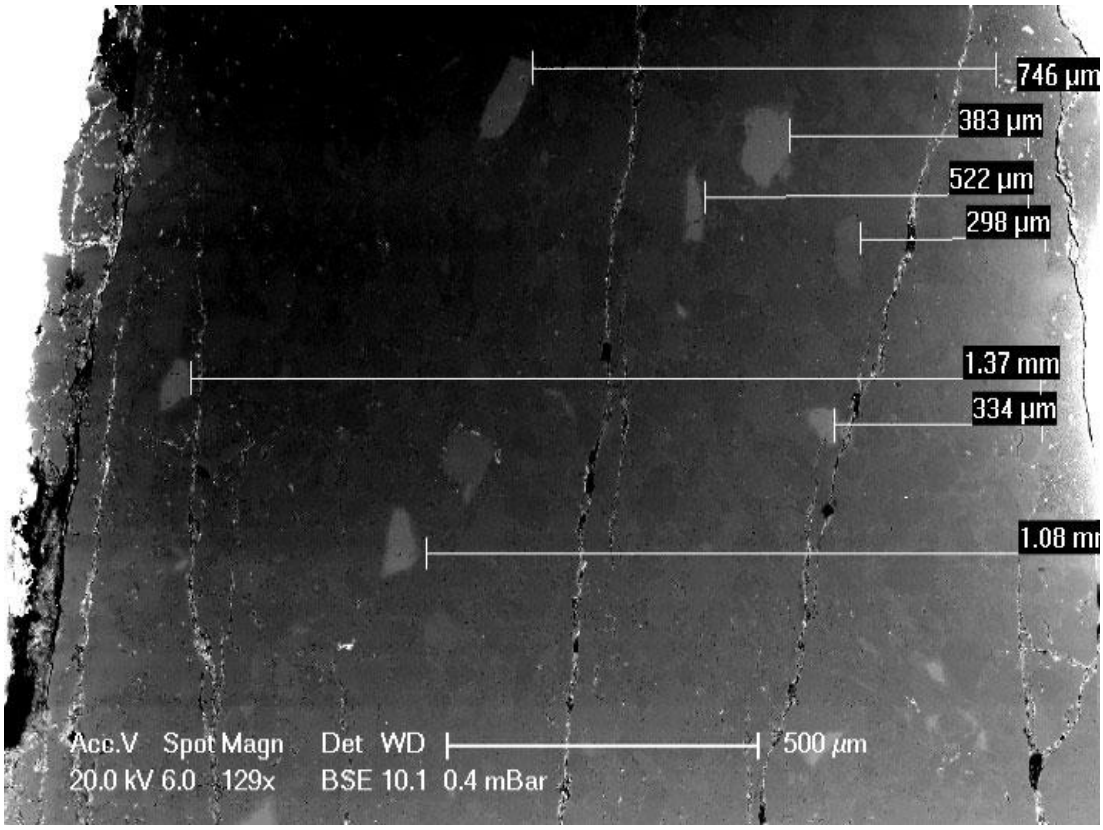

Figure 36: Run VGB4 showing all Olivine grains and Distances

Olivine grains are clearly visible as being lighter (higher mean density) than the surrounding Mg-spinel grains. The grains are well spaced at a variety of distances from the pyrophyllite interface which is at the right hand side of the image. Most grains have a smallest visible dimension of at least 50µm meaning that it was possible to place a SIMS analysis point on the grain without sampling the grain boundary. Annotated distances are those from the pyrophyllite interface to the grain in question.

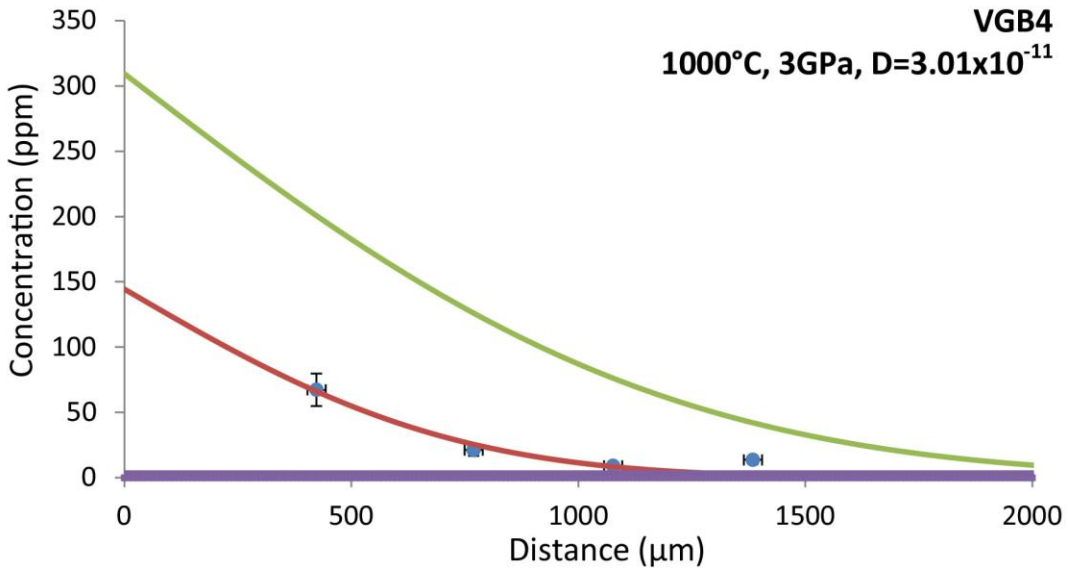

Figure 37: Concentration/Distance Plot for Run VGB4

4 grains at varying distances were located in the sample allowing the easy fitting of a diffusion law to the data. The red line is a model fit of a solution to Fick's Law to the experimental data. The green and purple lines represent the 90% confidence bounds for the fitting procedure. The closer the green and purple lines are to the red line, the more confident one can be of the quality of the fit. This proxixmity will be controlled by both the amount of data in the plot and the agreement of that data with the specified diffusion model. This measure of goodness of fit is discussed fully in section 2.6.1.5 Goodness of Fit.

3.6.2.4 VGB6,7,9,12-15,17,18

Following the completion of runs VGB1 – 5, and bearing in mind the limitations therein (discussed previously), VGB6 – 20 were run incorporating experimental re-designs. These runs provided the majority of the data for the investigation and the majority were deemed to have been successful.

Diffusion profiles took on a variety of different forms depending on the extent to which diffusion had progressed during an experimental run. All runs did not give the same shape profiles owing to the fact that it was exceedingly difficult to accurately predict the run duration which would give the ideal profile at a given temperature. No runs were found to have been completed with a duration which was too short (which would give a profile which was very steep at high proximity to the pyrophyllite interface, dropping to zero with only a very small increase in distance) but a number were found to have been run for excessive durations to varying degrees.

As previously mentioned, two solutions to Fick's second laws were solved for the concentration/distance data obtained. It was in situations where runs were run for longer than ideal that this procedure was particularly useful. By solving the law for two sets of boundary conditions (by considering the source phase differently) it was possible to ensure that the diffusion parameters obtained were realistic – i.e. they had been determined by two independent methods. In every case, the two methods gave the same answers.

Figure 38 to Figure 46 show concentration/distance plots for each of the successful runs. Analyses points are shown as blue dots with error bars in both the y-direction (concentration) and x-direction (distance from the pyrophyllite interface). In cases where error bars are not clearly visible it is due to the fact that they are smaller than/of similar size to the points. The solutions to Fick's Second Law for each dataset are shown as a red line. The calculated value of the diffusion coefficient associated with this solution is also shown along with the physical parameters of each run. In cases where multiple readings were recorded on a single grain, the multiple values have been averaged and one point is shown with the distance corresponding to the centre of the grain. The reason for doing this is to prevent multiple readings at a similar distance from skewing the non-linear regression fitting process.

Figure 46 which shows the concentration/distance plot for run VGB18 differs from those which precede it as a grain close to the spinel/pyrophyllite interface has recorded a concentration of approximately 4000ppm of H. This has then caused the fitted solution of Fick's law to intersect the concentration axis at a very high value. There is a significant chance that this concentration is metastable and was caused by the grain's very high proximity to the interface. As very few readings were obtained from this capsule and as there are no other grains at a similar distance to the interface, this result should have a relatively low degree of confidence attached to it.

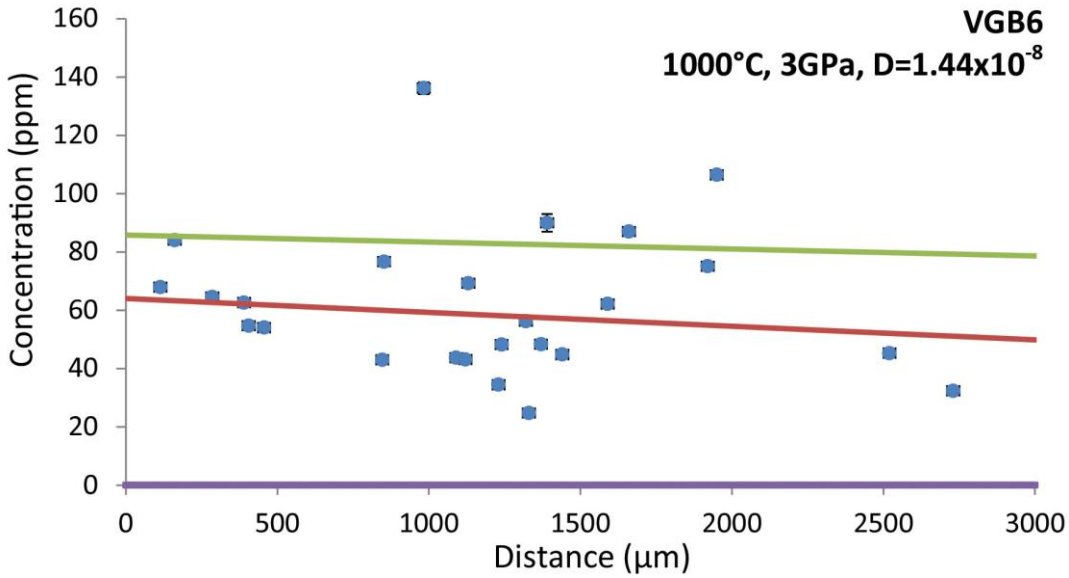

Figure 38: Concentration/Distance Plot for Run VGB6

Data and model fit. Details as in Figure 37

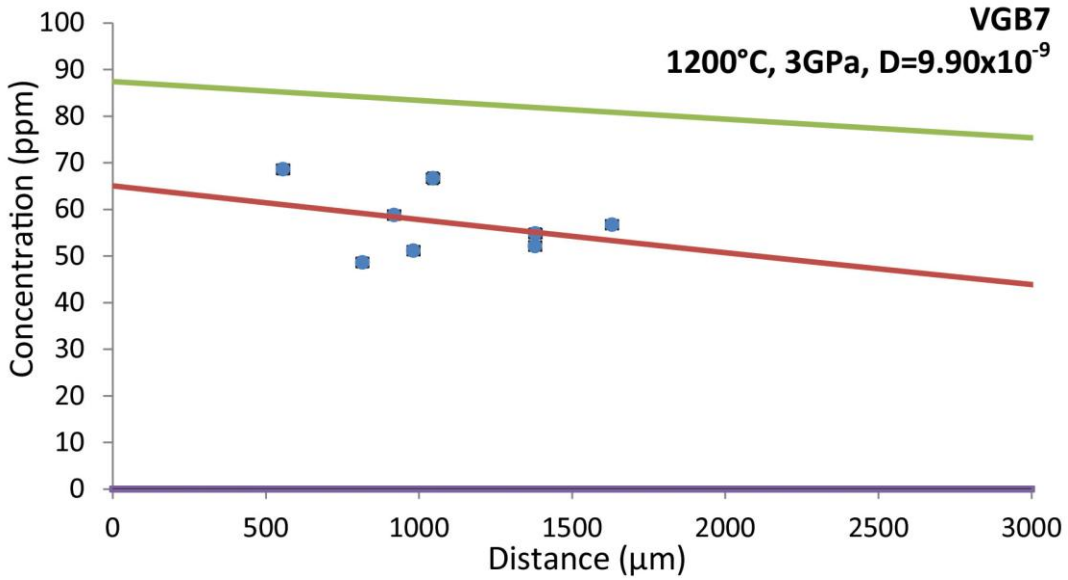

Figure 39: Concentration/Distance Plot for Run VGB7

Data and model fit. Details as in Figure 37

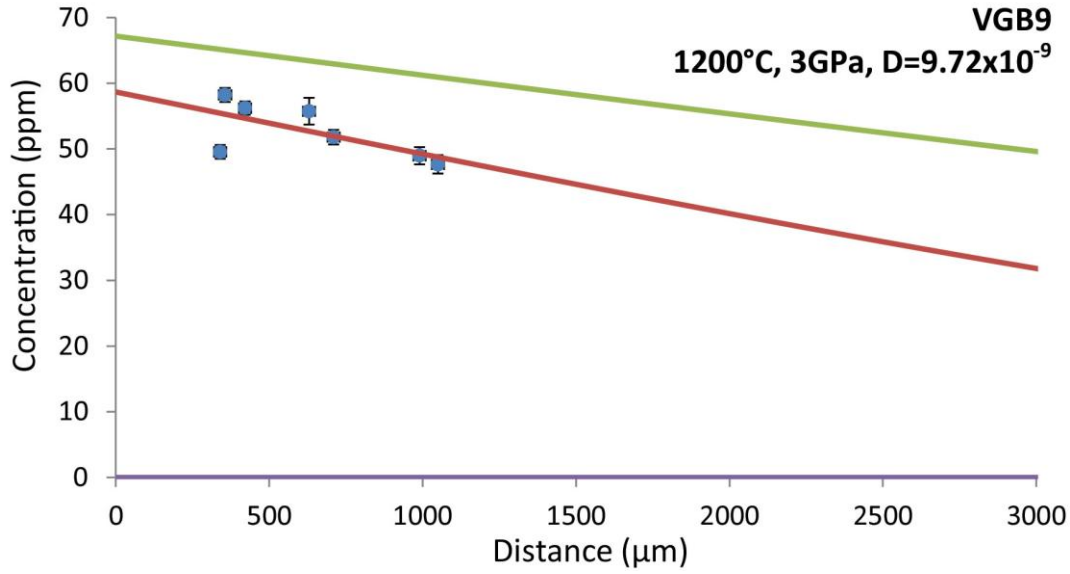

Figure 40: Concentration/Distance Plot for Run VGB9

Data and model fit. Details as in Figure 37

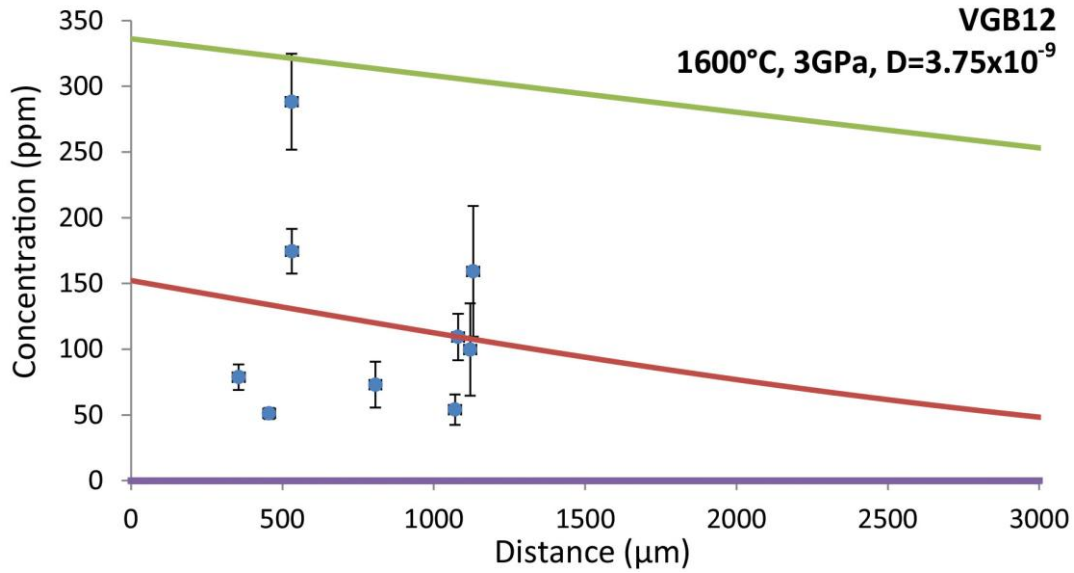

Figure 41: Concentration/Distance Plot for Run VGB12

Data and model fit. Details as in Figure 37

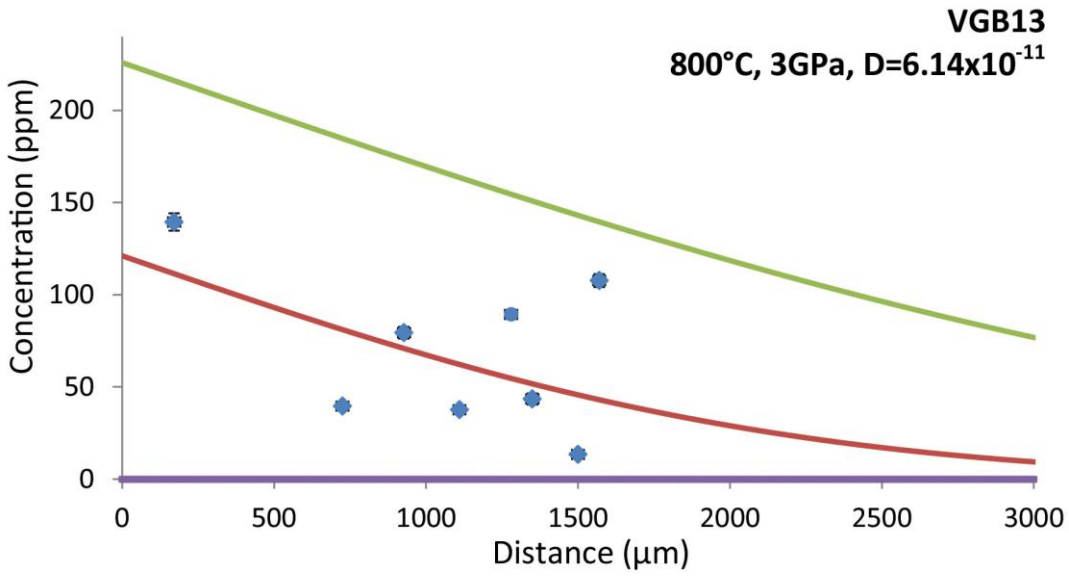

Figure 42: Concentration/Distance Plot for Run VGB13

Data and model fit. Details as in Figure 37

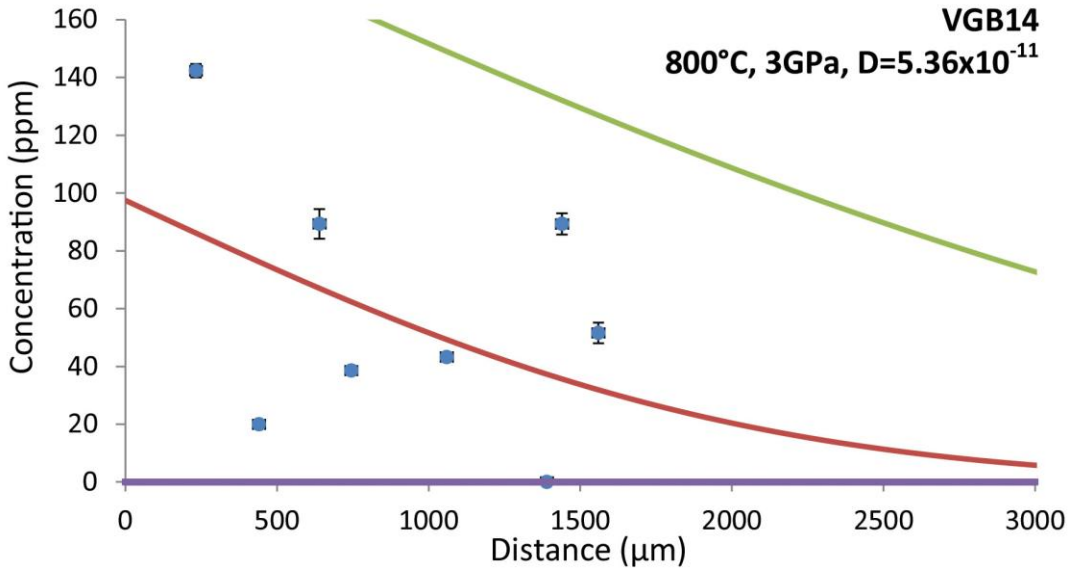

Figure 43: Concentration/Distance Plot for Run VGB14

Data and model fit. Details as in Figure 37

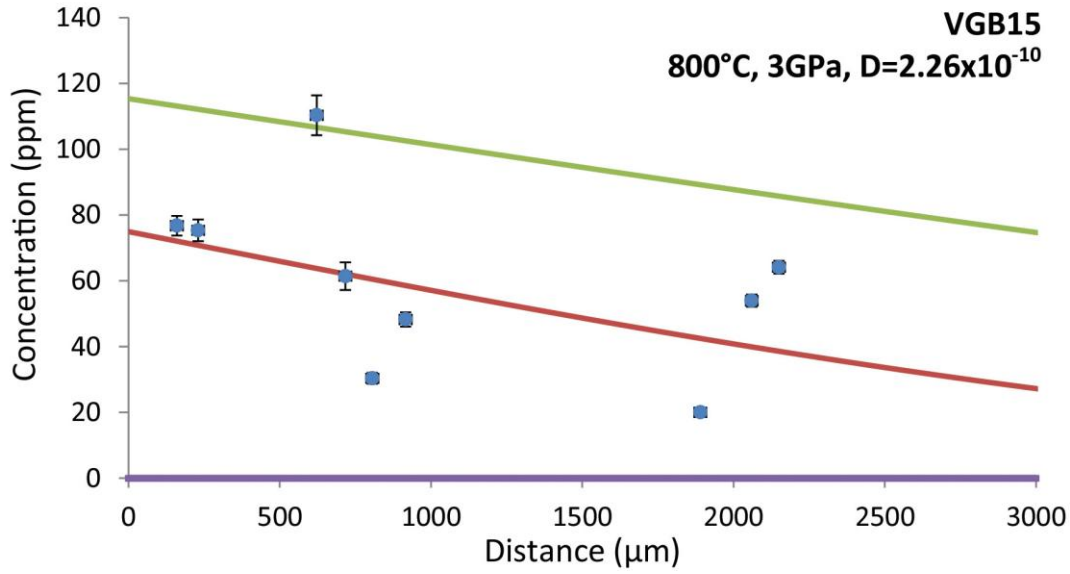

Figure 44: Concentration/Distance Plot for Run VGB15

Data and model fit. Details as in Figure 37

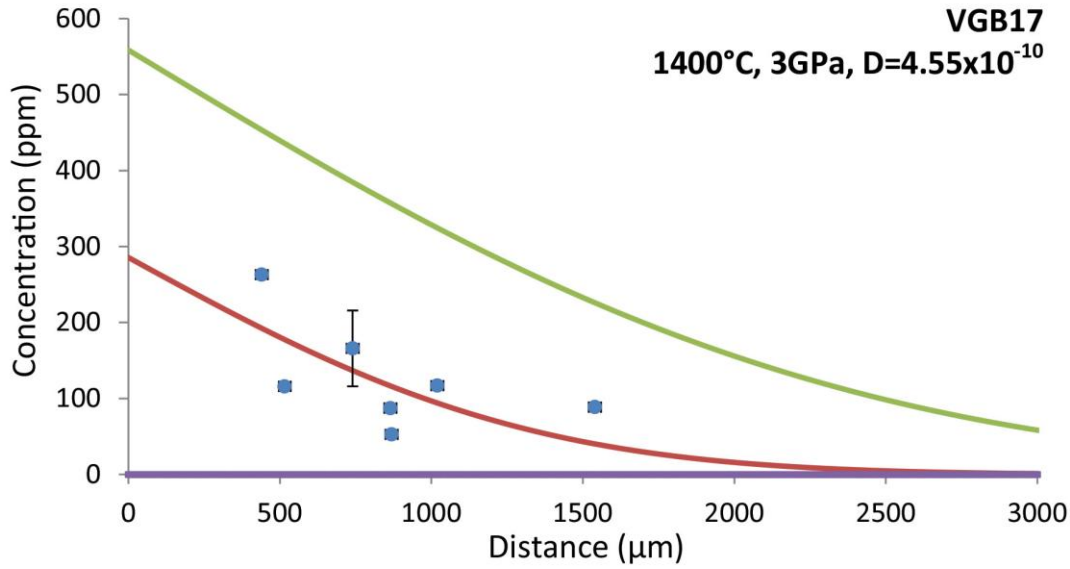

Figure 45: Concentration/Distance Plot for Run VGB17

Data and model fit. Details as in Figure 37

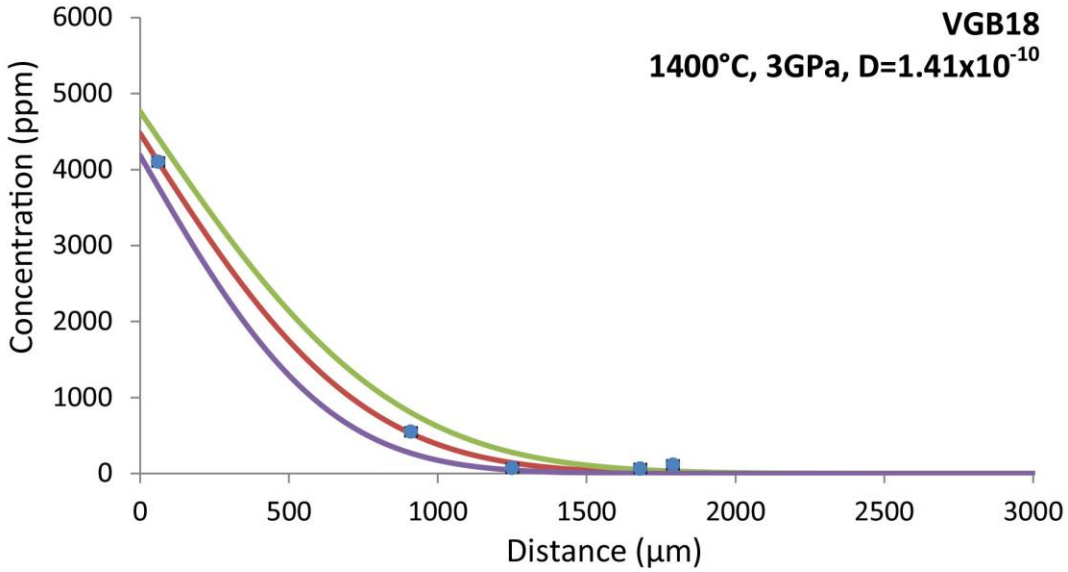

Figure 46: Concentration/Distance Plot for Run VGB18

Data and model fit. Details as in Figure 37

3.6.2.5 Unsuccessful Runs & Runs Not Analysed

3.6.2.5.1 VGB8

Run VGB8 was analysed but did not produce a diffusion coefficient. Figure 47 is a concentration/distance plot of the data obtained.

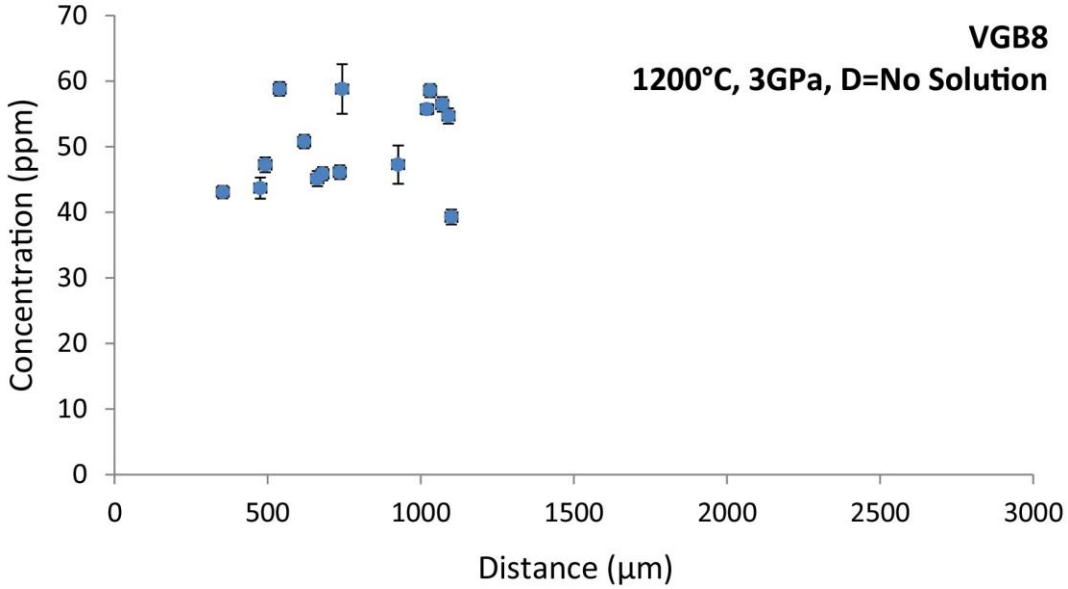

Figure 47: Distance/Concentration Plot for run VGB8

Points show no discernible pattern and as such it was not possible to fit a diffusion law to them. Thus, diffusion parameters could not be determined from this run.

As can be seen, the points are distributed in an essentially random fashion. In order for a diffusion law to be fit to the data there must be a decrease in concentration values as distance from the interface increases. As this is not the case for this data, the fitting software is unable to determine a solution to the diffusion law.

The likely explanation for this essentially random variation in concentration values within the capsule is that the run may well have been run for a significantly longer duration than it should have. As previously mentioned, this is in some ways inevitable in investigations of this nature as the speed of diffusion is not known (as this is what is being measured). Thus, whilst estimates can, and indeed were, made for the likely duration needed for a measurable diffusion profile to form, in this case the estimate was too high with the result that all of the grains measured took on a significant concentration of H thereby destroying an diffusion profile which may have formed earlier on. A second factor which may be significant is an unfortunate distribution of olivine grains (see Figure 48). Almost all of the grains which were present were in the half of the capsule which was closest to the pyrophyllite. This was simply a case of bad luck as it cannot be known which grains will be exposed during sample preparation (the surface which is exposed by sawing the capsule in half is essentially a random plane through the capsule). As a result, there are no readings in positions where low concentrations would be expected and as such, there is no tending towards zero in the diffusion profile.

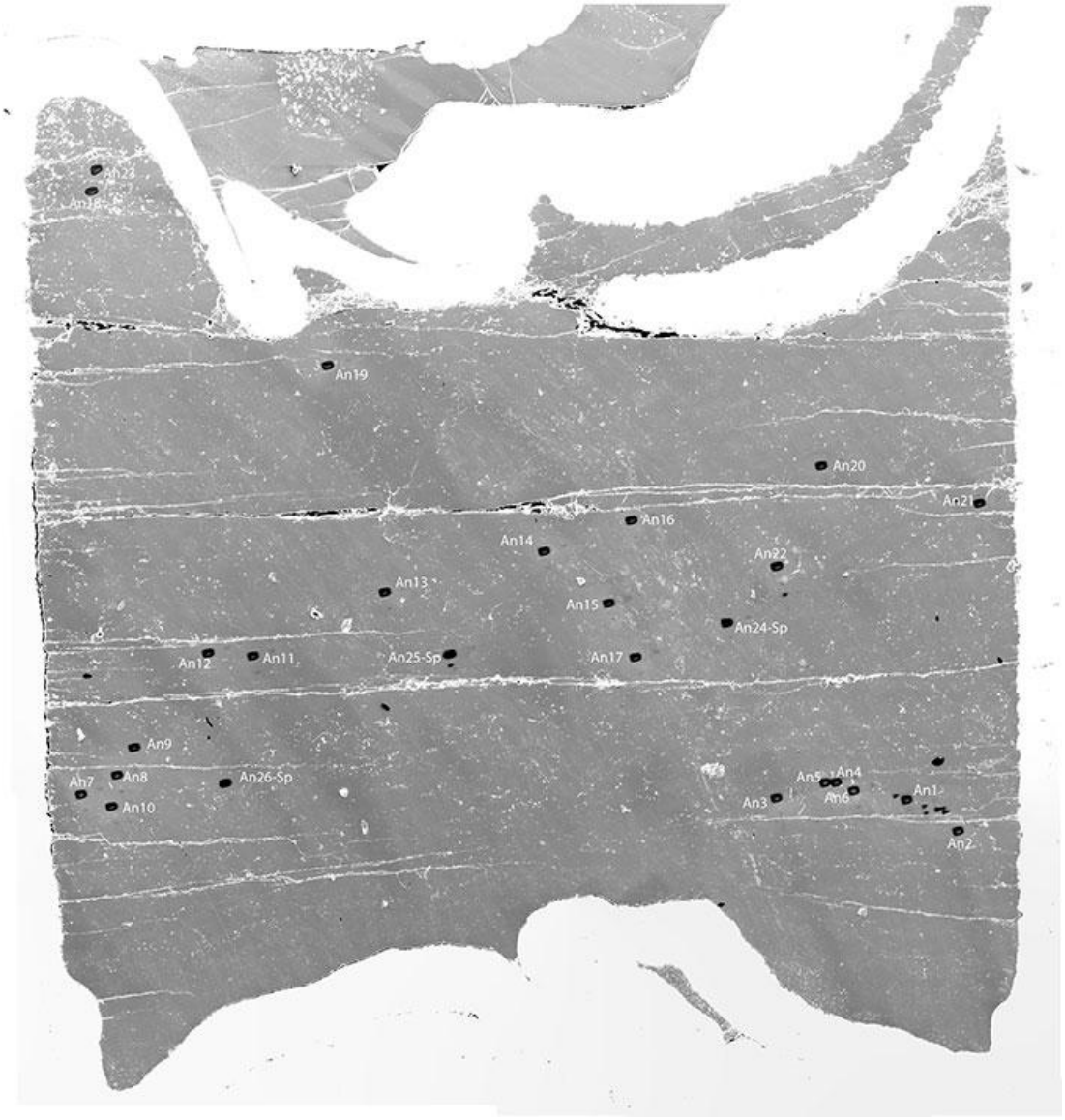

Figure 48: SEM Image of VGB8 showing Analysis Points

The majority of analysis points are towards the pyrophyllite end of the capsule. There were relatively few olivine grains exposed in VGB8 and of those few, a number were of significant size. As such, multiple analysis points were placed upon them. Once grains with multiple readings on had had their values averaged, there were fewer readings to plot. This, combined with the excessive duration of the run and the bunching of grains towards the pyrophyllite end of the capsule, resulted in the poor data which was obtained. The width of the capsule is approximately 3mm.

3.6.2.5.2 VGB10 & 11

Runs VGB10 & 11 were very difficult to analyse as when they were placed into the ion microprobe and viewed under its reflected light microscope, there was a red layer across the sample which made the identification of olivine grains for analysis impossible. Furthermore, SEM images of the samples (see Figure 49) showed that there were relatively few olivine grains exposed in the section samples. Those grains which were present often showed a strange texture with many cracks present throughout the grain (see Figure 50). The origin of this texture is unknown but it is thought that it may well have resulted from the rapid heating and/or cooling of the capsule which was required at run temperatures of 1600°C. This rapid temperature change may have caused very rapid changes to the grain such as thermal shock or very rapid exsolution of either volatiles or other phases. The combination of the relative lack of exposed olivine grains and the strange morphology of the few grains which were present resulted in uncertainty as to the viability of analysing these runs. There was of course a significant time restraint in conducting SIMS analysis – only a relatively short amount of time was available in each analysis session. As a result, and given that VGB12 (which was run at the same temperature as runs VGB10 & 11, 1600°C), had been successfully analysed, it was decided that these runs would not be analysed. Given more time and funds it would be ideal to re-polish the surfaces of these samples and complete further analysis such that more diffusion coefficients could be obtained for runs at 1600°C.

Figure 49: Run VGB11 Showing Relative Lack of Olivine Grains

There are very few olivine grains exposed in this sectioned capsule which is representative of both runs VGB10 & 11. Furthermore, a red smear was found on the surface of the sample when it was viewed under the reflected light microscope of the ion microprobe. As a result, neither run was analysed by SIMS. The width of the capsule is approximately 3mm.

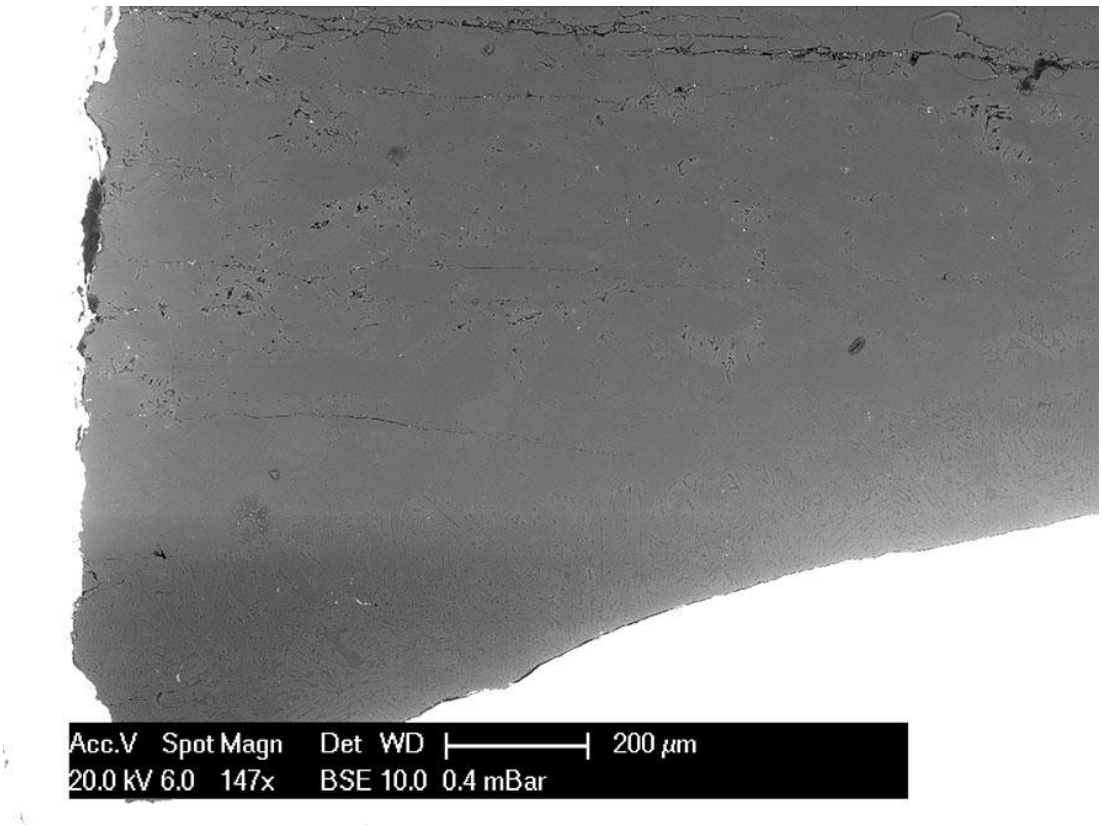

Figure 50: Olivine Grains in VGB10 showing Unexpected Texture

Relatively few grains are exposed in this sectioned capsule and, of the few which are exposed, many show an unexpected, cracked texture. It is suggested that this may have arisen due to the very rapid heating and cooling required when running an experiment at a temperature of 1600°C (see text for details). The width of the field of view is approximately 1.5mm.

3.6.2.5.3 VGB16

VGB16 was the only run of this experimental set which was aborted due to suspected issues with the piston cylinder apparatus. During the initial heating of run VGB16, unexpected and sudden variations in the voltage recorded by the thermocouple were observed. This was accompanied by an audible change in pitch of the normal operating noise of the transformer which powered the heating system. These observations indicated that there was a problem either with the furnace part of the experimental assemblage or that the thermocouple had broken. As the run had been intended to be one of long duration, it was decided that the run should be aborted instead of potentially wasting a large amount of time during which erroneous temperatures may have been recorded.

3.6.2.5.4 VGB19 & 20

Unexpected phases were discovered in experiments conducted at 650°C. SEM images of these runs showed a lightly coloured (in BSE imaging) phase not present in experiments conducted at higher temperatures (see
Figure 51). The duration of these experimental runs (VGB19 & 20) was approximately 71hours. An EDS spectrum obtained from a grain of this phase is shown in Figure 52. It should be noted that the EDS system is unable to detect elements lighter than C and so, if, for example, H forms a significant component of this phase it will not be shown in Figure 52. The spectrum shows a complex mineralogy with significant amounts of Si, Mg & Al present along with lesser amounts of Fe & Ca. The O content of the phase is estimated based on the abundance of other elements and the amount of O contained in their constituent oxides. It is possible that this phase is a hydrated reaction product of olivine and other capsule constituents, perhaps a chlorite. It is likely that it was able to form as a result of the long run durations and low temperatures of VGB19 & 20 permitting reactions to take place which would not have been stable at higher temperatures or would not occur without significant amounts of time. These runs demonstrate a limit to the conditions at which experiments can be run with this setup. The presence of this phase means that the runs could not be analysed to give valid diffusion data as this phase may well preferentially take on H as compared to olivine. This would mean that sinks with different affinities for H would be present within the same capsule and any measurements taken from this phase would not be directly comparable with olivine grains which have not been involved in a reaction. If these experiments were to be repeated in future, they would first be run with shorter durations. Whilst this would cause a steep diffusion profile it might well still be possible to obtain diffusion data from such a scenario.

Figure 51: BSE SEM Image of Capsule VGB20 showing unexpected phase

Spinel and olivine grains can clearly be seen in the main body of the capsule with the spinel forming the dark background material and olivine forming slightly lighter grains. The lightest grains are the unexpected phase. The width of the capsule is approximately 3mm.

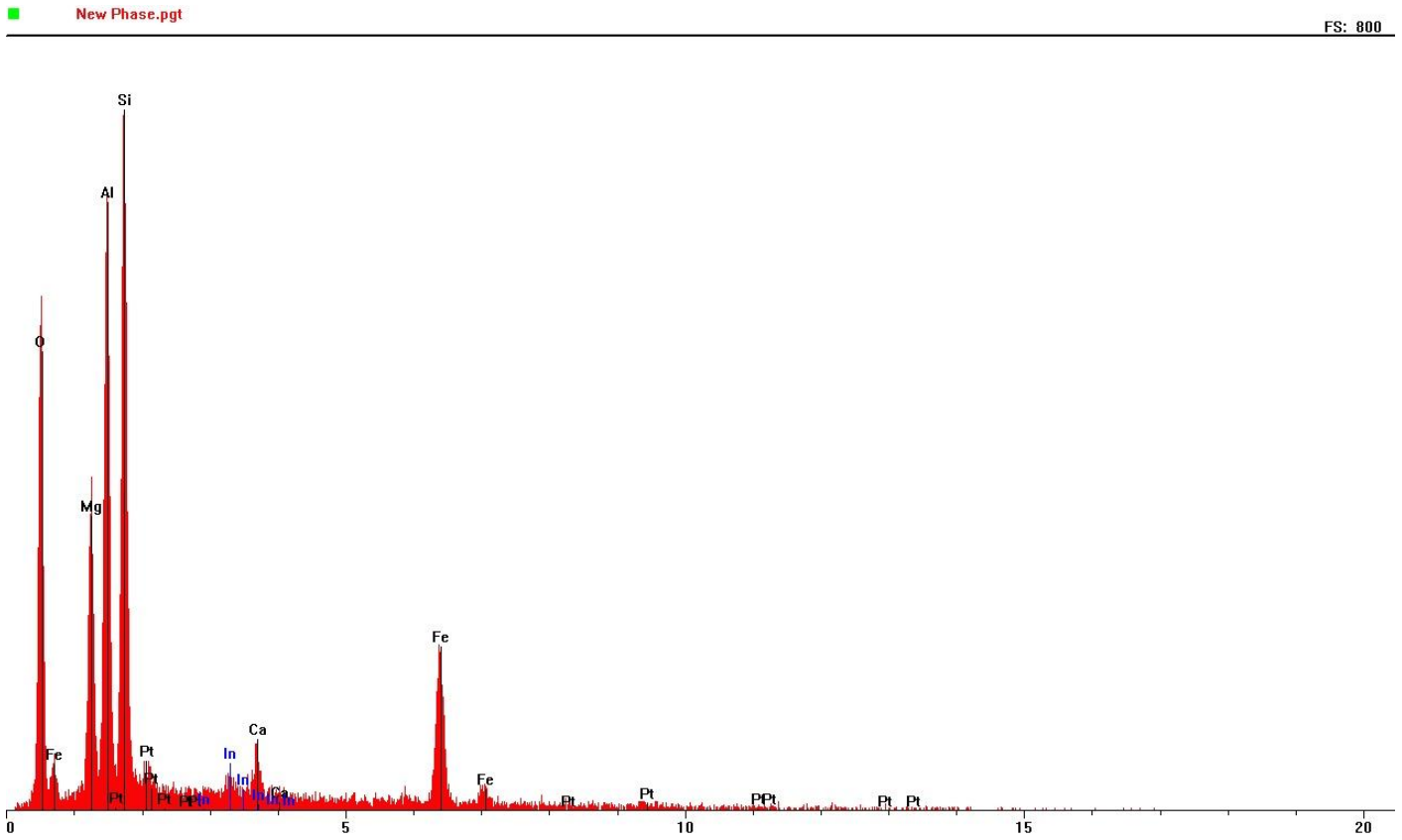

Figure 52: EDS Spectrum of Unexpected Phase Discovered in Runs VGB19 & 20

The phase is evidently a reaction product of olivine and Mg-spinel and is also likely to be hydrated. It was most likely able to form owing to the low temperature (650°C) and long duration (~71 hours) of runs VGB19 & 20. It is suspected that the phase may be chlorite, ideally EBSD analysis would be performed to confirm this.

3.6.3 Summary of All Run Results

Run ID	Temp (°C)	Pressure (GPa)	Duration (mins)	Diffusion Coefficient (m^2s^{-1})	Effective Concentration (ppm)
VGB4	1000	3	90	$3.01x10^{-11}$	144
VGB6	1000	3	66	$1.44x10^{-8}$	64
VGB7	1200	3	43	$9.90x10^{-9}$	65
VGB9	1200	3	30	$6.72x10^{-9}$	59
VGB12	1600	3	20	$3.75x10^{-9}$	152
VGB13	800	3	392	$6.14x10^{-11}$	121
VGB14	800	3	394	$5.36x10^{-11}$	98
VGB15	800	3	402	$2.26x10^{-10}$	75
VGB17	1400	3	20	$4.55x10^{-10}$	286
VGB18	1400	3	20	$1.41x10^{-10}$	4480

Table 5: Summary of Volatile Diffusion along Grain Boundaries Run Results

This data can then be plotted into an Arrhenius diagram (see section 1.3.2.3.1 The Effect of Temperature – General Case) showing the temperature dependence of grain boundary diffusion of H (Figure 53).

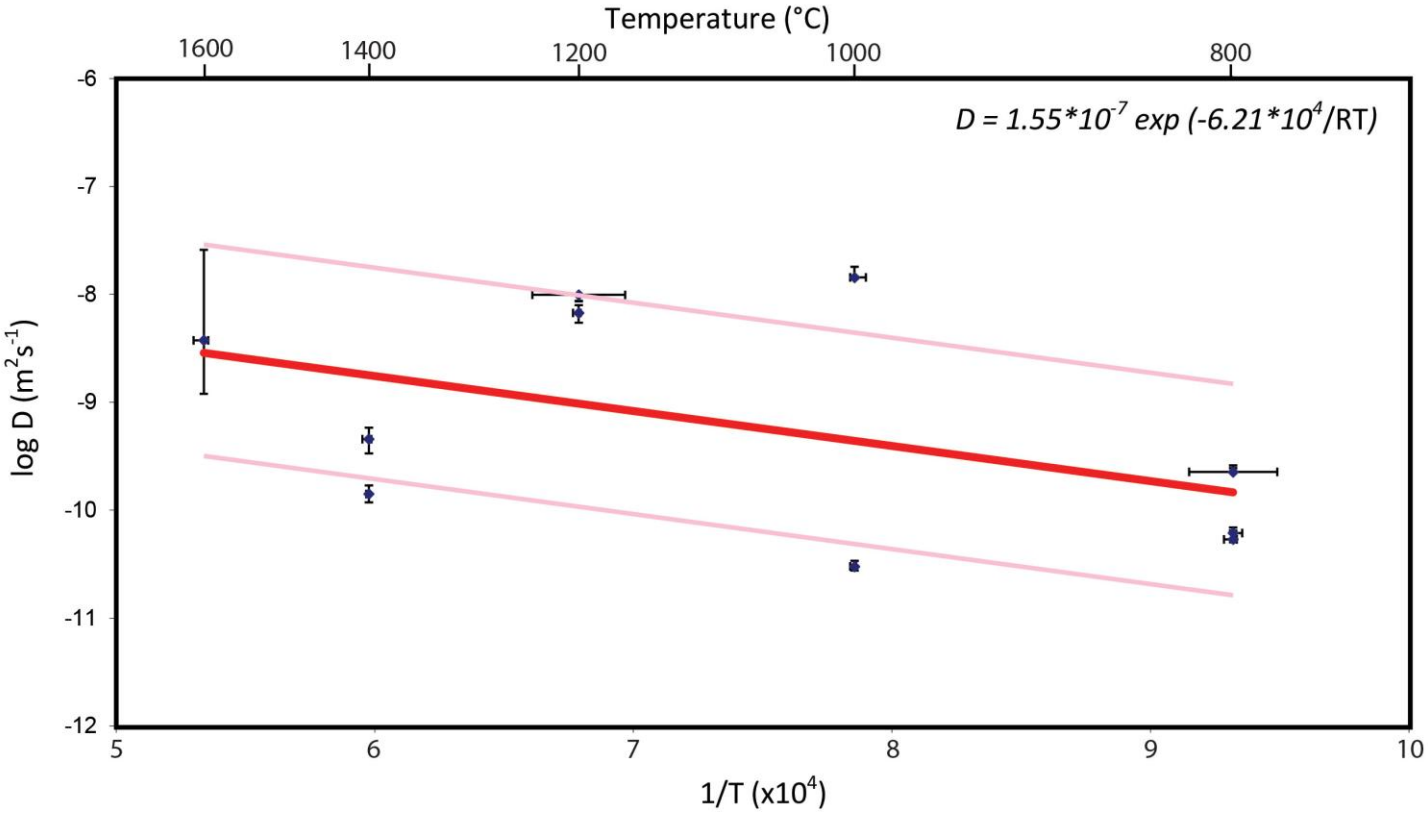

Figure 53 : Arrhenius Diagram showing Temperature Dependency of Grain Boundary Diffusion of H

A decrease in diffusivity with temperature is observed. The variation in temperature dependency observed is relatively small given the size of the temperature range. There is close agreement between all runs at the same temperature with the exception of runs at 1000°C. Given more time and funding it would be very useful to conduct further repeat experiments to improve the quality of the fit of the Arrhenius equation. The pair of pink lines represent the position of the 95% confidence bounds based upon the individual fittings carried out.

3.7 Discussion & Interpretations

3.7.1 Discussion of Factors which could affect Data

3.7.1.1 Diffusion of H within Olivine Grains

As olivine grains were used as a sink phase in this investigation, it is important to consider the movement of H from the grain boundaries surrounding the grain (along which it has been moving) to the point within the grain where the reading of H concentration is taken. An ideal way to analyse this is to look at large grains on which a number of analysis points can be placed. By making a first approximation of a "map" of H contents within the grain it should then be possible to start to understand how H moves from the boundaries towards the centre.

On a number of occasions olivine grains were found which were large enough to have several analyses conducted on them. Where this was possible multiple analyses were taken in an effort to understand the mechanism by which H entered olivine grains. This information is valuable both in terms of understanding how H moved around the capsule and how it moved within grains to the points at which its abundance was measured.

A large grain which was ideal for this purpose was found in run VGB7 (see Figure 54). In total, 11 analyses were performed on this grain. Analysis points were spread across the grain in an attempt to understand the mechanisms by which H entered the grain and also the diffusive process within the grain (which allowed the H to reach the individual points where analyses were recorded).

Figure 55 shows a histogram of H concentration readings taken from this grain. When this is viewed in combination with Figure 54 it becomes clear that the distribution of concentrations throughout the grain is rather complex. Whilst some aspects of the distribution are as one might reasonably expect (e.g. the lowest value concentration point is the most central - the furthest away from the grain boundaries surrounding the grain), other aspects are less expected (e.g. the presence of the second highest concentration analysis point in close proximity to the highest value point). This fairly random distribution is most likely a reflection of the internal structure of the olivine grain. The position of linear and planar defects within the grain, as well as the abundance and relative positioning of point defects will determine the ability of H to move to any given point within the grain. It is likely that those analysis points which sit on planar or linear defects will display the highest readings as H will be able to move along them in a way which is very similar to motion along a grain boundary. One factor of particular importance in the study of this particular grain is its size. As already

mentioned, this is a particularly large grain which is approximately 600µm in its largest dimension. In comparison, the largest dimension of many of the grains analysed here was of the order of 100 - 150µm. The fact that points within the very centre of this large grain have high concentrations which are similar to those at the edges is suggestive of the fact that those points in the centre of the grain are at equilibrium with the H contents at the grain boundary. Points which have anomalously low concentrations within the centre of a grain are likely to not be served by defects which could otherwise effectively deliver H to them. The chances of this occurring are much larger in a large grain as the outer portions of the grain are likely to have protected the inner portions of the grain from defect forming processes. Conversely, defects, particularly those caused by grinding, are likely to be more pervasive in smaller grains as the smaller size offers less resistance to their formation. As a test of this hypothesis, in some cases where grains of a suitable size were discovered, more than one analysis point was placed upon them to check the consistency of H distributions within them. These grains had a typical largest dimension on the order of 100 - 150µm and so were representative of the majority of grains. An example of such a grain is shown in Figure 56. Here, 3 analysis points (labelled An4, 5 and 6) were placed upon a single grain. Point An6 is considered to be unreliable and was rejected as, during post-SIMS SEM analysis, it was found that it penetrated the grain boundary and so was likely to give an anomalous result (see section 3.4.3.2 Analysis Point Defect Check). The concentrations recorded at points An4 and 5 were, respectively, 47ppm and 44ppm and as such were very consistent. This exercise was repeated many times and, in the vast majority of cases, a similar consistency was found. As such, a high confidence is attached to the belief that all olivine grains were able to quickly take in H from their grain boundaries, most likely due to pervasive defects within them. As such the H contents recorded from them can be relied upon.

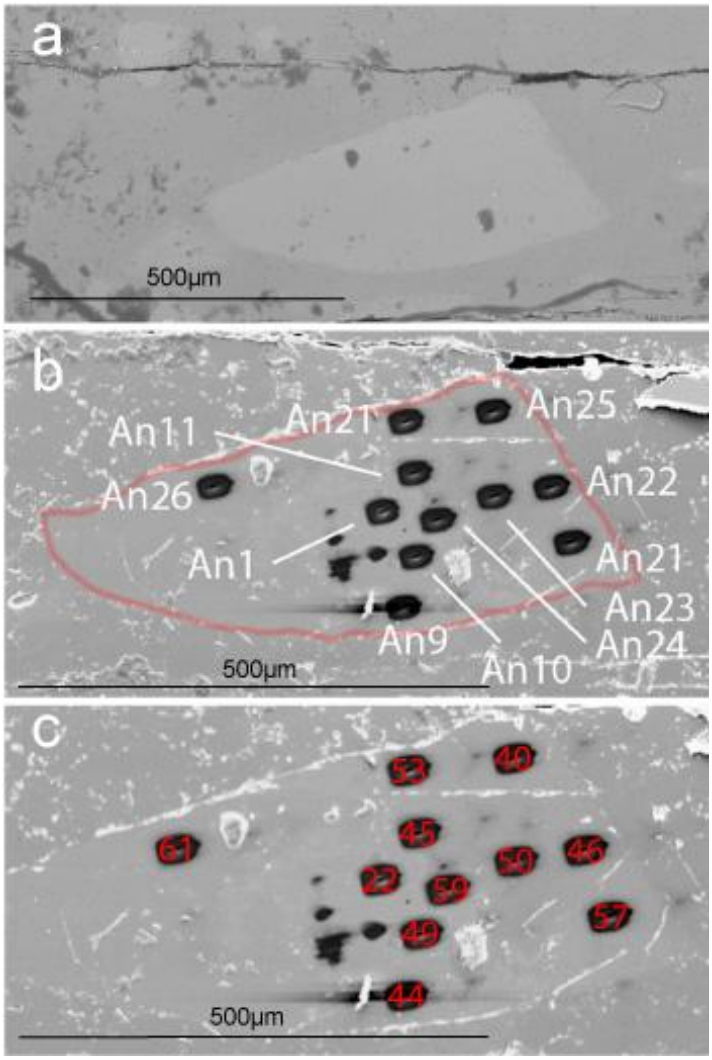

Figure 54: Large Olivine Grain with Multiple Analysis Points – VGB7

Multiple analyses were performed on a large olivine (approximately 600µm along its largest dimension) found in run VGB7. Image a shows the grain as it was sectioned and exposed on the surface of the polished sample. Image b shows the grain with its boundary highlighted and the 11 analysis points with their analysis ID numbers shown. Image c shows the grain with the H abundance values shown at each analysis point. In general there is relatively little variation in concentrations suggesting that the grain has fully equilibrated with the H which has reached it via grain boundary diffusion during the run. The point furthest from the edge of the grain with a concentration reading of 22ppm may indicate a diffusion gradient within the grain as the surrounding grain boundary acts as the source and the grain being the sink with diffusion occurring via the lattice mechanism.

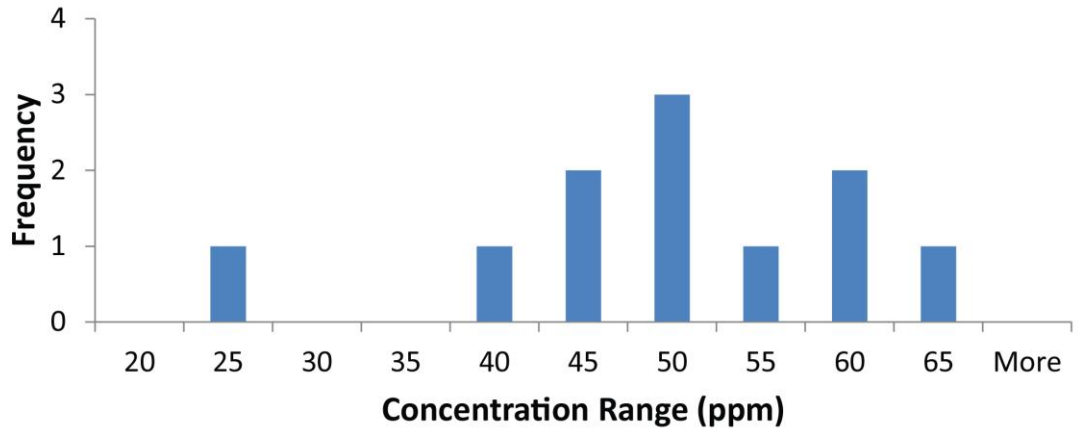

Figure 55: Histogram showing Frequency of Concentration Values Recorded from Large Grain in VGB7

There is a significant range of concentrations recorded within the grain but most values are centred upon concentrations of 50 – 55ppm. The lowest value of 22ppm represents the very centre of the grain and is a distance of approx. 150µm from the edge of the grain. This suggests that grains with a size of less than 250µm will show very little gradient in the concentration of H across them with the implication that they are fully equilibrated.

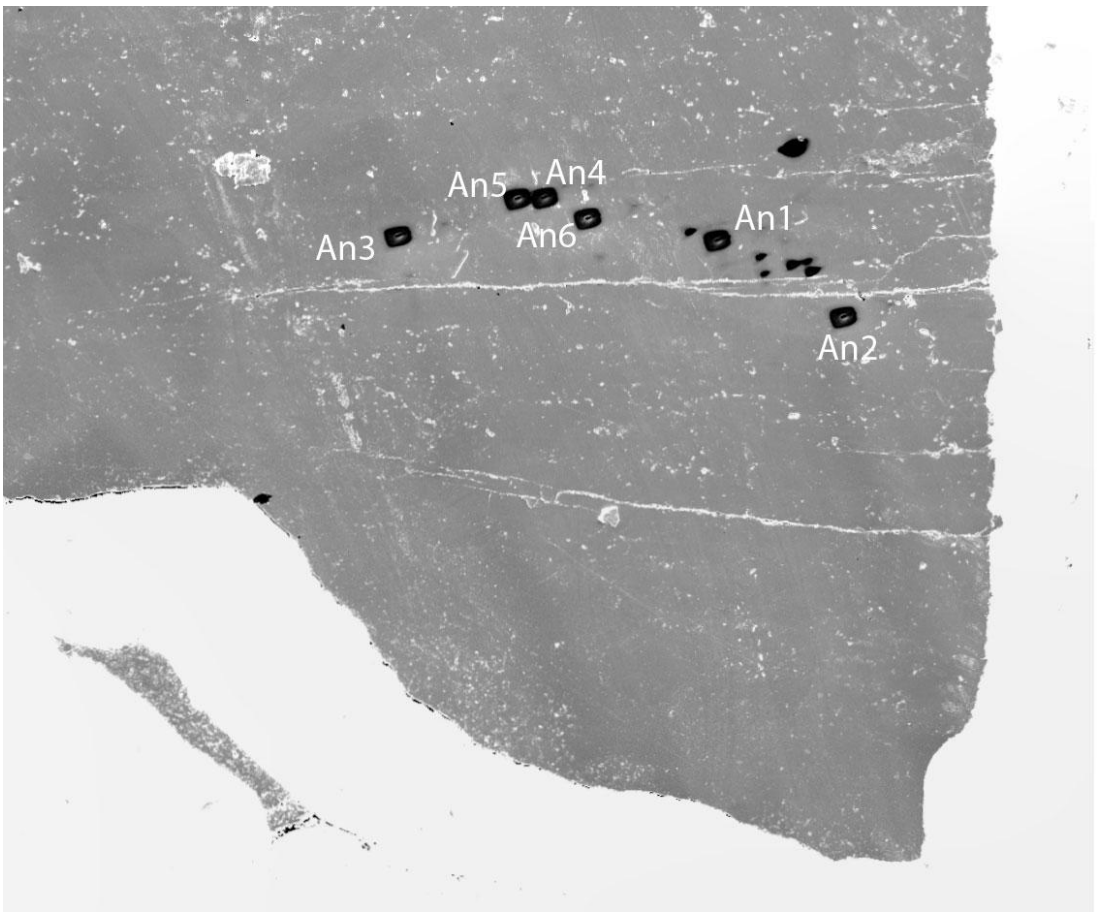

Figure 56: Close up of Analysis Points in VGB8

Analysis points An4,5 and 6 all lay on the same grain. An6 is discounted as it cuts the grain boundary but An4 and 5 are considered valid readings. An4 has a concentration of 47ppm of H and An5 has 44ppm. The width of the field of view here is approximately 1.5mm.

3.7.1.2 Diffusion through the Pyrophyllite Layer

The pyrophyllite layer has a thickness and so there is a certain amount of diffusion that must occur in order to get the H from the particular point at which it dissociates with a given formula unit of pyrophyllite to the interface with the spinel from which concentrations and so diffusion is measured. However, this dissociation should take place rapidly as the capsule is heated above approximately 600°C. This would then cause a reservoir of free H to be created which would then diffuse from the interface with the spinel into the remainder of the capsule. As such, the diffusion of H within the pyrophyllite is not considered to be a process which will greatly affect the degree of grain boundary diffusivity measured by the experiments.

As previously mentioned the effective position of the interface between the pyrophyllite and the spinel may change with time as more and more H leaves the pyrophyllite and begins travelling along the grain boundaries. The extent to which this occurs is not well known. It is

believed, from previous experience with experiments of this nature, that the size of this effect is likely to be small and most likely within the 20μm value used in calculating the error in diffusion coefficients. As such, any movement of the position of the interface has been accounted for.

3.7.1.3 Grain Boundary Fluid Phases

One area of particular concern in the measurement of grain boundary diffusion of H was that the H released from the pyrophyllite might form a grain boundary fluid phase which would potentially allow diffusion at a different, quite possible significantly faster rate than grain boundary diffusion in the absence of a fluid phase. In order to determine whether or not this had happened, a close examination of grain boundaries throughout capsules was undertaken to see if a quenched grain boundary fluid phase was present. At no point was such a texture found down to the micron scale at which grain boundaries were imaged. Furthermore, the values of diffusion coefficients calculated within this investigation are consistent with what would be expected based on previous studies. As such, it is not believed that grain boundary fluid phases formed or affected diffusivity.

3.7.1.4 Depth Profiling of H contents of Olivine

When performing SIMS analysis of H contents of olivine grains, a number of individual readings of abundance were taken and averaged to form the reported value. The method for performing such analyses required the rastering of the area of the analysis with the ion beam prior to measurements being recorded. As more and more analyses were recorded material was ablated by the ion beam causing the position of each sampling point to be deeper within the sample. This proved useful in removing any surface impurities from the analysis site but also had a secondary function; showing the variation of H contents within the olivine with depth through the grain. As previously stated, the section which was cut and polished through any given experimental capsule was essentially random as there was no control in the specific rotation of the capsule when it was mounted for cutting and also as there was no specific value for the distance through the capsule the cut was made at – although it was attempted to cut capsules approximately half way through. As such, it was not known to what extent any particular olivine grain was exposed. Whilst it was entirely possible that a grain was cut halfway through its thickness so that its maximum cross sectional area was shown, it was also possible (indeed more likely) that the cutting of the capsule meant that the grain was cut off centre and so showed a section with a less than maximal cross sectional area. This is significant as a grain which has been cut off centre will therefore have less depth through which analyses can be made before one intersects the grain boundary on the far side of the grain which would be expected to show significantly higher levels of H than the grain itself. In order to examine whether this had happened or not, each analysis site had all

of its readings reviewed to see if there were any notable inconsistencies in the readings recorded (see Figure 57).

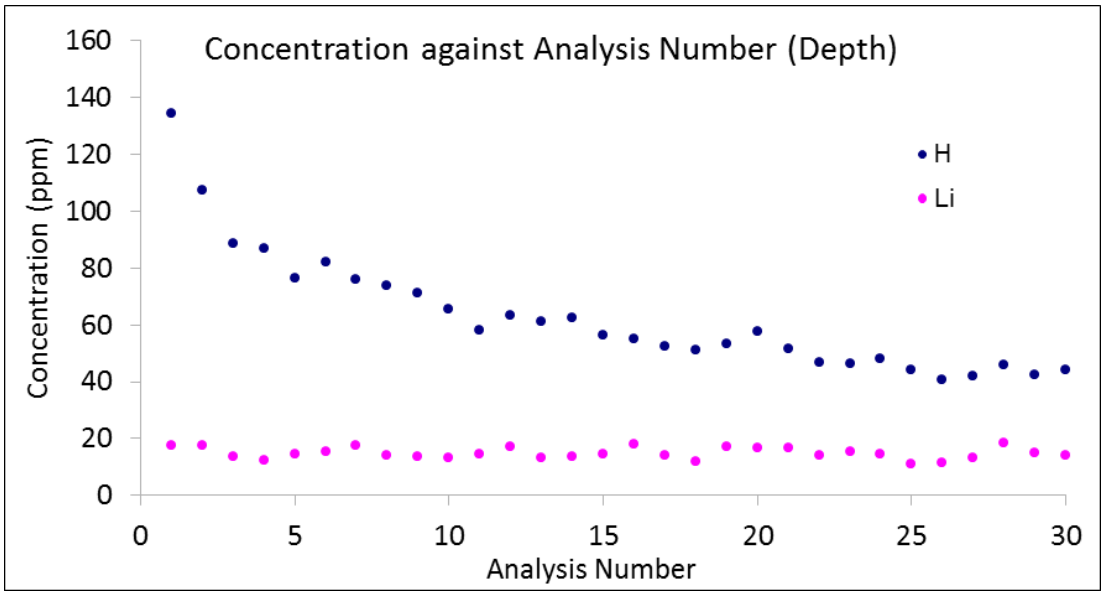

Figure 57: Progressive Concentrations Recorded from Multiple Analyses at a Single Site

Initial analyses are high as the ion beam progressively removes and analyses H on the surface of the grain. Subsequent analyses come from deeper in the grain and are considered more reliable. The reported value for this analysis point is calculated from the mean value of the final six analyses.

3.7.1.5 Capsule Edge Effects

During analysis sessions it was found that olivine grains close to the capsule edge (i.e. the sides of the capsule perpendicular to the H source) often had higher levels of H contained within them than would otherwise be expected given their distance from the pyrophyllite. In the light of this observation it was decided that the distance of a point from the nearest capsule edge would be recorded along with its distance from the pyrophyllite/spinel interface.

It is a non-trivial task to make a clear, quantitative analysis of the strength of the capsule edge effect. It was essential that this was done as it is a natural tendency to notice anomalous points and disregard those whose behaviour is closer to what is expected. By completing a quantitative analysis, the strength of any edge effect could be determined. Comparisons between runs are difficult because runs were completed over a range of different temperatures and comparison within a given run is complicated by the diffusion gradient between the pyrophyllite/spinel interface and the far end of the capsule. In order to make a proper measure of any capsule edge effect, a run from which many readings had been taken was selected – VGB6. The concentration value of each point was corrected, based on the calculated solution to Fick's Second Law so that the value was as it would be if it were a distance of 390µm from the interface (this distance was chosen as there was a point at 390µm which sat perfectly on the solution line – as such it formed a suitable basis from which to make the calculation). Figure 58 shows a plot of these corrected

concentrations against distance from the edge of the capsule. A broadly negative correlation can be clearly seen but the correlation is by no means strong. Whilst there is a little evidence to support an edge effect (i.e. higher concentrations at low distances from the edge of the capsule), it is not particularly strong and as such no corrections of this nature have been made to the data presented here. It would however be a very useful avenue of future research to determine how strong capsule edge effects might be, particularly with regard to volatiles with high mobilities.

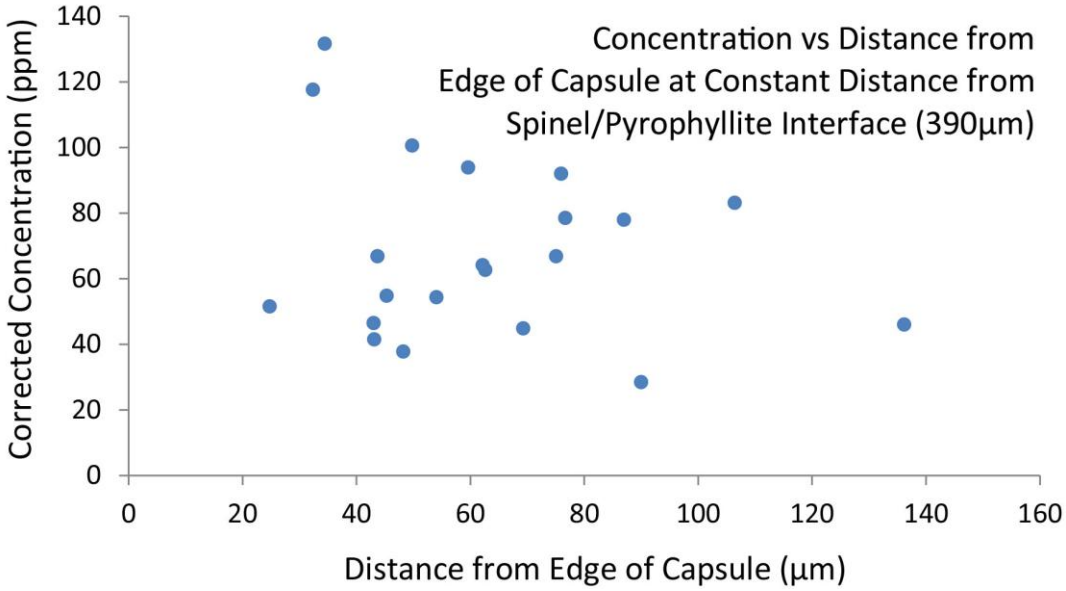

Figure 58: Concentration versus Edge Proximity Plot

There is a broadly negative correlation between distance from the edge of a capsule and the concentration recorded. However, the correlation is not particularly strong. Here, concentrations have been recorded to correct for distance from the pyrophyllite interface and all points are from the same run (VGB6).

3.7.1.6 Effect of Increased Diffusion Distance along Grain Boundaries

It is expected that diffusion along grain boundaries will be along a greater distance than the straight line route which would be measured in lattice diffusion. In her work of 2010, Demouchy [62] corrects for this effect using the following equation:

Equation 16: Grain Boundary Diffusion Distance Correction used by Demouchy

$$x_{\max} = \frac{x_{\min}}{d}\frac{d}{2}\pi$$

This equation considers a mass of perfectly spherical grains along the boundaries of which the diffusant is travelling. Here, x_{max} is the maximum distance possible for diffusion (i.e. along grain boundaries) and x_{min} is the minimum (i.e. straight line) distance. d is the diameter of grains. Having calculated a value for x_{max}, Demouchy then takes a mean of x_{max} and x_{min} and uses the result as the distance in the characteristic diffusion distance equation.

Whilst this method offers some form of approximation of the increased distance that a diffusant travelling along a grain boundary would experience, it is not used here for a number of reasons.

Firstly, the method essentially applies a multiplication of 1.27 to the measured distance. Whilst this may closely reflect reality in some cases it is unlikely that it will in all cases. From studies of capsules with an SEM during this investigation it is clear that whilst grain sizes may be homogenous at the start of a run, they frequently do not remain so. Typically large grains may exist in some regions and significantly smaller grains in others. It should of course be remembered that the observed grain morphology will be the result of many factors – e.g. dynamic evolution of grain boundaries during runs, mechanical twisting/grinding caused by the pressurisation and de-pressurisation of the run (see section 3.7.1.7 Dynamic changes to Diffusive Pathways during Experimental Runs). As such, the true degree to which grain boundary diffusion lengths are longer is very hard to know.

The second reason for not using this correction relates to the need to compare grain boundary diffusion to lattice diffusion. Fundamentally, in comparing the two one wants to know how much diffusant can travel to a given point in either regime. Thus, by not applying a correction factor for distance the grain boundary diffusion measured here is more comparable to lattice diffusion data. If the correction were applied and diffusion coefficients were calculated by the method described here (as opposed to the characteristic diffusion distance method as used by Demouchy which was not used here for reasons discussed previously), diffusivity would appear to be higher than it is thereby making the data potentially more unreliable.

Thus, whilst it may be ideal to perform a correction for the increased distance that a diffusant must travel in a grain boundary diffusion scenario it is not necessarily advisable to do so as an over-simplified method may introduce greater error and reduce how well diffusion data can be compared to data obtained in other scenarios. Grain size is of course an important factor and as such data should be reported as “at a given grain size”. It will be necessary to add a correction factor for grain size when applying the data obtained here to natural settings. However, by running experiments at the conditions characteristic of that setting a valid attempt can be made to understand that regime.

3.7.1.7 Dynamic changes to Diffusive Pathways during Experimental Runs

Previous workers have typically found that mineral grains put into experiments such as those being run here are different in shape and texture to those recovered at the end of runs. This process of annealing is common to many materials which are exposed to high temperatures and pressures as the material undergoes a process of equilibrating with its new environment. This process adds an extra layer of complexity to this investigation as when grains anneal thereby changing their shape so do their boundaries. Thus, in considering grain boundaries as a potential fast route for diffusion one must bear in mind their dynamic character as diffusion routes develop, close and change direction during the course of an experimental run. In addition to the annealing process which is likely to be slow and continue throughout a given run, one must also consider changes to grain boundaries which may be caused by mechanical changes to the high PT environment in which they sit. Specifically, such mechanical changes are likely to be of the form of stresses and strains imposed by deformation of the experimental capsule particularly during pressurisation, heating and cooling of run. In a natural environment this would be caused by processes such as convection and related tectonic forces. The timescale for such phenomena would of course be far greater than that of an experiment and there may be significant heterogeneity in the distribution and nature of the induced forces. It is useful to consider each of these three phases individually to assess the likely influence of deformation on GBD.

The initial pressurisation of an experimental run always took place prior to any heating and typically took approximately 20 minutes to complete. As this phase was completed at low temperature, it would be effectively impossible for any diffusion to occur. As such, the changes to grain boundaries during initial pressurisation are not important as those changes are already in place and completed prior to heating beginning. However, of potentially greater importance is the deformation which occurs when pressure is applied during a run when an experiment is at high temperature.

Over time, experiments using a piston cylinder apparatus lose pressure, normally as a result of the assemblage settling but also potentially due to any leaks (however small) in the pressure system. In order to overcome this loss of pressure it is necessary to apply more pressure as the run continues. In the case of the experiments run for this investigation, this was done using a hand pump at varying intervals when the experiment was checked. Short duration experiments were supervised at all times whereas those of a long duration were typically checked once every several hours once they had settled and were running smoothly. The longest intervals between checks were normally overnight. When using the hand pump to increase the pressure being applied to the experimental capsule care was always taken to apply the pressure as smoothly as possible but it was noted that on many occasions a creaking or cracking sound was heard as the Pyrex part of the assemblage

shifted in response to pressurisation. This shifting may have caused deformation to the capsule and therefore changes to the grain boundaries – potentially altering diffusion routes whilst diffusion was taking place. It is however unlikely that such deformation was particularly severe as if it was it would be expected that the capsule would fail. As such, there may have been changes to grain boundaries caused by the process but the degree of these changes is likely to be limited.

Once the run pressure had been applied, experiments were then heated up to the desired temperature. During this period the experimental assemblage and capsule reacted to the changes in temperature - it can be reasonably assumed that some deformation of the capsule took place during the process. As already discussed, the heating process took approximately 10 – 15 minutes depending on the temperature to be reached, of which a significant proportion of the time was taken up heating at lower temperatures – where very little diffusion would occur. At higher temperatures, particularly between approximately 600°C and 800°C, it was observed that the pressure being applied to the assemblage tended to drop off more rapidly than at other temperatures, both higher and lower. This is attributed to softening of the assemblage as it began to equilibrate to the increasing temperatures being applied to it. During this period it is highly likely that the softening and subsequent deformation of the assemblage caused a similar effect in the capsule, thereby changing the arrangement of grain boundaries and diffusion pathways. As diffusion would have been in the initial stages during this short period with dehydration of the pyrophyllite also beginning, it is unlikely that changes to grain boundary diffusive pathways would have had a large effect on the amount of diffusion measured at the end of the experiment. This is due mostly to the short duration of the heating period and the fact that the maximum periods of diffusion and deformation formed a small proportion of the period. It is of course worth noting that evolution of the grain boundary texture during heating is in itself not problematic as during the heating process only a small amount of diffusion will occur. Changes to grain boundaries during the stable part of the run or during cooling are potentially more problematic although in reality the whole apparatus was found to be very stable

Cooling is the final part of the run in which it is expected that significant deformation may have taken place. The act of quenching a sample typically took approximately 20 seconds to complete; hence diffusion can be considered to have been stopped practically instantaneously. As the quenching was performed a drop in pressure applied to the sample was recorded. To overcome this and ensure that the cooling was isobaric, pressure was applied with the hand pump so that the overall pressure was maintained at the level at which it had been for the duration of the run. Whilst this may well have caused deformation and altering of grain boundary diffusive pathways, it took place over a very small time period when diffusion was essentially being stopped instantaneously. Furthermore, the talc and

pyrex experimental assemblage had a considerably larger volume and were softer than the inner assemblage in which the capsule was located and as such will have taken up a significant proportion of any deformation. As a result this too should have had very little effect on measured diffusion.

Unfortunately it is not possible to analyse the effect that processes such as these might have when using the piston cylinder apparatusE so the extent of changes caused is not known. However, it is of course useful to bear in mind the potential for such changes, particularly as a possible explanatory mechanism for any unexplained measurements of textures which may be found.

Following the lines of logic outlined above, it is not expected that deformation during the pressurisation, heating and cooling phases had a significant effect on measured diffusivity. However, it is less clear if re-pressurisation during runs and annealing of grains would have had a significant effect. It is expected that both processes would have disrupted diffusive pathways but that the closing of certain pathways may well have been equalled out by the opening of others. Whilst this added complexity makes the understanding of such work more difficult it is in many ways a useful additional factor as it may well, in some regards, mirror natural processes more fully.

This process of deformation during an experimental run is likely to operate in all sets of experiments using the piston cylinder apparatus (along with other high pressure apparatus). As such, this discussion is equally applicable to the other experimental programs within this investigation.

[E] Such analysis is not possible when using the piston cylinder apparatus owing to the relatively small sample size which can be contained within a capsule – small enough that meaningful textures are unable to develop. The only technique which would enable a visualisation of changes to grain boundary structures during a run would involve in situ tomographic imaging – where the best possible resolution currently available is 2µm. Furthermore, rotational pressure cells are also available which allow controlled amounts of torque to be applied to a sample. An investigation using such apparatus would be a particularly interesting follow up to this work.

3.7.2 Discussion & Interpretation of Data

3.7.2.1 Consistency of Data with Other Workers' Findings

These findings are consistent with work conducted by Demouchy [61] and her data is shown alongside that obtained in this study in Figure 59. An important point of note is the relatively shallow gradient of the line of best fit to the data. This is indicative of GBD of H in this setting having a lower temperature dependency than the lattice diffusion of H in olivine as measured by other workers (in the various crystallographic directions as shown – lattice diffusion of H in olivine is shown as being the most relevant single crystal comparison to GBD of H under mantle conditions). Interestingly, the data obtained here shows a much lower temperature dependency compared to the most recent data of Demouchy & Mackwell (2003) [115]. The data is also in agreement with the GBD work of Demouchy (2010) [61] which was conducted along similar lines to that presented here. Despite the differences in methods and processing of data between the two investigations, her data sits neatly along with those produced here.

The fact that grain boundary diffusion of H appears to be only slightly quicker than lattice diffusion requires an explanation. As previously discussed, grain boundaries were suspected to provide fast pathways for diffusion owing to their more disordered nature. Possible reasons and explanations for these findings and methods to determine the validity of those explanations are discussed in the following sections.

.

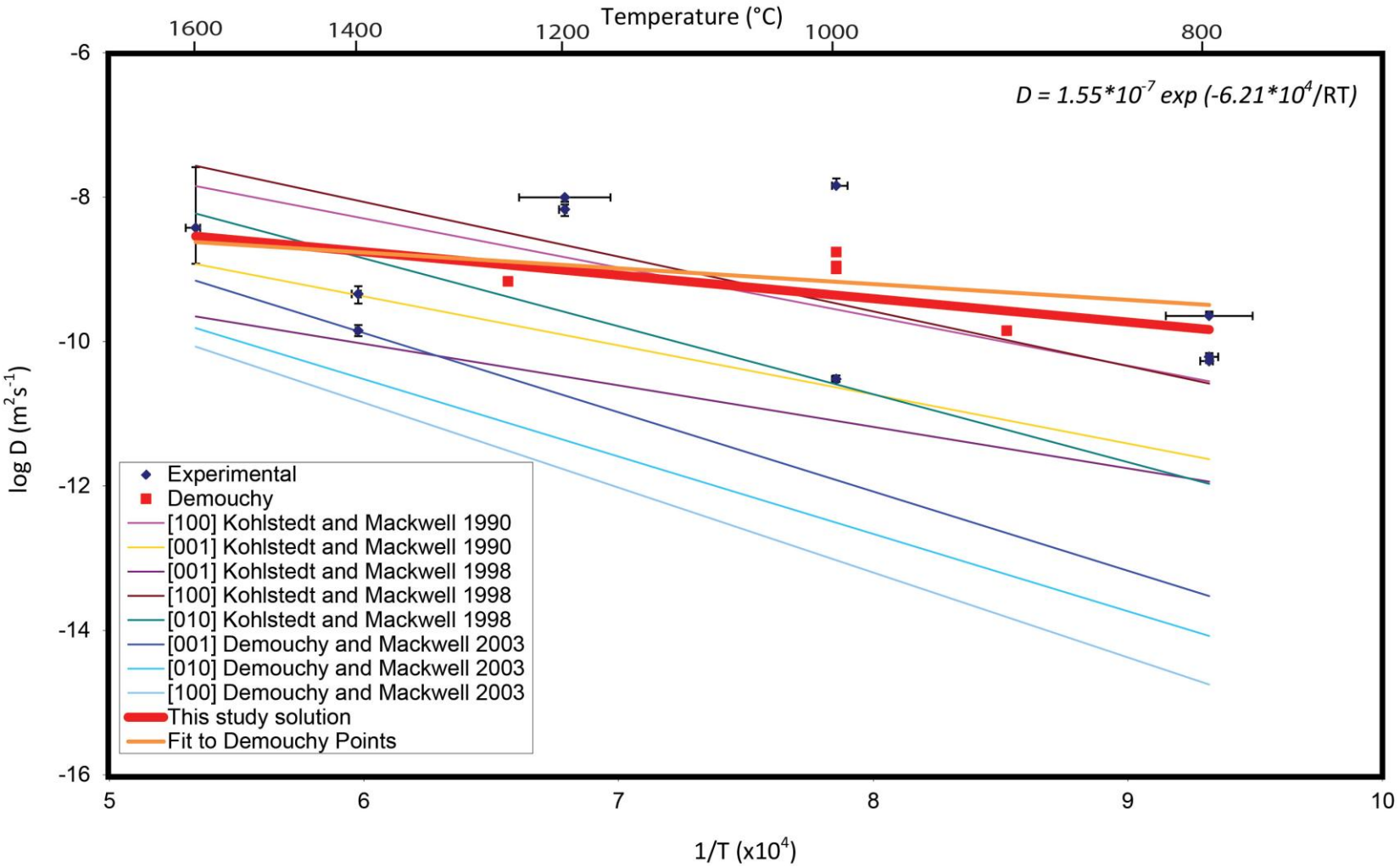

Figure 59: Arrhenius Plot of Diffusion Data from this study Combined with that of Other Workers

The thick red line shows the best fit of the data obtained here to an Arrhenius relationship, the red points are the data of Demouchy (2010) and the thinner, coloured lines are diffusivities of H in single crystal olivine as measured by other workers. Errors derived from the fitting of diffusion laws are not shown here, for a graphical representation of these the reader is referred to Figure 53.

3.7.2.2 Possible Explanations for Observations

The relatively small difference between grain boundary diffusion coefficients measured here and published single crystal data demands an explanation. Whilst the measured grain boundary diffusion coefficients do indeed describe faster diffusion than a number of studies, the measured rates coincide with some published single crystal data, particularly at high temperatures. There appears to be a greater deviation from the single crystal rates at lower temperatures in a direct parallel to the work on GBD of silver discussed in section 1.3.2.3.2 The Effect of Temperature on Grain Boundary Diffusion and shown in Figure 10. This similarity in diffusion rates along grain boundaries relative to the mineral lattice could be due to the size of the H ion. An H^+ ion (i.e. a proton) has a diameter of 1.7fm ($1.7x10^{-15}$m) and as such is significantly smaller than the architecture of a mineral lattice and also of a grain boundary which are structures on a scale of picometres to nanometres. This exceptionally small size implies that the energy associated with the jumping of an H^+ ion from the site to site and any associated lattice strain would be so small as to be easily overcome by energy supplied by the temperature of the surrounding conditions (or even, in effect, non-existent). As such, an H^+ ion could therefore be essentially blind to its surroundings and whether it was travelling along a grain boundary or through a mineral lattice. Furthermore, H has been observed to sit in interstitial positions within a mineral lattice and so should not require the presence of vacancies in the same way as larger ions do in order to diffuse through the lattice (see section 1.3.2.2.1 Lattice Diffusion for a discussion of lattice diffusion mechanisms and the role of vacancies). This is of course relevant to the issue of charge balancing and the need for a counter flow of an opposing charge such that the diffusant source region does not develop a charge excess. In the case of a diffusant such as H+ where the charge is single and positive, an electron, with a single negative charge could provide a suitable counter flow. Electrons are obviously in very ready supply for such a purpose and as such the need for a counter flow would not be expected to have any significant effect in reducing the diffusivity of H^+. As such, both the small size and low charge of H/H^+ go some way towards providing a hypothesis to accountfor the similarity in diffusion coefficients in grain boundary and lattice settings. In order to determine whether or not this hypothesis is true, it would therefore be of great use to conduct further investigations with a similar setup but using a volatile diffusant phase with a greater ionic diameter and/or a larger charge. The relative sizes of the differences between grain boundary and lattice diffusion rates with various diffusants would indicate whether or not the different properties of the diffusants responsible for the observed effects or not. It would also be interesting to see if there is a particular preference for grain boundary diffusion by larger ions with smaller ions showing a lesser difference in diffusivity between settings. It may be that there is a critical value of ionic diameter above which grain boundary diffusion becomes the dominant bulk diffusion mechanism. The effect of temperature on this relative effect would also be critical with GBD potentially becoming more and more important at lower temperatures. Furthermore, the relative size of the activation enthalpy (E_a) term could be important as this will reflect the mechanisms of diffusion and incorporation. Finally, the effect of pressure on work with different

diffusants would be of great interest. With a diffusant with a larger ionic diameter, one might expect pressure to have a greater effect as with depth (i.e. increasing pressure) minerals take on increasingly dense structures potentially making it more difficult for cations to be incorporated within them. It could be reasonably expected that this difficulty in incorporation would be greatest for large ions.

To this end, it was decided that a third experimental program would be carried out to determine if the size of the diffusant had a measurable effect on the utilisation of grain boundaries as a route for diffusion. This work was conducted with Li as the diffusant and is detailed and discussed in section 5 Grain Boundary Diffusion of Lithium.

3.7.2.3 Implications of GBD for Transport between Mantle Reservoirs

The finding that grain boundaries permit diffusion at a slightly greater rate than the mineral lattice in olivine under similar conditions is significant for the movement of water between reservoirs within the Earth. The findings have implications for the transport of water from the comparatively highly hydrous mantle transition zone to the much dryer upper and lower mantle. Traditional geochemical models suggest that the mantle is separated into distinct reservoirs owing to the different isotopic signatures possessed by ocean island basalts (OIB) and mid ocean ridge basalts (MORB). MORBs are typically depleted in incompatible elements and primordial isotopes with water content of approximately 0.01% whereas OIBs are much more enriched in incompatible elements and primordial isotopes and are significantly wetter with a water content of approximately 0.05%. The traditional model proposes that OIBs are derived from mantle plumes which sample the deep, lower mantle whereas MORBs are formed from depleted upper mantle, the upper and lower mantle reservoirs being separated by a boundary, most commonly thought of as the 660km seismic discontinuity. The seismic discontinuities observed between 410 and 660km are ascribed to phase changes in olivine (with some additional minerals) as with pressure it transforms to wadsleyite (β-Mg_2SiO_4) and ringwoodite (γ-Mg_2SiO_4) respectively before forming magnesiowustite (MgO) and perovskite ($MgSiO_3$) beyond 660km depth (see Figure 60). The phases found within the transition zone have significantly higher water solubilities than those out with.

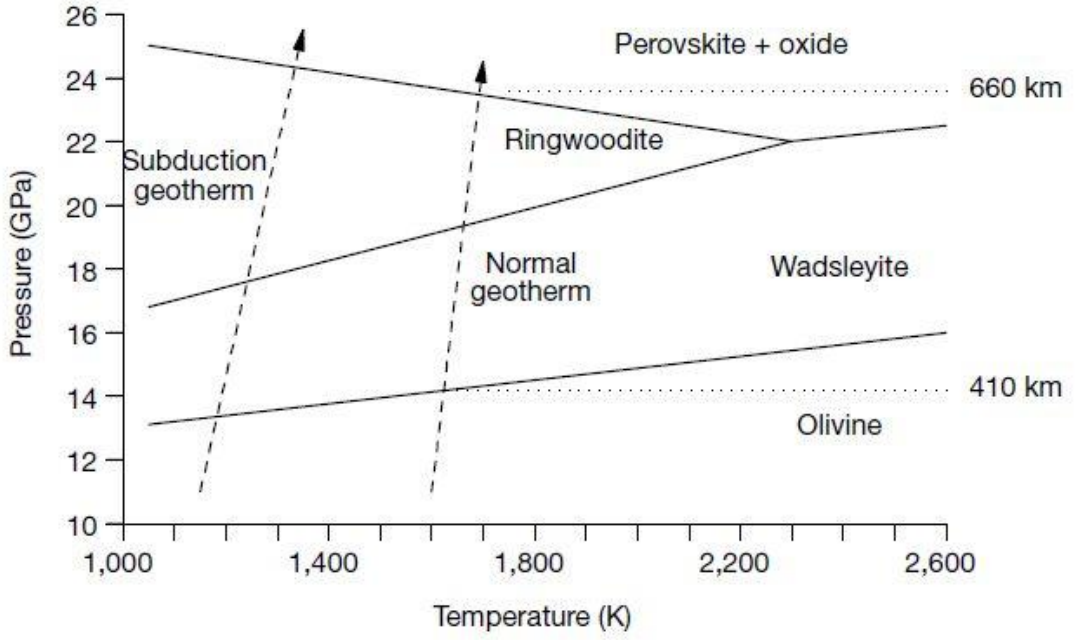

Figure 60: Stability of Mg_2SiO_4 under mantle conditions
From Helffrich & Wood 2001 [70].

A model has been proposed by Bercovici and Karato [116] to explain the origin of OIBs and MORBs without having parts of the mantle which are unable to mix with each other (see Figure 61). There

is a downward movement of mass as cool subducting slabs move beyond the transition zone. To counteract this downward movement a slow upward movement of lower mantle material (perovskite + magnesiowustite) is proposed (orange in Figure 61). Upon entering the transition zone this material takes in water at concentrations higher than the upper mantle phases are able to. As the material continues moving upwards, it moves beyond the 410km discontinuity where wadsleyite changes to olivine. As this reaction occurs, the water is expelled. The addition of free water then lowers the melting point of the mantle rocks at this point causing partial melting. Thus, a layer of melt is formed at the top of the transition zone. Incompatible elements which prefer to be in a melt relative to a mineral lattice move into this partial melt thereby producing the depleted upper mantle material from which MORB is derived. The melt layer is prevented from growing indefinitely by entrainment into subducting slabs thereby causing it to remain at a steady state (as the descending slabs are the cause of the upwelling of lower mantle material in the first place). The implication of this is that there is a highly hydrous melt layer at the top of the transition zone. Whilst the water from this layer is unable to enter the olivine mineral structure at particularly high concentrations it may still be able to diffuse from the transition zone into the upper or lower mantle via grain boundaries (or indeed from the core into the mantle). Grain boundaries may provide a route for diffusion where mineral lattices are already saturated with the diffusant thereby providing a significant flux which, although small compared to the total amount of diffusion possible from combined lattice and GBD could be geologically significant. As an example of the potential for transport of H along grain boundaries, Table 6 shows characteristic diffusion distances for H along grain boundaries (based upon the data obtained in this investigation) over a period of 3.2Ga (approximate time since the initiation of plate tectonics) at the temperatures characteristic of the 410km and 660km discontinuities and at the core/mantle boundary. As such, grain boundaries may provide a transport route for H between the transition zone and the lower mantle. They may also do so between the core and lower mantle. Given the calculated distances shown in Table 6 for diffusion over geological time, this process has the potential to transport significant amounts of water over geologically and geochemically significant distances. Combined with convective flow of the mantle, H is likely to be gradually re-incorporated into the lower mantle from the transition zone over geological time.

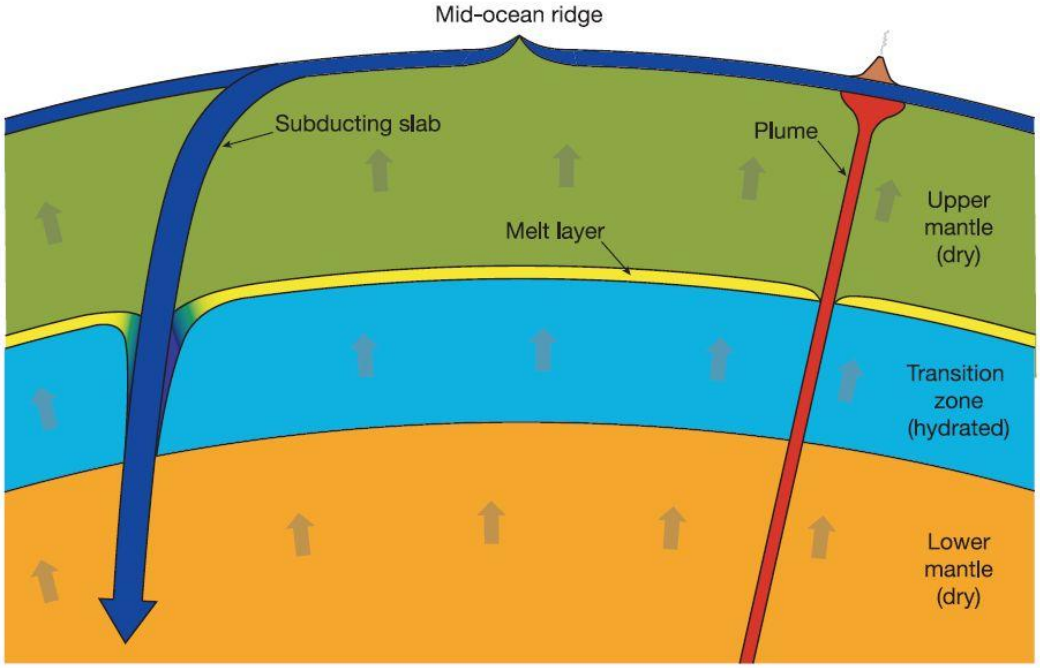

Figure 61: Transition Zone Water Filter Model

See text for full description of this model.

From Bercovici and Karato, 2003 [116].

Discontinuity	Temperature (°C)	Diffusion Coefficient (m^2s^{-1})	Characteristic Diffusion Distance (km)
410 km	1500	$2.29x10^{-9}$	15.2
660 km	1800	$4.22x10^{-9}$	20.6
CMB	3700	$2.36x10^{-8}$	48.8

Table 6: Characteristic Grain Boundary Diffusion Distances of H at various Discontinuities
Calculation based on diffusion for 3.2Ga (approximate time since initiation of plate tectonics) at the diffusion rates determined in this investigation. No correction has been made for pressure owing to lack of knowledge of the effect of this parameter. Characteristic diffusion distance is calculated as $\sqrt{Dt}$ *.*

3.7.2.4 Implications for Measurements of Mantle Conductivity

The movement of a charged species is the definition of an electrical current and as grain boundary diffusion of H will often be in the form of movement of H^+, it is reasonable to deduct that GBD of H may be responsible for a proportion of mantle conductivity. Karato (1990) [96] uses the Nernst-Einstein relation (Equation 17) to determine electrical conductivity of olivine under mantle conditions.

Equation 17: Nernst-Einstein Relation for Electrical Conductivity

$$\sigma = fDcq^2/kT$$

Where σ is electrical conductivity (in Sm^{-1}), f is a correlation factor approximately equal to 1, D is the diffusion coefficient (in m^2s^{-1}), c is concentration (in number of H^+ ions per m^3), q is the electrical charge of the species in question (in C, so the charge on a proton $1.6x10^{-19}$ C), k is the Boltzmann constant ($1.38x10^{-23}$ JK^{-1}) and T is temperature (in K).

By inputting the diffusivities calculated in this investigation into this equation, bulk conductivities can be calculated for various concentrations of mantle H_2O. These values are summarised in Table 7.

			100 ppmw H_2O	500 ppmw H_2O	1000 ppmw H_2O
T (°C)	T(K)	Diffusion Coefficient (m^2s^{-1})	Conductivity (Sm^{-1})		
800	1073	$1.46x10^{-10}$	$5.55x10^{-3}$	$2.78x10^{-2}$	$5.55x10^{-2}$
900	1173	$2.65x10^{-10}$	$9.19x10^{-3}$	$4.60x10^{-2}$	$9.19x10^{-2}$
1000	1273	$4.37x10^{-10}$	$1.40x10^{-2}$	$6.99x10^{-2}$	$1.40x10^{-1}$
1100	1373	$6.71x10^{-10}$	$1.99x10^{-2}$	$9.93x10^{-2}$	$1.99x10^{-1}$
1200	1473	$9.71x10^{-10}$	$2.68x10^{-2}$	$1.34x10^{-1}$	$2.68x10^{-1}$
1300	1573	$1.34x10^{-9}$	$3.47x10^{-2}$	$1.73x10^{-1}$	$3.47x10^{-1}$
1400	1673	$1.78x10^{-9}$	$4.33x10^{-2}$	$2.16x10^{-1}$	$4.33x10^{-1}$
1500	1773	$2.29x10^{-9}$	$5.25x10^{-2}$	$2.63x10^{-1}$	$5.25x10^{-1}$
1600	1873	$2.87x10^{-9}$	$6.23x10^{-2}$	$3.11x10^{-1}$	$6.23x10^{-1}$

Table 7: Calculated Bulk Conductivities based on the Grain Boundary Diffusivity measured here

Figure 62 shows the above data plotted with reference to the conditions which are characteristic of the upper mantle. It is clear that a mantle water contents of 100ppmw H_2O is sufficient to explain observed mantle conductivities and higher, localised abundances of water could lead to significantly higher values. As such, it is clear that GBD has the potential to have a large effect on mantle conductivity.

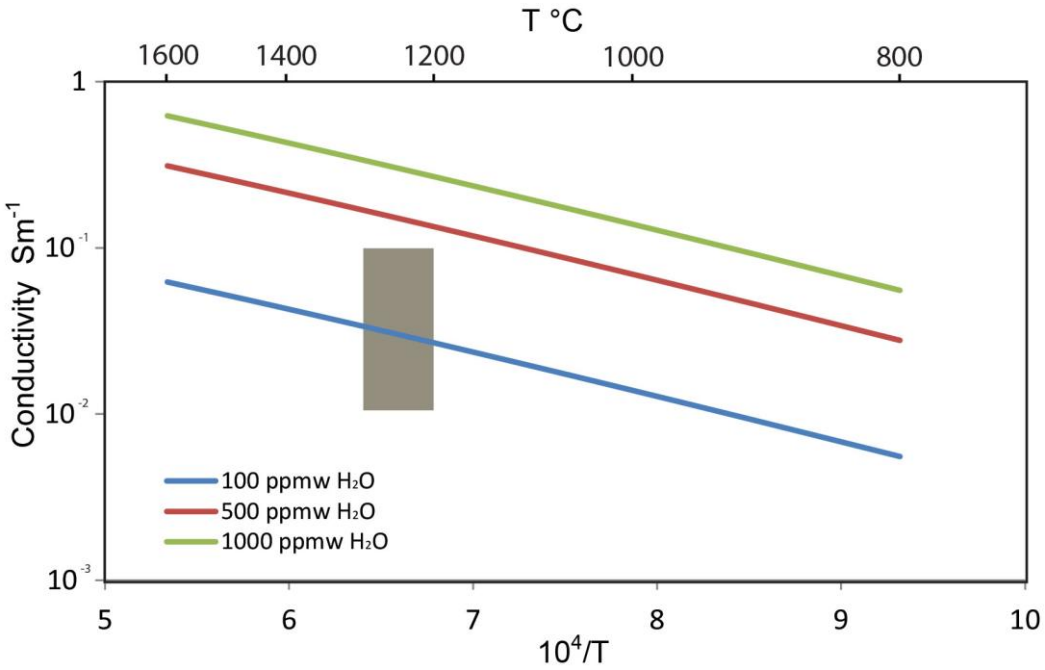

Figure 62: Plot of Bulk Conductivity vs Temperature based on the Diffusion Data obtained here *Conductivities have been calculated based on the diffusion coefficients which have been measured in this investigation. The grey box represents the temperature conditions and observed conductivities of the upper mantle. It is clear that GBD could be a mechanism responsible for the observed conductivities, even at relatively low concentrations. Locally higher concentrations of H_2O could lead to significantly higher conductivities.*

4 Grain Boundary Diffusion of Titanium in Quartz Experimental Program

4.1 Introduction

The use of measurements of the titanium contents of quartz was first suggested as a possible geothermometer in 1987 by Ostapenko et al. [117] before being developed by Wark and Watson in 2006 [2] (Equation 18) and further by Thomas et al [59] into a geothermobarometer (Equation 19) referred to as TitaniQ. This was then further developed by Huang & Audétat (2012) [118] (Equation 20).

Equation 18: TitaniQ Geothermometer Expression

$$Log(X_{Ti}^{qtz}) = (5.69 \pm 0.02) - \frac{(3765 \pm 24)}{T(K)}$$

(After Wark & Watson, 2006 [2])

Where X_{Ti}^{qtz} is the Ti content of quartz in ppm by weight.

Equation 19: TitaniQ Geothermobarometer Expression of Thomas et al.

$$RT \ln X_{TiO_2}^{quartz} = -60952 + 1.520 \cdot T(K) - 1741 \cdot P(kbar) + RT \ln a_{TiO_2}$$

(After Thomas et al., 2010 [59])

(Where $X_{TiO_2}^{quartz}$ is the mole fraction of TiO_2 in quartz and a_{TiO_2} is the activity of TiO_2 which, if rutile is present within the sample will equate to 1. *R* is the gas constant, *T* is temperature in K and *P* is pressure in kbar. If rutile is not present the activity of TiO_2 must be estimated by other means.)

Equation 20: TitaniQ Geothermobarometer Expression of Huang &Audétat

$$\log Ti_{(ppm)} = \frac{-0.27943 \cdot 10^4}{T - 660.53 \cdot (P^{0.35} / T)} + 5.6459$$

Since its initial development, the use of TitaniQ has been steadily increasing 10,100–110,[17] with critical studies of the technique taking place aimed at its refinement [118]. This geothermometer (and barometer with additional terms/refinement) is based on the simple observation that Ti concentrations in quartz are a proxy for equilibration temperature of the system with high concentrations of Ti indicating a higher temperature [2] as more Ti is able to substitute for Si in the

tetrahedral site of the SiO_2 crystal structure. Hence, if it is to be used for determining the thermal histories of the rocks to which it is applied, then knowledge of the mobility of Ti in quartz is essential. Recent research implies that the Ti in quartz thermometer may be used at much lower temperatures than previously thought, and implies that quartz is able to attain equilibrium Ti contents over geologically short periods at temperatures below 500˚C [4,10]. Mobility of Ti in quartz aggregates is thus the determining factor in the temporal sensitivity of the technique. A cooling quartz crystal will be able to hold progressively less Ti with the implication that Ti must be able to move out of the quartz lattice and into another phase – commonly exsolved needles of rutile (TiO_2). Thus, depending on the temperature dependence of Ti mobility in quartz and cooling rate, a 'closure temperature' (or range of temperatures) will mark the point at which cooling quartz crystals effectively become closed systems and retain a certain concentration of Ti. Conversely, a minimum temperature will be needed to mobilise Ti in quartz and 'reset' the Ti in quartz geothermometer in metamorphosing rocks. Studies of diffusion of Ti in monocrystalline quartz show slow diffusion rates which are not consistent with inferred timings of crystallisation e.g. cooling rates determined from textural information [3,4] (see Figure 63). Thus, there must be a quicker way for Ti to diffuse through quartz in real world examples. A simple solution to this problem is for the diffusion to occur along grain boundaries as diffusion through monocrystalline quartz is an unrealistically slow natural scenario. Indeed, GBD has been found to be dominant in some settings at lower temperatures, an example of this is discussed in section 1.3.2.3.2 The Effect of Temperature on Grain Boundary Diffusion, and is shown in Figure 10. This process may be further enhanced by the presence of additional species.

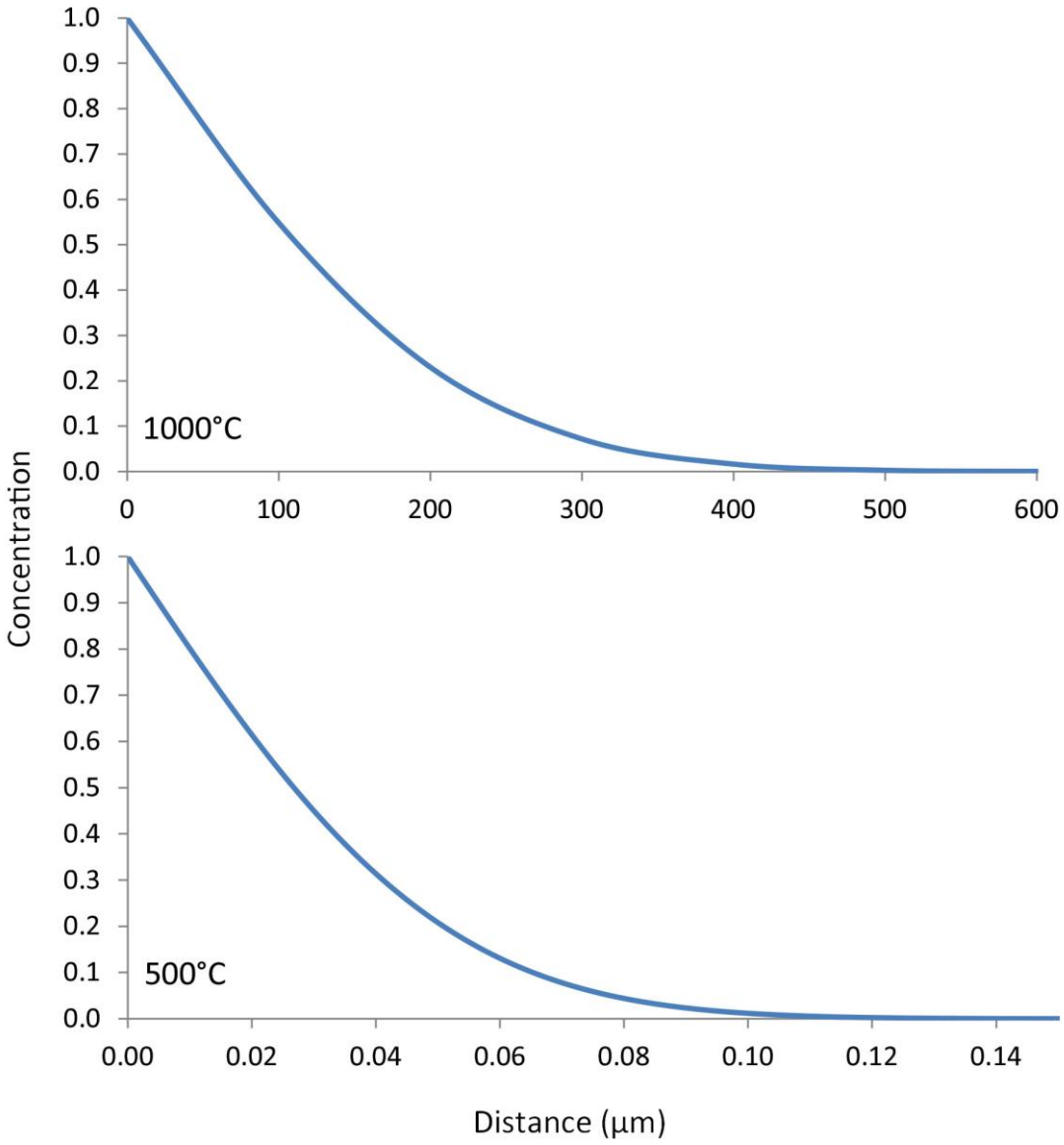

Figure 63: Modelled diffusion profiles for lattice diffusion of Ti in Monocrystalline Quartz at 1000°C & 500°C

Top. Diffusion would need to take place for in excess of 1000 years at 1000°C for measurable concentrations of Ti to be detected in quartz 500µm from the Ti source.

Bottom. The same calculation performed for a temperature of 500°C – note that in the same time period so little diffusion is able to occur that concentrations drop to 0 within 0.12µm of the source. This is indicative of the massive temperature dependence of diffusion.

From equations governing Ti diffusion in quartz determined by Cherniak et al., 2007 [3].

4.2 Methods Used & Their Development

In common with the other settings in which GBD is being investigated, method development was a key part of this aspect of the research, particularly in the early stages. Thus, once again, preliminary results were used to refine methods as problems were encountered and overcome. As such, at the start of the project, experimental work was carried out as much with the intention of using it to refine methods as it was for obtaining data to test hypotheses. As such, this section discusses the methods used in the investigation and specific method development whereas the data derived from experiments is discussed in the results section.

4.2.1 First Capsule Design

Capsule designs evolved throughout the project in response to experimental successes, failures and difficulties. The initial set up (Figure 64) utilised a carbon capsule containing quartz interlayered between platinum foils (acting as a Ti sink) with a central titanium foil acting as the Ti source. The reason for this design was that allowing Ti to alloy with Pt would be an effective way for the sink foils to accept Ti and the thickness of the foils would make them easy to analyse. Thus, in a parallel with the work conducted by Hayden & Watson[1,6] on carbon GBD, the amount of Ti diffusion would be determined by measuring the extent of alloying of the diffusant in a sink phase – in this case measuring the extent of Ti/Pt alloying. Quartz with a grain size of approx. 10 – 50μm was used to form the granular host medium through which the Ti would diffuse. This fine grain size was used as a starting point so that grain boundary diffusion would take place along a path as close to linear as possible. With increasing grain size diffusants will travel greater distances to reach a given point. Thus, smaller grain sizes allow more linear diffusion. Diffusion in a single linear direction is easier to analyse as corrections do not need to be made for increased distance travelled. However, it was expected (and observed) that a certain amount of annealing quartz grains would take place thereby causing grain sizes to increase and therefore ultimately requiring this increased distance to be taken into account.

The capsule design consisted of stacks of source and sink foils (see Figure 64) in a graphite capsule for use in a piston cylinder apparatus. Following experimental runs, capsules were mounted in epoxy resin, ground through (it was expected that if the capsules were sawn through they would be likely to fall apart owing to the brittleness of the graphite) and then finely polished for analysis. Initial analysis was by SEM and, in some cases semi-quantitative EDS analysis of compositions were recorded. This provided an assessment of the structural integrity of the capsule and allowed initial determination of any diffusion which may have taken place.

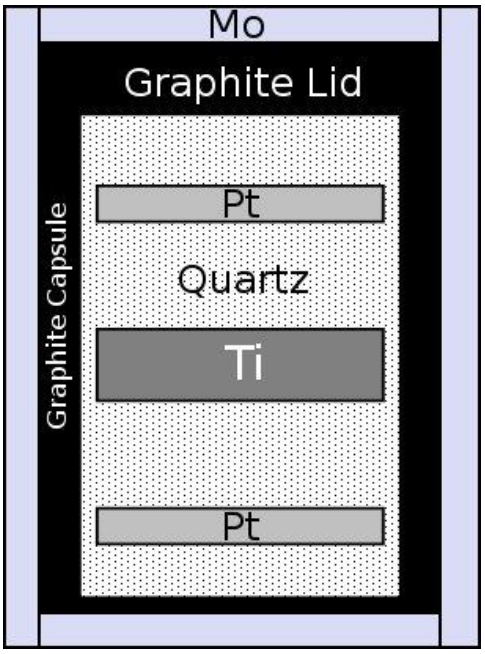

Figure 64: Schematic Initial Ti in Quartz capsule design

Pt and Ti foils are placed within the granular quartz host material. The number of foils used varied throughout the series of experiments in response to failures. From run TiQ3 onwards the capsule was wrapped in Mo foil (as shown above) in an attempt to increase its durability.

Following run TiQ1 (in which the capsule fragmented during decompression), it was decided that a small piece of Mo foil would be placed at either end of the capsule. This was done to add strength and reduce the risk of the capsule fragmenting. A second, very useful function was that the foils acted as markers of the top and bottom of the capsule. This was desirable owing to the difficulty associated with identifying the capsule when dismantling the recovered assemblage. Initially it was hoped that it would be possible to saw through capsules following their experimental run and then mount them such that the long axis cross section (as in Figure 64) was exposed for analysis. This would allow easy measurement of distances thereby permitting accurate calculation of diffusion coefficients.

After run TiQ2 which did not rupture but which used capsules from the same batch as TiQ1 which did, capsules with a reduced outside diameter were made so that in subsequent experiments, a layer of Mo foil could be wrapped around the capsule before it was placed in to the assembly. This was done to further reduce the risk of deformation of the capsule and also in the hope that the capsule could be sawn through to reveal its contents instead of the comparatively slow and difficult method of being ground through by hand (this method was not ideal as often several mm of capsule needed to be ground through in order to reach the centre of the capsule – thereby increasing the risk of creating an uneven surface on the epoxy disc). Capsules were not initially sawed owing to the brittleness of the capsule and thus the risk of the contents being spilled.

A second change made after the completion of run TiQ2 was the reduction in the number of Pt foils in the capsule. In TiQ2 a total of 5 Pt foils were present in addition to the central, thicker Ti foil. It was believed that the proximity of the 5 Pt foils in addition to the Ti foil may well have caused an alloy made up of Pt and Ti to form thereby causing the failure of the experiment (see Results section). Thus, in subsequent experiments, only two Pt foils were used (one either side of the Ti foil). Following this revision, the problem of channels of alloying Pt and Ti forming was averted.

The capsules of runs TiQ3 and TiQ4 were found to be split in half along the line of the central foil when recovered. It is not known if this was due to the change in foil arrangements or if it was related to the small change in capsule size to accommodate the Mo foil wrapping on the outside.

During SEM analysis of runs TiQ3 and TiQ4, it was found that (within the detection limits of the SEM EDS system) no Ti had travelled sufficiently far to enter the Pt sink foils. From this observation, it was decided that additional longer run duration experiments should be conducted to explore diffusion under these conditions, followed by analysis by EPMA. Analysis by EPMA was decided upon due to the lower detection limits of the method. Furthermore, a redesign of the experimental capsules was subsequently undertaken. Having observed little diffusion in runs TiQ3 and TiQ4 it was also proposed that other species might enhance Ti mobility in quartz in natural systems. In a number of systems it has been shown that the presence of H greatly enhances diffusion and self-diffusion of various species [5,105]. Thus, plans were made for subsequent experiments to be conducted in capsules containing water as a source of H to potentially allow faster GBD of Ti.

4.2.2 Second (Final) Capsule Design

Following the problems with early runs which are detailed above and also in section 4.6.1 First Experimental Set, an extensive re-design of the capsules was undertaken. Figure 65 shows a schematic representation of the design which was settled upon. In this set up the Ti capsule acts as the source of Ti diffusant as well as fulfilling the function of providing a vessel in which the run could take place. This design was ideal as it was very easy to set up and insert into the experimental assemblage. Hammer fit capsules have also been shown to effectively contain diffusants[119]. The choice of materials and the method of creation for the capsule are discussed in subsequent sections.

Figure 65: Titanium Diffusion in Quartz 2nd Experimental Set Capsule Design

4.2.3 Materials

In a parallel with the previously discussed work on GBD of volatiles, the choice of materials to be used in this aspect of the investigation was exceptionally important. Consideration of issues such as potential reactivity between capsule constituents and the physical behaviour of all components

under the conditions that would be applied during experimental runs was essential. The following subsections detail the materials which were chosen through multiple generations of experiments. Materials were selected based not only upon their suitability for testing the hypotheses of the investigation but also for their ability to fulfil the criteria set out here.

4.2.3.1 Capsule Materials

4.2.3.1.1 First Experimental Set Capsule Materials

The first set of experiments was conducted with a carbon capsule as this would not alloy with Ti which could have caused serious problems for capsule integrity. The graphite capsules were created by machining graphite rods which were purchased with the desired outside diameter of the finished capsules. The end of the rod was hollowed out to the desired depth before the capsule was cut off. Thin slices were also cut from the rod and bevelled to form the lids of the capsules. As no welding or other processing of the capsules was necessary, it was very easy to prepare them for the experimental runs. This was advantageous both in terms of ease of preparation but also in terms of the mechanical strength of the capsule. As it was not necessary to work the capsule after it had been created, there was no opportunity for weaknesses to be introduced into it. This in turn meant that these capsules were then far less likely to fail during high PT runs.

4.2.3.1.2 Second Experimental Set Capsule Materials

Later experiments were run with a different capsule design where the capsule itself was made of Ti and was the source for the experiments (see section 4.2.2 Second (Final) Capsule Design). The availability and relative low expense of Ti allowed for the making of robust capsules with hammer fit lids. This avoided the need for welding which might have caused diffusion of Ti prior to the start of the experimental run and which would require equipment that was not immediately available. Furthermore, in a direct parallel to the use of carbon capsules for the first capsule design, the lack of processing of the capsule after creation meant that no weaknesses were introduced to it thereby reducing the risk of failure. Capsules were created by machining rods of Ti in the same way as detailed in section 4.2.3.1.1 First Experimental Set Capsule Materials.

4.2.3.2 Sample Materials

4.2.3.2.1 First Capsule Design Sample Materials

The first set of experiments utilising the initial capsule design were run using Ti and Pt foils layered with quartz. The individual foils used in each experiment were simply punched from a larger sheet to make discs of a slightly smaller diameter than that of the capsule. This was done using a small punch created from a tube of steel with a tapered, sharpened end.

As the capsule design evolved during the initial set of experiments, the number of foils required changed but the materials remained the same. SiO_2 ground to a grain size of <100µm was used as the host medium.

4.2.3.2.2 Second Capsule Design Sample Materials

For the second set of experiments high purity sintered quartz was ground down to a fine grain size (<100µm) to provide the host medium. As the Ti capsule acted as the source material no other sample preparation was necessary. The ground quartz was simply loaded into the capsule and the hammer fit lid was hammered into position. In cases where water was added the capsule, approx. 5µL was placed into the bottom of the capsule prior to the loading of the quartz. In all other respects capsule setup in these cases was exactly the same as for “dry” experiments.

4.2.4 Construction of Experimental Capsules

4.2.4.1 First Capsule Design

The first set of experiments which utilised a carbon capsule and Ti and Pt foils as source and sinks respectively were constructed by layering up the components of the capsule. Thus, firstly finely ground quartz was inserted, followed by a Pt sink foil. Another layer of quartz was added above this and then, depending on the number of sink foils used in the particular run, another Pt sink foil or the central Ti source foil. As each layer of quartz was added the capsule was gently tapped against a hard surface to aid the quartz in settling. Layers were also compacted to ensure that all space within the capsule was filled. Quartz and sink foils were interlayered above the central source foil in symmetry with the bottom half of the capsule. The graphite lid of the capsule was then simply placed on top of the capsule which was then placed into an alumina capsule holder. The capsule holder and capsule were then placed into a standard experimental assemblage as previously described.

4.2.4.2 Second Capsule Design

Construction of experiments using the second capsule design was even simpler. Powdered quartz was loaded into the Ti capsule and compacted inside the capsule with a metal rod. Once the capsule was full of quartz the hammer fit lid was placed on top of it and gently tapped into position. When the lid was correctly in place it was hammered hard to ensure that a good fit had been achieved. Finally the capsule was placed into a holder and assemblage as described above.

Experiments were then run and retrieved as per the method described in section 2.2.1 The Piston Cylinder Apparatus and section 2.2.1.1 Sample Retrieval.

4.2.5 Run Conditions

Experimental runs were conducted at temperatures between 1000 and 1400°C. This was done to ensure that the temperature dependency of diffusion could be accurately determined. A pressure of 3GPa was used for all runs. This value was chosen as it is a value at which the piston cylinder apparatus was known to work well and so it was expected that this value would increase the ease of carrying out the experimental program. Whilst this value is not representative of the crustal pressures under which quartz veins are found (at pressures of up to approximately 1GPa), this value is a relatively small deviation and, as previously discussed, pressure is expected to have a comparatively small effect relative to temperature. Running all experiments at a pressure of 3GPa (between all aspects of the investigation) also enables results to be easily compared to one another. As such, it is considered that, given the advantages of running at this pressure, it is acceptable to do so. As discussed in the previous chapter on the grain boundary diffusion of volatiles, whilst pressure is not a variable which was investigated here, it would be very interesting to do so in any future work on this topic. Run durations were initially calculated by estimating how

much more quickly grain boundary diffusion could be as compared to published lattice diffusion rates. As such, this estimate was essentially a guess. Once initial runs had been completed, diffusion coefficients were calculated and then used to estimate the next set of durations. Details of the specific conditions used for each run are detailed in section 4.6.3 Summary of All Run Results).

Later experiments were run with water added in order to determine if this had any effect on the measured diffusivity. It was suspected that the addition of water may increase the diffusivity of the Ti (as has been observed in others workers' studies e.g. Demouchy et al. 2007 [120]) and as such run durations were decreased. Once again, the exact run duration which would be required for a diffusion profile which could be easily fitted to was not known. As such, the durations which were determined were essentially an educated guess based upon the results of previous runs.

4.3 Sample Preparation for Analysis Methods

4.3.1 Preparation of Capsules run with First Design

The first set of experiments which were run in carbon capsules (see section 4.2.1 First Capsule Design) were challenging to prepare for analysis owing to the exceptionally brittle nature of graphite in the recovered samples. Due to this it was not possible to saw through capsules to section them (as was done in the investigation into hydrogen GBD). Instead the complete capsules were laid on their side and encased in epoxy resin. Once the resin had hardened the entire block was then ground down to a point where the maximum cross section of the capsule was exposed (i.e. half the thickness of the capsule was ground through). This initial grinding was performed with coarse papers and then once the correct cross section of the capsule had been exposed finer papers were used to polish the samples to an acceptable smoothness for EPMA analysis. Samples were then carbon coated and examined in the SEM. It was at this stage that this set of experiments was discovered not to have worked effectively thereby triggering the re-design of the capsule. The reasons for the failure of this initial set of experiments are discussed in the subsequent results section.

4.3.2 Preparation of Capsules run with Second Design

Experiments run with the second capsule design were found to consistently break into discs when the capsule was removed from the experimental assemblage (see Figure 66 for an example of a disc from run TiQ6). This proved advantageous as it effectively produced multiple cross sections across the recovered capsules, allowing multiple measurements of diffusion coefficients from each capsule. By mounting the discs face down in epoxy resin, it was possible to polish them to a fine finish. As the Ti capsule was the source of Ti for these experiments, diffusion profiles could be measured by recording a series of points in a line starting at the interface between the Ti capsule and its quartz contents (see Analysis section).

Fracture of Ti capsules is believed to have only occurred in this series of experiments owing to the more brittle nature of Ti and possibly due to work hardening during compression, heating, cooling and also during the first few hours of an experimental run as the capsule settled into the high PT conditions created by the apparatus.

Prior to EPMA analysis it was necessary to coat samples in carbon and connect the samples with the metallic mount on which the resin block was placed with silver paint thereby creating a conductive pathway which prevented charge build up by the electron beam by allowing it to flow to ground.

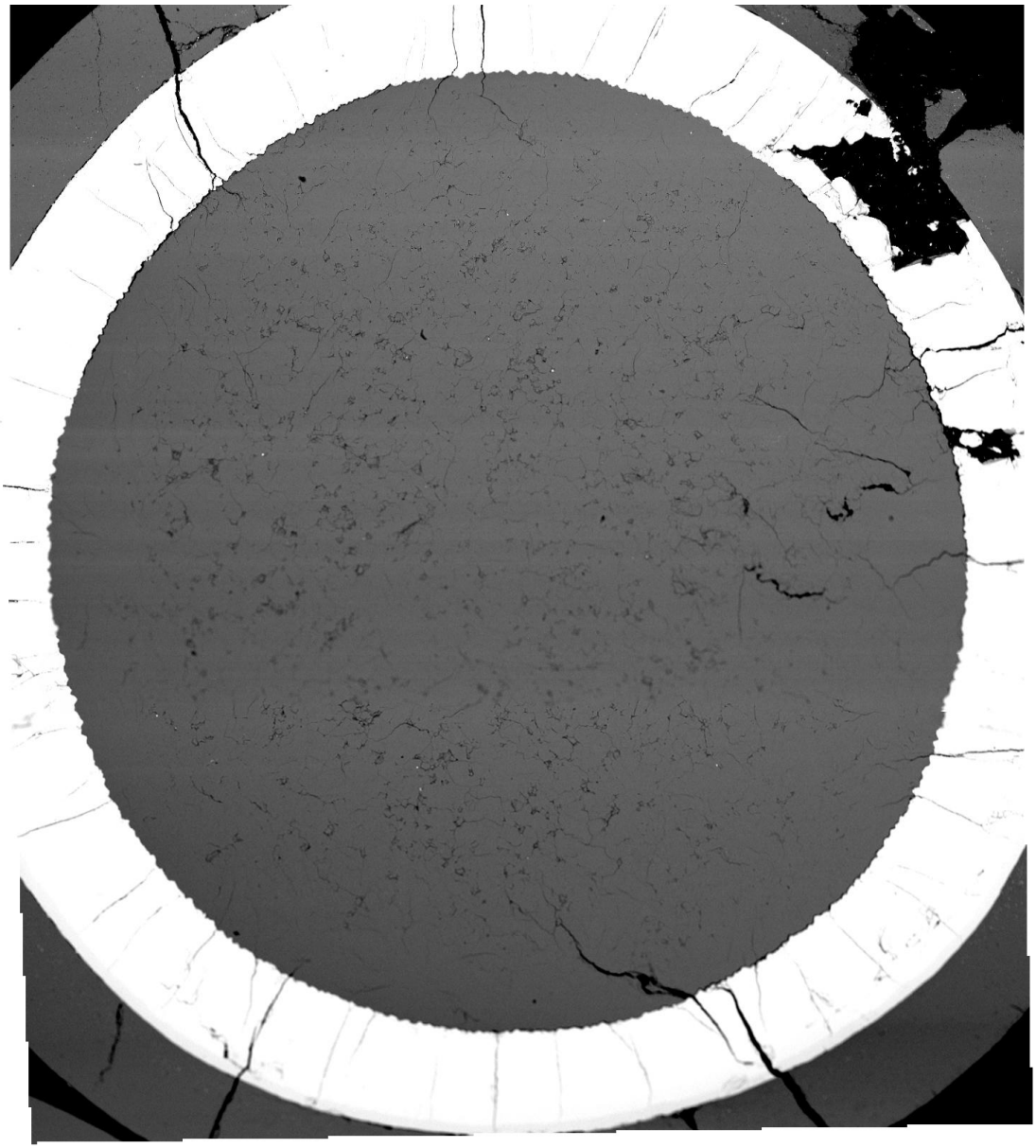

Figure 66: BSE SEM image of TiQ6B

Example of one disc derived from run TiQ6. The experimental capsule split into discs during recovery in each of runs TiQ5 – 12. As the Ti capsule was itself the source of Ti for diffusion along quartz grain boundaries in these experiments (white ring in the image), diffusivities were determined by measuring Ti contents of quartz radially, from the Ti capsule wall inwards in a perpendicular direction. The width of the field of view here is approximately 4mm.

4.4 Analysis of Completed Runs

Following the preparation of capsules, a number of processes were undertaken to analyse their contents. These included recording imagery and taking measurements of capsule slices along with the quantitative analysis which provided the numerical data for the calculation of diffusive properties.

4.4.1 Initial SEM Analysis

Capsules were analysed by SEM to check their integrity and in order to create imagery which would be used in the later stages of analysis to aid in identifying specific slices of capsules and in recording the location of analysis points.

As capsules had broken into a series of slices upon decompression it was necessary to be able to separately identify each slice. This was done by allocating a letter suffix to the name of the capsule. E.g. capsule TiQ5 was broken into slices TiQ5A, TiQ5B and TiQ5C. These identifiers were then appended to an image showing all slices and their spatial relationships to each other (see Figure 67). Each named slice could then be subsequently identified by comparing its morphology with that in the labelled diagram showing all slices.

High resolution images of each slice were also acquired and stitched together using image manipulation software to form maps of each slice. This was done with the intention of using the maps to log the position of lines of analysis points which would be completed during EPMA analysis. In practice these were not needed as the EPMA analysis was completed in such a way that lines could be identified from the properties which were recorded as part of the EPMA data.

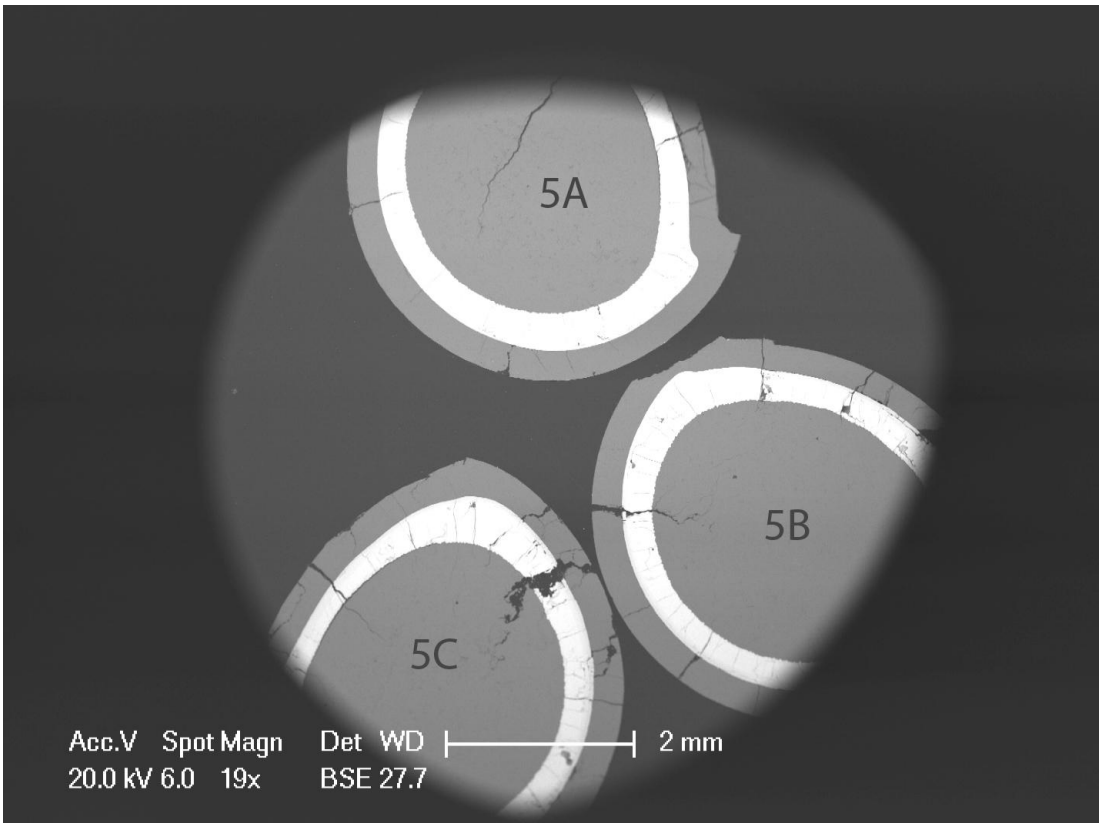

Figure 67: SEM Image Showing All Slices of Capsule TiQ5

Each slice of a given capsule was appended a letter to its identifier. Any slice within a capsule could then be identified by comparing its morphology with the image showing all slices within that capsule. An example of such an image for capsule TiQ5 is shown.

4.4.2 EPMA Analysis

EPMA analysis was conducted in two sessions with runs TiQ5 – 8 analysed first and then runs TiQ9 – 12 analysed at a later date. Analyses were primarily formed of linear profiles containing a number of points oriented perpendicular to the Ti/quartz interface. The first session was 1 day long and the second was 2 days. As such, some repeat lines for capsules TiQ5 – 8 were run as the length scale of diffusion had been determined from the first analysis session. The EPMA allowed the programming of analysis points so that the analysis could be performed when the user was not present. This allowed a large amount of data to be collected as analyses could be run overnight.

Initially, point readings were recorded close to the interface between the quartz and the Ti capsule manually (i.e. they were not programmed into the EPMA for automatic collection at a later stage) as it was necessary for the beam to be perfectly positioned so that the excitation volume did not include the capsule itself which would lead to unfeasibly high Ti concentrations being recorded. In certain cases where this is believed to have occurred, these points were rejected.

Once high proximity points had been recorded, lines of analysis points were set up originating very close to the extant points. These were programmed to be collected overnight and were interspersed with regular checks of standards. In practice there was very little variation in the reading of standards and it was not necessary to apply any further corrections to data.

Analyses were conducted using a 20kV beam at a current of 60nA. X-rays emitted from Ti atoms were counted on 3 large and 1 standard size PET detectors and Si was counted on one TAP crystal. Spot size was of the order of 2µm.

In some cases, line scans were performed. These were essentially quick, low quality data collection lines where data is continuously collected whilst the sample stage tracks in a specified direction. As such, they were a useful tool in obtaining a first order approximation of the length of a diffusion profile. The dataset derived from such an analysis was however very noisy and so was unsuitable for accurately fitting a diffusion law to.

4.4.3 Post-EPMA SEM Analysis

After the completion of data acquisition by EPMA, capsules were analysed by SEM with the primary aim of locating analysis points and measuring their distances from the interface with the capsule wall. This was necessary so that both a concentration and an accurate distance could be plotted for each given analysis point thereby allowing the determination of diffusion parameters. As the spacing of points was (at least nominally) known from the EPMA software it was, in theory, simply a case of measuring the distance of the first point of an analysis line from the Ti capsule wall and adding this value to all readings. However, it was found, during SEM analysis, that in some cases the length of the line of points was as much as 10% different to the reported value. This value was taken into account when determining errors in diffusion calculations (see section 4.5.2.1 Distance Errors).

Figure 68 is a SE image of a disc from run TiQ7 and shows a series of analysis points close to the capsule edge alongside a line of points. A scan line (where the sample stage constantly tracks during analysis giving a low quality line scan of Ti concentrations) is also visible.

Images of all analysis lines were also saved to maintain a record of all work completed.

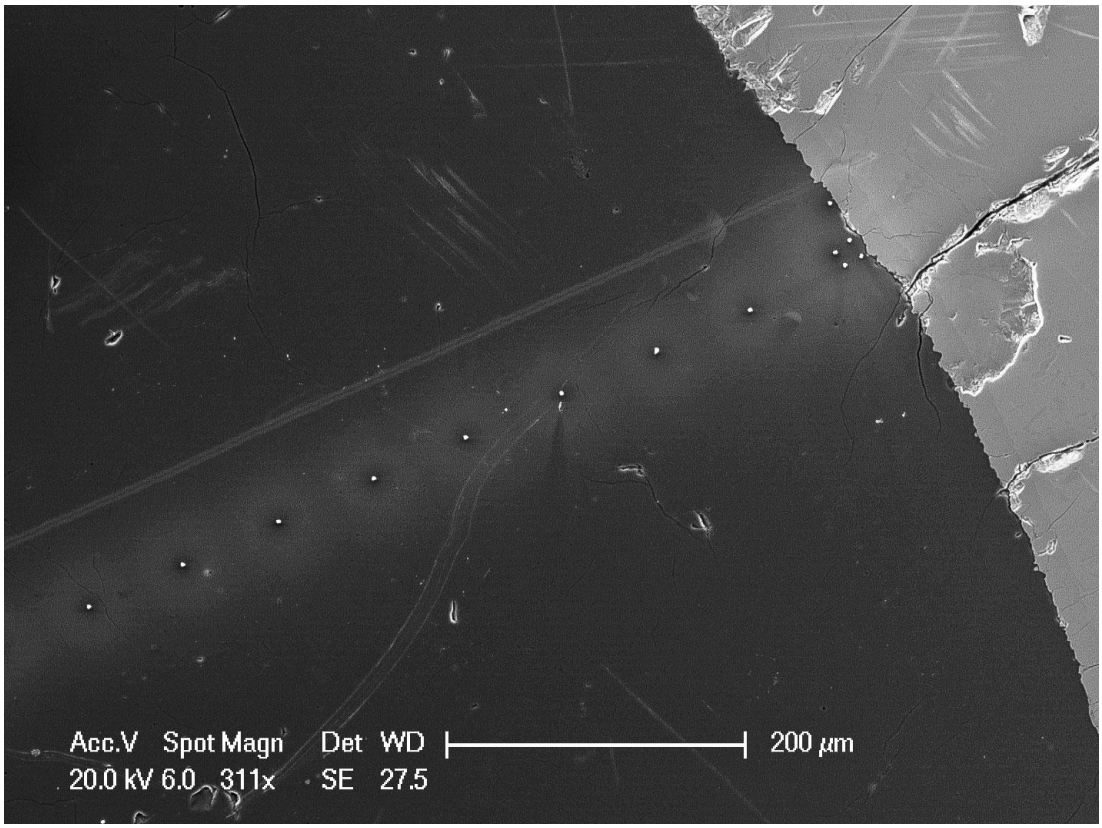

Figure 68: TiQ7 showing EPMA Analysis Points

Four high proximity points can be seen close to the interface between the Ti capsule wall and the polycrystalline quartz contents. The line of analysis points then extends, with analysis points at a regular spacing, inwards from the capsule wall in an essentially perpendicular orientation. A line scan is also visible above the main line of analysis points.

4.5 Treatment of EPMA Data

4.5.1 Calculation of Diffusion Parameters

The data obtained from EPMA analysis was extensively reviewed and processed to enable the extraction of diffusion coefficients and Arrhenius relationships. Errors were also carefully treated to determine the likely precision of the data obtained.

Diffusion coefficients were calculated using the Datafit curve fitting software by Oakdale Engineering using the exact same method as previously detailed in section 3.5.1 Calculation of Diffusion Parameters within the diffusion of volatiles along grain boundaries aspect of this investigation. The reader is directed to this section for a full discussion of the calculation methods used and the solutions of Fick's Laws which the data was fitted to. As diffusion of Ti in quartz (even along grain boundaries) was already known to be significantly slower than that of H along grain boundaries it was necessary to change the starting values for each of the two variables. A starting value of $1x10^{-15}$ m^2s^{-1} was used for the diffusion coefficient (denoted *a*) and a value of $1x10^{-3}$ m^2s^{-1} was used for the effective concentration at the interface (denoted *b*).

Background concentrations of Ti were determined by looking at the tail of the data obtained during line measurements and taking the mean of the final 5 measurements (in some cases a clearly anomalous point was within the last 5 values; when this occurred the anomalous point was not included in the calculation of the mean and instead values more typical of the tail of the data were used). This was then subtracted from each concentration value and the resultant figure was used in the calculation of the diffusion coefficient. These values were further checked by measuring the Ti contents of random grains at the centre of a capsule and comparing the values obtained with those in the line measurement tail.

4.5.2 Calculation of Errors

Absolute error values were estimated for each measured parameter. The estimations which were made and the logic by which these estimations were arrived at is detailed in section 2.6.1 Calculation of Errors. Where specific methods were required for this particular aspect of the investigation they are detailed below. These individual sources of error were combined as detailed in section 2.6.2 Combination of Errors.

4.5.2.1 Distance Errors

In the case of Ti diffusion in quartz experiments, the distance of an analysis point from the capsule edge could be clearly defined to a µm level of precision. Furthermore, in the case of points which were collected as parts of automated lines (i.e. a number of points at regular spacing between a defined start and end position), the EPMA software reported a spacing which could be used in the calculation of the diffusion parameters. This spacing was, however, simply the spacing between points and as such was in itself not meaningful. As such, these values had to

be corrected by adding on to them the distance of the first point from the Ti source. By doing this each point would then have the correct distance away from the capsule wall associated with it. It was noted during SEM analysis after the completion of EPMA work that some lines appeared to be marginally longer than the values reported by the EPMA suggested. These lines were measured and, in some cases were found to be as much as 10% longer than they should have been. This effect is attributed to a stage "backlash" effect whereby the sample stage does not return to exactly the correct position, particularly after a large move. As this effect is magnified with distance moved, points closer to the start of a line had a smaller absolute error than those further away. As such, it is felt that a proportional error gives a more accurate representation of the error experienced by each point. The error in the distance of any given point from the Ti source is calculated as +/- 10% of the measured distance. In many ways this potentially large error (some lines were approximately 200µm long giving an error of 20µm for the furthest points) is not greatly problematic as the largest errors are at (relatively) great distances along an analysis line where concentration has dropped to 0. These parts of the line contribute very little to the calculation of a diffusion coefficient. The critical parts of the line for fitting (i.e. those where the concentration is steepest) have (without fail) far smaller absolute errors and as such the fitting process can be tightly constrained.

4.5.2.2 Concentration Errors

There was a quantifiable error associated with the measurement of point concentrations of Ti content of quartz via EPMA. During the analysis of each point, a significant number (between 20 and 70) of individual analyses were recorded for each analysis point. The EPMA software recorded each of these values and used them in the calculation of the final reported value for each point. The error associated in reading the concentration of each analysis point is the standard deviation of all of the readings recorded at that analysis site and is as reported by the EPMA software.

4.5.2.3 Summary of Error Magnitudes

Parameter	Value
Time	120s
Concentration	Standard deviation of all readings recorded at given analysis site as reported by EPMA.
Distance from Interface	10% of measured distance
Temperature	Maximum deviation from nominal temperature

Table 8: Summary of Error Magnitudes for GBD of Ti in Quartz Experiments

4.6 Results

4.6.1 First Experimental Set

Initial runs of Titanium in quartz experiments utilising the first capsule design were conducted at high temperature to allow as large an amount of diffusion as possible to take place therefore causing higher concentrations of Ti in Pt to be recorded. This would allow for quick, easy analysis on basic instrumentation (e.g. EDS system on an SEM) to determine if the method was effective prior to embarking on a larger, more detailed study. A pressure of 1GPa was chosen as this is representative of a depth of 30km. This pressure is representative of the region in which one would expect mylonites, the rocks that the titanium in quartz thermometer has to date been mostly applied to, to be present. Initial experiments used several Pt sink foils (of thickness 0.05mm) to ensure that distance through which Ti (from the Ti source foil – 0.25mm thick) had to diffuse was minimal.

4.6.1.1 Summary of Run Parameters

Run ID	Temp (°C)	Pressure (GPa)	Duration (hr)	Comments
TiQ1	1600	1	68.5	Suspected thermocouple breakage: slight deviation from T set point possible. Capsule ruptured and Pt seen to be fragmented and disseminated throughout the capsule. Not analysed.
TiQ2	1400	1	20	Capsule remained intact. Layers of Pt and Ti appear to be distinguishable. Analysed in SEM. Links evident between Pt and Ti foils where alloying had taken place. No diffusion evident through quartz.
TiQ3	1200	1	70	Capsule found to be broken in half when removed from recovered assembly. Both halves prepared and one half analysed by SEM. No GBD evident.
TiQ4	1000	1	73	Capsule found to be broken in half when removed from recovered assembly. Both halves prepared and one half analysed by SEM. No GBD evident.

Table 9: Run Parameters & Comments for First Capsule Design Experiments

4.6.1.2 Specific Run Observations

4.6.1.2.1 TiQ1

Run TiQ1 was not successful for a number of reasons. It is believed that it may have suffered a thermocouple breakage and as such there is little control on the temperature that the run was subjected to. Furthermore, when the capsule was recovered it was found that it had ruptured and that the metal fragments had broken apart and disseminated throughout the capsule. This may well have occurred due to softening and extrusion of the metal foils within the capsule as a result of the lack of temperature control caused by the thermocouple breakage. As a result of all of these factors, this run was not analysed.

4.6.1.2.2 TiQ2 - 4

Runs TiQ2 – 4 were performed with the same basic set up as TiQ1. Unlike TiQ1, when these runs were recovered, the constituent metals of the capsule were not found to be widely disseminated. Instead, foils remained intact and capsules were not found to have ruptured. In some cases capsules were found to be broken in half when they were recovered. The texture of the recovered pieces was suggestive of the capsules having broken during decompression of the run and not rupturing during runs. Furthermore, no unexpected behaviour was observed in the temperature data recorded during any of these runs. As such it was considered that these runs had the potential to provide useful data.

As can be seen in Table 9, this set of experiments was conducted at a pressure of 1GPa instead of 3GPa as was the case for subsequent runs and also in other aspects of the investigation. The different parts of this investigation were, in practice run simultaneously and these particular runs were the first to be completed. These experiments were run at 1GPa in order to replicate the conditions of Earth's crust (1GPa corresponds to an approximate depth of 30km). It was found that the piston cylinder apparatus did not run as reliably at this pressure, particularly for long periods, as it did at higher pressures such as 3GPa – i.e. pressures were less stable for long durations. As a result, subsequent runs were completed at 3GPa. As discussed elsewhere, this variation in the experimental pressure from the pressures which might be found in some of the real world examples of the particular process in question is not envisaged to be particularly problematic owing to the relatively small effect that pressure is believed to have on diffusion parameters. It is suggested that it would be useful, in future, to conduct work on the effect of pressure on grain boundary diffusion.

Basic SEM analysis was completed of runs TiQ2-4. Images were collected in both BSE and SE modes to provide an understanding of the condition of the capsule and its contents. Estimates of point concentrations of the constituents of the capsules were also collected using the EDS system. In the case of TiQ2, these were not calibrated against standards and so only serve as

indications of composition at the sampling points. Point concentrations recorded from TiQ3 & 4 were calibrated against standards.

4.6.1.2.2.1 TiQ2

Run TiQ2 was the first run to survive the duration of the experiment with the capsule still intact and in many ways is the most complex to understand. The capsule was constructed with an arrangement of 2 Pt foils, a Ti foil and a further 3 Pt foils (moving left to right in Figure 69). In Figure 69, the lightest coloured material is Pt, the sparse, intermediate grey material (particularly common in the central large lens of Pt and at the edges of some of the Pt structures) is Ti (rich material) and the darkest grey is quartz. All phases were observed to contain small concentrations of the other components indicating high mobility within the capsule.

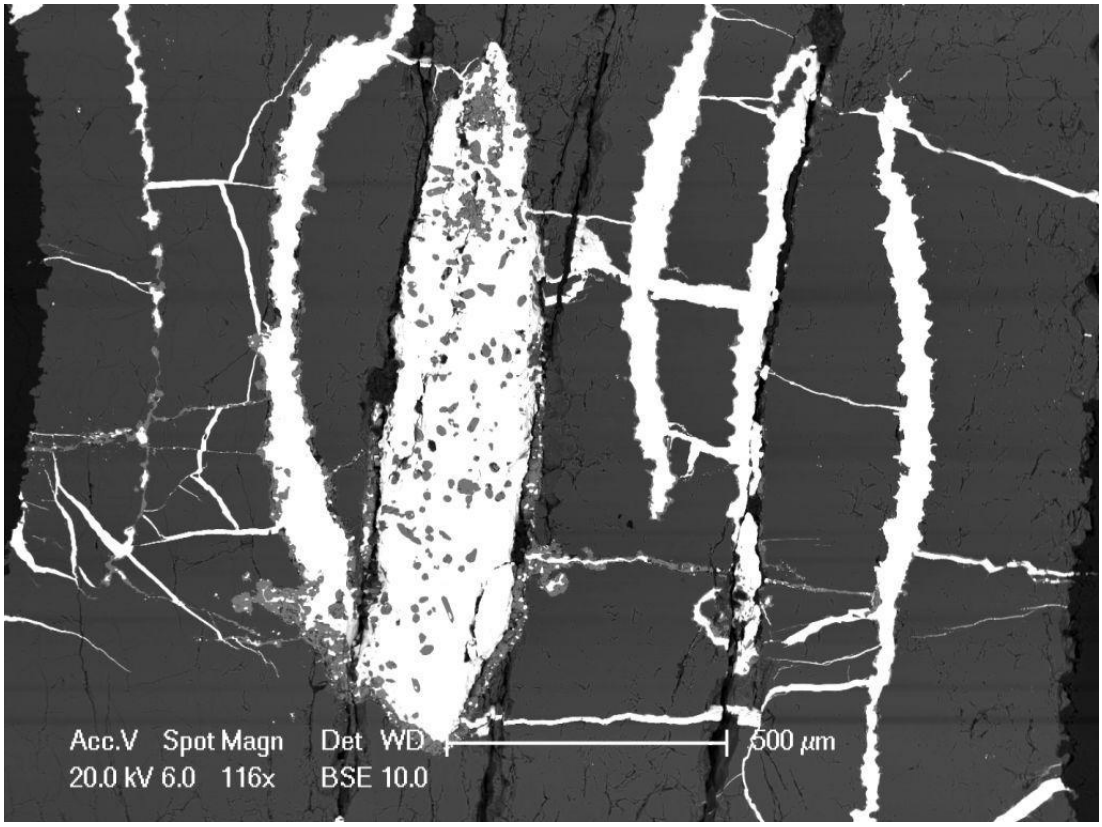

Figure 69: Back-scattered electron image of sample TiQ2

The central, thicker Ti foil has alloyed with the outer, thinner Pt foils via melt channels. Thus, any Ti detected in the Pt foils is most likely there due to alloying via these channels as opposed to via diffusion through quartz (or along its grain boundaries).

The central, largest lens of material was originally entirely Ti. However, imagery and EDS measurements indicate that following the run, the lens was largely composed of Pt. Point analyses of the area give average compositions of 59% Pt, 23% Ti and 18% Si (all expressed as atomic percentages – not calibrated against standards).

The outer Pt foils typically contained 15 – 20 atomic % Ti. They were linked to the central Ti foil by what appear to be melt channels containing in excess of 90 atomic % Ti. This suggests that the vast majority of the Ti present in the foils travelled along these channels. It is presumed that a combination of the proximity of the foils and deformation under load led to the formation of the channels. At the run temperature (1400˚C), the Pt foil is likely to have been sufficiently soft to allow it to extrude between the grains making up the quartz matrix. It is likely that this process was promoted by deformation of the capsule during compression, heating and potentially during the first couple of hours of the run as the capsule settled into the high PT conditions. Once in contact with the Ti foil, rapid alloying would have been able to occur (see Figure 70 for an indication of the depression of melting points with alloying of Pt and Ti). The resulting alloy could potentially be softer than the materials from which it was derived thereby promoting further flow. Furthermore, there is some suggestion from the phase diagram that it may just have been possible that the alloy could melt if its composition was close enough to the eutectic point. Flow of the Pt foils would be enhanced by any deformation of the sample assembly resulting from initial compression. This scenario is problematic as once flow has occurred within an experimental capsule, runs cannot be used to determine GBD for reasons which are discussed elsewhere.

Following run TiQ2, it was evident that changes needed to be made to the design of experimental runs in order to avoid similar problems occurring again. It was predicted that the flow of sink foils and run failure could be minimised by taking the following steps: (1) Increasing distance between foils to decrease probability of contact. (2) Conducting experiments at lower (more geologically relevant) temperatures (under which Pt will be less likely to flow). (3) Using an alternative sink foil which is less likely to flow at high T. (4) Decreasing the grain size of the quartz matrix. All of these steps were incorporated into the capsule design for runs TiQ3 & 4.

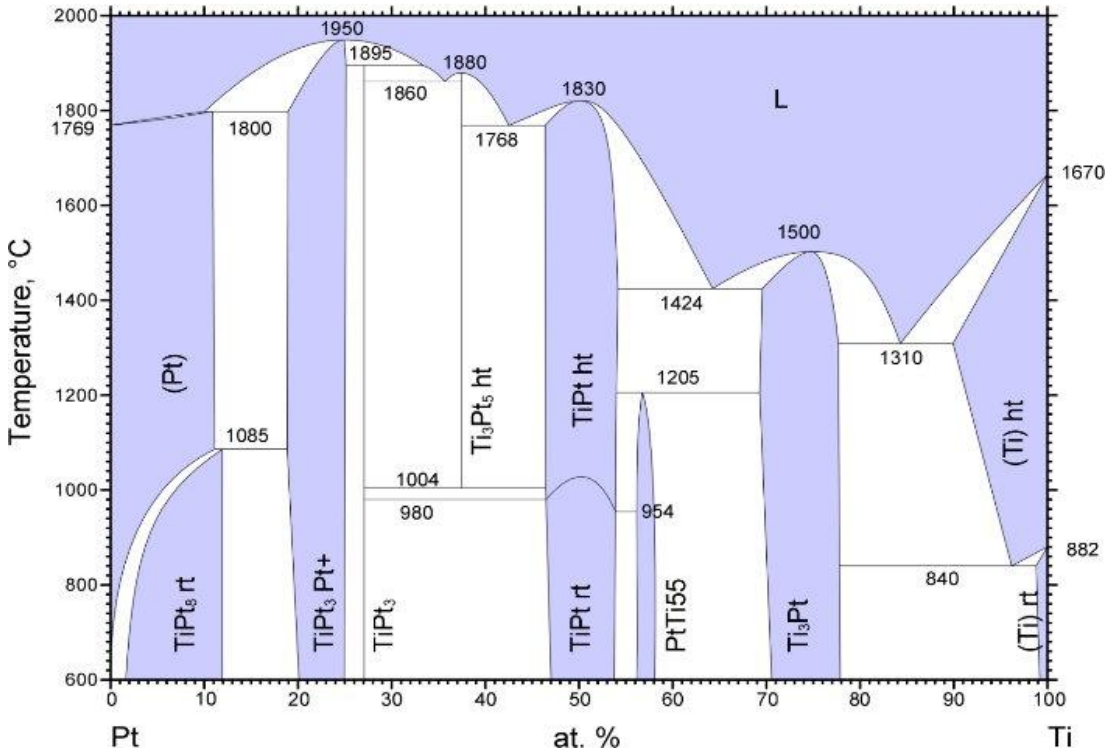

Figure 70: Pt-Ti phase diagram

Ambient pressure alloying of Pt and Ti can cause massive deviations in melting points. Hence alloying as occurred in run TiQ2 could cause the formation of melt channels as observed.

From Biggs et al., 2004 [121]

4.6.1.2.2.2 TiQ3 & 4

Following the changes to the setup which were decided upon after run TiQ2, subsequent experiments were conducted at lower temperature and using a smaller number of foils to prevent alloying and run failure. As can be seen in Figure 71, which is representative of both runs TiQ3 and TiQ4, the problem of channels forming between the Ti and Pt phases was avoided by reducing the number of Pt foils in the capsule. The deformation and extrusion of the Pt foil is also markedly reduced at lower T. EDS point measurements (calibrated against standards) were unable to detect any Ti in the Pt foils (within the detection limits of the EDS system used). Furthermore, it was not possible to detect any Ti within the quartz even at very high proximity to the Ti. This is not surprising as, in the case of lattice only diffusion, one would expect concentrations to drop to 0 within 2µm of the source within these experimental conditions. The EDS method was unable to detect any Ti residing at grain boundaries. This could be due to either the spatial restraints (spot size was 5µm compared to a predicted grain boundary widths of approx. 5nm) or that very little diffusion had occurred. As a result it was decided that EDS analysis would not provide the necessary resolution or sensitivity to detect Ti in quartz in the concentrations which were likely to be present. Thus, it was decided that future runs would be analysed by EPMA. Furthermore, it was decided that the capsule design should be changed so that there was a larger Ti source and no foils so that the problems experienced in run TiQ2 were

not repeated. These considerations were taken into account when designing the second experimental set.

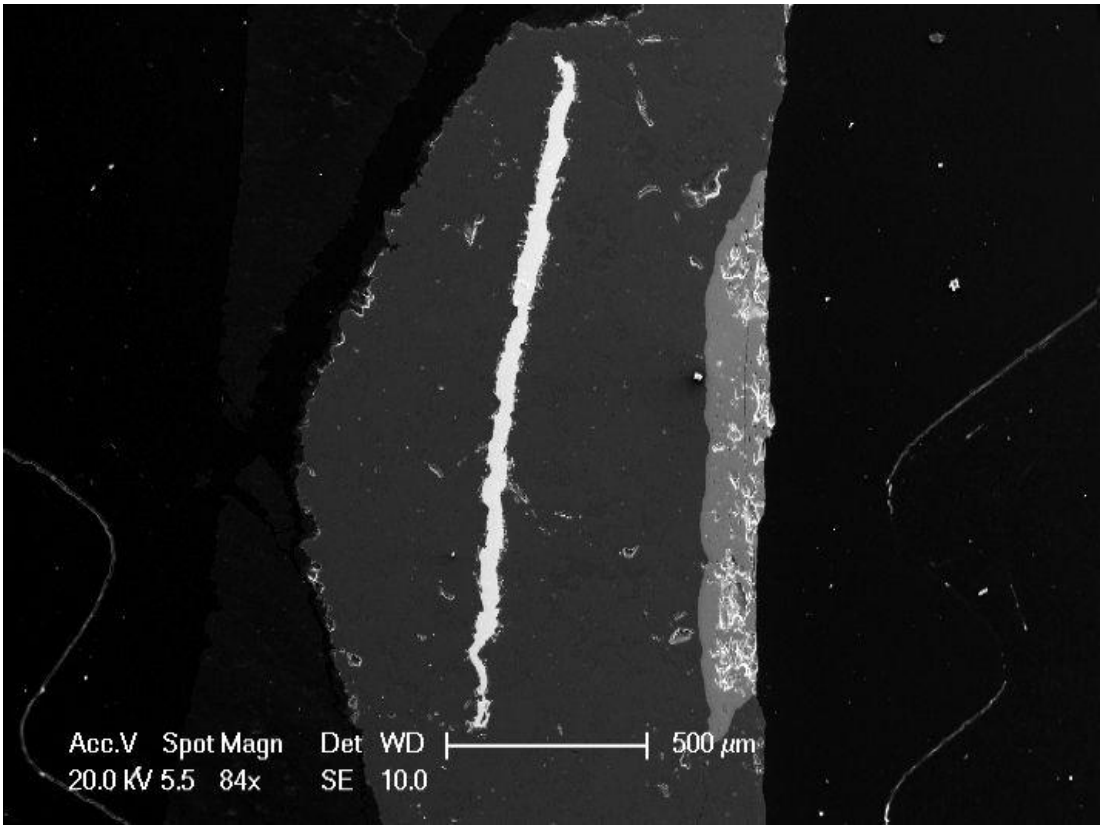

Figure 71: Secondary electron image of half of TiQ3

The lightest area is the Pt foil, the next lightest is the Ti foil, the medium grey is the quartz host and the darkest grey is the carbon capsule. The capsule has split along the line of the central Ti foil. The other half of the capsule is effectively a mirror image of this.

4.6.2 Second Experimental Set

Following the failure to obtain data from runs TiQ1 – 4, an experimental re-design was undertaken. The design for this second set of experiments is shown in section 4.2.2 Second (Final) Capsule Design and the materials and methods used are discussed subsequently. This design proved to be very successful and provided all of the quantified diffusion data reported here. As previously mentioned, the capsules were found to break into a series of discs upon decompression and during recovery. Whilst this was initially considered to be problematic, this was in fact very useful as it allowed for very effective diffusion measurements to be taken by measuring the Ti contents of quartz in a series of points extending radially from the capsule edge. Here, specific observations and results from each run are reported.

4.6.2.1 Summary of Run Parameters

Run ID	Temp (°C)	Pressure (GPa)	Wet/Dry	Duration (hr:min)
TiQ5	1400	3	Dry	23:50
TiQ6	1400	3	Dry	25:31
TiQ7	1200	3	Dry	45:55
TiQ8	1300	3	Dry	50:44
TiQ9	1000	3	Dry	96:46
TiQ10	1000	3	Dry	72:44
TiQ11	1000	3	Wet	97:09
TiQ12	1000	3	Wet	20:15

Table 10: Run Parameters of Second Capsule Design Experiments

4.6.2.2 Specific Run Observations

4.6.2.2.1 TiQ5 - 10

Runs TiQ5 – 10 were those from which the vast majority of the data in this aspect of the investigation was obtained. These experiments were run dry (i.e. with no water added to the capsule) and at temperatures ranging between 1000°C and 1400°C. Lower temperatures were not investigated in this aspect of the investigation owing to the very large amounts of time which were suspected to be needed for a measurable diffusion profile to form under such conditions. Figure 72 to Figure 77 show concentration/distance plots for runs TiQ5 – TiQ10 inclusive. In each case, the blue points are all of the data points collected from a given run (i.e. where sets of points were collected from each of a number of capsule "discs" derived from a given experiment, the points from each disc are amalgamated into a single concentration/distance plot). Initially, concentration/distance data was plotted for single discs only as it was suspected that the differing distances of each disc from the lid or base end of the capsule, which, along with the capsule walls, acted as a source of Ti. Upon inspection of the data from each of these individual lines it

was found that there was good consistency between all discs from a given experiment and so data was amalgamated into one plot per experiment. It was found that when this was done, better fits to an Arrhenius equation could be made. In each case profiles are shown extending a distance of 200µm from the capsule wall (i.e. the interface with the Ti source). Data collected from early analysis sessions (where it was not known how long diffusion profiles might be) frequently included points at greater distances than this but is not shown here as, in all cases, the concentrations were, within background, zero. A test was performed to check if the removal of these values from a dataset would affect the value of the diffusion coefficient which was returned by the non-linear regression fitting technique – no differences were found. Error bars reflect the values discussed in section 4.5.2 Calculation of Errors. In cases where error bars are not clearly visible they are within the size of the plotted point. It is clear that there are larger potential errors in the data at greater distances from the Ti source. However, in almost all cases, the area in which these larger errors are present is in the region where concentration of Ti in quartz has dropped to zero. As such, these points have little to no bearing on the determination of the diffusion coefficient.

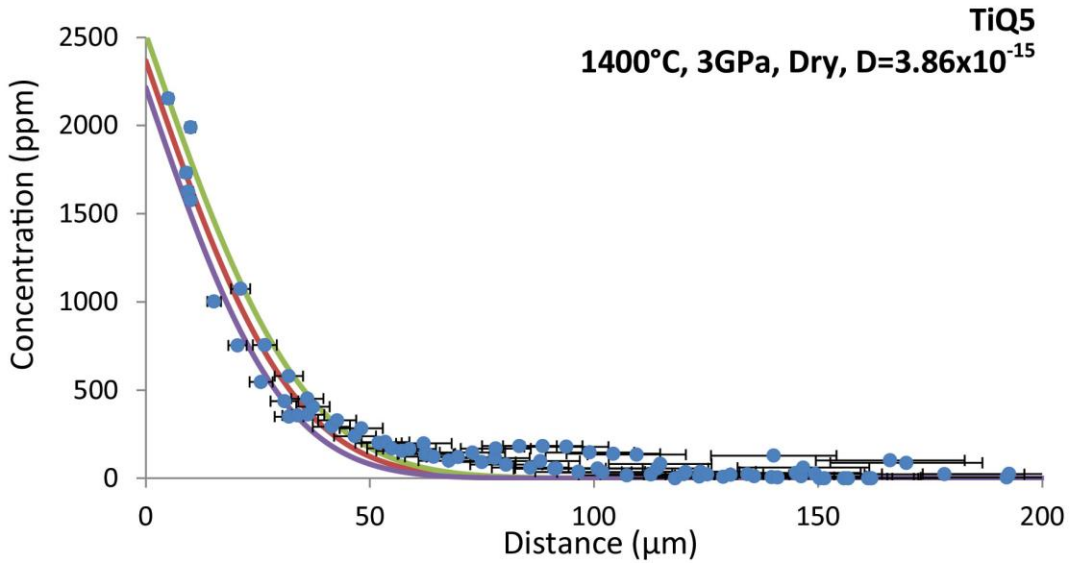

Figure 72: Concentration/Distance Plot of Run TiQ5

Data and model fit. Details as in Figure 37

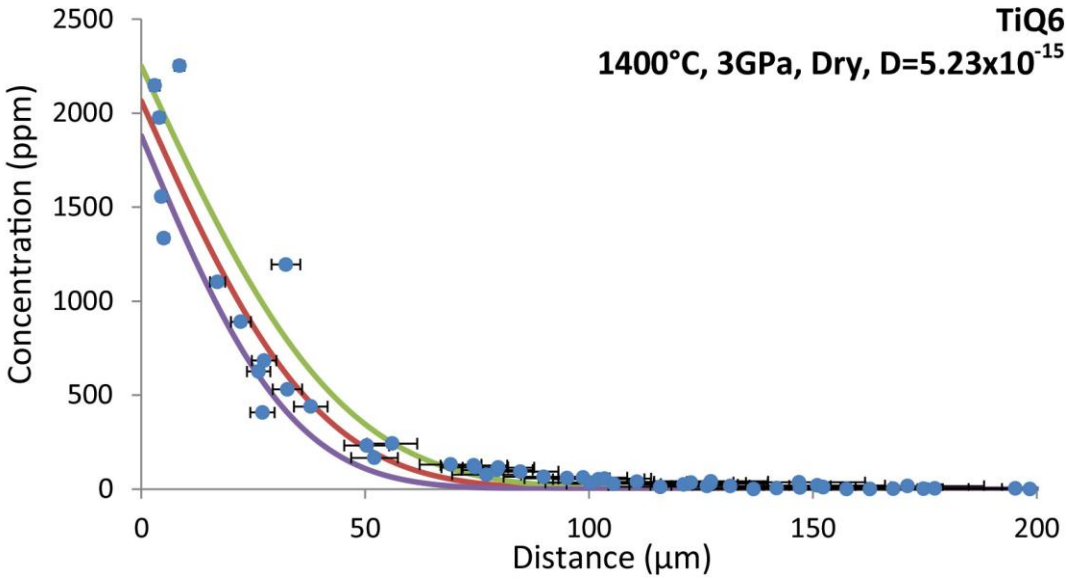

Figure 73: Concentration/Distance Plot of Run TiQ6

Data and model fit. Details as in Figure 37

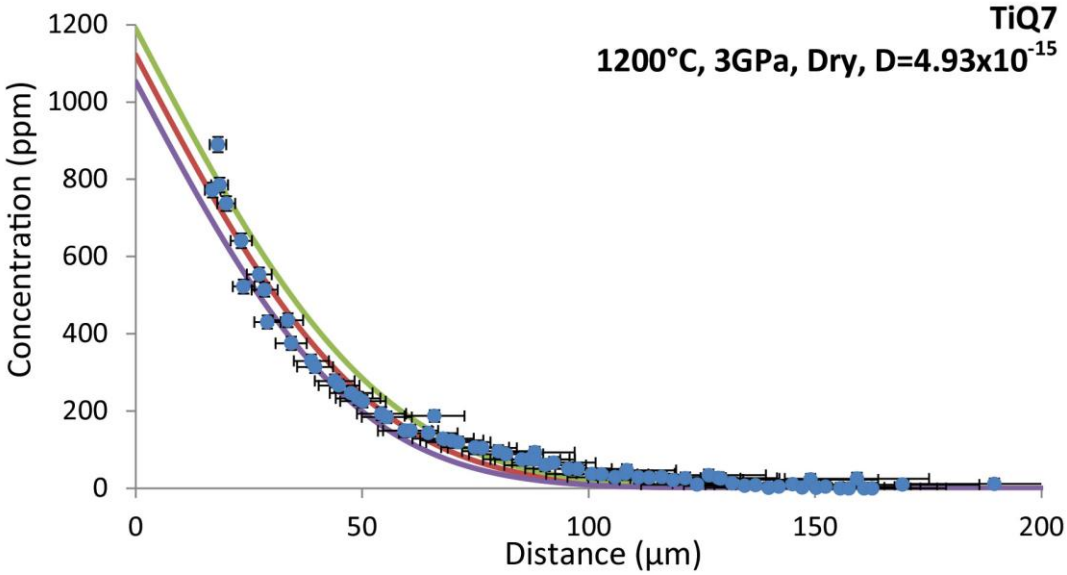

Figure 74: Concentration/Distance Plot of Run TiQ7

Data and model fit. Details as in Figure 37

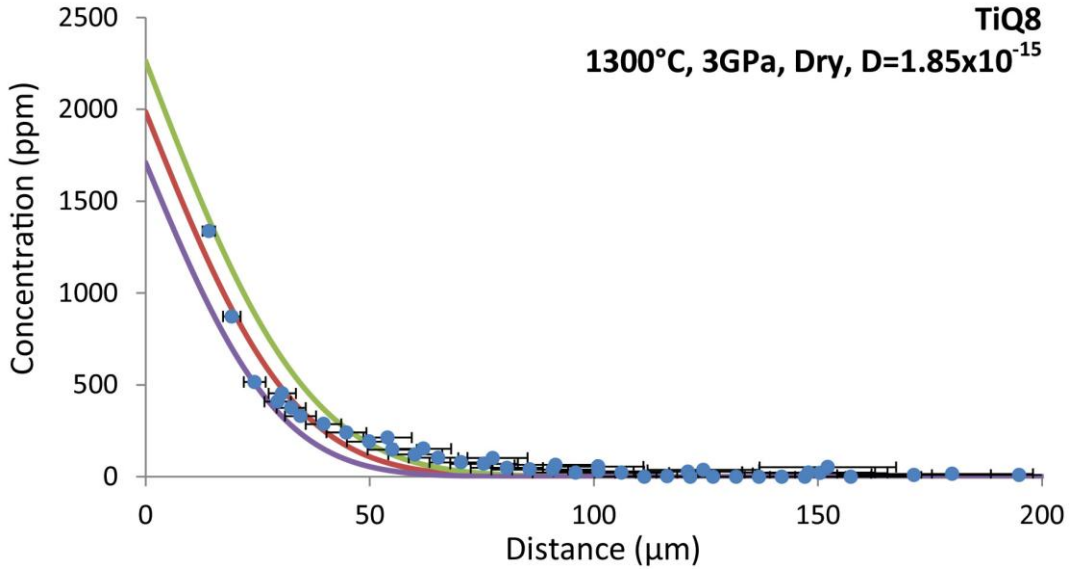

Figure 75: Concentration/Distance Plot of Run TiQ8

Data and model fit. Details as in Figure 37

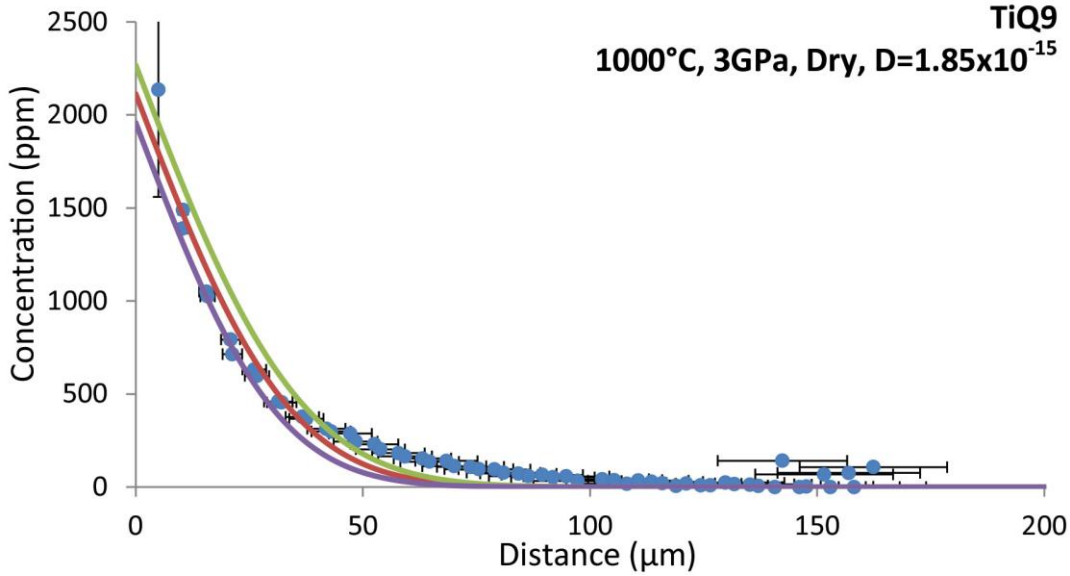

Figure 76: Concentration/Distance Plot of Run TiQ9

Data and model fit. Details as in Figure 37

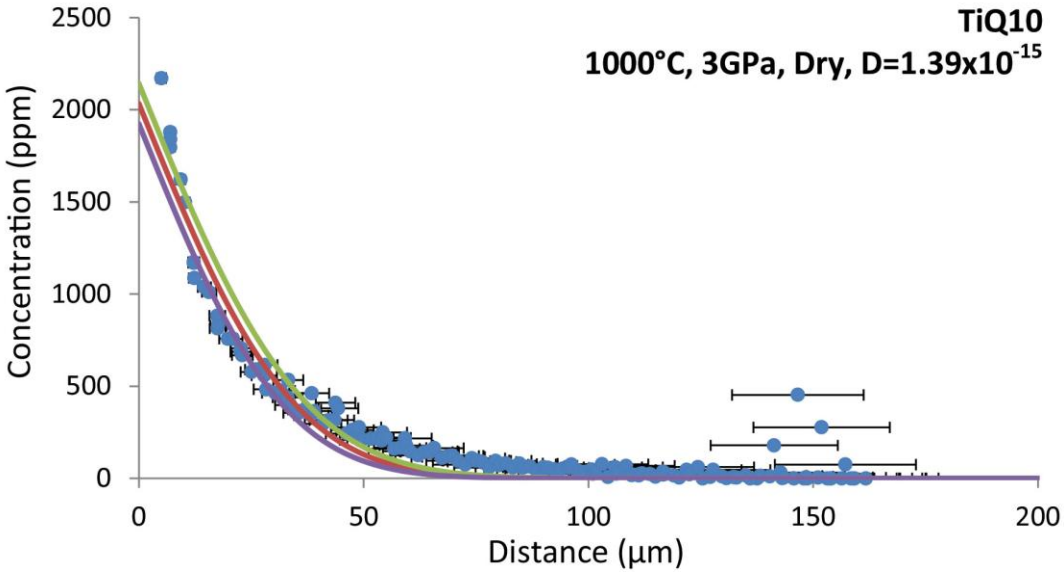

Figure 77: Concentration/Distance Plot of Run TiQ10

Data and model fit. Details as in Figure 37

4.6.2.2.2 TiQ11

Unlike the previous runs, TiQ11 contained water so as to test the hypothesis that its inclusion might increase Ti diffusion rates. As such it was considered to be a very important run as it would provide useful data to understand the effect of water on Ti diffusion. It was found during SEM analysis of the run that a melt phase had developed and travelled along grain boundaries. This phase can clearly be seen picking out grain boundaries in Figure 78. EPMA readings were taken along a line in a similar way to all other runs.

Figure 79 & Figure 80 show diffusion profiles recorded from EPMA analysis of run TiQ11 (specifically of disc TiQ11A). Figure 79 shows the profile as it was originally recorded. Within the profile are many very high concentration points with concentrations as high as 600,000ppm. Values such as this (indeed values of more than a few thousand ppm) are higher than the maximum permitted solubility of Ti in quartz at the conditions of the experimental run in question. As such, the presence of concentrations of this magnitude is indicative of the formation of Ti bearing phases, possibly TiO_2 (rutile) within the sample. It is likely that very high concentration points of this nature are a result of the direct sampling of rutile by the incident electron beam. This TiO_2 rich phase may also be in the form of very fine lamellae within the quartz structure. In order to test such a hypothesis, very high resolution investigation using equipment such as a TEM (Transmission Electron Microscope) would be necessary. The implications of this observation are discussed in section 4.7.1.6 Development of Fluid Phases.

Figure 80 shows the same diffusion profile but with the points with concentrations higher than permitted by the run conditions removed. As such, the points shown are believed to represent the

Ti contents of the quartz instead of the presence of Ti phases. It is clearly evident that the figure shows a realistic diffusion profile. As such, it may be possible to derive diffusivities from this run albeit with a low degree of confidence. The degree of confidence associated with the measurement is discussed in subsequent sections.

Whilst it is highly desirable for analysis of this run to generate useful diffusion data, owing to it having contained water, it must be rejected if a proper understanding of the mechanisms at play suggest that grain boundary diffusion cannot be isolated.

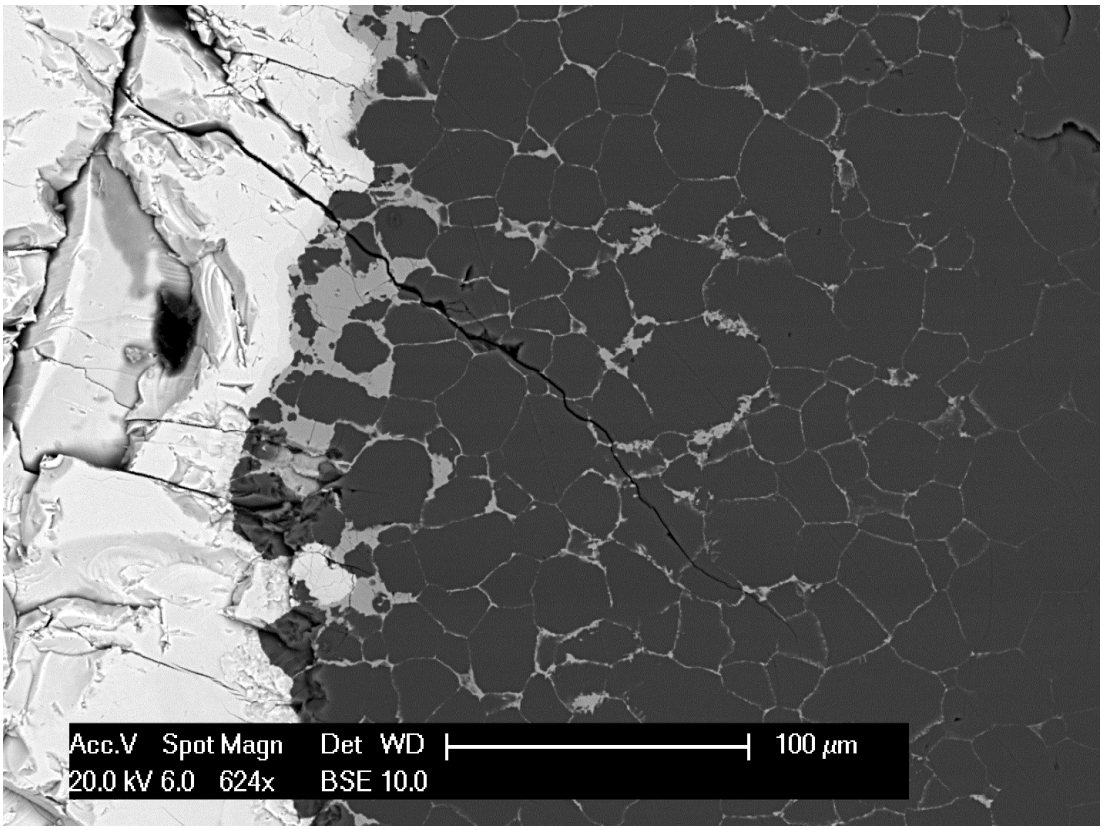

Figure 78: BSE SEM Image of TiQ11A showing TiO_2 at Grain Boundaries

A TiO_2 phase is present at and delineates quartz grain boundaries. The shade of the phase represents its mean density. The way in which the phase is incorporated at grain boundaries is suggestive of it having been present as a fluid during the experimental run.

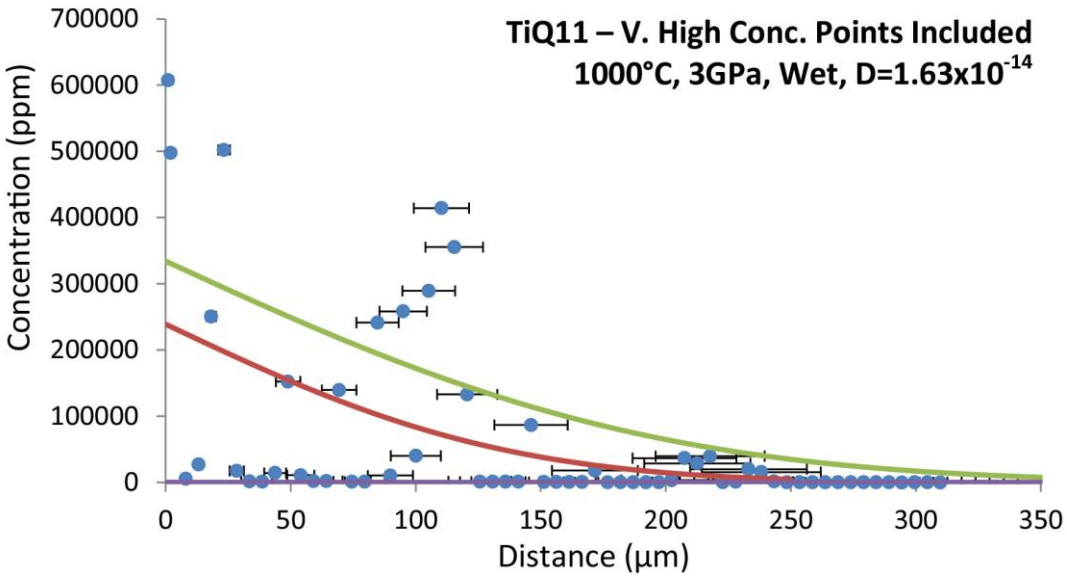

Figure 79: Concentration/Distance Plot of Run TiQ11 with Very High Concentration Points Included

The inclusion of water in this run has led to exceptionally high concentrations of Ti being recorded from analysis lines. The concentrations of the points which are clearly visible as being above the 0 value line are higher than the solubility limit of Ti in quartz at the temperature and pressure of the run. Details as in Figure 37

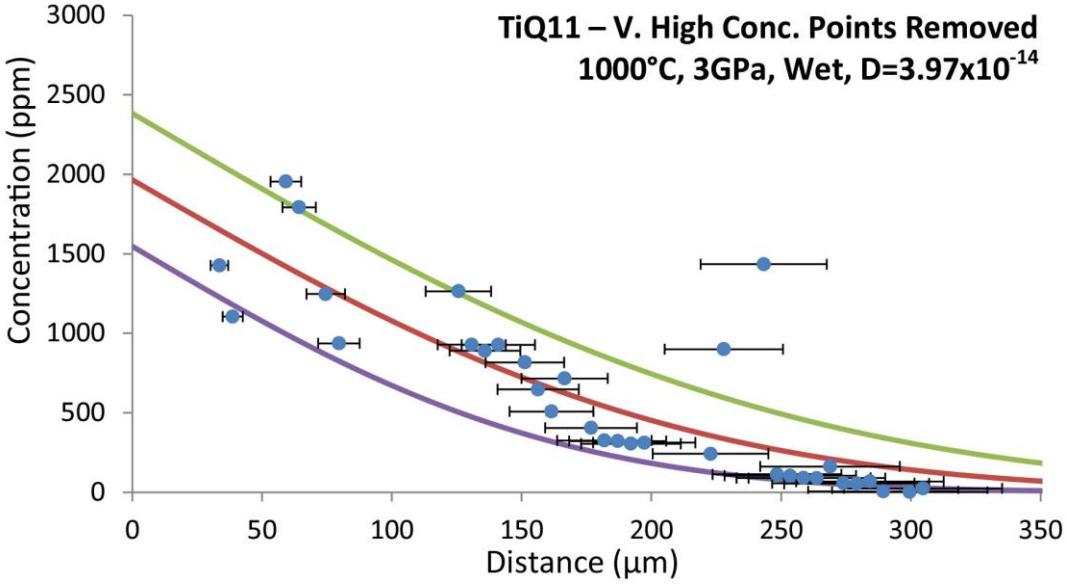

Figure 80: Concentration/Distance Plot of Run TiQ11 with Very High Concentration Points Removed

Only points which are within the solubility limit of Ti in quartz at the run conditions are included. A far more typical dataset is found to exist. Details as in Figure 37

4.6.2.2.3 TiQ12

Only 2 discs were recovered from run TiQ12, both of which came from the ends of the capsule. Once polished, only a very little amount of quartz was exposed on each disc. Of the quartz which was exposed, only a very thin smear was present (owing to a small amount of topography in the capsule lid and base). As such, data acquisition from the run was exceptionally difficult. Figure 81 shows SE images of the two discs which were recovered from TiQ12.

In practice it was not possible to obtain any useful diffusivity data from run TiQ12. This was due to its extremely fragmented nature and the very thin layers of quartz which were present as "smears" on the Ti surfaces. The thinness of these smears and their proximity to the Ti surfaces meant that they had exceedingly variable Ti contents and as such it was not possible to fit a diffusion law to any of the data obtained.

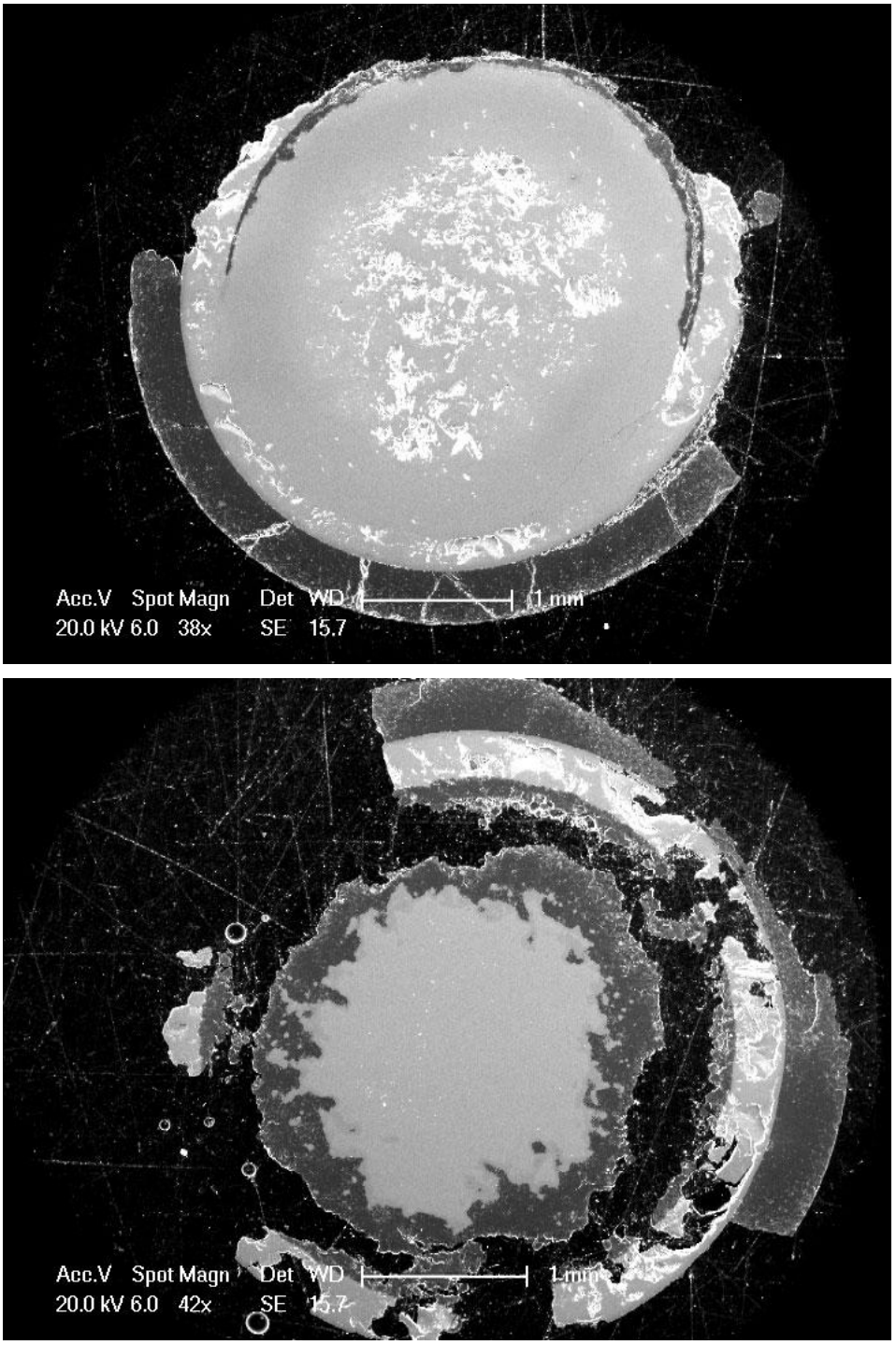

Figure 81: Capsule TiQ12 Discs A & B

Top image is disc TiQ12A and bottom image is disc TiQ12B. In both cases the lightest coloured material is Ti. The small amounts of darker material inside of the ring of Ti (the capsule wall) is quartz. In disc A only very small rims of quartz are present and in disc B it is not possible to tell how far the fragments of quartz were from the Ti source as the capsule is so fragmented.

4.6.3 Summary of All Run Results

Data was obtained from 7 of the 8 experimental runs which were deemed to have been successfully completed within this series. Results are detailed in Table 11.

Run ID	Temp (°C)	Pressure (GPa)	Wet/ Dry	Duration (hr:min)	Diffusion Coefficient (m^2s^{-1})	Initial Conc. (ppm)
TiQ5	1400	3	D	23:50	$3.86x10^{-15}$	2370
TiQ6	1400	3	D	25:31	$5.23\ x10^{-15}$	2060
TiQ7	1200	3	D	45:55	4.93 x10-^{15}	1120
TiQ8	1300	3	D	50:44	$1.85\ x10^{-15}$	1990
TiQ9	1000	3	D	96:46	$1.85\ x10^{-15}$	1990
TiQ10	1000	3	D	72:44	$1.39\ x10^{-15}$	2030
TiQ11	1000	3	W	97:09	$3.97\ x10^{-14}$ Low reliability	1960 Low reliability
TiQ12	1200	3	W	20:15	Unable to determine	Unable to determine

Table 11: Summary of Ti Diffusion along Quartz Grain Boundaries Run Results

These results are summarised in the form of an Arrhenius diagram in Figure 82 which clearly shows that there temperature has a relatively weak effect on diffusivity in this system.

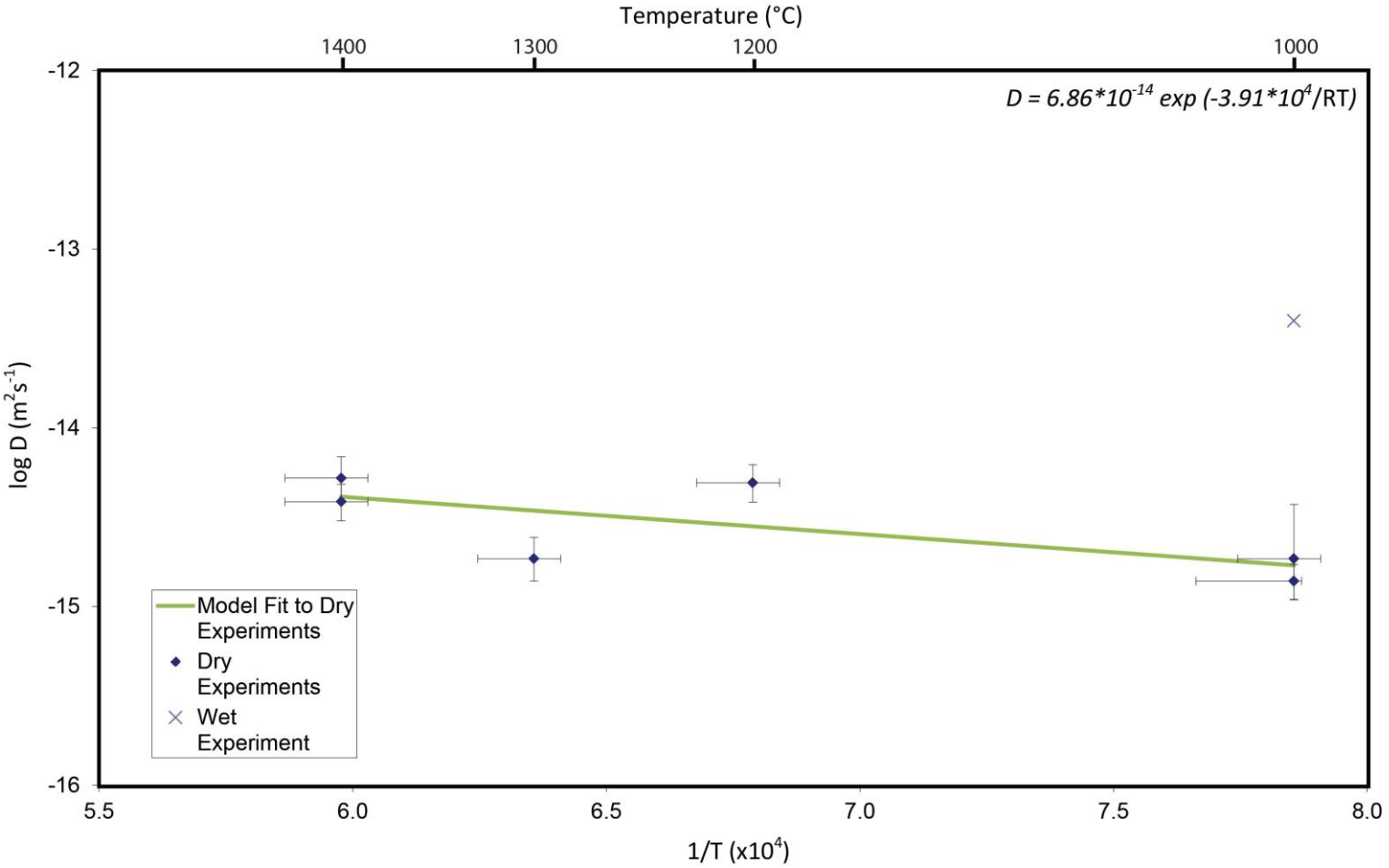

Figure 82: Arrhenius Diagram showing Temperature Dependency of Grain Boundary Diffusion of Ti in Quartz

Variation in diffusivities with temperature is clear with the measured effect being weak. An Arrhenius equation can easily be fitted to the measured data. Errors associated with the fitting process fall within the range of the individual error bars shown for each run.

4.7 Discussion & Interpretations

4.7.1 Discussion of Factors which could Affect Data

4.7.1.1 Diffusion into quartz grains

Unlike in the previous work on grain boundary diffusion of volatiles, a host medium which is able to preclude lattice diffusion through itself has not been used here. Indeed, as the host medium is also the sink medium it is necessary that a certain amount of lattice (or associated) diffusion of Ti in quartz must occur in order to allow Ti to travel from grain boundaries into grains to the point at which they are detected by EPMA. Whilst grain boundary diffusion cannot be isolated here in the same way as in the previous work, the very slow lattice diffusion rates published by other workers from well designed experiments using single crystals [3] can be compared to values of Ti mobility determined here, and the relative rates of GB vs lattice diffusion compared. Within the timescales and conditions of the experiments conducted here, lattice diffusion can only account for a very small portion of the total diffusion which has occurred during a given run. Previous studies on lattice diffusion of Ti in quartz used perfect crystals with no visible defects. This work has utilised sintered quartz which has subsequently been ground in preparation for this work. As such, it has undergone a significant amount of mechanical working which is likely to have introduced a large number of defects into the crystal structure. It is these defects which are likely to be extensive throughout the crystal and may be linear, planar or indeed more complex, which may well allow Ti to effectively move into the centre of grains. Even relatively large quartz grains with a diameter of a large enough size that it would not be possible for them to equilibrate with regard to Ti within the timescale of an experimental run by lattice diffusion alone record Ti concentrations which are significantly above background levels when they are in close proximity to the Ti source.

4.7.1.2 Return Diffusive Flow

In many cases a reaction texture was identified, using BSE imaging, which was indicative of changes having occurred to the Ti capsule during the experimental run. The relative darkness of phases within these BSE images was suggestive of the rim having developed a lower than previous mean atomic density during the run. This would suggest that, even though this phase was the source of diffusant for this run, there was a return flow of some chemical species. It is considered likely that Si may have diffused into the Ti wall. An example of such a texture can be seen in Figure 83. A full analysis of such features was not undertaken primarily due to time constraints. Whilst it is interesting to note such features, they are not considered to be of great relevance to the data obtained from such experiments.

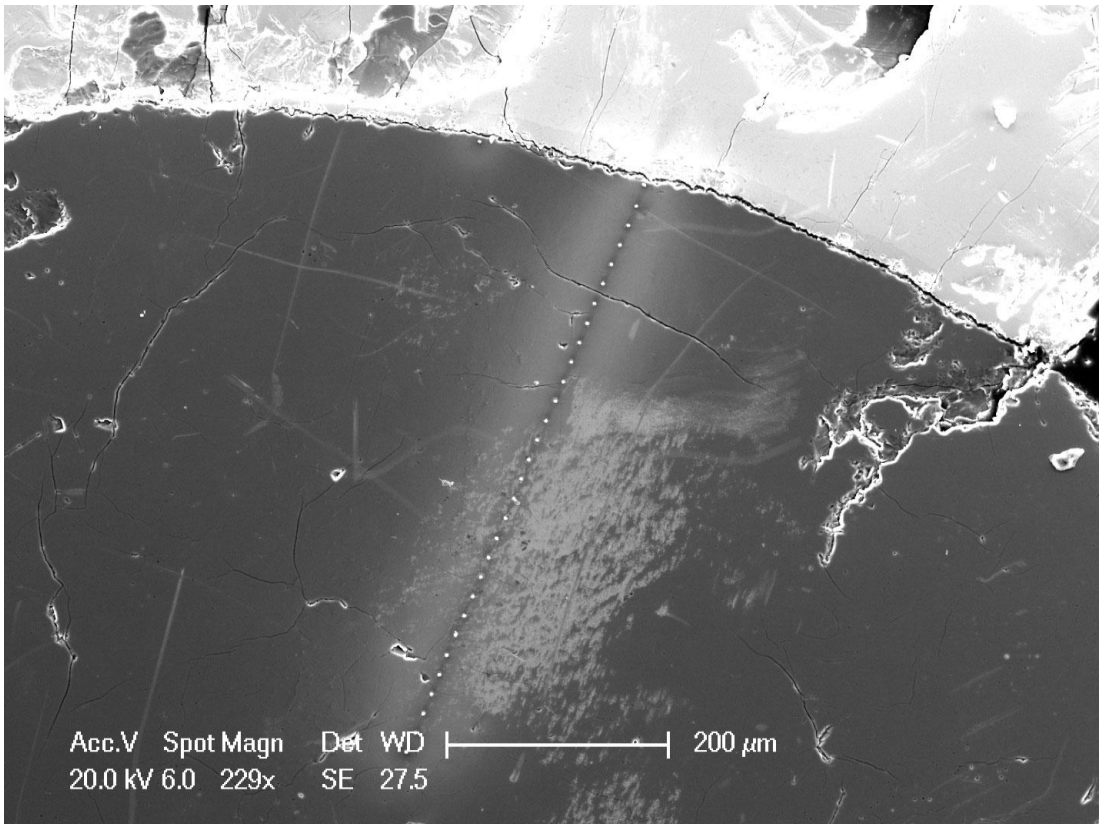

Figure 83: Example of a Reaction Rim at the Interface of Ti & Quartz

A reaction rim can be seen at the interface of the Ti capsule wall and the quartz contents. A series of EPMA analysis points can also be clearly seen. Other images collected in BSE imaging mode are suggestive of the rim being made of either disbursed TiO_2 or that Si has taken up residence within the Ti structure.

4.7.1.3 Dynamic Changes to Diffusive Pathways

Dynamic changes to diffusion pathways are likely to have taken place during the running of experiments within this aspect of the investigation – as is the case with all aspects. Changes in the available routes for diffusion as the run progresses have the potential to change the values of diffusion parameters and as such it is essential that the effects of such a process are fully considered. A full discussion of this issue can be found in section 3.7.1.7 Dynamic changes to Diffusive Pathways during Experimental Runs. Whilst the discussion is framed in the context of grain boundary diffusion of volatiles, the concepts and processes which are detailed are equally applicable here.

4.7.1.4 Variations in Ti Solubility with Pressure

The solubility of Ti in quartz varies with pressure and previous work on the subject has considered relatively low pressures. As such, it is necessary to consider the effect of pressure variations on the solubility of Ti in quartz at the conditions used in this investigation. Determining the maximum concentration at which Ti could be present in the quartz under

such conditions is a non-trivial exercise. Here, calculations have been performed using the data of Wark and Watson [2] and Thomas et al. [59] to estimate Ti solubility at the high PT conditions used in the experimental runs. The experiments used as the basis of these works were conducted at pressures of 5 – 20 kbar (0.5 – 2GPa) whereas the work conducted here was at a pressure of 3GPa. Figure 84 and Figure 85 show the relationship between pressure, temperature and Ti content in quartz that they found (NB This is a topic of ongoing research and debate and refinements are currently being published on a regular basis e.g. Huang & Audétat 2012 [118], as such the precise quantification of the relationship may be subject to change but it does appear that the overall relationship is sound). The relationships show that at higher pressure, less Ti can be accommodated in quartz. This effect is the inverse of that for temperature where increasing temperatures allow increasing solubility. As such, the interplay of the two effects is important in determining how much Ti can be taken up by quartz. This in turn is of great importance in calculations of diffusivity as grains will only be able to record Ti contents within solubility limits (before separate Ti rich phases form).

During experimental runs, it was found that the piston cylinder apparatus lost pressure as the experimental assemblage reacted to and settled into the high pressure conditions in which it found itself. As such, runs were in practice continually losing pressure at a low rate and were periodically returned to their nominal pressure. This has the implication that at certain points, particularly when long duration experiments were left to run overnight, runs were under lower pressure conditions than planned. Given the information discussed above on the effect of pressure on solubility, this has the implication that Ti may have been more soluble in the quartz than would otherwise be expected. If this is indeed the case it may lead to higher than expected diffusion coefficients being calculated as more Ti present in the quartz than should be. However, Ti contents exceeding the solubility limit are only likely to occur very close to the Ti source and so are only likely to be detected in one or two of the most proximal analysis points. As such, the points, which are part of a large dataset will have some influence on the fitting of a diffusion law but the effect of a slightly higher than expected value will be very minimal and in all likelihood well within the error bars as defined by other sources of error. As such, variations in Ti solubility caused by pressure variations are expected to have very little effect on the overall quality of data obtained in this investigation.

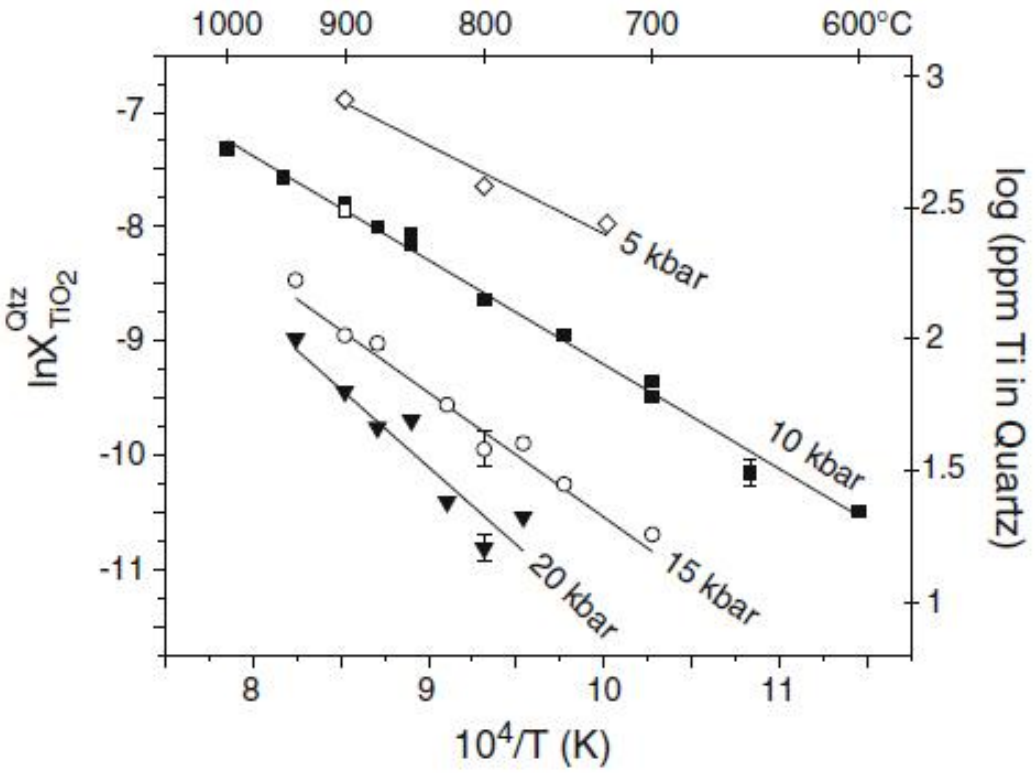

Figure 84: Temperature and Pressure Dependence of Ti content of Quartz

Four experimental series conducted at different pressures are shown and least squares fits have been performed. Ti content decreases with temperature and with increasing pressure. From Thomas et al. [59]

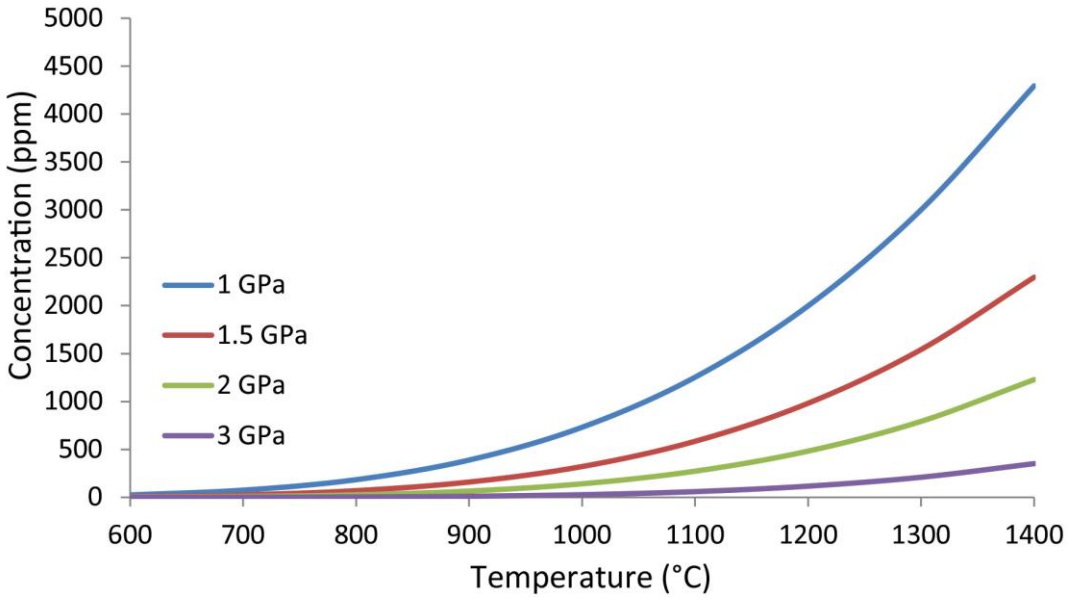

Figure 85: Predicted Variability of Ti solubility in Quartz with Temperature and Pressure *Experiments conducted by Thomas et al. went up to pressures of 2GPa, the 3GPa line is therefore an extrapolation of this figure, as are the calculated solubilities at temperatures greater than 1000°C. There is doubt regarding the viability of this extrapolation (see text). Based on the relationships described in Thomas et al.,* [59].

4.7.1.5 Method of Data Analysis

As the second set of experiments with the new capsule design were analysed in two batches, it was possible to refine the measurements recorded in the first batch for certain samples. This was possible as the first batch to be analysed gave a value for the diffusion coefficient which could then be used to determine the likely length of the diffusion profiles to be analysed in the second analysis section. A good example of this development in measurements can be seen in the concentration/distance plots for run TiQ5 (Figure 86).

By doing this it was possible to progressively improve the quality of the data recorded even though the starting point was one of only being able to guess at diffusivities to within a few orders of magnitude. In practice, the diffusion coefficients determined from low and high resolution line profiles were very similar and it was because of this that, ultimately, all datasets for a given experimental run were combined. By doing this, a true representation of the diffusivity in a given run could be determined as the effects of background noise in datasets was diminished by the large number of other, non-noisy points.

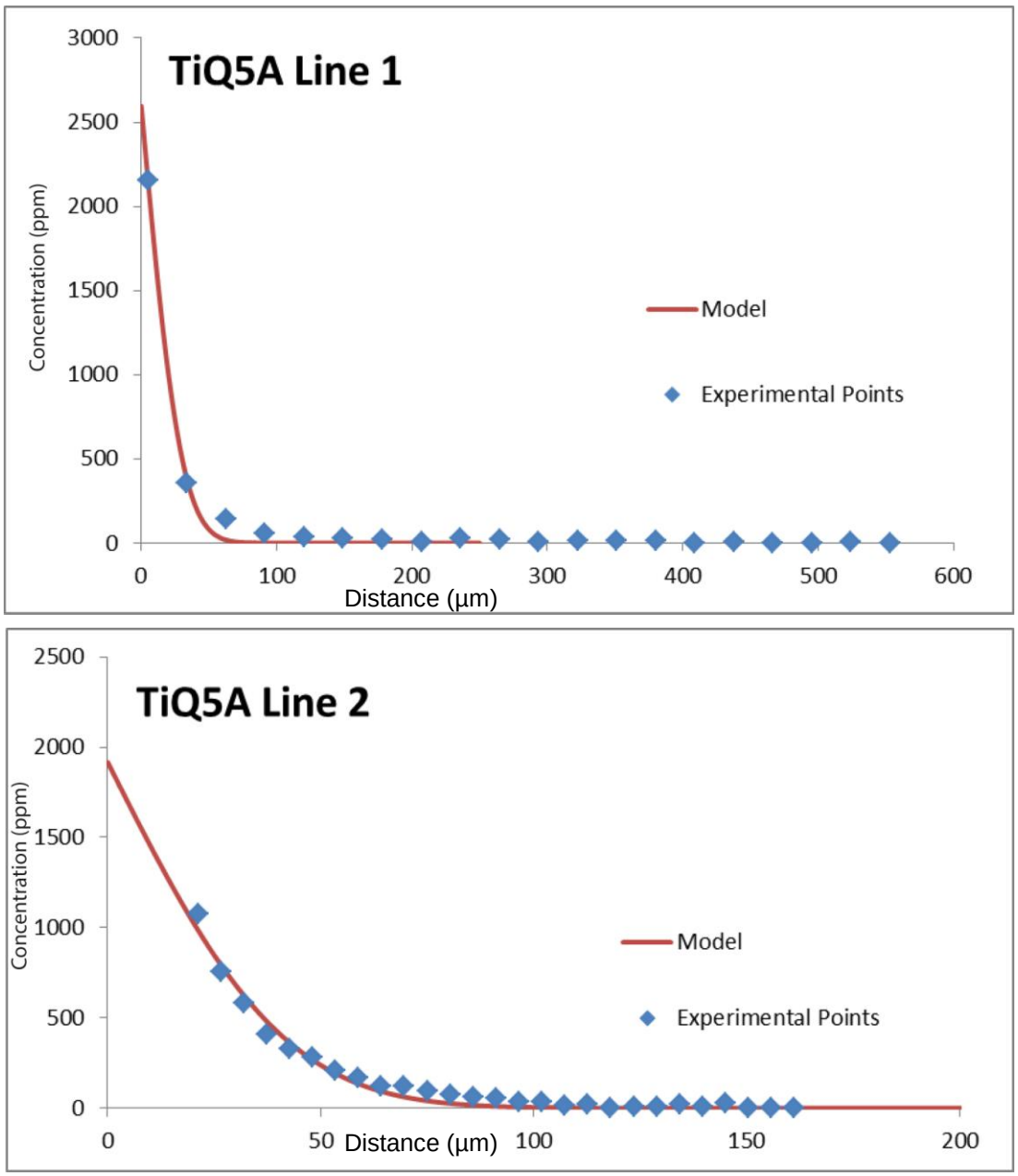

Figure 86: Concentration/Distance Plots from the same Run at Different Point Spacings

The two respective datasets were recorded at different times with the upper set recorded first and the lower set recorded second. The length of the profile recorded in the upper set is significantly longer owing to the lack of knowledge of diffusivity at the time of the analysis being recorded. As such, there is relatively little data available at the high proximity end of the profile where the slope of the model fit line (and so the value of the diffusion parameters) is defined. The lower set was recorded after diffusivity had been broadly determined and so it was possible to record a profile of the approximate length to gain as much resolution as possible in the critical part of the profile. Ultimately the diffusion parameters calculated from each profile were very similar.

4.7.1.6 Development of Fluid Phases

No evidence for the development of fluid phases was found in either of the stages of SEM analysis conducted on dry experimental runs (TiQ5 – 10). Runs were carried out under conditions where the constituents of the capsule were not expected to melt. However, the final two runs (TiQ11 & 12) were conducted with water added to the capsule. BSE SEM images of TiQ11 (Figure 78) suggest that a fluid phase may have developed and travelled along grain boundaries. This phase appears as one of intermediate brightness between that of Ti capsule wall diffusant source and the quartz contents of the capsule (see section 2.4.1 Scanning Electron Microscopy (SEM) for a discussion of the mechanism by which such images are generated) suggesting that it may have formed by an interaction of the Ti, quartz and water under the conditions of the run. The identification of the phase as having been a fluid during the run is based upon its textural appearance. SEM EDS & EPMA WDS analysis suggest that its composition is TiO_2 – rutile. Given the possibility that the phase may have existed as a fluid during the run, the data obtained from the run must be treated with a degree of caution. This is due to the fact that the motion of the fluid along grain boundaries may be mechanically driven with the fluid reacting to the pressure of the run by forcing its way along grain boundaries. Furthermore, the fluid is likely to act as a conduit for diffusion of Ti which may very well operate at a different rate to the grain boundary diffusion which is the subject of the investigation. Such processes are likely to produce a very noisy dataset and this is what was observed during SEM imaging.

Once a fluid phase has developed it may quickly move along grain boundaries. As soon as the fluid is in contact with a grain, Ti contained within it will be able to begin diffusing into that grain. As the fluid phase may move from its source, along grain boundaries very quickly once it has formed, the amount of time it may take to reach a distal grain may be very short compared to a standard grain boundary diffusion scenario where fluid phases are not involved. As such, Ti levels detected in such grains may be higher than they otherwise would be given their distance from the Ti source. This will lead to higher than correct diffusion coefficients being obtained. As such, an appropriate degree of confidence must be attached to any quantified parameters derived from runs where fluid phases have been discovered.

As previously mentioned, it is likely that fluid phases developed in run TiQ11 and, as a result, the diffusion parameters obtained from analysis of the run must be treated with a very low degree of confidence. This is due to the fact that transport via grain boundary and grain edge fluid mechanisms cannot be decoupled and as such it is impossible to know how much grain boundary diffusion has contributed to the observed diffusivity. This is particularly inconvenient as this run was the only successful experiment which was run with water included. It is likely that the presence of water assisted the formation of the fluid phase and

it is suspected that it may also have caused increased grain boundary diffusivity. In future follow ups to this work it would be advisable to reduce the temperature of wet runs in order to reduce the chances of additional phases forming. A full investigation into fluid assisted grain boundary diffusion would involve a significant experimental program in itself and would be an excellent follow up to this work.

4.7.1.7 Range of Temperatures Investigated

The experiments which were run for this aspect of the investigation were conducted at temperatures of between 1000 and 1400°C. This was done to ensure that enough diffusion occurred within the duration of a run for a measurable diffusion profile to be generated. It was known in advance of the work that lattice diffusion rates for Ti in quartz are exceedingly slow and it was also known that typically grain boundary diffusion coefficients are approximately 3 – 5 orders of magnitude higher. As such, it was possible to determine that if experiments were conducted at temperatures of less than 1000°C, it was likely that so little diffusion would occur that a measurable diffusion coefficient may not form within the timescales available to run experiments. In practice the combination of timings and conditions which were used allowed good diffusion profiles to form to which a solution of Fick's Second Law could easily be fitted. There is a however a negative aspect to running the experiments at such high temperatures and this is one of geological relevance. This set of experiments has essentially been carried out under conditions more representative of earth's mantle than of the crust where quartz exists. This is not considered to be a significant problem for a number of reasons. Firstly, the temperature dependence of diffusion, as shown in Figure 87, is, in all similar scenarios, able to be extrapolated to lower temperatures without encountering any difficulties (this approach is common in studies of diffusion). When plotted on an Arrhenius plot, temperature dependencies are consistently able to be fitted to a linear model therefore implying that extrapolation is straightforward. Furthermore, the findings, at the temperatures of the investigation are consistent with the use of the TitaniQ geothermometer which, from the experiences of other workers appears to work well. As such, it is not considered that the deviation in temperatures used in this investigation as compared to the natural settings at which TitaniQ is applied, is problematic.

4.7.1.8 Validity of Pressure Investigated

The pressure at which this work was conducted is significantly higher than that under which the constituents of the experiments would be found in nature. As previously discussed, this is primarily due to the operation of the piston cylinder apparatus and the desire to run an efficient experimental program. Whilst it would of course be ideal to run the full experimental program at conditions which are representative of the natural setting, it is not considered, in this case, problematic that this was not done here. The primary reason for this is that, in general terms, pressure is not considered to have a particularly strong effect on diffusivity,

certainly the strength of any effect is significantly less than that of temperature. It would of course also be very interesting to investigate the effect of varying pressure on the grain boundary diffusion of Ti in quartz as indeed it would be very useful to measure the effect of pressure on grain boundary diffusion in a more general sense. However, this volume of work would need to be the subject of a future investigation. Here, owing to the small effect pressure has on diffusivity, and, in the absence of further knowledge on the subject, it is considered that the data obtained here on the mechanics of grain boundary diffusion is relevant in the discussion of diffusion in natural quartzes.

4.7.2 Discussion & Interpretation of Data

4.7.2.1 Comparison with Other Workers' Data

As expected, diffusion of Ti in a multi-granular setting is significantly quicker than that in a single crystal thereby suggesting that GBD forms a significant component of bulk diffusion. Figure 87 shows an Arrhenius plot of the diffusion data which has been obtained here along with data for single crystal diffusion as measured by Cherniak et al. [3]. It is clearly evident that not only is grain boundary diffusion significantly faster than lattice diffusion in this setting (i.e. the line for grain boundary diffusion plots higher, at a less negative value) but also that there is a different gradient to the line indicating differing temperature dependencies of diffusion in the setting. It should of course be noted that the best fit line to the measured diffusion coefficients is not flat, it does have a gradient with which diffusivity decreases with temperature but the gradient is a very shallow one. This indicates that temperature has a weak effect on diffusivity in this scenario. Of particular interest is the markedly different gradients of the two lines. Grain boundary diffusion is faster than lattice diffusion at all measured temperatures but the difference is significantly greater at low temperatures. This is a direct parallel with the work on self-diffusion of silver discussed in section 1.3.2.3.2 The Effect of Temperature on Grain Boundary Diffusion, and shown in Figure 10. This observation is interpreted as being a function of the mechanism by which grain boundary diffusion operates as compared to lattice diffusion. In a lattice diffusion scenario, as temperature increases the diffusant gains increasingly large amounts of energy which allows it to progressively overcome the activation energy of making diffusive jumps through the mineral lattice. These results suggest that there is a far smaller activation energy associated with motion along a grain boundary. This is most likely due to the mode of incorporation of Ti in quartz (SiO_2). Ti resides in SiO_2 by sitting in one of the sites normally occupied by an Si ion. As such, vacant Si sites are required in order to permit lattice diffusion. There is an energy associated with making a diffusive jump between sites and this energy must take into account any energy that is utilised to enable the jump. This might include stretching the mineral lattice to let the relatively large Ti ion move through it. Alternatively, the diffusive

process may be facilitated by the hopping of Si vacancies to positions which are suitable to facilitate the hopping of Ti between vacancies and so through the quartz. As such, a complex interplay of mechanisms may occur to permit diffusion through a natural, imperfect lattice – especially when large species such as Ti are diffusing which are unable to utilise interstitial sites. Grain boundaries, on the other hand, are visualised as regions of long range order and partial short range disorder, with much higher concentrations of vacancies and more complex defect structures; the implication here is that less energy may be required in order to move a given species along them. As the long range, ordered lattice is not present in this scenario, there may be less energy required in order to move along a grain boundary as it is not (as) necessary to deform a mineral lattice. If there is only a very small activation energy associated with moving along a grain boundary and as such very little energy is needed to overcome it, then increasingly high temperatures will have little effect in speeding up diffusion as the activation energy will have been overcome already at low temperatures. As such, whilst increased temperatures may increase the kinetic energy of molecules of diffusant, thereby allowing them to move slightly faster along grain boundaries, the fact that they will have very little effect in overcoming activation energies will mean that there is an overall very small temperature dependency.

Of critical importance is the fact that the work which has been conducted here was completed at temperatures which were significantly higher than those where the application of the TitaniQ geothermo(baro)meter is most critical (primarily due to exceedingly long experimental durations being required to investigate such temperatures). The difference in diffusion rates between grain boundary and lattice diffusion for Ti in quartz will be even greater at lower temperatures thereby making grain boundary diffusion even more important. As such, the importance of grain boundary diffusion will be even greater than that demonstrated in the data obtained here. To date Ti mobility in quartz has been massively underestimated based upon data from single crystal experiments and this investigation, by demonstrating the far quicker nature of grain boundary diffusion is exceptionally important in understanding the true mobility and thus how an analytical method such as TitaniQ can provide accurate results.

As such, whilst the data obtained here is a significant deviation from that obtained by other workers, it is, for the reasons explained above, entirely consistent with a logical understanding of grain boundary diffusion of Ti in quartz.

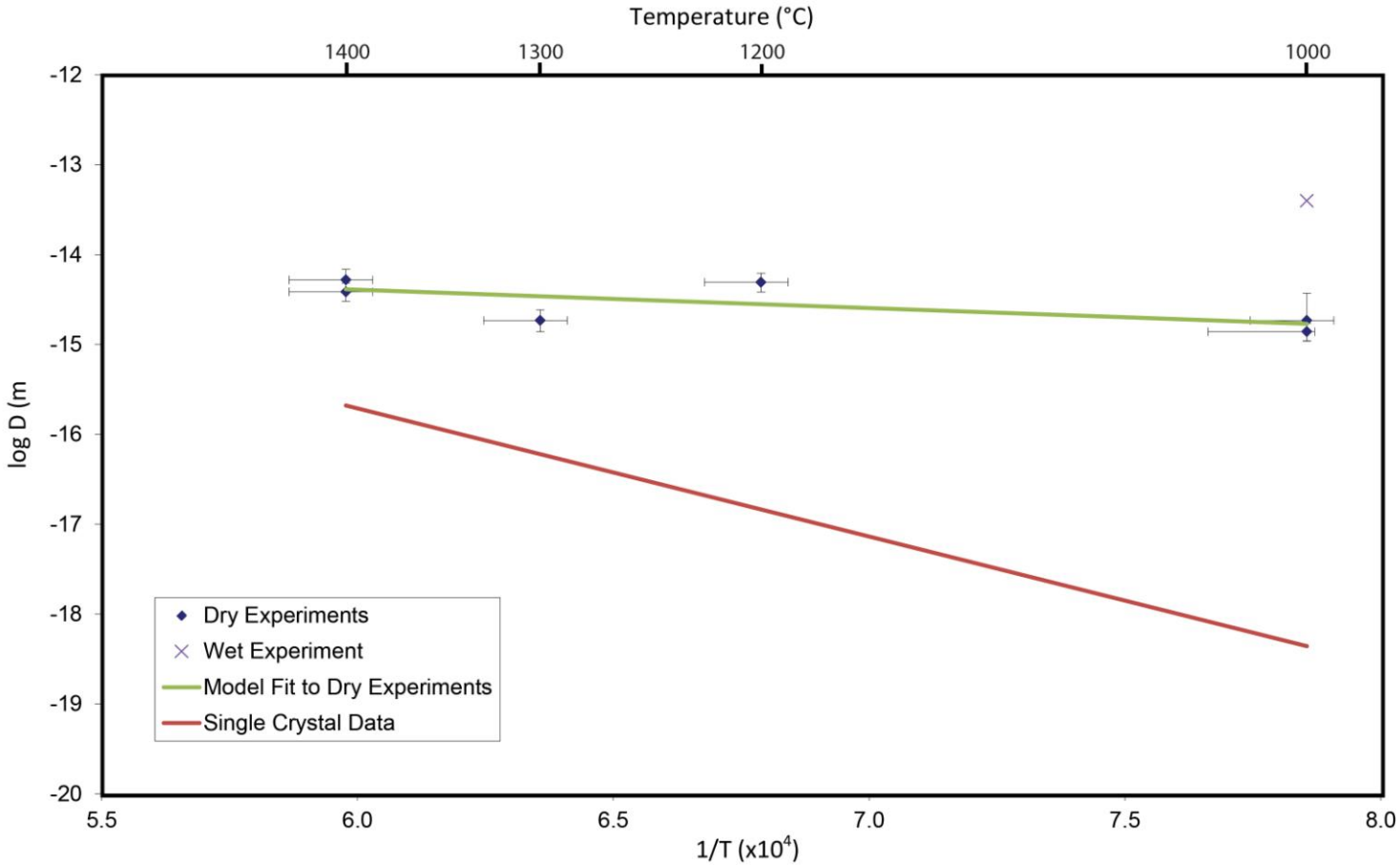

Figure 87: Arrhenius Plot Showing Comparison between Grain Boundary and Lattice Diffusion Data for Ti in Quartz

The measured grain boundary diffusion coefficients are approximately 1 order of magnitude higher at 1400°C and approximately 4 orders of magnitude quicker at 1000°C. The single wet experiment has a diffusion coefficient 1 order of magnitude quicker still but the reliability of this data point is in serious doubt. Errors associated with the fitting process fall within the range of the individual error bars shown for each run.

4.7.2.2 Deviation of Data from Ideal Solutions

The relationship between the positioning of points and the best fit solution of Fick's Second Law to them on concentration/distance plots is suggestive of a complex mechanism being at play in the incorporation of Ti into quartz. It is commonly observed in many of the measured diffusion profiles that in certain regions of the profile measured concentrations are lower than would be expected from a solution of Fick's Second Law and in other places concentrations are higher. An example of this is shown in Figure 88.

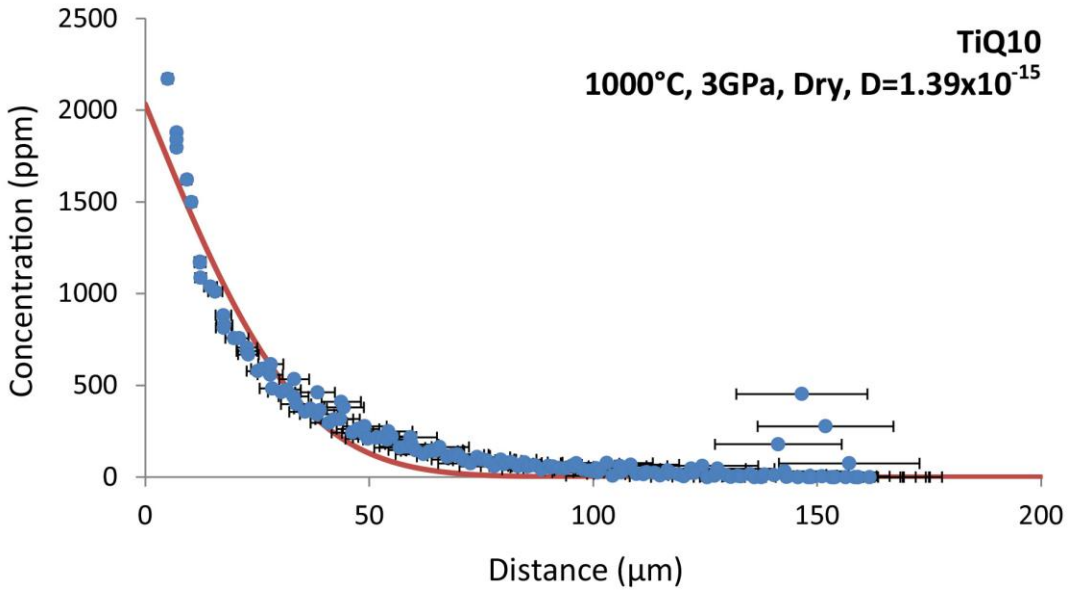

Figure 88: Example of Deviation of Measured Points from Ideal Diffusion Solution
Many points at relatively high proximity to the interface (low distance value) plot below the model solution and many points at greater distances plot above the curve.

This observation is suggestive of either un-determined mechanisms being involved in the incorporation of the Ti into the quartz or that incorrect solutions have been used for the determination of diffusion parameters. It should of course be noted that this deviation is only observed in this aspect of the investigation and this is likely related to the fact that far more data is present in each distance/concentration plot, thereby allowing a far more constrained fit to the data to be produced.

Alternative solutions to Fick's Laws have been investigated to see if these might result in a better fit. Unfortunately no such improvement of fit has been found. Further work on the mathematical description of the diffusion in this setting combined with a study of the distribution of diffusant in relation to grain boundaries may provide a further insight into this problem. Such future work is discussed towards the end of this report.

4.7.2.3 Implications of Findings

The faster diffusivity measured in a grain boundary diffusion scenario supports the use of the TitaniQ geothermometer. Whilst published lattice diffusion rates [3] did not support the use of the technique owing to the long timescales which were required for lattice diffusion of Ti to enable equilibration with quartz, (and contrary to information from other techniques which could confirm the temperatures obtained with TitaniQ) this investigation provides a mechanism by which equilibration can take place rapidly in a geologically realistic scenario. As such, this work confirms the validity of using the technique at lower temperatures as, with grain boundary diffusion being less affected by temperature that lattice diffusion, mobility will still be high enough at low temperatures for full equilibration to occur.

In demonstrating that grain boundary diffusion provides a fast pathway for the diffusion of Ti in quartz, this work has provided the theoretical basis for the use of the TitaniQ geothermometer at low temperatures. Without the theoretical basis provided by this work, and based upon single crystal diffusivity data which has been widely used before, Ti diffusion in quartz would be too slow to allow the use of TitaniQ. As such, this work has been of great use to all users of the technique. However, this work also suggests that in high temperature terrains, the technique may underestimate peak temperatures because of the rapidity with which Ti can diffuse from fine grain quartz bodies. I.e. the technique should not be used to study fine grained rocks equilibrated at high temperature.

Whilst runs which included the addition of water in the experimental capsule were not successful in providing reliable diffusion data here, they do provide some indication that the presence of water may well increase grain boundary diffusivity. This also supports the use of TitaniQ as in natural, chemically dirty systems, water is likely to be present and may be involved in the diffusive process.

A significant aim of this aspect of the investigation, for which the experimental work was the first to be completed, was to aid in the development of methods and techniques for use in other parts of the investigation. In this respect the work was entirely successful as lessons learned from the experiments and analysis completed here were utilised in all other aspects.

5 Grain Boundary Diffusion of Lithium

5.1 Introduction

Following the investigation into hydrogen diffusion along grain boundaries and the hypothesis derived from the results that the very small ionic size of hydrogen could be responsible for its "blindness" to its surroundings it was decided that a series of experiments should be designed to test the hypothesis. In order to do this, grain boundary diffusion experiments needed to be performed with a diffusant with a larger ionic radius – lithium was chosen as an ideal element for this purpose.

Dohmen et al. [122] performed a study of Li diffusion in single crystal olivine and found that two diffusion mechanisms work in tandem.

Figure 89 shows a typical diffusion profile from their study. A number of "regions" within the profile are clearly evident (labelled I – III). Region I is defined by a steep profile at high proximity to the interface with the diffusant source. Region II is characterised as a plateau with a very low gradient where concentration drops off linearly with depth. Region III defines a final drop in concentrations down to the background level. Dohmen et al. found that the end of region III coincided with the maximum penetration distance of ^{6}Li. Dohmen et al. proposed that this complex diffusion behaviour is well modelled by a partitioning of Li between interstitial and metal (octahedral) sites with Li being able to diffuse different distances depending on the mechanism utilised by specific molecules of diffusant. With diffusion of Li in single crystal olivine having been accurately modelled it is possible to make a clear comparison between diffusion in single and poly-crystalline settings.

The ionic radius of Li^{+} is 90pm ($90x10^{-12}m$) as compared to 53pm for H or ~1.7fm ($1.7x10^{-15}m$) for a proton (H^{+}) and as such is significantly larger. In many regards however, its behaviour is relatively similar – when ionised it takes on a charge of +1 and both elements are volatile in character. In comparison, Ti has an atomic radius of 176pm and thus is significantly larger. Given that it is able to take on a +4 charge (despite having an ionic radius of ~75pm) it is unsuitable to utilise interstitial positions within a mineral lattice (unlike Li and H) and so, in the case of diffusion through quartz must occupy an Si site. As such, a study into the diffusion of Li in a polycrystalline setting will be very informative as its behaviour appears to be intermediate between that of H and Ti (i.e. its diffusion through a mineral lattice can take place via both an interstitial mechanism and by occupying cation sites). Furthermore such a study will be particularly interesting as a coupling of mechanisms is likely to occur.

Here, we seek to measure diffusion coefficients of Li in polycrystalline olivine in the hope of determining the difference in diffusivities between lattice and grain boundary settings. By comparing the observed differences to those found in the case of H, it is hope that the mechanisms of and factors affecting grain boundary diffusion can be illuminated.

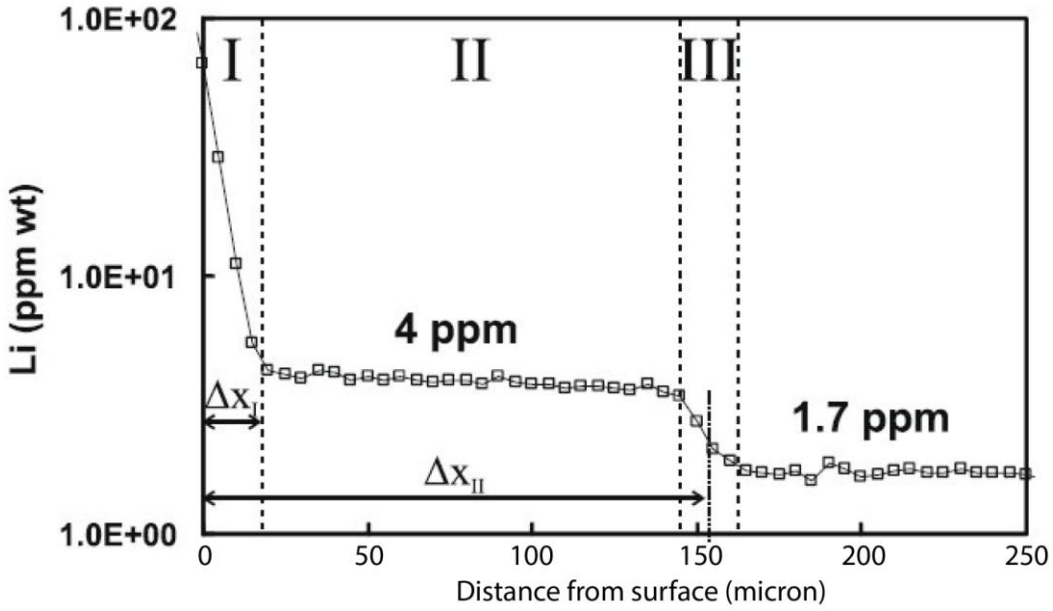

Figure 89: Li Diffusion in Single Crystal Olivine

Dohmen et al. suggest that the diffusion profile observed here is best described by a combination of diffusion mechanisms where Li utilises both metal and interstitial sites within the olivine lattice.

From Dohmen et al. (2010) [122].

5.2 Methods

This section of the work was the last to be completed and so benefitted from the method development which had been undertaken in the previous sections of the investigation. It was decided, owing to the success of the work on H diffusion, and due to a desire to obtain data which could be easily compared, that a design very similar to that used in the H work would be utilised. Unlike the H work, it was not possible to preclude the diffusion of H in olivine – the host medium (nor would it be desirable to do so as olivine is also the sink medium) and so the amount of diffusion which could take place within olivine had to be taken into account when determining grain boundary diffusivities. Given that this approach had previously worked well in the work on Ti diffusion in quartz where lattice diffusion also could not be precluded but could be accounted for (in that case lattice diffusion occurred so slowly as to be completely insignificant within the duration of the experimental run) it was not expected that this would be a problem. This in itself is not problematic as the bulk diffusivity is that which will operate in a natural setting and as such is particularly useful to determine.

5.2.1 Capsule Design

The decision to use a similar capsule design to that utilised in the grain boundary diffusion of H section of the investigation meant that determining a suitable set up for investigation of Li grain boundary diffusion was straightforward. In common with all experiments run with the intention of measuring chemical diffusion it was necessary to design an arrangement which had distinct source and sink components. This was achieved by placing the source material at one end of the capsule and then having the polycrystalline host and sink material forming the rest of the contents. As such, a simple design was settled upon, a schematic representation of which is shown in Figure 90.

Figure 90: Lithium GBD Capsule Design

Li-orthosilicate is loaded into the base of a gold capsule and acts as the source of Li diffusant. Multi-granular olivine is then loaded above the Li-orthosilicate and is the host medium. The nominal capsule diameter is 3mm and the nominal height is approximately 4.5mm.

5.2.2 Materials

5.2.2.1 Capsule Material

Gold was chosen as the capsule material as it would not react with Fe or Mg derived from the olivine. Its use placed a limit on the upper temperature at which runs could be conducted as gold is able to melt under the higher temperatures achievable with the piston cylinder apparatus [123]. This is clearly shown in Figure 91. As a result, a maximum run temperature of 1150°C was decided upon (see section 5.2.4 Run Conditions for a full discussion of the conditions used). Gold was also an easy material to work with, particularly with regard to welding, making the overall capsule creation process very straightforward. Furthermore, gold would allow the passage of electrons through its structure thereby allowing the oxygen fugacity to be buffered by the furnace.

5.2.2.2 Sample Materials

As previously discussed, it was decided that this set of experiments would be run with a source material and host/sink material. The materials that were chosen for each of these roles were selected for their suitability in representing the process which was being

investigated and also for their behaviour under the conditions at which experiments would be run. As such, the materials used for this experimental program had to be carefully chosen.

5.2.2.2.1 Source Material

A source material was required which, under ambient conditions contained Li which was then released as the material was heated up to the desired experimental conditions. Li-orthosilicate (Li_4SiO_4) was identified as a good potential candidate for this material. This material was selected for two reasons. Firstly, the material is rich in Li (23 wt%) making it an efficient material with which to introduce Li to the experimental capsule. It is also known to be widely used as a flux in the manufacture of ceramics, indicating that it dissociates upon heating thereby releasing Li. It is this thermal decomposition which is essential for the material's use in this context as it allows diffusant to be released into the capsule. The reaction progresses as follows:

$Li_4SiO_4 \rightarrow Li_2SO_3 + Li_2O_{(g)}$
(from Cruz et al., 2006 [124])

Li_2O is then able to dissociate to give free Li. Furthermore, the material is ideal as its SiO_4 content is very similar to that of olivine alongside which it is present in an experimental capsule. As a result, there is little potential for any unintended reactions to occur.

5.2.2.2.2 Host/Sink Material

In this set of experiments, the host and sink phases are one and the same, in a direct parallel with the work on Ti diffusion in quartz. It is valid to do this as Li diffuses sufficiently slowly within a mineral lattice that the total distances it could travel within the duration of an experimental run are fairly insignificant relative to the scale of the capsule. It was also desired that the host/sink phase was of a mineralogy which had previously been studied so that the rate of lattice diffusion had been well characterised. This would then make it significantly easier to determine the relative magnitude of the effect of ionic size. In order to fulfil these criteria, olivine was selected as the host/sink phase.

5.2.3 Construction of the Experimental Capsule

3mm gold tubing was cut to 10mm lengths before being washed in acetone in an ultrasonic bath and then briefly annealed in a blue flame. These cylinders were then closed off at one end by means of a 3 point crimp. This end was then welded shut and flattened using a 3mm pin press. The open capsules were then washed again in acetone in an ultrasonic bath. The contents were then loaded. Lithium orthosilicate ($LiSiO_4$) powder with a nominal grain size of ~150µm (100 mesh) was placed into the bottom of the cylinder to a thickness of approximately 0.5mm. Olivine of grain size >100µm was then placed above the $LiSiO_4$ to a

thickness of approximately 2.5mm. At each stage the capsule was tapped against a hard surface and the contents were pressed down to ensure that no free space was left inside the capsule. The inner rim of the capsule was then cleaned to ensure that no grains of either mineral could get trapped inside the top crimp when it was made. If grains were trapped inside the crimp the welding process would be impeded as the gold would not melt properly. The top crimp, like the bottom one was a 3 point crimp. This was then welded shut in exactly the same way as the bottom crimp. The top crimp was then flattened in the 3mm pin press. The capsule was then passed through the press a number of times without compressing it against a solid base. The purpose of this step was to ensure that the diameter of the capsule was maintained at 3mm.

The same experimental assemblage was used as in the other sections of the investigation (see section 2.2.1 The Piston Cylinder Apparatus). As 3mm tubing was being used it was necessary to use a capsule holder with a 3mm internal diameter. Inevitably some points of the capsule had a greater diameter than 3mm due to the re-shaping that had taken place during construction of the capsule. In order to make the capsule fit, the holder was very gently filed using a file with a circular cross section. It was essential that this was done exceptionally gently as the holders were very crumbly in nature. Once the capsule had been made to fit into the holder, the components were then placed into the assemblage in the same way as previously detailed.

5.2.4 Run Conditions

Experimental runs were conducted at temperatures between 800 and 1100°C and as such conditions were representative of the upper mantle. A pressure of 3GPa was used for all runs. This value was chosen primarily to ensure that results obtained from this set of experiments were comparable with those obtained from the work on grain boundary diffusion of H. Furthermore and as previously discussed, the piston cylinder apparatus was known to work well at this pressure and so it was expected that this value would increase the ease of carrying out the experimental program. Pressure was not investigated as a variable here but it would be very interesting to do so in any future work. Run durations were initially calculated by estimating how much more quickly grain boundary diffusion might be compared to published lattice diffusion rates. A rough estimate of approximately 3 orders of magnitude was arrived at (based upon comparisons of grain boundary and lattice diffusion in other settings). Once initial runs had been completed, diffusion coefficients were calculated and then used to estimate the next set of durations. Specific conditions used for each run are detailed in section 5.6.3 Summary of All Run Results).

In practice, some significant experimental difficulties were experienced whilst running these experiments. Many of these were caused by the comparatively (with regard to Pt as used in

previous parts of the investigation) very soft nature of the gold capsule material at elevated temperatures compared to surrounding, brittle, ceramic components. This caused capsules to tear on some occasions thereby causing the failure of the run. Furthermore, whilst all experiments were conducted under conditions which would not cause the gold to melt (Figure 91), if the gold were to come into contact with another metal – for example Pt from the thermocouple then the resulting alloy would have a lower melting point thereby allowing melting to occur. This eventuality did indeed occur during the experimental program and is discussed in section 5.6.2.3 LiGB4.

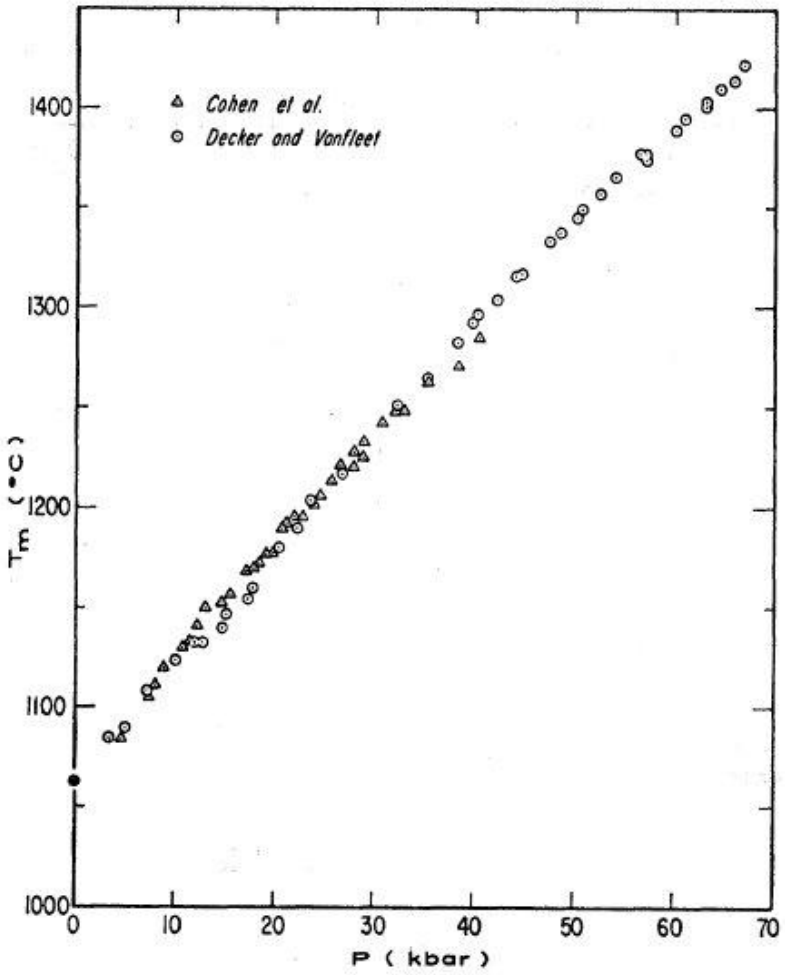

Figure 91: Melting Curve for Gold at Pressures up to 7Kbar

The melting curve shows a broadly linear increase in the melting point of gold with increasing pressure. At the pressure at which these experiments were run, 3Gpa (30 Kbar) melting occurs at approximately 1230°C. Thus, an upper temperature of 1150°C was decided upon to eliminate the possibility of the capsule melting.

From Mitra et al., 1967 [123].

5.3 Sample Preparation for Analysis

Following the completion of experimental runs and the retrieval of the capsule from the assemblage, capsules were very carefully cut in half using a circular saw before being mounted in epoxy resin. In each case both halves of each capsule were mounted so as to increase the number of grains that could be analysed from any one run. At each stage great care was taken to ensure that capsules were kept clean and that cracks did not take up fluids used in the preparation procedure. Once mounted in the resin block the capsules were polished on increasingly fine polishing sheets to achieve a satisfactory finish and flat surface to allow for SIMS analysis. Following checks for integrity and capsule map creation (which were performed uncoated in the SEM – See section 2.4.1.3 Conductive Coatings) samples were gold coated for analysis by SIMS.

5.4 Analysis of Completed Runs

5.4.1 Initial SEM Analysis

Once runs had been completed, recovered and prepared for analysis they were checked for capsule integrity and maps were created of them using the SEM.

5.4.1.1 Capsule Integrity Checks

Capsule integrity checks were conducted at low magnification in a combination of SE and BSE modes. Fundamentally checks were performed in order to ensure that none of the capsule contents had escaped or otherwise interacted with material from outside of the capsule which might contaminate it and potentially affect the diffusive processes being investigated.

5.4.1.2 Capsule Map Creation

Following integrity checks, capsule maps were created. This was done by recording a series of images, normally in BSE mode, which overlapped each other. Typically an area of approximately 1/4 - 1/6 of the capsule was recorded in each image. By ensuring that there was an overlap it was then possible to “stitch” images together using the Adobe Photoshop software. This resulted in an image or map of the entire capsule which could be printed at A3 size and use to navigate around the sample during SIMS analysis. An example of a capsule map created for this set of experiments is shown in Figure 92.

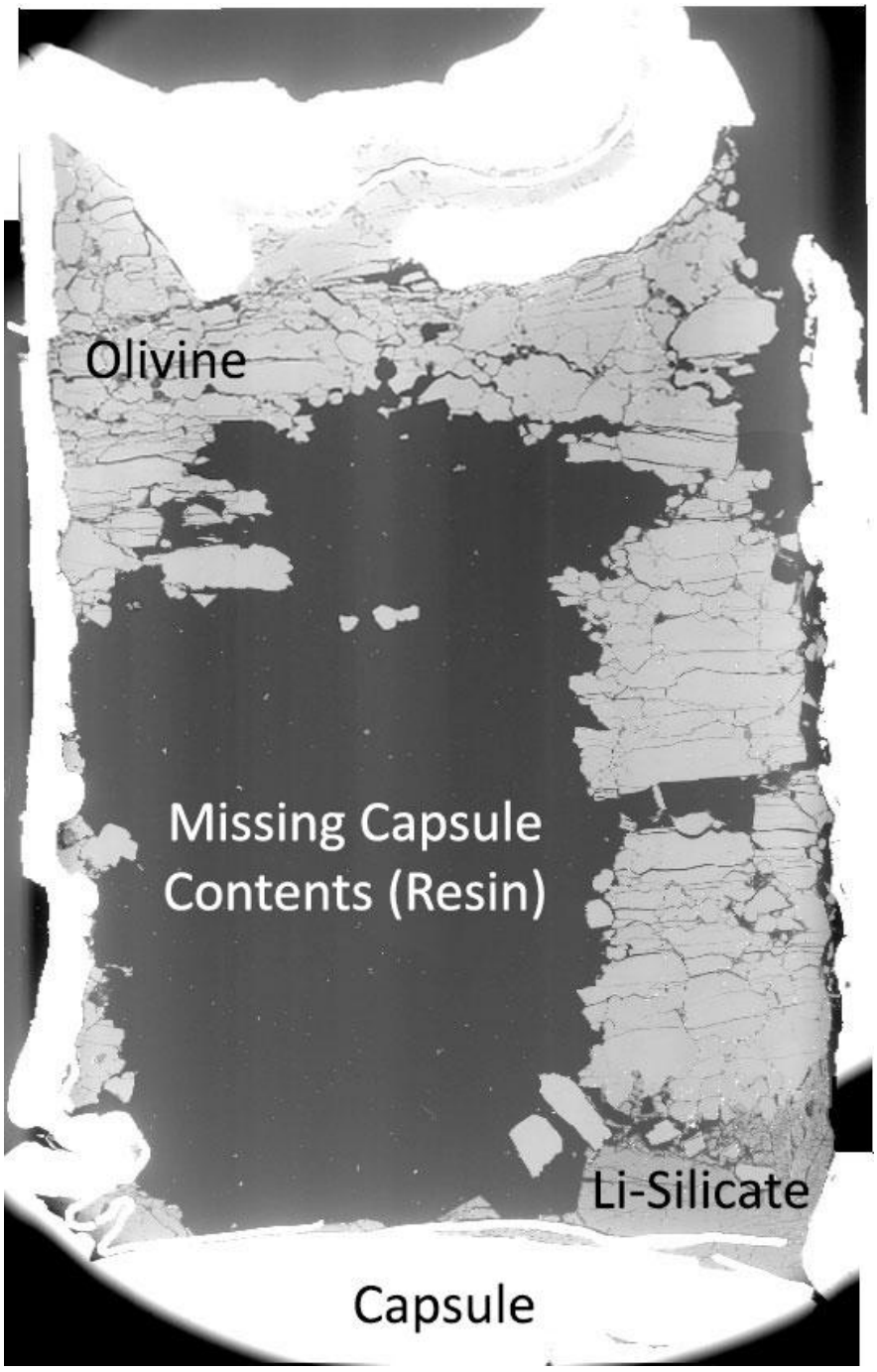

Figure 92: BSE SEM Image of a Capsule Map for Li Grain Boundary Diffusion Experiments
The image is created from the digital stitching together of a series of smaller images recorded using the SEM. Capsule width is approximately 3mm.

5.4.2 SIMS Analysis

SIMS analysis was conducted on 4 of the completed experiments within this series (see section 5.6.2 Specific Run Observations for details of runs). The purpose of SIMS analysis was to record accurate quantifications of Li contents within olivine grains at varying distances

from the interface between Li-orthosilicate and olivine. All analyses were completed within one analysis session (1 day).

Samples were loaded into the instrument on the day of analysis. Analysis of Li was significantly more straightforward than analysis of H owing to significantly lower background concentrations and a far higher relative ion yield. As such, it was not necessary to "pump down" samples in a vacuum chamber for an extended period of time prior to analysis.

Analysis points were selected whilst using the SIMS instrument. As the host and sink phase were one and the same, analysis points could be selected by essentially choosing random points within the sectioned capsule subject to certain rules. The most significant of these was that analysis points should not, at any point break grain boundaries. If this were done there was a great chance that significantly higher than correct readings would be recorded as Li which was being stored at grain boundaries was measured as opposed to that which had travelled along grain boundaries before entering olivine grains. The olivine which was loaded into the experimental capsules prior to the commencement of runs had a grain size of greater than 100µm. As a result, the vast majority of grains which could be observed using the light microscope coupled to the ion microprobe were clearly visible and significantly larger than the size of an analysis point. As such, it was a simple task to ensure that analysis points were positioned in such a way as to not straddle grain boundaries with the beam.

Prior to the collection of concentration data, the sites of analysis points were rastered using the ion beam to remove the gold coating at the site along with any impurities, thereby reducing the risk of obtaining noisy data. The size of this rastered area was approximately 20 x 25µm. Samples were then analysed by a 5nA ^{16}O beam which had been accelerated to 10kV with an energy offset of 75V. Si^{4+} and Li^{+} were collected and counted by the mass spectrometer part of the SIMS instrument with total analysis times being of the order of 300s per analysis point. With such short analysis times it was possible to collect a large amount of data within the single day of allocated instrument time.

During analysis the capsule maps (which had previously been made using the SEM) were extensively annotated with the locations and ID numbers of each of the analysis point. This was essential as it enabled each point to be identified later and have its measured concentration associated with a distance between the point and the pyrophyllite/spinel interface.

5.4.3 Post-SIMS SEM Analysis

Following SIMS analysis, samples were once again analysed by SEM. The aims of this analysis were to check that analysis points had not broken grain boundaries and to measure the distances of analysis points from the Li-orthosilicate/olivine interface.

In practice it was found that no grains broke grain boundaries as it was straightforward, during SIMS analysis, to locate grain boundaries and avoid them (owing primarily to the consistent grain size of the olivine).

The distances of analysis points from the Li-orthosilicate/olivine boundary were measured using a tool on the SEM which allowed the determination of distances between any two defined points on a given image. Distances were measured from the centre of analysis points to the nearest point on the interface. As previously discussed, whilst the contact between the Li-orthosilicate and olivine was nominally flat, in practice it was found that once experiments had been run it inevitably took on a significant topography. As such, finding the nearest point on the interface was a somewhat inexact procedure. This uncertainty was taken into account in the determination of errors in the measurement of distances. In some cases parts of the contents of capsules were not present in the section, polished sample. This was due primarily to the granular and friable nature of samples after runs. Furthermore, the mechanism by which samples were prepared may well have further encouraged loose grains to be removed from the sample. As a result, and as can be seen in Figure 92, in some cases significant portions of the interface were missing. In such cases it was necessary to make an estimation of the original position of the interface based upon its trend where it is present. Whilst there was a degree of uncertainty associated with this estimate, this too is taken into account in the determination of distance errors (see section 2.6.1.1 Distance Errors).

Having identified analysis points based upon the maps which had been annotated during SIMS analysis, the appropriate distances to the interface were associated with them thereby allowing the creation of concentration/distance plots and thus the calculation of the parameters of diffusion.

5.5 Treatment of SIMS Data

5.5.1 Calculation of Diffusion Parameters

The data obtained from SIMS analysis was extensively reviewed and processed to enable the extraction of diffusion coefficients and Arrhenius relationships. Errors were also carefully treated to determine the precision of the data obtained.

Diffusion coefficients were calculated using the Datafit curve fitting software by Oakdale Engineering using the exact same method as previously detailed in section 2.5 Non-Linear Regression Analysis. The reader is directed to this section for a full discussion of the calculation methods used and the solutions of Fick's Laws which the data was fitted to.

5.5.2 Calculation of Errors

Absolute error values were estimated for each measured parameter. The estimations which were made and the logic by which these estimations were arrived at is detailed in section 2.6.1 Calculation of Errors. Where specific methods were required for this particular aspect of the investigation they are detailed below. These individual sources of error were combined as detailed in section 2.6.2 Combination of Errors.

5.5.2.1 Concentration Errors

There was a quantifiable error associated with the measurement of point concentrations of Li content of olivine grains via SIMS. Approximately 10 individual analyses were recorded for each analysis point. Owing to the relative ease of analysing Li by SIMS there was very little variation between individual readings. The error that has been used here is the maximum variation that was observed during the acquisition of the data and this is 10ppm.

5.5.2.2 Summary of Error Magnitudes

Parameter	Value
Time	120s
Concentration	10ppm
Distance from Interface	20µm
Temperature	Maximum deviation from nominal temperature

Table 12: Summary of Error Magnitudes for GBD of Li Experiments

5.6 Results

5.6.1 Summary of Run Parameters

In total, 5 experimental runs were carried out for this aspect of the investigation. Of these, 4 were successfully completed and 1 suffered capsule failure. The parameters of each run are summarised below in
Table 13.

Run ID	Temperature	Pressure	Durations (hrs)
LiGB1	1000°C	3GPa	6
LiGB2	800°C	3GPa	21.5
LiGB3	800°C	3GPa	22
LiGB4	1000°C	3GPa	0.5 - Capsule Failure
LiGB5	1100°C	3GPa	3

Table 13: Summary of Run Parameters for Grain Boundary Diffusion of Li Experiments

5.6.2 Specific Run Observations

5.6.2.1 LiGB1 & 2

Runs LiGB1 & 2 were the first two of this experimental series to be completed. Neither showed any mechanical problems and both were initially deemed to have been successful. Figure 93 is an SEM image of half of the prepared LiGB1 capsule. It can clearly be seen that a number of olivine grains have been picked out by the polishing process leaving holes which appear as black areas as they are filled with epoxy resin.

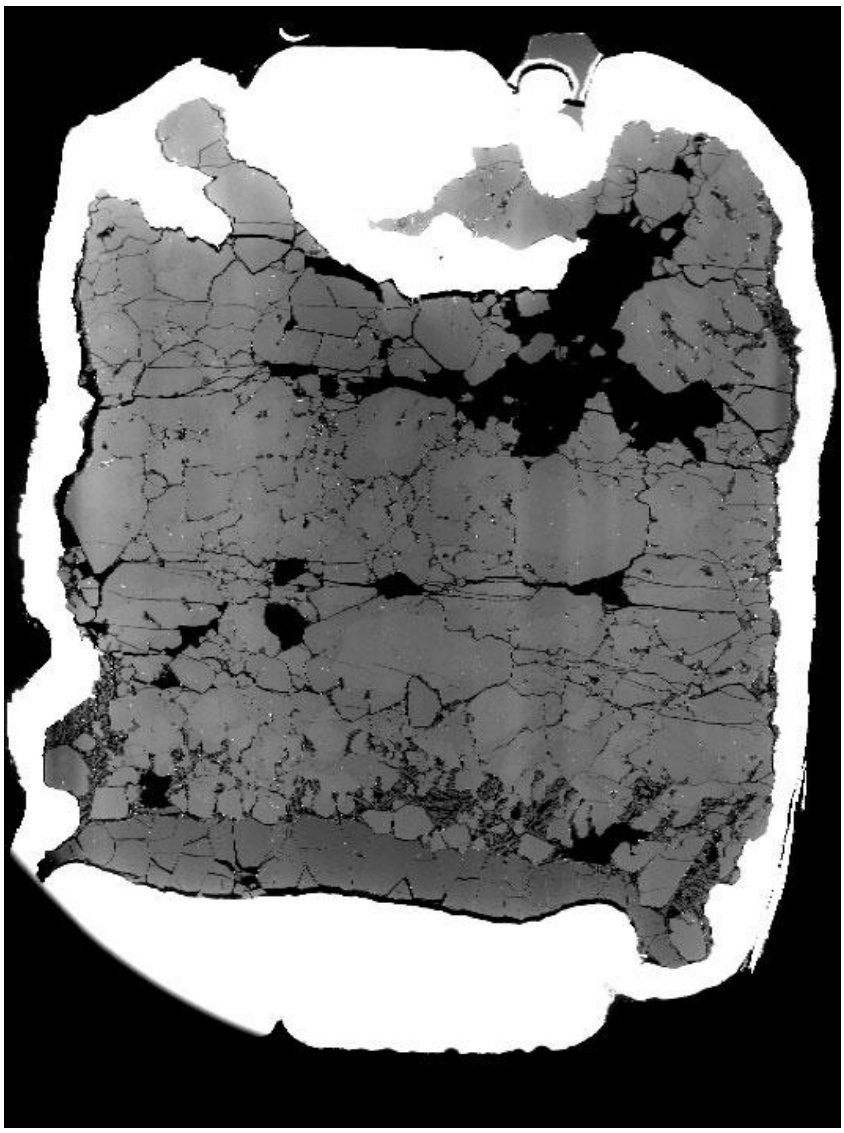

Figure 93: Representative Section of Run LiGB1

The capsule is clearly completely intact and the Li-orthosilicate is visible towards the bottom of the image. A number of grains of olivine have been 'picked out' by the polishing process leaving holes which appear as black areas as they have been filled with epoxy resin. Olivine grains can clearly be seen to be greater than 100µm. The width of the capsule here is approximately 3mm. It is possible that a small amount of melt has developed and resides close to the Li source.

Whilst both runs LiGB1 & 2 operated well and were initially deemed to have been successful, the analysis of SIMS data showed that it would not be possible to extract useful diffusion parameters from the runs. Figure 94 & Figure 95 are concentration/distance plots of runs LiGB1 & 2. It is clear from inspection of the spots that there is no clear downward trend in concentration of Li in olivine with distance from the diffusant source. As such it was not possible for the curve fitting software to fit a solution to Fick's Second Law to the data and so

diffusion could not be quantified. The likely reason for this is that these experiments were run for too long and Li was able to diffuse the entire length of the capsule and then gradually increase its concentration throughout the entire capsule. LiGB1 & 2 were run for 6 and 21.5 hours respectively and as such had plenty of time for this process to occur. This problem essentially resulted from not knowing the rate at which grain boundary diffusion of Li would operate (as of course should be the case given that this is what is being investigated). As a result, there was an element of guess work involved in determining the duration which was necessary for a diffusion profile to develop during a run. In this case that guess work was unfortunately wrong. As such, runs LiGB1 & 2 have not provided any useful data for this investigation. Furthermore, the presence of textures which may be indicative of melt having developed serve to further reduce any confidence which would otherwise be associated with the run.

Figure 94 also shows a calculated solution to Fick's Law which would be expected for this run based upon the Arrhenius relationship determined from other, successful runs. It is shown for reference only and demonstrates how a lack of relationships within a dataset can lead to it not being possible to find a suitable solution.

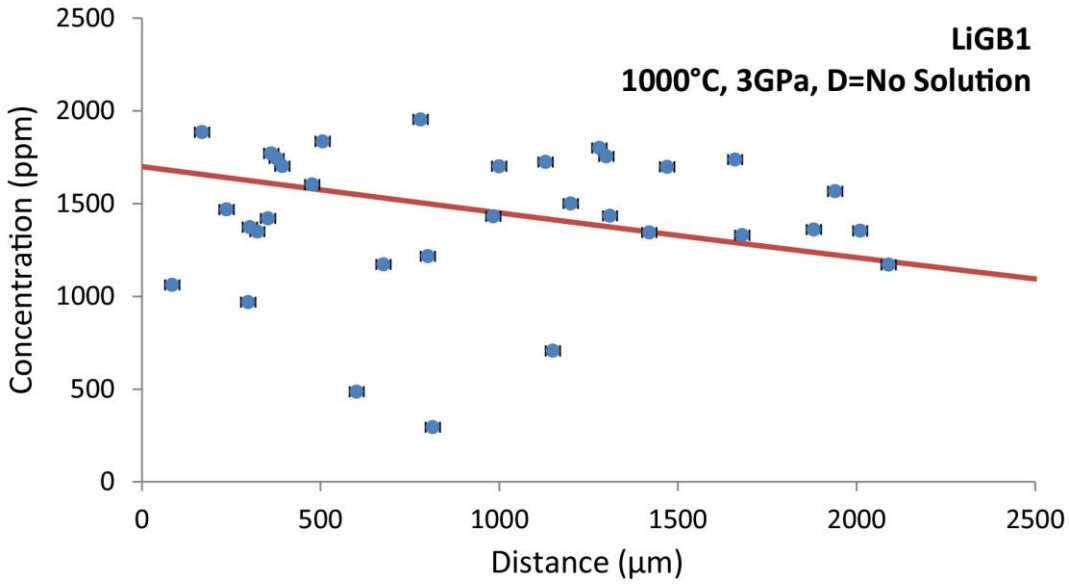

Figure 94: Concentration/Distance Plot for Run LiGB1

The red line shows the diffusion profile which would be expected given the estimation of the Arrhenius Law made from the other runs carried out. It is not derived from the dataset shown here but appears to be an acceptable solution..

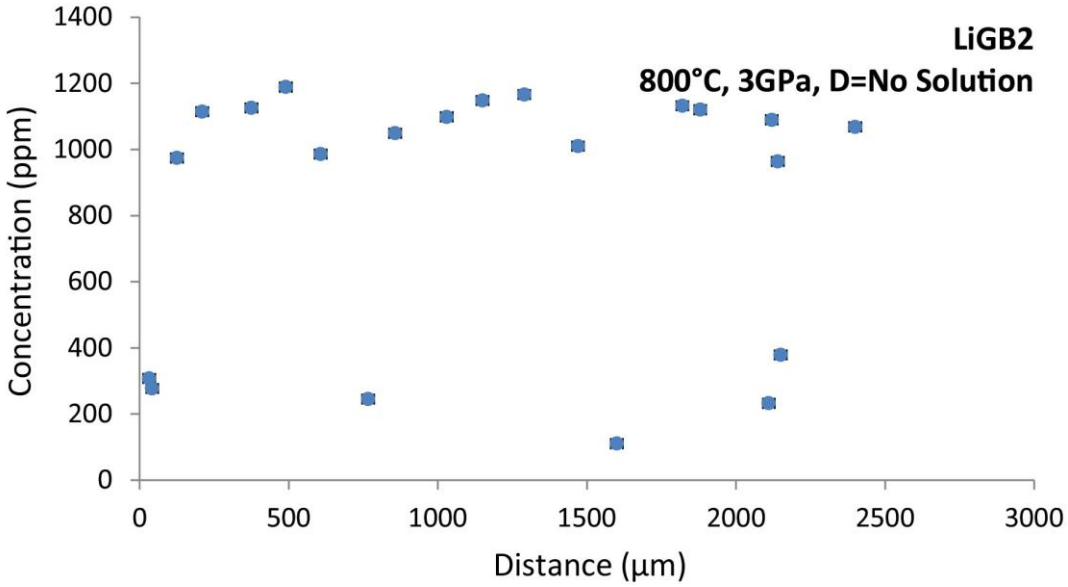

Figure 95: Concentration/Distance Plot for Run LiGB2

In Figure 94 & Figure 95 vertical (concentration) error bars are within the size of the data point.

5.6.2.2 LiGB3 & 5

LiGB3 & 5 were the two most successful runs in this part of the investigation and have provided all of the data that has been obtained on the grain boundary diffusion of Li. Experimental durations were of a suitable length to enable measurable diffusion profiles to form without saturating the entire capsule with Li as happened in runs LiGB1 & 2. The curve fitting software was able to fit solutions to Fick's Second Law to the data and this model is shown along with all measured experimental points in Figure 96 & Figure 97. The data and its implications are discussed in section 5.7 Discussion & Interpretations.

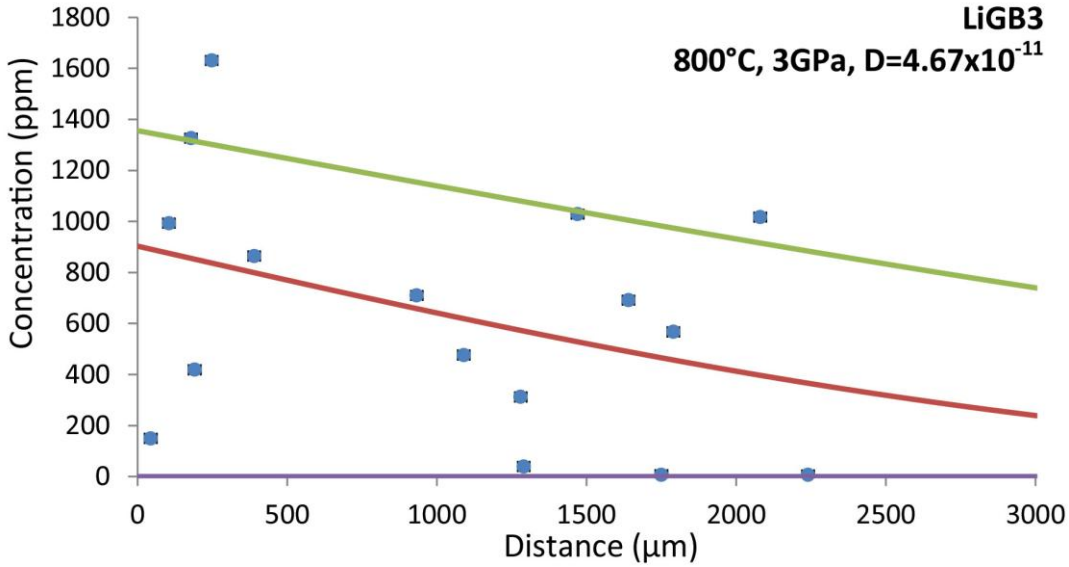

Figure 96: Concentration/Distance Plot for Run LiGB3

Data and model fit. Details as in Figure 37

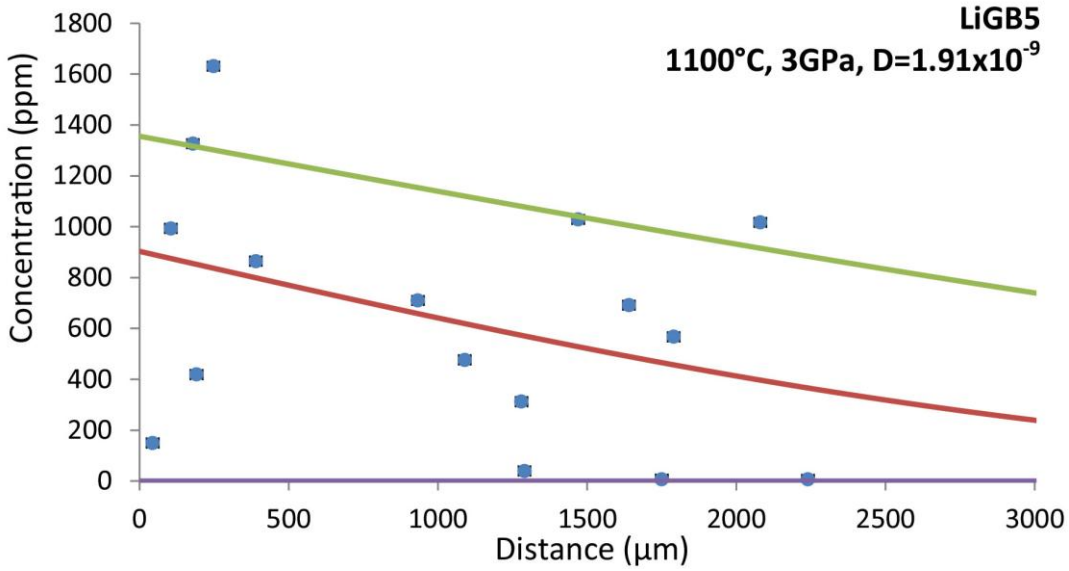

Figure 97: Concentration/Distance Plot for Run LiGB5

Data and model fit. Details as in Figure 37

In Figure 96 & Figure 97 vertical (concentration) error bars are within the size of the data point.

5.6.2.3 LiGB4

No data was obtained from run LiGB4. This was due to the capsule failing during the experimental run. From the morphology of the recovered capsule it is believed that a piece of the experimental assemblage was broken during construction which allowed part of the Pt

or Pt/Rh wire which formed the thermocouple to come into contact with the capsule. Under the high PT conditions of the experimental run this caused alloying and subsequent melting of the capsule. This theory is further backed up by readings taken from the control system of the piston cylinder apparatus which showed significant variations in the voltages recorded across the thermocouple despite there being no variation in the input power. As a result of this melting and subsequent exposure of the contents of the capsule to the environment of the assemblage, this run was deemed to have failed and was not mounted or analysed. As such no data has been derived from it.

5.6.3 Summary of All Run Results

Run ID	Temp (°C)	Pressure (GPa)	Duration (hh:mm)	Diffusion Coefficient (m^2s^{-1})	Effective Concentration (ppm)
LiGB1	1000	3	06:02	Unable to Determine	Unable to Determine
LiGB2	800	3	21:30	Unable to Determine	Unable to Determine
LiGB3	800	3	21:33	$4.67x10^{-11}$	903
LiGB4	1000	3	~00:15	Capsule Failure	Capsule Failure
LiGB5	1100	3	03:04	$1.91x10^{-9}$	2370

Table 14: Summary of All Li Grain Boundary Diffusion Results

The diffusion data which has been obtained can be shown on an Arrhenius plot to reveal the temperature dependency of diffusion in this setting. This is shown in Figure 98

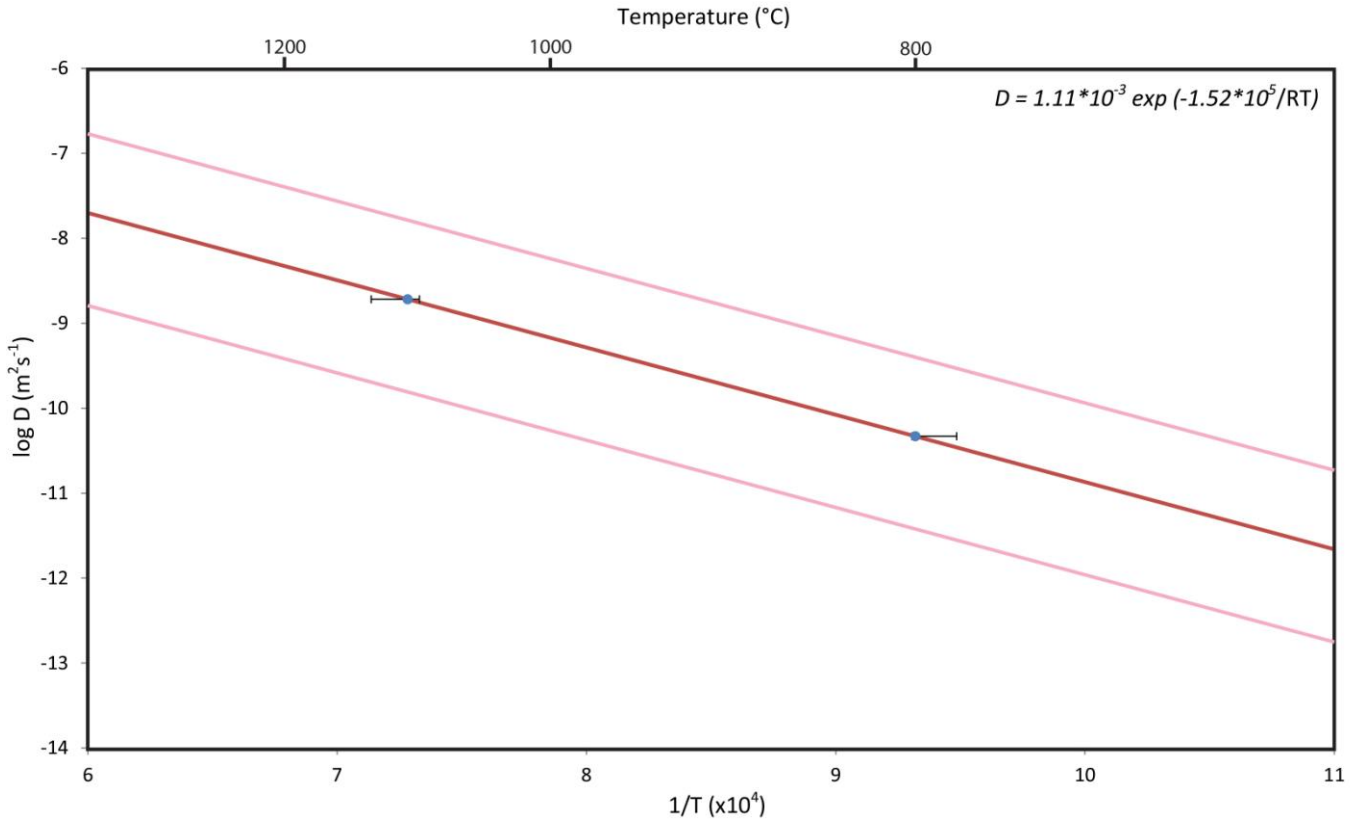

Figure 98: Arrhenius Plot Showing Measured Temperature Dependency of Grain Boundary Diffusion of Li in Olivine

It is possible for an Arrhenius relationship to be determined based on the two data points which were obtained. Measurements derived from experiments are shown as blue points and the Arrhenius model is shown as a red line. A relatively strong temperature dependency of diffusion is observed. Error bars for the diffusion coefficients are very small and are within the size of the data point. There is significant uncertainty in this data owing to the lack of data points. This is discussed in detail in the main text. The pink lines represent the 95% confidence bounds based upon the fitting process that was used to determine diffusion coefficients.

5.7 Discussion & Interpretations

5.7.1 Discussion of Factors which Could Affect Results

The majority of the factors which could have an effect on the data obtained here are exactly the same as those which might have an effect on the quality of data obtained for the work on the grain boundary diffusion of H (from which this particular aspect of the investigation acts as a direct follow-up). As such, the reader is referred to section 3.7.1 Discussion of Factors which could affect Data for a discussion of such factors.

5.7.1.1 Amount of Data Obtained

Only a very small amount of data was able to be collected from this set of experiments – only two runs were conducted with appropriate durations to allow the formation of measurable diffusion profiles. As a result the data obtained here must be thought of as an initial quantification of grain boundary diffusion of Li in olivine and should be followed up with future work. In a parallel with the early sets of experiments in the previous two aspects of this investigation, the data obtained from these runs may be used to accurately determine experimental durations of future runs therefore allowing more to be obtained over a wider range of temperatures. This would allow a far more accurate determination of diffusivity in this setting. Previously investigated aspects of this investigation observed significant scatter in diffusivities between experimental runs but it was still possible for an Arrhenius Law to fit well. It is expected that a similar situation would occur here if more data were obtained.

It should of course be noted that the aim of this aspect of the investigation was to act as a follow up to the much larger experimental program which was conducted into the grain boundary diffusion of H. As such, whilst only a limited amount of data has been obtained here, it does begin to illuminate the mechanisms of grain boundary diffusivity and as such is of use. Furthermore, as all of the experiments which have formed this investigation have been conducted at similar temperatures and pressures, there is a great deal of comparability between them. Thus, even where there is uncertainty in data (such as here) it is still possible to gain a clear indication of the relative speeds of grain boundary diffusion in the different scenarios as compared to previously measured lattice diffusion data. Given more time and resources it would of course be very desirable to continue this study further in the ways outlined above.

5.7.1.2 Combination of Diffusive Mechanisms

As previously discussed, Dohmen et al. [122] proposed that Li lattice diffusion was governed by two simultaneously operating mechanisms utilising both metal and interstitial sites within the lattice. As such, the diffusivity that they measured was a complex process. Here, the

process which has occurred is potentially even more complex. As a host phase was used which was unable to preclude the entry of Li into it (as opposed to the work on grain boundary diffusion of H where Mg-spinel was able to preclude H from entering it) both the mechanisms described by Dohmen et al. and grain boundary diffusion must have been operating. As a result, the diffusivity which has been measured is a result of the combined effect of all three processes. The magnitude of the effect of each of these components of bulk diffusion will vary depending on the rate at which that mechanism operates. This is because within a given experimental duration, diffusion which proceeds more quickly will allow diffusant to travel further through the capsule. As such, the total amount of diffusant observed at a given point may be made up of differing contributions. Closer to the source of diffusant, higher proportions of the observed concentrations will have arrived at that point via slower diffusion mechanisms. Conversely, further away, the majority of the diffusant present can only be present due to the fastest mechanisms. Figure 99 shows a representation of this logic for the particular scenario under investigation here.

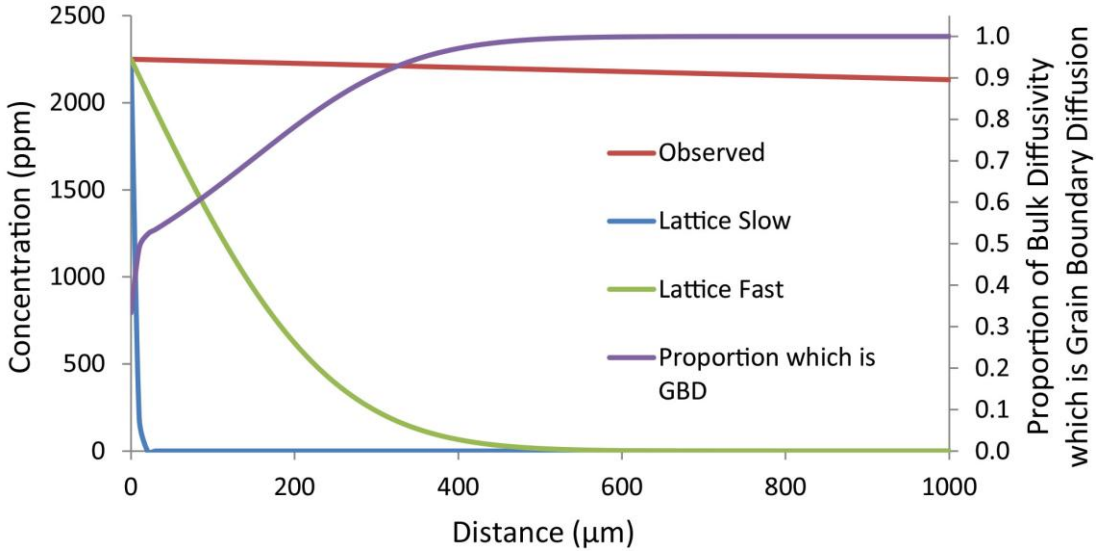

Figure 99: Comparison of Li Diffusive Mechanisms

At high proximity to the diffusant source (i.e. low distance on the x-axis) the fast lattice and slow lattice mechanisms make significant contributions to the bulk diffusivity. At distances of greater than ~20µm the slow lattice mechanism makes very little contribution and at distances of greater than 500µm the fast lattice mechanism makes no contribution. The observed data set is based on the data obtained in this investigation and the lattice mechanisms are based on the work of Dohmen et al.. The calculation of diffusion profiles is based upon an experiment running at 1000°C for 48 hours. The value of the effective concentration at the interface between the host and source is 2250ppm which was a commonly observed value in the datasets which made up this investigation.

When this logic is applied to the specific conditions of experiments completed as part of this investigation it is possible to estimate the proportion of diffusant present at any given point which has arrived there by a grain boundary diffusion mechanism. Figure 100 is similar to Figure 99 but has been re-calculated for the conditions of run LiGB5.

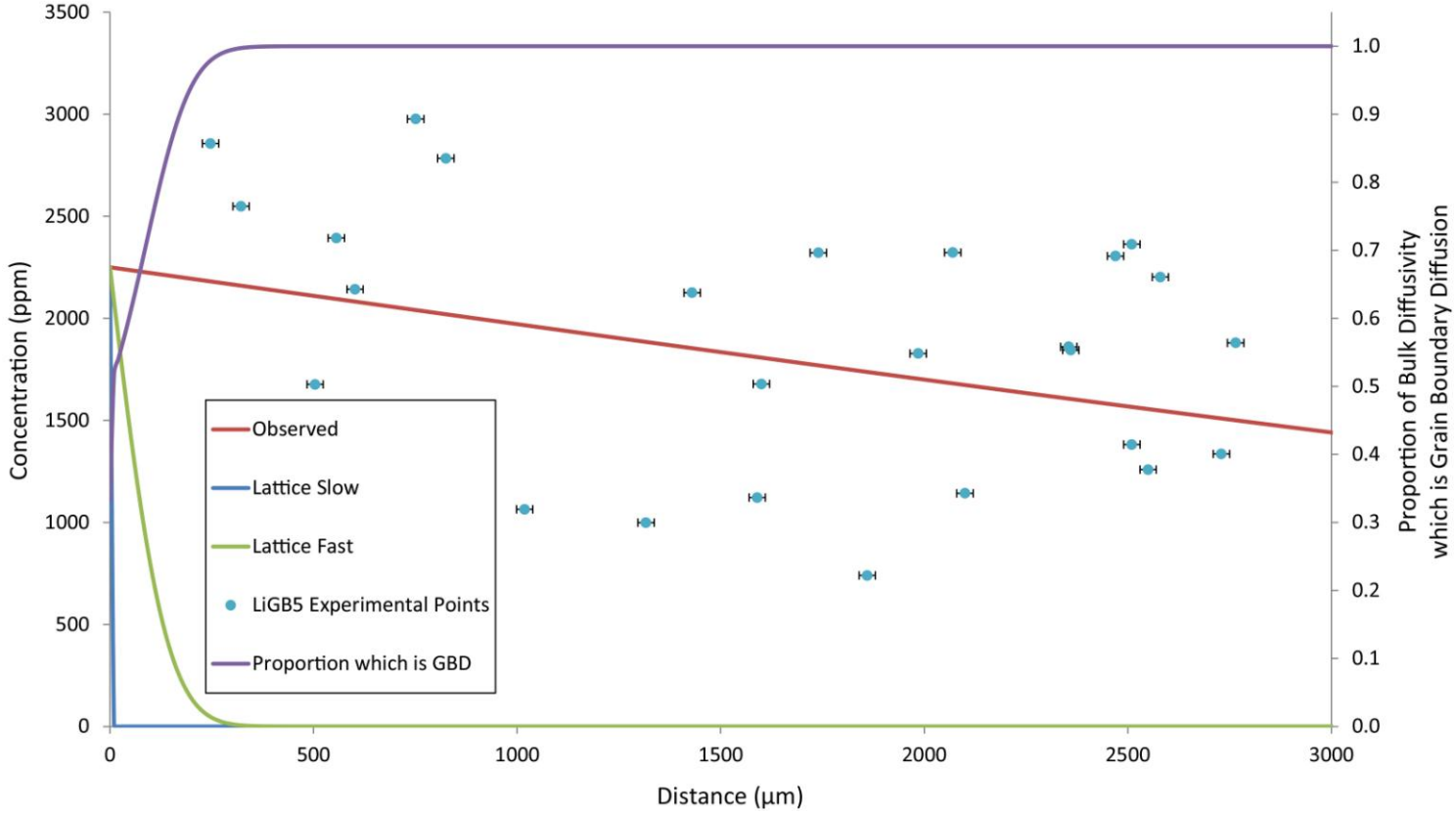

Figure 100: Mechanism Comparison Graph for Run LiGB5

Only two of the measured analysis points are within the part of the capsule where the fast lattice component of diffusion may have an effect. All other points are within the portion where grain boundary diffusion is proposed to be dominant suggesting that this forms the majority of the bulk diffusive process. It should of course be noted that lattice diffusion must occur when diffusant reaches the grain in question and this may cause an overall lowering of the total diffusivity.

As can be seen in Figure 100, the contribution of mechanisms other than grain boundary diffusion to the measured concentrations can only be very light and only the two highest proximity data points are likely to have a significant fast lattice diffusion component. This calculation was made by calculating lattice diffusivities using the Arrhenius relationship defined by Dohmen et al. at the same temperature as run LiGB5. From this data, model diffusion profiles were calculated and compared to that which was determined from the data obtained from run LiGB5. The calculated concentration values were considered as a proportion of the total amount of diffusion measured with grain boundary diffusion being considered as being responsible for the rest of the Li present at that point. These proportions were then plotted as the purple curve. It should of course be noted that in order for diffusant to travel from a grain boundary to an analysis site which may be well within the centre of a grain, it may be necessary for the diffusant to travel to that analysis site via lattice diffusion (it may of course be that in practice the diffusant molecule travels to the analysis site by a combination of mechanisms, particularly if long range defects are present which would likely allow diffusion to occur in a very similar way to grain boundary diffusion). As such, Figure 100 shows that diffusion from a grain edge to its centre is entirely possible within the timescale of the run as long as the total distance that the diffusant has to travel is no greater than approximately 250µm. This scenario is valid as all observed olivine grains within this experimental series were found to be less than 250µm in size. Thus, in essence, measurements of smaller grains are more reliable at large distances from the source than measurements from larger grains.

Thus, given the conditions under which the experiments have been conducted here, the measured diffusion parameters give a true reflection of the grain boundary diffusion process. Any diffusion which has occurred through the mineral lattice is likely to have a very small impact on the concentrations which have been measured. However, this lattice diffusion is important in ensuring that the diffusant which has travelled along grain boundaries is able to reach analysis sites.

5.7.1.2 Dynamic Changes to Diffusive Pathways

Dynamic changes to diffusion pathways are likely to have taken place during the running of experiments within this aspect of the investigation – as is the case with all aspects. Changes in the available routes for diffusion as the run progresses have the potential to change the values of diffusion parameters and as such it is essential that the effects of such a process are fully considered. A full discussion of this issue can be found in section 3.7.1.7 Dynamic changes to Diffusive Pathways during Experimental Runs. Whilst the discussion is framed in the context of grain boundary diffusion of volatiles, the concepts and processes which are detailed are equally applicable here.

5.7.2 Discussion & Interpretation of Data

5.7.2.1 Comparison with Other Workers' Data

The data obtained here shows that grain boundary diffusion of Li in olivine is significantly faster than that observed in a single crystal scenario. To date, no other work has been conducted on grain boundary diffusion of Li in this setting and as such it is not possible to make a direct comparison between this work and that conducted by other workers. However, the magnitude of the difference between Li diffusivity in grain boundary and lattice scenarios (approximately 4 orders of magnitude faster at 800°C and 3 orders of magnitude faster at 1100°C) is consistent with differences observed elsewhere, especially when the mechanisms which control Li diffusion in olivine are considered (see section 5.7.1.2 Combination of Diffusive Mechanisms for a specific discussion of the different mechanisms). Figure 101 shows the Arrhenius relationship shown above in Figure 98 alongside Arrhenius relationships for the fast and slow lattice mechanisms of Li diffusion in olivine. It is evident that there is a slightly lower temperature dependency in the grain boundary diffusion scenario (as evidenced by a shallower gradient). The difference in gradients is, however, rather small. It should of course be stated once again that this data is based on just two data points and as such there is a low degree of confidence associated with it. However, the results which have been presented are consistent with expectations, given the observations that have been made in other aspects of the investigation and more widely in the published literature, and as such, are potentially more reliable than initially thought. Possible reasons for this temperature dependence are discussed in section 5.7.2.2 Possible Explanations for Observations. Grain boundary diffusion in this setting appears to be between 2 & 3 orders of magnitude (i.e. at least 100 times) faster than the fastest known lattice mechanism for Li in olivine with the clear implication, as already discussed, that within the short duration of experimental runs, grain boundary diffusion can be easily isolated. Given this significantly faster measurement of diffusivity, even bearing in mind the lack of data and other sources of error discussed here, grain boundary diffusion is the most likely scenario to explain this much increased value.

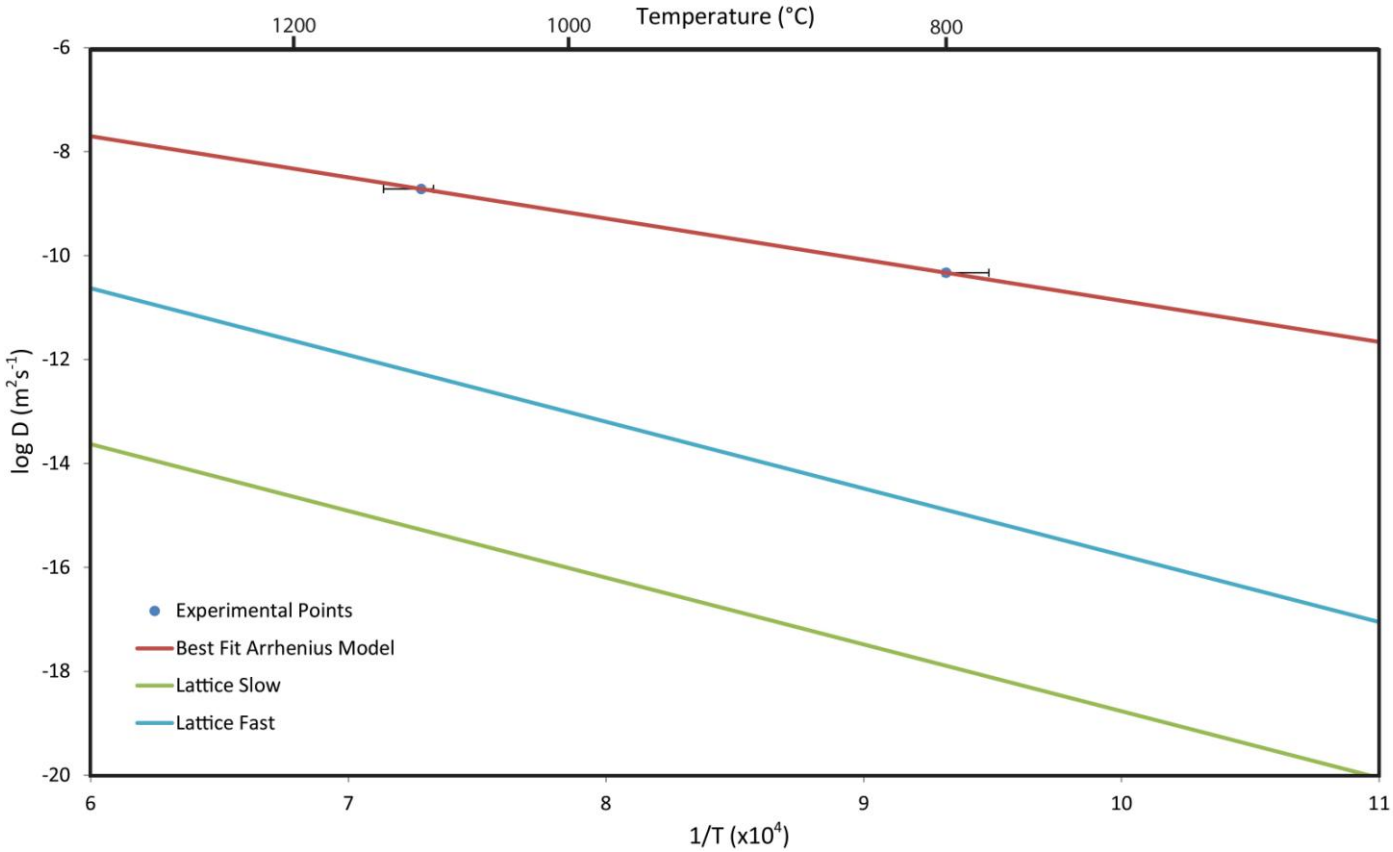

Figure 101: Arrhenius Plot showing Comparison between Measured Grain Boundary Diffusion Data and Single Crystal Data for Diffusion of Li

Lattice diffusion rates are significantly lower than grain boundary diffusion rates within the measured temperature range. Lattice diffusion rates are also marginally more temperature dependent than grain boundary diffusivity (as evidenced by a steeper line for the single crystal scenario). Error bars for diffusivity are very small and within the size of the data point. Errors based on the fitting process are not shown for clarity, the reader is referred to Figure 98

5.7.2.2 Possible Explanations for Observations

The primary explanation for the observations described above is that, in a parallel with the other sections of this investigation, grain boundary diffusion forms the majority of the bulk diffusive process. Diffusion of Li is a complex process owing to the ability of the element to occupy both interstitial and lattice sites within the olivine mineral lattice (all comparisons with lattice diffusion scenarios are made with reference to olivine here for the purposes of consistency between different parts of the investigation and also geological relevance owing to the mantle abundance of olivine). As such, the bulk diffusive process appears to be made up of a combination of factors including the two lattice diffusive mechanisms described by Dohmen et al. [122] and grain boundary diffusion as has been previously discussed. Li is a particularly interesting species to study with regard to this process owing to its volatile nature and its size. Whilst it is significantly larger than H, it is still relatively small compared to many other species and so forms a very interesting intermediate step in the study of grain boundary diffusion of various species. The larger size of Li (as compared to H) seems to have an obvious effect on its diffusive behaviour, which is much more dependent on local atomic environment and possibly also counterflux of oppositely charged species. It is this interaction with mineral structure and local bonding environment which is also responsible for the relative temperature dependencies of the two processes. Of particular interest here is that the temperature dependency of grain boundary diffusion appears to be very similar to that for lattice diffusion – both the fast and slow mechanisms. This is in complete contrast to observations in other aspects of this investigation.

There are a number of possible reasons for this observation. The first may simply be that an insufficient amount of data has been obtained to make a clear assessment of the temperature dependency of grain boundary diffusion in this setting. As only two experiments were successfully completed within this experimental program, only a low degree of confidence can be attached to the results obtained here. A variation in diffusivity of perhaps a few tens of per cent could significantly change the measured temperature dependence. Such variability has been commonly observed in other experimental programs within this investigation. These variations would not necessarily be caused by errors resulting from inherent sources of error within the instrumentation used or experimental setup but simply as a function of the natural variability common to all experiments using natural materials. Variations in the composition of starting materials or in the rates of many of the processes operating during an experiment could cause such deviations from model values to occur. However, as more and more data is collected such variability will tend to average out and the true signal from the data can be found. As such, in this case, it is likely that more data is needed before a proper understanding of the temperature dependence found here can be developed.

Despite the difficulties posed by the lack of data collected here it is clear that grain boundary diffusion in this setting does indeed proceed significantly more quickly than lattice diffusion. It is very unlikely that two separate determinations of the process would be simultaneously incorrect by a large number of orders of magnitude in the same direction. The fact that both data points show grain boundary diffusion to be at least 2.5 orders of magnitude faster than lattice diffusion is highly suggestive that the data obtained here is valid. Furthermore, the increasingly large gap between grain boundary and lattice settings as temperature lowers is consistent with all other comparisons of grain boundary versus lattice diffusion thereby adding further confidence to the data.

Thus, whilst it would be greatly advantageous to obtain further data in this aspect of the investigation, it is felt that the data which has been obtained provides a clear indication of the relative speed of grain boundary diffusion as compared to lattice diffusion. Observations are consistent with comparisons in the investigations into Ti and H and are suggestive of an overall framework to understand grain boundary diffusion based upon the radii of the diffusing species. This framework is further discussed in the following sections.

5.7.2.3 Implications for Work on Grain Boundary Diffusion of H

The aim of the work into the grain boundary diffusion of Li was to provide some evidence to support the hypothesis derived from the work on H grain boundary diffusion that ionic size had a significant effect on grain boundary diffusivity. The hypothesis derived from the H GB measurements was that diffusion of species with larger ionic radii would be much more energetically favourable via grain boundaries as opposed to through crystal lattices, due to the significantly greater lattice strain associated with accommodating larger species and the lower concentration of pre-existing vacancies or defects within the bulk of crystals compared to grain boundaries. Diffusion of species with larger radii occurs via a series of 'jumps' between lattice or interstitial sites, conceptually visualised as being facilitated by metal site vacancies – a process which is thought to be more energetically expensive than grain boundary diffusion. As such, if the hypothesis were true, a greater difference between the grain boundary and lattice diffusion rates would be observed in a system with a large ionic radius. This is indeed what has been found. The difference between diffusivities in the two scenarios is approximately 4 orders of magnitude at lower temperatures (800°C) in the case of H with the difference decreasing to approximately 1 order of magnitude at higher temperatures (1600°C). In the case of Li, differences are closer to 3 orders of magnitude, even at higher temperatures, with even larger differences at lower temperatures. Whilst the reliability of the data on Li is limited owing to the very small dataset, the measured data does seem to indicate that the hypothesis may be true. In order to further prove it, significantly more work on the grain boundary diffusion of Li would be required to expand the dataset and refine the Arrhenius relationship based upon it. However, as this particular aspect of the

work was a late addition to this research with the aim of furthering the understanding of the H data, it is felt that it has been exceptionally useful.

This work has also gone some way towards further understanding of the work on Ti diffusion in quartz. In the case of Ti diffusion in quartz, the literature values for lattice diffusion were so slow as to be essentially non-existent within the duration of the experimental run. Here, owing to the mechanisms of lattice diffusion of Li in olivine as discussed above, one of the lattice diffusion mechanisms is sufficiently fast to allow a significant concentration of Li to be built up in grains within a given distance from the source within the duration of the experiment (with the precise distance being significantly governed by temperature). This work has allowed the diffusivity of Ti in quartz to be put into greater context as Li is in many ways intermediate in terms of its diffusive behaviour between H and Ti. Where the diffusion of Ti can be seen as that of a heavy end member which can only move by occupying large sites in a mineral lattice and H can be seen as the very small and light end member which is able to utilise interstitial sites, Li is able to use both mechanisms and as such its behaviour is very instructive. Of particular interest is the relative temperature dependence of Li grain boundary diffusion which appears to be fairly similar to that of the other two scenarios investigated. The two data points which were obtained here suggest that the temperature dependence is a little stronger than in the other scenarios but it would be necessary for more data to be obtained before any statements can be made on this with any significant degree of confidence.

An important point to note, particularly with regard to this work on Li is that the partitioning of diffusants between different diffusive routes will be critical in understanding bulk diffusivities. Fundamentally for a particular mechanism to be the dominant route it must be faster with a greater abundance of diffusant using it instead of other routes. As such, it would in effect be useful to calculate weightings for the diffusive routes and apply them to calculations such as those shown in Figure 99 & Figure 100.

Thus, the work on Li diffusion is considered to have been a very useful addition to this study and has helped in gaining an understanding of H diffusion. The comparison of the three scenarios that have been studied in this investigation is further discussed in the subsequent two sections.

6 Grain Boundary Diffusion Meta Study

Over the time that diffusion has been studied, a large amount of data has been produced describing the diffusion of various elements and compounds within various host materials of geological interest. Much of the data that has been obtained is single crystal data i.e. the diffusion coefficient reported is that obtained for pure lattice diffusion. Whilst this data is essential in understanding the interaction between diffusants and host phases, it does not tell the full story, particularly with regard to natural scenarios. Given that all natural geological materials are polycrystalline it is absolutely essential that a full understanding of the effect of polycrystallinity on diffusivity is understood. Recently, the perceived importance of grain boundary diffusion has been increasing with the result that more studies are being carried out into the process, thereby increasing the volume of published data available. It is as a part of this community-wide research into diffusion in polycrystalline materials that this investigation hopes to add data and understanding.

By comparing and contrasting published diffusion data (from both poly- and mono-crystalline regimes) and that obtained in the various parts of this investigation one can gain an insight into how the new data fits with the existing dataset and the relative importance of grain boundary and lattice diffusion coefficients in natural settings.

A multitude of factors affect diffusivity. Figure 102 is an Arrhenius plot showing the diffusivities at a range of temperatures of a range of diffusants in quartz. Diffusivities are shown to vary over more than 12 orders of magnitude depending on the temperature and diffusant in question. It is particularly instructive to consider diffusion at an atomic level in order to develop an understanding of factors which may have a bearing on it. When considering a diffusant one must consider both its chemical and physical properties at the atomic level. Of particular interest will be the charge possessed by the diffusant and its size or ionic radius. A general observation which can be made of Figure 102 is that smaller low charge ionic species tend to gather in the upper right part of the Arrhenius plot (suggesting fast diffusivities, even at lower temperatures) and larger, higher charge species tend to concentrate in the lower left part of the diagram (slower diffusion, even at higher temperatures). It is also evident that in all cases lines slope down and to the right showing that diffusivity decreases as temperature decreases. This is true in all cases but the gradient of the lines varies indicating variable temperature dependencies of the respective diffusivities. This dependency will, in turn, be affected by the mechanisms by which diffusants move through the quartz lattice. As a diffusant moves through a host phase charges must remain balanced. If the diffusant is an ionic species with an inherent charge and it is moving from a source to a sink region (i.e. is undergoing chemical diffusion) then that flow of charge must be countered by some other flow in the opposite direction. This

may occur in the form of coupled or counter-movement of vacancies within the lattice in that return flow direction. If a site within a lattice is ideally/normally occupied by a positively charged cation but is, in this case, vacant, then it will possess a net negative charge equal in magnitude to the positive charge that the cation which would normally occupy it possesses. As such, diffusion of a species with a charge of +2 through a mineral lattice could be charge balanced by the return flow of vacancies which represent missing Mg^{2+} or Fe^{2+} ions. More highly charged diffusants could require a counter flow of groups of vacancies or other negatively charged species. As such, as charge increases the requirements for charge balancing also increase. These charge balancing steps may become rate limiting and ultimately define the rate at which diffusion can occur through a lattice thereby giving the distribution of diffusivities with charge as seen in Figure 103.

Thus, the diffusion of any species through a mineral lattice must be treated on its own merit and the observed behaviour will be a result of the interaction of the chemical and physical properties of both the mineral and the diffusant. Grain boundary diffusion on the other hand presents a different, potentially more complex scenario. Instead of the comparatively simple scenario where diffusants move through a lattice by making discrete jumps between specified sites or positions, grain boundary diffusion is visualised as diffusion along amorphous, long range disordered regions. In order to avoid the local build-up of net charge it must still be necessary for charge balancing to occur but it is likely to operate via quite different mechanisms with local atomic environments permitting the process. As such, grain boundary diffusion is something of an unknown quantity. This is why it was the subject of this investigation.

Figure 104 acts to summarise the data obtained in this investigation and to compare it to comparable studies performed by other workers. It is clear that in all cases that lattice diffusion is significantly slower than grain boundary diffusion. Also of particular interest is the relative diffusivity of the different species shown. Possible reasons for this distribution of diffusivities are discussed elsewhere within this report.

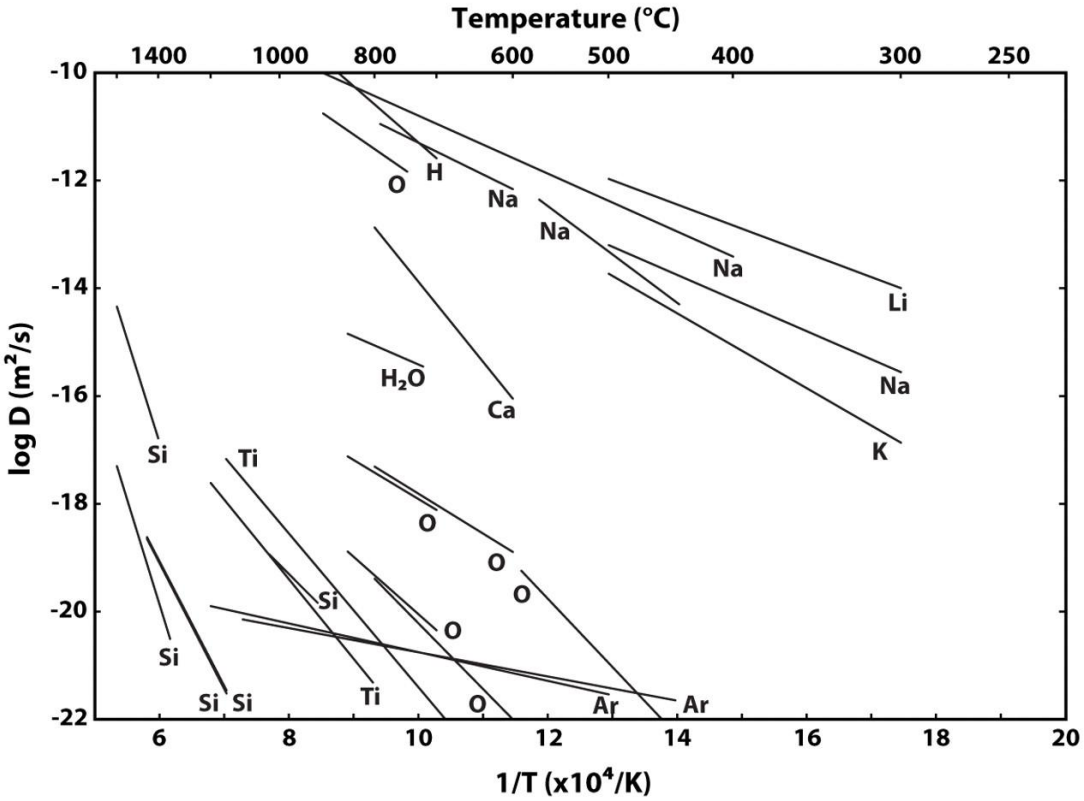

Figure 102: Diffusion Coefficients of Multiple Species in Single Crystal Quartz

In general, cations with higher charges have lower diffusivities and correspondingly higher activation energies.

From Brady & Cherniak 2010 [125]

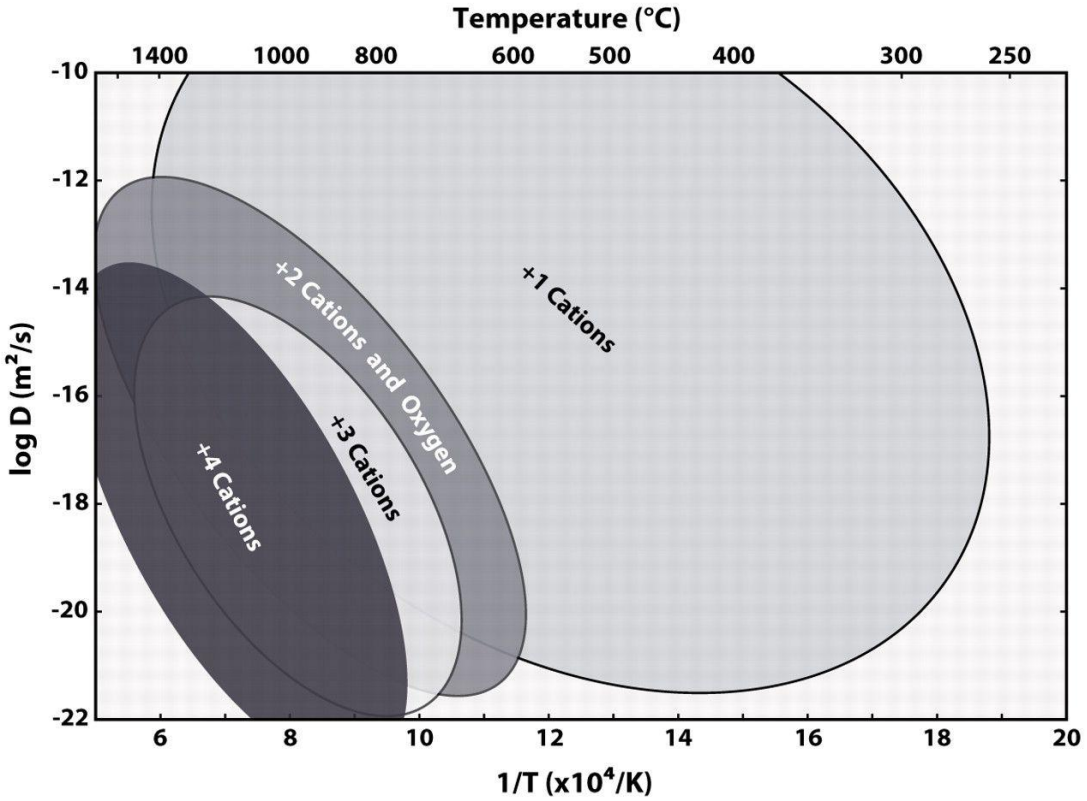

Figure 103: Schematic Arrhenius Diagram of Range of Diffusion Coefficients for Cations of Varying Charge

Cations with smaller charges consistently diffuse more quickly. In some cases such species are able to diffuse utilising interstitial mechanisms thereby foregoing the need for the presence of metal site vacancies.

From Brady & Cherniak 2010 [125]

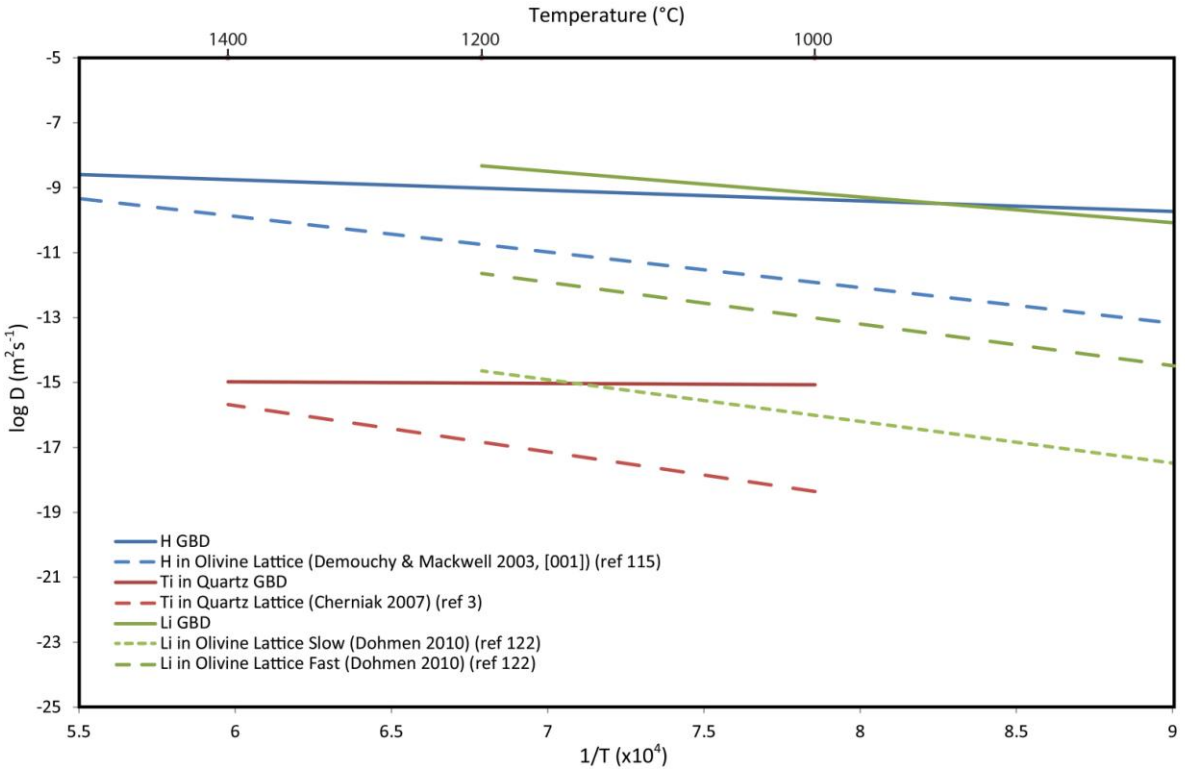

Figure 104: Arrhenius Plot Showing Experimental Data Obtained Here with Lattice Diffusion Comparisons

Solid lines show the grain boundary diffusion data obtained here and dashed lines are the lattice counterparts as discussed in the text. It is clear that smaller, low charge cations diffuse more quickly than larger, higher charge cations. Here Li shows faster bulk diffusivity than H but this may be due to the combined effects of a fast lattice diffusion mechanism and a lack of data obtained in the experimental program. The difference between lattice and grain boundary diffusivities appears to be relatively consistent between Ti & H but different for Li suggesting that the hypothesis regarding ionic sizes controlling the difference in rates may be only partly true. NB, No correction has been made here for differences in grain size Figures in square brackets are the miller index plane along which diffusion was measured.

As previously discussed, very little work has been completed on grain boundary diffusion, particularly of light elements under scenarios of geological relevance. As such, there is very little work to compare the data obtained here with. However, two studies by Demouchy [61,62] and one by Hayden & Watson [1] form useful comparisons as they too study light elements as diffusants in grain boundaries. Figure 105 shows the Arrhenius relationships obtained as part of this investigation for H & Li grain boundary diffusion (with all of the previously discussed caveats still associated with them – particularly with regard to the reliability of the line for Li which is based on evidence from only two data points).

Figure 105 makes a number of observations regarding the context of this investigation clear. Firstly, the results obtained here for H diffusion along spinel grain boundaries (i.e. isolated grain boundary diffusion) are in excellent agreement (given differences between experiments, analysis and uncertainties) with those obtained by Demouchy. As such, it is fairly certain that the data obtained here is valid and a useful addition to the dataset has been made. However, the main observation here is that H grain boundary diffusivities are significantly quicker than those for grain boundary diffusion of C. The relationship between H & Li is however more complex with the Li line crossing all of the measured lines for H. As previously discussed, this is likely to be due to a combination of factors including the relative lack of data so far collected on the system and the interplay of lattice and grain boundary diffusion mechanisms (these factors are discussed in much greater depth in section 5.7 Discussion & Interpretations). The line for Li is also extrapolated to temperatures outside of the range investigated. The overall position of the line for Li is, however, suggestive of its diffusivity being faster than that of C (by up to four orders of magnitude at higher temperatures), and potentially, with the collection of more data, potentially less than H. Such a result would suggest that the size/mass of a diffusant has an effect on its grain boundary diffusivity (as well as the more obvious effect on lattice diffusivity where incorporation of diffusants into lattice sites dictates overall diffusivity).

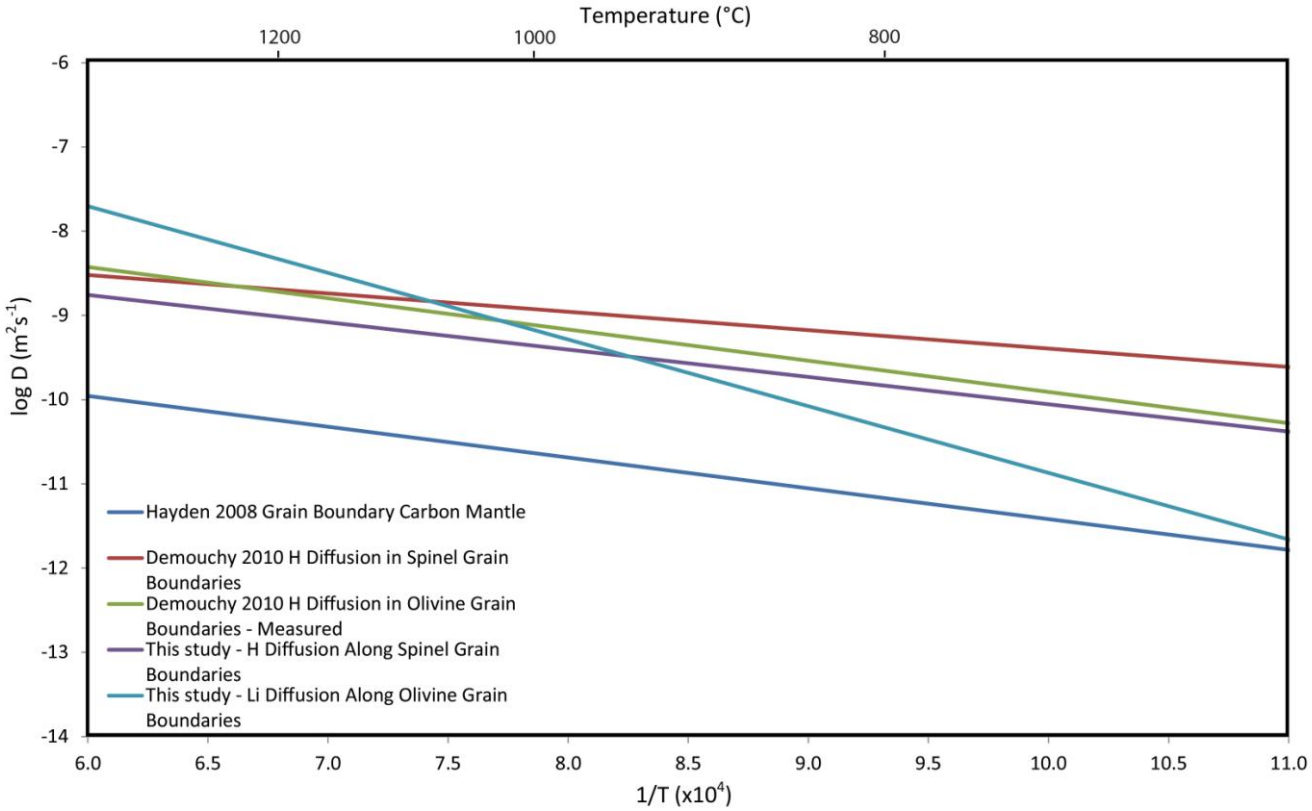

Figure 105: Comparison of Light Diffusant Arrhenius Profiles with those Obtained by Other Workers

The work conducted here on H agrees closely with that of Demouchy (2008 & 2010) [61,62] *in both of the scenarios that she investigated. The curve labelled Hayden 2008 is based on data from Hayden and Watson*[1] *C is seen to diffuse significantly more slowly (approx. 1 – 1.5 orders of magnitude) than H across the reported temperature range. The line for Li shows a significantly stronger temperature dependency than for the other two species. This is likely due to both the nature of the experiments conducted (where lattice diffusion was a significant component of bulk diffusivity) and possibly due to errors caused by the very small dataset (2 points).*

Thus, the data obtained in this investigation very much complements and adds to that which has previously been obtained by other workers. It is clear that a combination of ionic radius and charge combined with the effects of temperature control whether or not the bulk diffusive mechanism in a given setting is via grain boundaries or the mineral lattice. Variations in the temperature dependencies between comparative systems (i.e. Ti lattice diffusion vs Ti grain boundary diffusion) show that as temperature decreases the difference between diffusivities increases with grain boundary diffusion being a lot faster than lattice diffusion. As such, grain boundary diffusion must be significantly more important at lower temperatures. It may be that there are more energetically favourable pathways along grain boundaries meaning that diffusants can avoid high-energy jumps between adjacent sites which would be required within a mineral lattice.

As previously discussed, grain boundary diffusion is more important at lower temperatures where it forms a larger proportion of bulk diffusivity and may also enhance the total amount of diffusion taking place. Figure 106 shows a modelled temperature profile for the lower crust and mantle including a subducting plate. It is clear that certain regions of the mantle are significantly cooler due to the subduction and such regions will therefore be particularly conducive to grain boundary diffusion being a dominant mechanism.

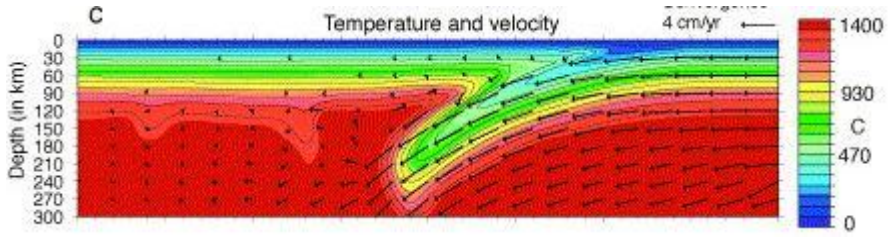

Figure 106: Modelled Crust & Mantle Temperature Profile

Grain boundary diffusion will form a larger proportion of bulk diffusivity and bulk diffusivity may itself be significantly greater in cooler regions. The cooler areas shown here, particularly those in yellow, green and blue are such regions. Here a tectonic plate is modelled as being subducted. The cooler temperatures caused by this subduction will cause grain boundary diffusion to be more prevalent and it may well be a key mechanism in liberating chemical species from the subducted plate.

Image from Doin & Henry 2001 [126]

Much like variations in temperature, there will also be variations in grain size throughout the mantle. Regions with larger grain sizes may well cause lower grain boundary diffusion rates as diffusants have to travel further around grain boundaries. Conversely, particularly fine areas would likely lead to faster grain boundary diffusion. As such, the contribution made by

grain boundary diffusion to bulk diffusivity will vary with grain size variations throughout the mantle also. Such a variation will require a scaling of the data obtained here.

The primary function of this investigation has been to provide a quantification of grain boundary diffusion processes in three separate settings and to utilise the data obtained from them to further our understanding of the mechanism as a whole. The conceptual understanding of grain boundary diffusion was in place prior to the commencement of this work but here we have performed a significant amount of quantification which was not previously present.

7 Conclusions & Further Work

Grain boundary diffusion has been shown to be a quicker process than lattice diffusion in multiple settings. Specifically, H grain boundary diffusion has been shown to be approx. 1 order of magnitude quicker at high temperatures of approx. 1400°C as compared to 4 orders of magnitude quicker at 800°C. In comparison, Ti diffusion in quartz is 0.5 orders of magnitude faster than lattice diffusion at 1400°C whereas at 1000°C it is 4 orders of magnitude faster. The case for Li is less certain owing to the lack of data as previously discussed, but, based on that which has been obtained, grain boundary diffusion is 3 orders of magnitude faster than the fastest lattice diffusion mechanism at 1200°C and 5 orders of magnitude faster at 800°C. It is clear that the difference in the structure of grain boundaries relative to a mineral lattice enables quicker transport of diffusing species. The extent to which grain boundary diffusion rates differ from lattice diffusion rates varies primarily with the chemical and physical properties of the diffusant, and temperature. Work by Demouchy suggests that the specific nature of the host phase may not have a particularly large effect on grain boundary diffusivity as she showed that H grain boundary diffusivity in olivine and spinel occurred at similar rates in the two phases [61,62]. More specifically, the partitioning of diffusants between lattice and grain boundary transport routes varies depending on the mechanism of lattice diffusion (i.e. what sort of sites are occupied within a mineral lattice) and the availability of any required vacancies within that structure. Furthermore, the nature of the grain boundary environment (i.e. the distribution and availability of unbonded anions) will also have a significant effect.

Here the grain boundary diffusivities of three species within three specific settings has been determined. In the case of H diffusion, lattice diffusion was eliminated by the choice of the host medium and in the case of Ti the process was effectively eliminated by the exceedingly slow lattice diffusion in the setting. Lattice diffusivity was not entirely precluded in the work on Li diffusion, although in this case (and indeed, many others) the lattice diffusion rates had previously been well quantified by other workers therefore making it possible to determine what contribution the various mechanisms made to the bulk diffusive process.

Comparison of the measured grain boundary diffusivities with relevant lattice diffusion equivalents shows that grain boundary diffusion processes are less temperature dependent than lattice diffusion processes. Whilst diffusivities do increase when diffusion is along grain boundaries, the rate of this increase is small as compared to that observed in a lattice diffusion scenario. This has the implication that grain boundary diffusion makes a far more significant contribution to bulk diffusivity at low temperatures (at temperatures of less than approximately 900°C grain boundary diffusion is at least two orders of magnitude quicker than its lattice diffusion equivalent). At higher temperatures diffusivities in the two settings

tend to become increasingly similar (as lattice diffusion proceeds significantly more quickly – as such, the rates converge). For grain boundary diffusion to be important in terms of the bulk mantle it needs to be significantly faster than lattice diffusion. This is due to the fact that, as compared to the number of potential diffusion routes through a mineral lattice, there are far fewer pathways available for diffusants to travel along grain boundaries. Furthermore, diffusion distances along grain boundaries must be longer than the straight line route through the middle of a grain and as grain sizes increase this distance can only increase thereby diminishing the importance of grain boundary diffusion. As grain size variations through the mantle are unknown, the importance of grain boundaries (both in terms of diffusion and as hosts for incompatible elements) can only be estimated as currently the abundance of such boundaries is unknown.

Grain boundary diffusion has the potential to provide a fast transport mechanism in many geological settings. It also has the potential to be of great significance in the fields of materials science. In situations where a diffusant is present within a phase at its maximum permitted concentration (i.e. the host phase is saturated by the diffusant), grain boundaries provide a mechanism to permit diffusion. As such, transport of chemically important species such as H between reservoirs within the earth may be significantly more common than previously thought. Furthermore, the transport of such species may play a controlling influence on certain measured properties of the earth e.g. conductivity.

The understanding of grain boundary diffusivity is also critical in the understanding of equilibration of minerals with the elements within their environment. As temperatures drop and crystallisation progresses, lattice diffusion rates drop rapidly thereby preventing diffusion across the necessary distances within the available timescales. This has major implications for the reliability of techniques which use the chemical content of minerals to determine the history of those minerals. Grain boundary diffusion provides an explanatory mechanism for such techniques by providing fast diffusive pathways which remain viable as temperature decreases.

The concept of closure temperatures is of course very important here as previously discussed. In effect, very slow diffusivities at low temperatures mean that there is effectively a temperature below which diffusion can be considered to be insignificant, even over geological time, due to its sluggishness. Grain boundary diffusion effectively permits lower closure temperatures as grain boundaries still permit relatively rapid diffusion at low temperatures owing to its low temperature dependency. This is of course dependent on a route from the grain boundary to the centre of the grain being present. This not only has implications for techniques such as TitaniQ but also potentially for chronometric techniques which assume that certain elements are no longer mobile below a certain temperature. If

these species are in fact able to move, there may be a degree of re-equilibration that is able to occur below the nominal closure temperature thereby altering the content of that species. This may then give an incorrect assessment of age using the technique. As a result, it may be wise to reconsider the application of such chronometric techniques in light of the work detailed here.

As such, this work has provided a valuable insight into grain boundary diffusion in three geologically relevant settings and has obtained evidence which illuminates the interplay of factors at play as chemical and physical parameters vary. Whilst further work would be exceptionally useful in refining the precision and accuracy of the data obtained, it is felt that the work which has been conducted here has provided a very useful contribution to a field which is currently lacking experimental data.

As mentioned in many of the preceding sections, there are a number of potential avenues for further work which could be completed to complement and further develop the work presented here.

A primary factor which could be investigated is the effect of pressure on grain boundary diffusion coefficients. This effect would be expected to be relatively small based upon the effect of pressure on lattice diffusion which has been published by other workers [5]. Access to equipment such as a multi-anvil cell, a diamond-anvil cell would be required for studies at higher pressure than that which can be achieved with the piston cylinder. Lower pressure studies could be completed with gas pressure vessels or cold seal apparatus. The choice of the specific piece of apparatus used for investigations at different pressures would dictate the nature of the capsule which could be used in such settings. Typically, the higher the pressure that is used, the smaller an experimental sample must be. Given that there is a minimum grain size which is needed for the analysis of the work being conducted here and also given that the work is on polycrystalline scenarios (requiring the presence of numerous crystals), as capsules get smaller experiments may become less relevant as fewer grains are present. Furthermore, any capsule edge effects may become more significant as capsule size is reduced.

The published effect of pressure on Ti solubility in quartz is significant, and as such, any variation in the experimental pressure will have a direct effect on the measured diffusivity (when concentrations of Ti in quartz are high i.e. close to or at saturation). Thus, pressure control is essential. During the experimental runs pressure could drop significantly overnight meaning that diffusivities for the run would be overestimated (as solubility increased with decreasing pressure). Hence, in future work of this nature using similar equipment the addition of computer control to regulate the conditions of the experiment would be greatly

advantageous as more reliable data could be obtained. Subsequent to the completion of this investigation, these additions have been made and as such, future investigations will be able to take advantage of such improvements.

It would be advantageous to extend the range of temperatures over which experiments are run. Here, experiments were typically run at temperatures greater than 800°C. The reason for this was to ensure that enough diffusion took place within the available timescale of an experiment that a measurable diffusion profile would develop. In order to run experiments at lower temperatures, considerably longer durations would be needed owing to the exponential relationship between diffusivity and temperature. In practice, the addition of automated control to a piston cylinder apparatus would be very useful if this was done as experiments could then be left to run unattended for greater periods of time. For some diffusants at particularly low temperatures, durations of weeks or months may be necessary.

Element mapping of large grains derived from grain boundary experiments would provide very useful data. The technique would provide useful information on the way in which diffusants travelled from grain edges to the points within grains where they were analysed. Ideally this would be done on a scale of nanometres. Some first order element maps could have been performed as part of this investigation but were not due to constraints of instrument capability and time. Also, the resolution of instruments available during this investigation was on the scale of micrometres. Whilst this information would be useful, the most useful information would involve collecting nanometre scale element maps in the region of grain boundaries, potentially allowing for the identification of long range imperfections in the mineral lattice which may provide fast routes into the centre of a grain. The investigation of such imperfections could, itself be a field of useful research.

It would be a worthwhile to further investigate capsule edge effects. In order to do this a number of experiments would have to be run under the same conditions so that similar diffusion profiles formed in each run. It would then be possible to take readings of point concentrations of diffusants at various distances from a capsule edge thereby allowing a determination of the strength of the effect caused by an edge to be determined. These investigations would of course have to be altered depending on the capsule geometry used for a given set of experiments.

A further study into the effect of composition would be advantageous, potentially using a ground up natural peridotite (or potentially a machined cylinder) as the diffusion medium. An investigation into chemically dirty systems would be very interesting – particularly in the light of other workers' findings that grain boundaries are effective reservoirs for incompatible elements [23]. As various species reside at grain boundaries, they may bond to unbonded O

ions at the surface of that lattice structure. As such, there is likely to be a relative lack of unbonded O in such situations thereby creating a lack of sites to enable diffusants to jump between.

It would be advantageous to run repeats of a significant amount of the data obtained in the pursuit of providing better diffusion profiles for the fitting algorithms to work on. As the aim of the investigation was to determine diffusion coefficients it was not possible to accurately predict how long an experiment would need to run for such that an ideal diffusion profile could be obtained. An ideal profile is one in which there are many points on the slope of the profile which most affect the outcome of the fitting procedure. It is of course very difficult to achieve this in the work on the diffusion of volatiles along grain boundaries as each measurement point must be a separate olivine grain of greater than 30µm diameter (ideally at least 50µm). As the section through the capsule that is seen is essentially random and therefore a random selection of the olivine grains within the sample is sampled it is highly unlikely that enough grains will ever be revealed to get a large number of points making up the diffusion profile. It would be possible to increase the number of grains that would be exposed by increasing the total number of olivine grains within the capsule. This would however be a potentially risky strategy as a very large number of olivine grains could cause numerous grains to be in contact with each other thereby forming a continuous network of grains that would permit lattice diffusion. This would then directly affect the diffusion data which is being collected in a study of GBD.

This investigation also shows how difficult it can be to obtain high quality data on grain boundary diffusion. As with any experimental program, the successful acquisition of data relies on all steps of a long and complex process being completed correctly. Furthermore, experimental design has had to be carried out with great care so as to ensure that valid diffusion data was obtained. As such, it is considered a significant achievement that diffusion data which is consistent between experiments and with the work conducted by other investigators has been obtained and interpreted to add to the body of knowledge in this field.

Further to the suggested experimental improvements detailed below, it is also important to consider the wider context of the findings of this research. Fundamentally, it has been found that there are very clear differences in diffusivity of light elements and Ti in quartz between the respective scenarios of grain boundary and lattice diffusion. In some cases these differences occur over several orders of magnitude. The magnitude of the differences is dependent on the second major finding of the work; the temperature dependency of grain boundary diffusion. In general, this has been found to be significantly less than that of lattice diffusion (i.e. temperature has a less significant effect on grain boundary diffusivity as

compared to lattice diffusivity). It is clearly evident that the process of grain boundary diffusivity is very different to that of lattice diffusivity. Lattice diffusivity has previously been well constrained with conceptual models having been developed which envisage it as occurring as a series of discrete hops between different sites with a counter flux of charged species utilising a series of defects which facilitate bulk transport. This understanding is based upon decades of experiments performed over a large portion of Pressure-Temperature-Composition parameter space using a variety of experimental and analytical techniques. It is also based upon more recent atomistic simulations of diffusion and the stability of different defects and the energies associated with hopping between these. It is very clear that a similar suite of models and concepts need to be developed for grain boundary diffusion. This is particularly important when one considers the massive ubiquity of grain boundaries and as such the huge influence they may potentially have. The development of such an understanding will be significantly more difficult than for lattice diffusion – particularly as we are now only beginning to study grain boundaries in earnest. Grain boundaries cannot be constrained by traditional crystal diffusion techniques; as such, we need to utilise other approaches to gain an understanding. Accordingly, new analytical and experimental methods need to be developed.

A large number of questions can also be asked of grain boundaries which have not been specifically addressed here. Grain boundaries appear to be regions of long range disorder which have, to date, not been characterised to a particularly detailed extent. As such, future work should aim to understand the atomic environment of grain boundaries. This may very well be a very difficult task to complete. However, by using high resolution analytical techniques (e.g. TEM) it should be possible for progress to be made. It may be that the disordered nature of grain boundaries makes them, in many regards, analogous to melts with some limited local ordering but no long range order. As such, there may be a gradual continuum between the ordered mineral lattice and the partially disordered grain boundary. The similarity in grain boundary diffusivity of H in spinel and olivine grain boundaries may imply that grain boundaries are quite similar between different hosts and as such that the overall disorder of the grain boundary environment overcomes the differences in the structure of the host phases. Differences in chemistry between host phases may or may not have an effect on diffusivity in the same way as their structure. Given that the (at least partially) disordered nature of grain boundaries appears to have a significant bearing on diffusion along them, it may be that glasses, which are disordered, amorphous solids, may therefore be a good proxy for grain boundaries thereby more easily allowing their study. Furthermore, a study of grain boundary diffusion in nano-materials would be of interest – particularly with regard to seeing if the smaller grain size permits significantly faster diffusion. It may also be possible, with a greater basis of experimental work to link modelling of grain boundary diffusion with the experimental counterpart.

It is conceptual issues such as these, based upon an understanding of the physical nature of grain boundaries which need to be elucidated in order to allow a full understanding of the processes occurring at grain boundaries. Grain boundaries appear to be complex structures and this work has provided data which is suggestive of some of the controlling factors on diffusion along them. Further work will be required by future investigators in order to answer the questions posed here.

8 Acknowledgements

It goes without saying that any large piece of work would be impossible to complete without the help, assistance and support of a great many people and this project has been no exception. I have been very lucky to have been surrounded by some truly excellent scientists but more importantly a fantastic group of friends and family.

My first thanks must go to my supervisor and all round good chap, Geoff Bromiley without whom this work would not have been possible. He has been approachable and friendly at all times and always a wealth of knowledge. Thank you also to Dr Ian Butler for assistance in the laboratories of Grant Institute. I must also express my gratitude towards all of the support staff in the workshop and Mike Hall in the sample preparation lab without whom the practical work simply could not have happened. I was very lucky to work with some truly excellent analysts at EMMAC and I must extend thanks to them not only for their assistance in the work which forms this thesis but also for quite literally getting me to where I am today – I would not have the job that I now do if it were not for their expertise and willingness to teach. So thank you to John Craven, Nicola Cayzer, Cees-Jan de Hoog, Richard Hinton and Chris Hayward.

The PhD students at the School of GeoSciences are, in my opinion exceptionally lucky as they study within a huge, academically excellent and broad school which affords them the opportunity to both work with and socialise with a great many others in a similar situation to themselves. This has undoubtedly been one of the great joys of my time at Edinburgh. My first thanks in this regard must go to Jenny Rapp whom I knew well from our undergrad days at Bristol. Had it not been for her welcoming me to Edinburgh for Hogmanay during a trip home from working in Australia I might very well never have thought about studying for a PhD again. The early years of the PhD were hugely fun and amongst others I must thank Dan, Caroline, Louise, Ruth, Matt, Skippy, Amber, Sian, Rhian, Dave, Shaun Nick, Rob, Rosie and many others for that. The later generations of attic dwellers seem to be carrying on in the fine traditions left by those before them and so all the best to Darren, Maddy, Rachel, Romesh, Erica, Matt and the great many others whom I have undoubtedly shared a pint or two with. My house mates over the years have made living in Edinburgh a great joy and in addition to those mentioned above (you know who you are) I would like to extend special thanks to Andrew, Lizzie and Lofty in particular for all the good times in the Viewforth flat.

I must also thank my new employers, Oxford Instruments for being willing to employ me even before the submission of my thesis. I am very much enjoying working there and look forward to a long and prosperous future with the company.

Very importantly I would like to thank my parents, Derek & Christine Hiscock for everything over the last 29(!) years. Your support and encouragement has meant everything. Finally, thank you to the wonderful Francesca Snow who, over the last 2.5 years has made me happier than I ever have been and has been there for me through all of the inevitable frustrations that a life working in science brings.

Apologies to all those whom I have almost certainly missed from this list. A life is the sum product of all of everything that has been done and all the interactions that person has had – I am grateful for them all and wish everyone who has helped me along the way the absolute best.

9 References

1. Hayden, L. A. & Watson, E. B. Grain boundary mobility of carbon in Earth's mantle: A possible carbon flux from the core. *Proceedings of the National Academy of Sciences* **105,** 8537 –8541 (2008).
2. Wark, D. A. & Watson, E. B. TitaniQ: a titanium-in-quartz geothermometer. *Contrib Mineral Petrol* **152,** 743–754 (2006).
3. Cherniak, D. J., Watson, E. B. & Wark, D. A. Ti diffusion in quartz. *Chemical Geology* **236,** 65–74 (2007).
4. Pennacchioni, G., Menegon, L., Leiss, B., Nestola, F. & Bromiley, G. Development of crystallographic preferred orientation and microstructure during plastic deformation of natural coarse-grained quartz veins. *J. Geophys. Res.* **115,** 23 PP. (2010).
5. Watson, E. B. & Baxter, E. F. Diffusion in solid-Earth systems. *Earth and Planetary Science Letters* **253,** 307–327 (2007).
6. Hayden, L. A. & Watson, E. B. A diffusion mechanism for core-mantle interaction. *Nature* **450,** 709–711 (2007).
7. Shewmon, P. G. *Diffusion in Solids*. (McGraw-Hill, 1963).
8. Hirschmann, M. M., Aubaud, C. & Withers, A. C. Storage capacity of H2O in nominally anhydrous minerals in the upper mantle. *Earth and Planetary Science Letters* **236,** 167–181 (2005).
9. Bolfan-Casanova, N. Water in the Earth's mantle. *Mineral Mag* **69,** 229–257 (2005).
10. Kohn, M. J. & Northrup, C. J. Taking mylonites' temperatures. *Geology* **37,** 47–50 (2009).
11. Storm, L. C. & Spear, F. S. Application of the titanium-in-quartz thermometer to pelitic migmatites from the Adirondack Highlands, New York. *Journal of Metamorphic Geology* **27,** 479–494 (2009).
12. Sato, K. & Santosh, M. Titanium in quartz as a record of ultrahigh-temperature metamorphism: the granulites of Karur, southern India. *Mineralogical Magazine* **71,** 143–154 (2007).
13. Wark, D. A., Hildreth, W., Spear, F. S., Cherniak, D. J. & Watson, E. B. Pre-eruption recharge of the Bishop magma system. *Geology* **35,** 235–238 (2007).
14. Wiebe, R. A., Wark, D. A. & Hawkins, D. P. Insights from quartz cathodoluminescence zoning into crystallization of the Vinalhaven granite, coastal Maine. *Contributions to Mineralogy & Petrology* **154,** 439–453 (2007).
15. Vazquez, J. A., Kyriazis, S. F., Reid, M. R., Sehler, R. C. & Ramos, F. C. Thermochemical evolution of young rhyolites at Yellowstone: Evidence for a cooling but periodically replenished postcaldera magma reservoir. *Journal of Volcanology and Geothermal Research* **188,** 186–196 (2009).
16. Seifert, W. *et al.* Distinctive properties of rock-forming blue quartz: inferences from a multi-analytical study of submicron mineral inclusions. *MINERALOGICAL MAGAZINE* **75,** 2519–2534 (2011).
17. Bergman, H. & Piazolo, S. The recognition of multiple magmatic events and pre-existing deformation zones in metamorphic rocks as illustrated by CL signatures and numerical modelling: examples from the Ballachulish contact aureole, Scotland. *International Journal of Earth Sciences* **101,** 1127–1148 (2012).
18. Altenberger, U. *et al.* The Garzón Massif, Colombia-a new ultrahigh-temperature metamorphic complex in the Early Neoproterozoic of northern South America. *Miner Petrol* **105,** 171–185 (2012).
19. Spear, F. S. & Wark, D. A. Cathodoluminescence imaging and titanium thermometry in metamorphic quartz. *Journal of Metamorphic Geology* **27,** 187–205 (2009).
20. Rusk, B. G., Lowers, H. A. & Reed, M. H. Trace Elements in Hydrothermal Quartz: Relationships to Cathodoluminescent Textures and Insights into Vein Formation. *Geology* **36,** 547–550 (2008).
21. Behr, W. M. & Platt, J. P. A naturally constrained stress profile through the middle crust in an extensional terrane. *Earth and Planetary Science Letters* **303,** 181–192 (2011).
22. Hiraga, T., Anderson, I. M. & Kohlstedt, D. L. Chemistry of grain boundaries in mantle rocks. *American Mineralogist* **88,** 1015–1019 (2003).

23. Hiraga, T., Anderson, I. M. & Kohlstedt, D. L. Grain boundaries as reservoirs of incompatible elements in the Earth's mantle. *Nature* **427,** 699–703 (2004).
24. Suzuki, K. Grain-boundary enrichment of Incompatible Elements in some Mantle Peridotites. *Chem Geol* **63,** 319–334 (1987).
25. Waff, H. S. & Holdren, G. R. The Nature of Grain Boundaries in Dunite and Lherzolite Xenoliths: Implications for Magma Transport in Refractory Upper Mantle Material. *J. Geophys. Res.* **86,** 3677–3683
26. Joesten, R. Grain-Boundary Diffusion Kinetics in Silicate and Oxide Minerals. In Ganguly, J. (Ed.), Diffusion, Atomic Ordering and Mass Transport. *Advances in Physical Geochemistry* **8,** 345–395 (1991).
27. Walker, R. J. & Walker, D. Does the Core Leak? *Eos Trans. AGU* **86,** P. 237 (2005).
28. Brandon, A. D. & Walker, R. J. The debate over core-mantle interaction. *Earth and Planetary Science Letters* **232,** 211–225 (2005).
29. Orman, J. A. V., Fei, Y., Hauri, E. H. & Wang, J. Diffusion in MgO at high pressures: Constraints on deformation mechanisms and chemical transport at the core-mantle boundary. *Geophys. Res. Lett.* **30,** 4 PP. (2003).
30. Hayden, L. A. & Watson, E. B. Grain boundary mobility of siderophile elements in MgO. *Geochimica et Cosmochimica Acta* **70,** A238 (2006).
31. Wood, B. J. Carbon in the core. *Earth and Planetary Science Letters* **117,** 593–607 (1993).
32. Scott, H. P., Williams, Q. & Knittle, E. Stability and equation of state of Fe3C to 73 GPa: Implications for carbon in the Earth's core. *Geophysical Research Letters* **28,** 1875–1878 (2001).
33. Huang, L., Skorodumova, N. V., Belonoshko, A. B., Johansson, B. & Ahuja, R. Carbon in iron phases under high pressure. *Geophys. Res. Lett.* **32,** 4 PP. (2005).
34. Mishin, Y. & Herzig, C. Grain boundary diffusion: recent progress and future research. *Materials Science and Engineering: A* **260,** 55–71 (1999).
35. Dohmen, R. & Milke, R. Diffusion in Polycrystalline Materials: Grain Boundaries, Mathematical Models, and Experimental Data. *Reviews in Mineralogy and Geochemistry* **72,** 921–970 (2010).
36. Zhang, Y. & Cherniak, D. J. in *Diffusion in Minerals and Melts* (Zhang, Y. X. & Cherniak, D. J.) **72,** 1–4 (Mineralogical Soc Amer, 2010).
37. Tirone, M. *et al.* Rare earth diffusion kinetics in garnet: Experimental studies and applications. *Geochimica et Cosmochimica Acta* **69,** 2385–2398 (2005).
38. Zhang, Y. H2O in Rhyolitic Glasses and Melts: Measurement, Speciation, Solubility, and Diffusion. *Rev. Geophys.* **37,** 493–516 (1999).
39. Fogel, R. A. & Rutherford, M. J. The solubility of carbon dioxide in rhyolitic melts; a quantitative FTIR study. *American Mineralogist* **75,** 1311–1326 (1990).
40. Blank, J. G., Stolper, E. M. & Carroll, M. R. Solubilities of carbon dioxide and water in rhyolitic melt at 850°C and 750 bars. *Earth and Planetary Science Letters* **119,** 27–36 (1993).
41. Shcheka, S. S., Wiedenbeck, M., Frost, D. J. & Keppler, H. Carbon solubility in mantle minerals. *Earth and Planetary Science Letters* **245,** 730–742 (2006).
42. Baker, L. L. & Rutherford, M. J. Sulfur diffusion in rhyolite melts. *Contributions to Mineralogy and Petrology* **123,** 335–344 (1996).
43. Aiuppa, A. *et al.* H2S fluxes from Mt. Etna, Stromboli, and Vulcano (Italy) and implications for the sulfur budget at volcanoes. *Geochimica et Cosmochimica Acta* **69,** 1861–1871 (2005).
44. De Moor, J. M. *et al.* Degassing at Anatahan volcano during the May 2003 eruption: Implications from petrology, ash leachates, and SO2 emissions. *Journal of Volcanology and Geothermal Research* **146,** 117–138 (2005).
45. Teng, F.-Z., McDonough, W. F., Rudnick, R. L. & Walker, R. J. Diffusion-driven extreme lithium isotopic fractionation in country rocks of the Tin Mountain pegmatite. *Earth and Planetary Science Letters* **243,** 701 – 710 (2006).
46. Béjina, F., Jaoul, O. & Liebermann, R. C. Diffusion in minerals at high pressure: a review. *Physics of The Earth and Planetary Interiors* **139,** 3–20 (2003).

47. Winther, K. T., Watson, E. B. & Korenowski, G. M. Magmatic sulfur compounds and sulfur diffusion in albite melt at 1 GPa and 1300-1500 degrees C. *American Mineralogist* **83,** 1141–1151 (1998).
48. Freda, C., Baker, D. R. & Scarlato, P. Sulfur diffusion in basaltic melts. *Geochimica et Cosmochimica Acta* **69,** 5061–5069 (2005).
49. Wark, D. A. & Watson, E. B. Interdiffusion of H2O and CO2 in metamorphic fluids at ~490 to 690°C and 1 GPa. *Geochimica et Cosmochimica Acta* **68,** 2693–2698 (2004).
50. Koga, K. T., Walter, M. J., Nakamura, E. & Kobayashi, K. Carbon self-diffusion in a natural diamond. *Phys. Rev. B* **72,** 024108 (2005).
51. Kroger, F. & Vink, H. Relations between the Concentrations of Imperfections in Crystalline Solids. *Solid State Physics - Advances In Research And Applications* **3,** 307–435 (1956).
52. Wright, K. & Catlow, C. R. A. A computer simulation study of (OH) defects in olivine. *Physics and Chemistry of Minerals* **20,** 515–518 (1994).
53. Claire, A. D. L. The analysis of grain boundary diffusion measurements. *British Journal of Applied Physics* **14,** 351–356 (1963).
54. Hiraga, T. & Kohlstedt, D. L. Equilibrium interface segregation in the diopside-forsterite system I: Analytical techniques, thermodynamics, and segregation characteristics. *Geochimica et Cosmochimica Acta* **71,** 1266–1280 (2007).
55. Hiraga, T., Hirschmann, M. M. & Kohlstedt, D. L. Equilibrium interface segregation in the diopside-forsterite system II: Applications of interface enrichment to mantle geochemistry. *Geochimica et Cosmochimica Acta* **71,** 1281–1289 (2007).
56. Behrens, H. & Nowak, M. The mechanisms of water diffusion in polymerized silicate melts. *CONTRIBUTIONS TO MINERALOGY AND PETROLOGY* **126,** 377–385 (1997).
57. Watson, E., Sneeringer, M. & Ross, A. Diffusion of dissolved carbonate in magmas: Experimental results and applications. *Earth and Planetary Science Letters* **61,** 346–358 (1982).
58. Hamann, S. The influence of pressure on electrolytic conduction in alkali silicate glasses. *Aust. J. Chem.* **18,** 1–8 (1965).
59. Thomas, J. B. *et al.* TitaniQ under pressure: the effect of pressure and temperature on the solubility of Ti in quartz. *Contributions to Mineralogy & Petrology* **160,** 743–759 (2010).
60. Zhang, X. Y., Cherniak, D. J. & Watson, E. B. Oxygen diffusion in titanite: Lattice diffusion and fast-path diffusion in single crystals. *Chemical Geology* **235,** 105–123 (2006).
61. Demouchy, S. Hydrogen diffusion in spinel grain boundaries and consequences for chemical homogenization in hydrous peridotite. *Contributions to Mineralogy and Petrology* doi:10.1007/s00410-010-0512-4
62. Demouchy, S. Diffusion of hydrogen in olivine grain boundaries and implications for the survival of water-rich zones in the Earth's mantle. *Earth and Planetary Science Letters* **295,** 305–313 (2010).
63. Regenauer-Lieb, K. & Kohl, T. Water solubility and diffusivity in olivine: its role in planetary tectonics. *Mineral Mag* **67,** 697–715 (2003).
64. Sleep, N. H. Evolution of the mode of convection within terrestrial planets. *J. Geophys. Res.* **105,** PP. 17,563–17,578
65. Solomatov, V. S. & Moresi, L. N. Three regimes of mantle convection with non-Newtonian viscosity and stagnant lid convection on the terrestrial planets. *Geophysical Research Letters* **24,** 1907–1910 (1997).
66. J. Allègre, C., Staudacher, T. & Sarda, P. Rare gas systematics: formation of the atmosphere, evolution and structure of the Earth's mantle. *Earth and Planetary Science Letters* **81,** 127–150 (1987).
67. Dixon, J. E., Dixon, T. ., Bell, D. . & Malservisi, R. Lateral variation in upper mantle viscosity: role of water. *Earth and Planetary Science Letters* **222,** 451–467 (2004).
68. Mysen, B. O. & Boettcher, A. L. Melting of a Hydrous Mantle: I. Phase Relations of Natural Peridotite at High Pressures and Temperatures with Controlled Activities of Water, Carbon Dioxide, and Hydrogen. *J. Petrology* **16,** 520–548 (1975).
69. Workman, R. K. & Hart, S. R. Major and trace element composition of the depleted MORB mantle (DMM). *Earth and Planetary Science Letters* **231,** 53–72 (2005).

70. Helffrich, G. R. & Wood, B. J. The Earth's mantle. *Nature* **412,** 501–507 (2001).
71. Ringwood, A. Composition of the Core and Implications for the Origin of Earth. *GEOCHEM J* **11,** 111–135 (1977).
72. Murakami, M., Hirose, K., Yurimoto, H., Nakashima, S. & Takafuji, N. Water in Earth's Lower Mantle. *Science* **295,** 1885–1887 (2002).
73. Meade, C., Reffner, J. A. & Ito, E. Synchrotron Infrared Absorbance Measurements of Hydrogen in MgSiO3 Perovskite. *Science* **264,** 1558–1560 (1994).
74. Bolfan-Casanova, N., Keppler, H. & Rubie, D. C. Water partitioning between nominally anhydrous minerals in the MgO-SiO2-H2O system up to 24 GPa: implications for the distribution of water in the Earth's mantle. *Earth and Planetary Science Letters* **182,** 209–221 (2000).
75. Bell, D. R. & Rossman, G. R. Water in Earth's Mantle: The Role of Nominally Anhydrous Minerals. *Science* **255,** 1391–1397 (1992).
76. Wang, W. & Sueno, S. Discovery of a NaPx–En inclusion in diamond: possible transition zone origin. *Mineralogical Journal* **18,** 9–16 (1996).
77. Turner, G., Burgess, R. & Bannon, M. Volatile-rich mantle fluids inferred from inclusions in diamond and mantle xenoliths. *Nature* **344,** 653–655 (1990).
78. Kellogg, L. H., Hager, B. H. & van der Hilst, R. D. Compositional Stratification in the Deep Mantle. *Science* **283,** 1881–1884 (1999).
79. Schilling, J.-G. Iceland Mantle Plume: Geochemical Study of Reykjanes Ridge. *Nature* **242,** 565–571 (1973).
80. Hofmann, A. W. Mantle geochemistry: the message from oceanic volcanism. *Nature* **385,** 219–229 (1997).
81. Fisk, M. & Kelley, K. A. Probing the Pacific's oldest MORB glass: mantle chemistry and melting conditions during the birth of the Pacific Plate. *Earth and Planetary Science Letters* **202,** 741–752 (2002).
82. Hirth, G. & Kohlstedt, D. L. Water in the oceanic upper mantle: implications for rheology, melt extraction and the evolution of the lithosphere. *Earth and Planetary Science Letters* **144,** 93–108 (1996).
83. Yoder, C. F. *et al.* Secular variation of Earth's gravitational harmonic J2 coefficient from Lageos and nontidal acceleration of Earth rotation. *Nature* **303,** 757–762 (1983).
84. Stephenson, F. R. & Morrison, L. V. Long-Term Fluctuations in the Earth's Rotation: 700 BC to AD 1990. *Philosophical Transactions: Physical Sciences and Engineering* **351,** 165–202 (1995).
85. Sabadini, R., Yuen, D. A. & Boschi, E. Polar Wandering and the Forced Responses of a Rotating, Multilayered, Viscoelastic Planet. *J. Geophys. Res.* **87,** 2885–2903 (1982).
86. Robertson, D. *et al.* The application of geodetic radio interferometric surveying to the monitoring of sea-level. *GEOPHYS J ROY ASTR S* **87,** 3–13 (1986).
87. Spada, G., Ricard, Y. & Sabadini, R. Excitation of true polar wander by subduction. *Nature* **360,** 452–454 (1992).
88. Cathles, L. M. *The viscosity of the earth's mantle [by] Lawrence M. Cathles, III*. (Princeton University Press, 1975).
89. Farrell, W. *et al.* Glacial isostasy and relative sea-level - global finite-element model. *TECTONOPHYS* **50,** 81–110 (1978).
90. Peltier, W. & Tushingham, A. Validation of the ICE-3G model of Wurm-Wisconsin deglaciation using a global data-base of relative sea-level histories. *J GEOPHYS RES* **97,** 3285–3304 (1992).
91. Argus, D. F. Postglacial rebound from VLBI geodesy: On establishing vertical reference. *Geophys. Res. Lett.*
92. Milne, G. A. *et al.* Space-Geodetic Constraints on Glacial Isostatic Adjustment in Fennoscandia. *Science* **291,** 2381–2385 (2001).
93. Park, K.-D. *et al.* Investigation of glacial isostatic adjustment in the northeast U.S. using GPS measurements. *Geophys. Res. Lett.* (2002).
94. Kohlstedt, D., Paterson, M. & MacKwell, S. The Role of Water in the Deformation of Olivine Single Crystals. *J GEOPHYS RES* **90,** 1319–1333 (1985).
95. Paterson, M., Gerald, J. F. & Karato, S. Rheology of Sythetic Olivine Aggregates - Influence of Grain-size and Water. *J GEOPHYS RES* **91,** 8151–8176 (1986).

96. Karato, S. The Role of Hydrogen in the Electrical Conductivity of the Upper Mantle. *Nature* **347,** 272–273 (1990).
97. Gürer, A., Bayrak, M. & Gürer, Ö. F. Magnetotelluric images of the crust and mantle in the southwestern Taurides, Turkey. *Tectonophysics* **391,** 109–120 (2004).
98. Gatzemeier, A. & Tommasi, A. Flow and electrical anisotropy in the upper mantle: Finite-element models constraints on the effects of olivine crystal preferred orientation and microstructure. *Physics of The Earth and Planetary Interiors* **158,** 92–106 (2006).
99. Mackwell, S. J. & Kohlstedt, D. L. Diffusion of Hydrogen in Olivine: Implications for Water in the Mantle. *J. Geophys. Res.* **95,** PP. 5079–5088 (1990).
100. Kohlstedt, D. L. & Mackwell, S. J. Diffusion of Hydrogen and Intrinsic Point Defects in Olivine. *Zeitschrift für Physikalische Chemie* **207,** 147–162 (1998).
101. Duba, A. & Constable, S. The Electrical Conductivity of Lherzolite. *J. Geophys. Res.* 11885 – 11899 (1993).
102. Xu, Y., Shankland, T. J. & Duba, A. G. Pressure effect on electrical conductivity of mantle olivine. *Physics of The Earth and Planetary Interiors* **118,** 149–161 (2000).
103. Mainprice, D., Canova, G., Chastel, Y. & Tommasi, A. Viscoplastic self-consistent and equilibrium-based modeling of olivine lattice preferred orientations: Implications for the upper mantle seismic anisotropy. *J GEOPHYS RES* **105,** 7893–7908 (2000).
104. Karato, S. & Li, P. Diffusion Creep in Perovskite: Implications for the Rheology of the Lower Mantle. *Science* **255,** 1238–1240 (1992).
105. Wang, Z., Hiraga, T. & Kohlstedt, D. L. Effect of H+ on Fe–Mg interdiffusion in olivine, (Fe,Mg)2SiO4. *Appl. Phys. Lett.* **85,** 209 (2004).
106. Arculus, R. & Delano, J. Siderophile element abundances in the upper mantle: evidence for a sulfide signature and equilibrium with the core. *Geochimica et Cosmochimica Acta* **45,** 1331–1343 (1981).
107. Duba, A. G. & Shankland, T. J. Free carbon & electrical conductivity in the Earth's mantle. *Geophys. Res. Lett.*
108. Biellmann, C., Gillet, P., Guyot, F., Peyronneau, J. & Reynard, B. Experimental evidence for carbonate stability in the Earth's lower mantle. *Earth and Planetary Science Letters* **118,** 31–41 (1993).
109. Dasgupta, R. & Hirschmann, M. M. Effect of variable carbonate concentration on the solidus of mantle peridotite. *American Mineralogist* **92,** 370–379 (2007).
110. Dasgupta, R., Hirschmann, M. M. & Smith, N. D. Water follows carbon: CO2 incites deep silicate melting and dehydration beneath mid-ocean ridges. *Geology* **35,** 135–138 (2007).
111. Deer, W. A., Howie, R. A. & Zussman, J. *An Introduction to the Rock-Forming Minerals*. (Prentice Hall, 1996).
112. Bromiley, G. D., Nestola, F., Redfern, S. A. T. & Zhang, M. Water incorporation in synthetic and natural MgAl2O4 spinel. *Geochimica et Cosmochimica Acta* **74,** 705–718 (2010).
113. Rossman, G. R. & Smyth, J. R. Hydroxyl contents of accessory minerals in mantle eclogites and related rocks. *American Mineralogist* **75,** 775–780 (1990).
114. Kohlstedt, D. L., Keppler, H. & Rubie, D. C. Solubility of water in the α , β and γ phases of (Mg,Fe)2SiO4. *Contributions to Mineralogy and Petrology* **123,** 345–357 (1996).
115. Demouchy, S. & Mackwell, S. Water diffusion in synthetic iron-free forsterite. *Physics and Chemistry of Minerals* **30,** 486–494 (2003).
116. Bercovici, D. & Karato, S. Whole-mantle convection and the transition-zone water filter. *Nature* **425,** 39–44 (2003).
117. Ostapenko, G., Bamarnik, M. & Gorogotskaya, L. Isomorphism of titanium substitution for silicon in quartz: experimental data. *Mineral. Zh.* **9,** 30–40 (1987).
118. Huang, R. & Audétat, A. The titanium-in-quartz (TitaniQ) thermobarometer: A critical examination and re-calibration. *Geochimica et Cosmochimica Acta* **84,** 75–89 (2012).
119. Bromiley, G. D., Keppler, H., McCammon, C., Bromiley, F. A. & Jacobsen, S. D. Hydrogen solubility and speciation in natural, gem-quality chromian diopside. *American Mineralogist* **89,** 941–949 (2004).

120. Demouchy, S., Mackwell, S. & Kohlstedt, D. Influence of hydrogen on Fe–Mg interdiffusion in (Mg,Fe)O and implications for Earth's lower mantle. *Contributions to Mineralogy and Petrology* **154,** 279–289 (2007).
121. Biggs, T., Cornish, L. A., Witcomb, M. J. & Cortie, M. B. Revised phase diagram for the Pt-Ti system from 30 to 60 at.% platinum. *Journal of Alloys and Compounds* **375,** 120–127 (2004).
122. Dohmen, R., Kasemann, S. A., Coogan, L. & Chakraborty, S. Diffusion of Li in olivine. Part I: Experimental observations and a multi species diffusion model. *Geochimica et Cosmochimica Acta* **74,** 274–292 (2010).
123. Mitra, N. R., Decker, D. L. & Vanfleet, H. B. Melting Curves of Copper, Silver, Gold, and Platinum to 70 kbar. *Phys. Rev.* **161,** 613–617 (1967).
124. Cruz, D., Bulbulian, S., Lima, E. & Pfeiffer, H. Kinetic analysis of the thermal stability of lithium silicates (Li4SiO4 and Li2SiO3). *Journal of Solid State Chemistry* **179,** 909–916 (2006).
125. Brady, J. B. & Cherniak, D. J. in *Diffusion in Minerals and Melts* (Zhang, Y. X. & Cherniak, D. J.) **72,** 899–920 (Mineralogical Soc Amer, 2010).
126. Doin, M.-P. & Henry, P. Subduction initiation and continental crust recycling: the roles of rheology and eclogitization. *Tectonophysics* **342,** 163–191 (2001).

10 Appendices

10.1 Grain Boundary Diffusion of Volatiles Run Parameters

Run ID:	VGB1
Pressure (GPa):	3
Temp:	1000
Duration (Total) (s):	18000
Duration at Run T (s):	17640
Date:	40456

Cumulative Time (hours)	OP	V	A	mV	uV	T	Deviation from Nominal T	Notes
00:00	15	40		1.81	1810	238	-762	
00:01	20	50	5	3.5	3500	409	-591	
00:02	25	60	6	5.4	5400	584	-416	
00:03	30	75	7	7.85	7850	792	-208	
00:04	33	80	7.7	9.75	9750	942	-58	
00:06	34.2	85	8	10.52	10520	1001	1	T
00:09	34.2	85	8	10.55	10550	1003	3	
00:13	34.2	85	8	10.6	10600	1007	7	
00:17	34.2	85	8	10.53	10530	1002	2	
00:23	34.2	85	8	10.53	10530	1002	2	
00:27	34.2	85	8	10.47	10470	997	-3	
00:38	34.2	85	8	10.56	10560	1004	4	
00:55	34.4	85	8	10.56	10560	1004	4	
01:20	34.4	85	8	10.54	10540	1003	3	
01:47	34.4	85	8	10.51	10510	1000	0	
02:08	34.5	87	8	10.53	10530	1002	2	
02:26	34.5	87	8	10.49	10490	999	-1	
03:12	34.7	87	8	10.55	10550	1003	3	
03:57	34.7	87	8	10.56	10560	1004	4	
04:34	34.7	87	8	10.51	10510	1000	0	
05:00	34.7	87	8	10.5	10500	1000	0	Q
Max positive T deviation:			7	Max negative T deviation:				-3

Run ID:		VGB2						
Pressure (GPa):		3						
Temp (C):		1000						
Duration (Total) (s):		74340						
Duration at Run T (s):		73860						
Date:		40457						
Cumulative Time	OP	V	A	mV	uV	T	Deviation from Nominal T	Notes
00:00	10.5				0	0	-1000	
00:02	15	40		1.52	1520	206	-794	
00:03	20	50	5	2.94	2940	354	-646	
00:04	25	60	5	4.51	4510	504	-496	
00:05	30	75	6	6.61	6610	689	-311	
00:06	35	85	7	9.16	9160	896	-104	
00:07	36.5	90	7	10.25	10250	981	-19	
00:08	36.8	92	7	10.5	10500	1000	0	T
00:14	36.8	92	7	10.51	10510	1000	0	
00:20	36.8	92	7	10.51	10510	1000	0	
00:32	36.8	92	7	10.48	10480	998	-2	
00:54	36.9	92	7	10.51	10510	1000	0	
02:05	36.9	92	7	10.46	10460	997	-3	
02:54	37.1	92	7	10.49	10490	999	-1	
03:37	37.2	95	7.1	10.51	10510	1000	0	
04:02	37.2	95	7.1	10.51	10510	1000	0	
05:37	37.3	95	7.1	10.5	10500	1000	0	
06:09	37.5	95	7.1	10.5	10500	1000	0	
20:30	37.5	95	7.1	9.48	9480	921	-79	
20:39	38.5	98	7.1	10.55	10550	1003	3	Q
Max positive T deviation:			3	Max negative T deviation:				-79

Run ID:		VGB3						
Pressure (GPa):		3						
Temp (C):		1000						
Duration (Total) (s):		71760						
Duration at Run T (s):		71100						
Date:		40497						
Cumulative Time	OP	V	A	mV	uV	T	Deviation from Nominal T	Notes
00:00	10.5				0	0	-1000	
00:02	15	40		1.52	1520	206	-794	
00:04	20	50	5	2.94	2940	354	-646	
00:05	25	60	5	4.51	4510	504	-496	
00:06	30	75	6	6.61	6610	689	-311	
00:07	35	85	7	9.16	9160	896	-104	
00:09	36.5	90	7	10.25	10250	981	-19	
00:11	36.8	92	7	10.5	10500	1000	0	T
00:19	36.8	92	7	10.51	10510	1000	0	
00:33	36.8	92	7	10.51	10510	1000	0	
00:55	36.8	92	7	10.48	10480	998	-2	
01:12	36.9	92	7	10.51	10510	1000	0	
01:31	36.9	92	7	10.46	10460	997	-3	
02:38	37.1	92	7	10.49	10490	999	-1	
03:36	37.2	95	7.1	10.51	10510	1000	0	
04:21	37.2	95	7.1	10.51	10510	1000	0	
18:01	37.3	95	7.1	10.5	10500	1000	0	
19:56	37.5	95	7.1	10.5	10500	1000	0	Q
Max positive T deviation:			0	Max negative T deviation:				-3

Run ID:		VGB4						
Pressure (GPa):		3						
Temp (C):		1000						
Duration (Total) (s):		6180						
Duration at Run T (s):		5400						
Date:		40499						
Cumulative Time (hrs)	OP	V	A	mV	uV	T	Deviation from Nominal T	Notes
00:00	10.5				0	0	-1000	
00:01	15	40		1.52	1520	206	-794	
00:03	20	45	5	2.71	2710	331	-669	
00:05	25	60	6	4.3	4300	484	-516	
00:07	30	75	7	6.59	6590	687	-313	
00:10	35	80	8	9.31	9310	908	-92	
00:13	35.7	80	8	10.52	10520	1001	1	T
00:34	36.5	90	8	10.49	10490	999	-1	
00:57	36.6	92	8	10.47	10470	997	-3	
01:29	37	95	8	10.5	10500	1000	0	
01:43	37	95	8	10.5	10500	1000	0	Q
Max positive T deviation:			1	Max negative T deviation:				-3

Run ID:		VGB5						
Pressure (GPa):		3						
Temp (C):		1000						
Duration (Total) (s):		21600						
Duration at Run T (s):		21120						
Date:		40500						
Cumulative Time (hrs)	OP	V	A	mV	uV	T	Deviation from Nominal T	Notes
00:00	10.5				0	0	-1000	
00:01	14.2	35		1.34	1340	185	-815	
00:02	19.5	45	5	2.85	2850	345	-655	
00:04	24.2	60	5.5	4.4	4400	493	-507	
00:05	30	75	6.5	6.77	6770	702	-298	
00:07	35	85	8	9.87	9870	952	-48	
00:08	35.8	88	8	10.56	10560	1004	4	T
00:20	35.4	85	8	10.51	10510	1000	0	
01:20	35.5	88	8	10.48	10480	998	-2	
02:18	35.6	88	8	10.5	10500	1000	0	
03:48	35.6	88	8	10.5	10500	1000	0	
06:00	35.6	88	8	10.5	10500	1000	0	Q
Max positive T deviation:			4	Max negative T deviation:				-2

Run ID:		VGB6						
Pressure (GPa):		3						
Temp (C):		1000						
Duration (Total) (s):		4320						
Duration at Run T (s):		3962						
Date:		40633						
Cumulative Time (hrs)	OP	V	A	mV	uV	T	Deviation from Nominal T	Notes
00:00	10.6	20		0.3	300	51	-949	
00:01	15.9	40		1.35	1350	186	-814	
00:02	22	60	5	2.8	2800	340	-660	
00:04	28	60	6	4.68	4680	519	-481	
00:05	32.2	80	7	6.48	6480	678	-322	
00:06	38.7	100	8	10.51	10510	1000	0	T
00:15	38.6	100	8	10.5	10500	1000	0	
00:20	38.5	100	8	10.54	10540	1003	3	
00:27	38.3	100	8	10.54	10540	1003	3	
00:31	38.3	100	8	10.5	10500	1000	0	
00:41	38.4	100	8	10.5	10500	1000	0	
00:51	38.4	100	8	10.47	10470	997	-3	
00:59	38.7	100	8	10.6	10600	1007	7	
01:12	38.7	100	8	10.6	10600	1007	7	Q
Max positive T deviation:			7	Max negative T deviation:				-3

Run ID:		VGB7						
Pressure (GPa):		3						
Temp (C):		1200						
Duration (Total) (s):		3180						
Duration at Run T (s):		2582						
Date:		40633						
Cumulative Time (hrs)	OP	V	A	mV	uV	T	Deviation from Nominal T	Notes
00:00	12	25		0.78	780	117	-1083	
00:01	17	40	5	2.21	2210	280	-920	
00:02	22	55	5	3.79	3790	437	-763	
00:03	27	60	6	5.53	5530	595	-605	
00:08	40.3	100	9	13.21	13210	1199	-1	
00:10	41.2	100	9	12.93	12930	1179	-21	T
00:28	41.4	105	9	12.69	12690	1161	-39	
00:40	41.4	105	9	13.31	13310	1206	6	
00:53	41.4	105	9	13.31	13310	1206	6	Q
Noted that possible thermocouple movement, report this datapoint as T +/- 40C								
Max positive T deviation:			40	Max negative T deviation:				-40

Run ID:		VGB8						
Pressure (GPa):		3						
Temp (C):		1200						
Duration (Total) (s):		4140						
Duration at Run T (s):		3600						
Date:		40640						
Cumulative Time (hrs)	OP	V	A	mV	uV	T	Deviation from Nominal T	Notes
00:00	11.1	20		0.46	460	74	-1126	
00:01	14.5	40		1.32	1320	183	-1017	
00:02	17.4	40	5	1.86	1860	243	-957	
00:03	20.1	60	5	2.57	2570	317	-883	
00:04	23.2	60	5	3.33	3330	392	-808	
00:05	27.7	70	6	4.89	4890	538	-662	
00:06	32.6	85	6	7.2	7200	738	-462	
00:07	37.8	85	6	9.95	9950	958	-242	
00:09	41.9	110	8	13.15	13150	1194	-6	T
00:18	42.1	110	8	13.18	13180	1197	-3	
00:23	42.2	110	8	13.16	13160	1195	-5	
00:45	42.7	110	8	13.16	13160	1195	-5	
00:56	42.8	110	8	13.16	13160	1195	-5	
01:04	42.9	110	8	13.2	13200	1198	-2	
01:09	42.9	110	8	13.2	13200	1198	-2	Q
Max positive T deviation:			-2	Max negative T deviation:				-6

Run ID:		VGB9						
Pressure (GPa):		3						
Temp (C):		1200						
Duration (Total) (s):		2040						
Duration at Run T (s):		1802						
Date:		40645						
Cumulative Time (hrs)	OP	V	A	mV	uV	T	Deviation from Nominal T	Notes
00:00	20	60	5	2.65	2650	325	-875	
00:01	25	60	6	4.51	4510	504	-696	
00:02	33	80	8	8.4	8400	836	-364	
00:03	39	100	9	12.5	12500	1147	-53	
00:04	40.2	100	9	13.25	13250	1202	2	T
00:10	40.2	100	9	13.2	13200	1198	-2	
00:16	40.4	100	9	13.16	13160	1195	-5	
00:34	40.4	100	9	13.16	13160	1195	-5	Q
Max positive T deviation:			2	Max negative T deviation:				-5

Run ID:		VGB10						
Pressure (GPa):		3						
Temp (C):		1600						
Duration (Total) (s):		1440						
Duration at Run T (s):		1142						
Date:		40647						
Cumulative Time (hrs)	OP	V	A	mV	uV	T	Deviation from Nominal T	Notes
00:00	10.5				0	0	-1600	
00:02	28	65	6	5	5000	548	-1052	
00:03	38	80	7	9.85	9850	950	-650	
00:04	42	100	8	12.78	12780	1168	-432	
00:05	48.5	105	9	16.6	16600	1440	-160	
00:07	51.8	120	10	18.82	18820	1598	-2	T
00:11	52	140	11	18.8	18800	1596	-4	
00:20	52.3	140	11	18.64	18640	1585	-15	
00:24	52.5	140	11	18.74	18740	1592	-8	Q
Max positive T deviation:			-2	Max negative T deviation:				-15

Run ID:		VGB11						
Pressure (GPa):		3						
Temp (C):		1600						
Duration (Total) (s):		1380						
Duration at Run T (s):		1082						
Date:		40665						
Cumulative Time (hrs)	OP	V	A	mV	uV	T	Deviation from Nominal T	Notes
00:00	23.7	60	5	3.69	3690	427	-1173	
00:01	37.6	95	6.5	9.91	9910	955	-645	
00:02	43	105	8	13.6	13600	1227	-373	
00:04	51.4	115	9	18.1	18100	1546	-54	
00:05	53	120	11	18.8	18800	1596	-4	T
00:07	53	140	11	18.84	18840	1599	-1	
00:10	53.4	140	11	18.74	18740	1592	-8	
00:15	53.8	140	11	18.6	18600	1582	-18	
00:18	53.9	140	11	18.84	18840	1599	-1	
00:21	53.9	140	11	18.83	18830	1599	-1	
00:23	53.9	140	11	18.88	18880	1602	2	Q
Max positive T deviation:			2	Max negative T deviation:				-18

Run ID:		VGB12						
Pressure (GPa):		3						
Temp (C):		1600						
Duration (Total) (s):		1500						
Duration at Run T (s):		1200						
Date:		40673						
Cumulative Time (hrs)	OP	V	A	mV	uV	T	Deviation from Nominal T	Notes
00:00	10.5				0	0	-1600	
00:01	22	60		2.68	2680	328	-1272	
00:02	30	75	5	5.26	5260	571	-1029	
00:03	45	120	8	13.45	13450	1216	-384	
00:04	51	135	9	16.45	16450	1429	-171	
00:05	55.5	145	10	18.74	18740	1592	-8	T
00:08	55.9	145	10	18.83	18830	1599	-1	
00:11	55.9	145	10	18.83	18830	1599	-1	
00:18	56.4	150	10	18.8	18800	1596	-4	
00:25	56.4	150	10	18.8	18800	1596	-4	Q
Noted T deviations 1586C to 1606 C								
Max positive T deviation:			6	Max negative T deviation:				-14

Run ID:		VGB13						
Pressure (GPa):		3						
Temp (C):		800						
Duration (Total) (s):		23820						
Duration at Run T (s):		23520						
Date:		40674						
Cumulative Time (hrs)	OP	V	A	mV	uV	T	Deviation from Nominal T	Notes
00:00	14	35		1.34	1340	185	-615	
00:01	20	50	5	3.04	3040	364	-436	
00:03	25	60	6	4.65	4650	516	-284	
00:04	30	75	7	6.72	6720	698	-102	
00:05	32.3	80	7	7.99	7990	803	3	T
00:13	32.3	80	7	8	8000	804	4	
00:44	32.3	80	7.5	7.97	7970	802	2	
01:44	32.5	80	7.5	7.96	7960	801	1	
02:40	32.5	80	7.5	7.99	7990	803	3	
03:35	32.5	80	7.5	7.99	7990	803	3	
05:14	32.5	80	7.5	7.99	7990	803	3	
06:37	32.5	80	7.5	8	8000	804	4	Q
Max positive T deviation:			4	Max negative T deviation:				0

Run ID:		VGB14						
Pressure (GPa):		3						
Temp (C):		800						
Duration (Total) (s):		23940						
Duration at Run T (s):		23642						
Date:		40679						
Cumulative Time (hrs)	OP	V	A	mV	uV	T	Deviation from Nominal T	Notes
00:00	10.6	20		0.25	250	43	-757	
00:01	18	40		1.79	1790	236	-564	
00:02	25	60	5	3.4	3400	399	-401	
00:03	30	75	5.5	5.04	5040	552	-248	
00:05	35.9	90	6.5	7.97	7970	802	2	T
00:11	35.6	90	6.5	7.94	7940	799	-1	
00:41	35.5	90	6.5	7.97	7970	802	2	
01:32	35.5	90	6.5	7.92	7920	798	-2	
02:45	35.9	90	6.5	7.9	7900	796	-4	
03:56	35.4	90	6.5	7.94	7940	799	-1	
05:45	35.5	90	6.5	7.94	7940	799	-1	
06:39	35.5	90	6.5	7.94	7940	799	-1	Q
Max positive T deviation:			2	Max negative T deviation:				-4

Run ID:		VGB15						
Pressure (GPa):		3						
Temp (C):		800						
Duration (Total) (s):		24360						
Duration at Run T (s):		24120						
Date:		40681						
Cumulative Time (hrs)	OP	V	A	mV	uV	T	Deviation from Nominal T	Notes
00:00	15	40		1.64	1640	219	-581	
00:01	20	50	5	3.05	3050	365	-435	
00:02	25	60	6	4.44	4440	497	-303	
00:03	30	75	6.5	6.27	6270	660	-140	
00:04	33.4	80	7	7.98	7980	802	2	T
00:11	32.9	80	7	7.98	7980	802	2	
01:12	33.5	80	7	7.96	7960	801	1	
03:23	33.3	80	7	8	8000	804	4	
04:10	32.8	80	7	8	8000	804	4	
05:08	32.8	80	7	7.86	7860	793	-7	
06:46	32.8	80	7	7.86	7860	793	-7	Q
Noted T unstable quote as +/- 20C								
Max positive T deviation:			20	Max negative T deviation:				-20

Run ID:		VGB17						
Pressure (GPa):		3						
Temp (C):		1400						
Duration (Total) (s):		1440						
Duration at Run T (s):		1202						
Date:		40709						
Cumulative Time (hrs)	OP	V	A	mV	uV	T	Deviation from Nominal T	Notes
00:00	12	25		0.73	730	111	-1289	
00:01	30	75	6.5	6.09	6090	644	-756	
00:02	37	95	8	9.65	9650	935	-465	
00:03	46	120	10	15.5	15500	1362	-38	
00:04	47.1	120	10	16.08	16080	1403	3	T
00:09	46.9	120	10	16.05	16050	1401	1	
00:16	47.2	120	10	16.02	16020	1399	-1	
00:21	47.3	120	10	15.94	15940	1393	-7	
00:24	47.3	120	10	15.94	15940	1393	-7	Q
Max positive T deviation:			3	Max negative T deviation:				-7

Run ID:		VGB18						
Pressure (GPa):		3						
Temp (C):		1400						
Duration (Total) (s):		1440						
Duration at Run T (s):		1200						
Date:		40709						
Cumulative Time (hrs)	OP	V	A	mV	uV	T	Deviation from Nominal T	Notes
00:00	15	40		1.48	1480	201	-1199	
00:01	24	60	5.5	3.93	3930	450	-950	
00:02	30	75	6.5	6.2	6200	654	-746	
00:03	44	115	9	13.94	13940	1251	-149	
00:04	47.7	110	10	16.05	16050	1401	1	T
00:14	47.4	120	10	16	16000	1397	-3	
00:17	47.5	120	10	16.03	16030	1399	-1	
00:24	47.5	120	10	16.03	16030	1399	-1	Q
Max positive T deviation:			1	Max negative T deviation:				-3

Run ID:		VGB19						
Pressure (GPa):		3						
Temp (C):		650						
Duration (Total) (s):		256500						
Duration at Run T (s):		256140						
Date:		40715						
Cumulative Time (hrs)	OP	V	A	mV	uV	T	Deviation from Nominal T	Notes
00:00	10.5	20		0.39	390	64	-586	
00:02	15.5	40		1.86	1860	243	-407	
00:03	20	50	5	3.29	3290	389	-261	
00:04	25	60	6	5.04	5040	552	-98	
00:06	27.6	70	6.5	6.17	6170	651	1	T
00:13	27.6	70	6.5	6.18	6180	652	2	
00:26	27.6	70	6.5	6.18	6180	652	2	
01:38	27.6	70	6.5	6.17	6170	651	1	
19:15	27.6	70	6.5	6.16	6160	650	0	
21:14	27.6	70	6.5	6.18	6180	652	2	
23:18	27.6	70	6.5	6.17	6170	651	1	
01:48	27.6	70	6.5	6.17	6170	651	1	
19:11	27.6	70	6.5	6.14	6140	649	-1	
21:16	27.6	70	6.5	6.16	6160	650	0	
23:06	27.6	70	6.5	6.16	6160	650	0	
01:15	27.6	70	6.5	6.15	6150	649	-1	
19:53	27.6	70	6.5	6.14	6140	649	-1	
21:15	27.5	70	6.5	6.15	6150	649	-1	
23:15	27.5	70	6.5	6.15	6150	649	-1	Q
Max positive T deviation:			2	Max negative T deviation:				-1

Run ID:		VGB20						
Pressure (GPa):		3						
Temp (C):		650						
Duration (Total) (s):		253560						
Duration at Run T (s):		253020						
Date:		40721						
Cumulative Time (hrs)	OP	V	A	mV	uV	T	Deviation from Nominal T	Notes
00:00	10.5	20		0.35	350	58	-592	
00:02	15	40		1.6	1600	215	-435	
00:03	20	50	5	2.97	2970	357	-293	
00:09	30.3	75	6.5	6.03	6030	639	-11	T
00:15	30.2	75	6.5	6.08	6080	643	-7	
00:40	30.3	75	6.5	6.01	6010	637	-13	
00:55	30.4	75	6.5	6.09	6090	644	-6	
01:14	30.8	75	6.5	6.05	6050	641	-9	
01:38	30.8	75	6.5	6.52	6520	681	31	
01:39	30.2	75	6.5	6.19	6190	653	3	
02:13	30.2	75	6.5	6.01	6010	637	-13	
02:14	30.5	75	6.5	6.07	6070	642	-8	
03:08	30.5	75	6.5	6.46	6460	676	26	
03:09	30.2	75	6.5	6.22	6220	655	5	
03:52	30.2	75	6.5	6.14	6140	649	-1	
21:34	30.2	75	6.5	6.05	6050	641	-9	
21:35	30.4	75	6.5	6.05	6050	641	-9	
23:48	30.4	75	6.5	5.92	5920	629	-21	
23:49	30.7	75	6.5	6.04	6040	640	-10	
01:16	30.7	75	6.5	6.4	6400	671	21	
01:17	30.4	75	6.5	6.3	6300	662	12	
02:24	30.4	75	6.5	6.27	6270	660	10	
02:25	30.3	75	6.5	6.21	6210	655	5	
04:00	30.3	75	6.5	5.9	5900	628	-22	
04:01	30.4	75	6.5	5.91	5910	629	-21	
00:30	30.4	75	6.5	5.95	5950	632	-18	

00:31	30.5	75	6.5	6	6000	636	-14	
21:33	30.6	75	6.5	6.3	6300	662	12	
21:34	30.5	75	6.5	6.24	6240	657	7	
22:26	30.5	75	6.5	6.41	6410	672	22	Q
Max positive T deviation:			31	Max negative T deviation:				-22

10.2 Grain Boundary Diffusion of Ti in Quartz Run Parameters

Run ID:			TiQ5					
Pressure (GPa):			3					
Temp (C):			1400					
Duration (Total) (s):			85800					
Duration at Run T (s):			85200					
Cumulative Time (hr:mm)	OP	V	A	mV	uV	T	Deviation from Nominal T	Notes
00:00	10.5			0.31	310	52	-1348	
00:01	17.0	20		1.99	1990	257	-1143	
00:02	20.0	40	1.0	2.85	2850	345	-1055	
00:03	23.0	50	1.0	3.79	3790	437	-963	
00:05	28.0	60	2.0	5.68	5680	608	-792	
00:07	35.0	65	3.0	9.61	9610	932	-468	
00:10	45.4	85	5.5	16.11	16110	1405	5	T
00:14	45.4	120	10.0	16.01	16010	1398	-2	
00:17	45.5	120	10.0	15.97	15970	1395	-5	
00:32	46.1	120	10.0	16.00	16000	1397	-3	
00:59	46.4	120	10.0	15.99	15990	1396	-4	
01:29	46.7	120	10.0	16.04	16040	1400	0	
02:09	46.7	120	10.0	16.00	16000	1397	-3	
02:47	46.9	120	10.0	16.03	16030	1399	-1	
03:17	46.9	120	10.0	16.04	16040	1400	0	
19:35	46.9	120	10.0	15.61	15610	1370	-30	
19:38	47.5	120	10.5	16.02	16020	1399	-1	
20:42	47.9	120	10.5	16.09	16090	1404	4	
21:45	47.8	120	10.5	16.25	16250	1415	15	
21:46	47.5	120	10.5	16.05	16050	1401	1	
23:11	47.6	120	10.5	16.00	16000	1397	-3	
23:50	47.6	120	10.5	16.22	16220	1413	13	Q
Max positive T deviation:		14.9	Max negative T deviation:				-30.4	

Run ID:			TiQ6					
Pressure (GPa):			3					
Temp (C):			1400					
Duration (Total) (s):			91860					
Duration at Run T (s):			91320					
Cumulative Time (hrs)	OP	V	A	mV	uV	T	Deviation from Nominal T	Notes
00:00	10.5	20		0.33	330	55	-1345	
00:01	15.0	40		1.57	1570	211	-1189	
00:02	20.0	50	1.0	2.99	2990	359	-1041	
00:03	25.0	60	2.0	4.68	4680	519	-881	
00:04	30.0	75	4.0	6.74	6740	700	-700	
00:06	35.0	85	6.0	9.59	9590	930	-470	
00:07	40.0	100	8.0	12.93	12930	1179	-221	
00:09	46.1	120	10.0	16.10	16100	1404	4	T
00:15	45.6	120	10.0	16.00	16000	1397	-3	
00:31	45.6	100	10.0	15.80	15800	1383	-17	
00:32	45.9	100	10.0	16.00	16000	1397	-3	
01:02	45.9	100	10.0	15.78	15780	1382	-18	
01:03	46.5	100	10.0	16.03	16030	1399	-1	
01:49	46.6	100	10.0	16.01	16010	1398	-2	
03:48	46.8	100	10.0	16.00	16000	1397	-3	
05:42	47.1	100	10.0	16.05	16050	1401	1	
21:47	48.3	125	10.5	16.04	16040	1400	0	
00:53	48.1	125	10.5	15.30	15300	1348	-52	
01:31	48.1	125	10.5	15.86	15860	1387	-13	Q
Max positive T deviation:		4.2	Max negative T deviation:				-52.4	

Run ID:			TiQ7					
Pressure (GPa):			3					
Temp (C):			1200					
Duration (Total) (s):			252060					
Duration at Run T (s):			251700					
Cumulative Time (hrs)	OP	V	A	mV	uV	T	Deviation from Nominal T	Notes
00:00	10.5	20		0.11	110	20	-1180	
00:01	15.0	40		1.57	1570	211	-989	
00:02	20.0	50	5.0	3.14	3140	374	-826	
00:03	25.0	60	6.0	4.83	4830	533	-667	
00:04	30.0	75	6.5	7.01	7010	722	-478	
00:05	35.0	85	8.0	10.37	10370	990	-210	
00:06	39.1	100	9.0	13.29	13290	1204	4	T
00:08	39.0	100	9.0	13.28	13280	1204	4	
00:26	39.1	100	9.0	13.16	13160	1195	-5	
00:51	39.2	100	9.0	13.17	13170	1196	-4	
01:19	39.4	100	9.0	13.22	13220	1199	-1	
01:54	39.5	100	9.0	13.23	13230	1200	0	
02:35	39.7	100	9.0	13.28	13280	1204	4	
03:14	39.7	100	9.0	13.28	13280	1204	4	
22:07	39.7	100	9.0	12.80	12800	1169	-31	
22:08	40.4	100	9.0	13.21	13210	1199	-1	
00:21	40.5	100	9.0	13.20	13200	1198	-2	
01:48	40.6	100	9.0	13.26	13260	1202	2	
22:01	40.6	100	9.0	13.07	13070	1189	-11	Q
Max positive T deviation:		4.5	Max negative T deviation:				-30.8	

Run ID:			TiQ8					
Pressure (GPa):			3					
Temp (C):			1300					
Duration (Total) (s):			182640					
Duration at Run T (s):			163620					
Cumulative Time (hrs)	OP	V	A	mV	uV	T	Deviation from Nominal T	Notes
00:00	10.5	20		0.05	50	9	-1291	
00:02	15.0	40		1.05	1050	151	-1149	
00:06	30.0	75	5.5	4.93	4930	542	-758	
00:08	40.0	100	8.0	11.11	11110	1045	-255	
00:10	45.1	115	9.0	14.44	14440	1287	-13	T
00:37	45.1	115	9.0	14.62	14620	1299	-1	
03:12	45.7	120	10.0	14.59	14590	1297	-3	
05:14	45.7	120	10.0	14.68	14680	1304	4	
05:17	44.7	120	10.0	14.61	14610	1299	-1	
06:33	44.8	120	10.0	14.59	14590	1297	-3	
07:09	45.0	120	10.0	14.62	14620	1299	-1	
01:26	45.0	120	10.0	14.07	14070	1260	-40	
01:28	46.1	120	10.0	14.61	14610	1299	-1	
03:55	46.4	120	10.0	14.66	14660	1302	2	
07:56	46.4	120	10.0	14.34	14340	1279	-21	
07:58	47.0	120	10.0	14.64	14640	1301	1	
00:07	47.0	120	10.0	15.10	15100	1333	33	
01:42	47.0	120	10.0	15.02	15020	1328	28	
02:25	47.0	120	10.0	14.80	14800	1312	12	
02:44	47.0	120	10.0	14.89	14890	1319	19	Q
Max positive T deviation:		33.4	Max negative T deviation:				-39.8	

Run ID:			TiQ9					
Pressure (GPa):			3					
Temp (C):			1000					
Duration (Total) (s):			348660					
Duration at Run T (s):			348360					
Cumulative Time (hrs)	OP	V	A	mV	uV	T	Deviation from Nominal T	Notes
00:00	10.5	20		0.33	330	55	-945	
00:01	15.0	40	5.0	1.89	1890	246	-754	
00:03	25.0	60	6.0	5.37	5370	581	-419	
00:05	34.9	80	8.0	10.53	10530	1002	2	T
00:13	34.8	80	8.0	10.57	10570	1005	5	
00:21	34.8	80	8.0	10.51	10510	1000	0	
01:07	35.0	80	8.0	10.48	10480	998	-2	
03:04	35.3	80	8.0	10.51	10510	1000	0	
04:32	35.3	85	8.0	10.50	10500	1000	0	
22:07	35.3	85	8.0	10.33	10330	987	-13	
22:08	35.7	85	8.0	10.50	10500	1000	0	
01:03	35.7	90	8.0	10.58	10580	1006	6	
01:04	35.6	90	8.0	10.50	10500	1000	0	
04:02	35.6	90	8.0	10.45	10450	996	-4	
04:03	35.8	90	8.0	10.52	10520	1001	1	
21:48	35.8	90	8.0	10.51	10510	1000	0	
21:49	35.8	90	8.0	10.50	10500	1000	0	
00:32	35.9	90	8.0	10.48	10480	998	-2	
00:03	35.9	90	8.0	10.45	10450	996	-4	
00:05	36.1	90	8.0	10.52	10520	1001	1	
00:51	36.1	90	8.0	10.51	10510	1000	0	Q
Max positive T deviation:		5.6	Max negative T deviation:				-13.3	

Run ID:			TiQ10					
Pressure (GPa):			3					
Temp (C):			1000					
Duration (Total) (s):			262260					
Duration at Run T (s):			261840					
Cumulative Time (hrs)	OP	V	A	mV	uV	T	Deviation from Nominal T	Notes
00:00	10.5	20		0.30	300	51	-949	
00:01	15.0	40	5.0	1.42	1420	194	-806	
00:02	20.0	60	6.0	2.82	2820	342	-658	
00:03	25.0	60	7.0	4.12	4120	467	-533	
00:04	30.0	75	8.0	6.40	6400	671	-329	
00:07	37.4	90	8.0	10.54	10540	1003	3	T
00:12	37.2	90	8.0	10.51	10510	1000	0	
00:40	37.4	90	8.0	10.49	10490	999	-1	
01:06	37.1	90	8.0	10.51	10510	1000	0	
01:36	37.6	90	8.0	10.53	10530	1002	2	
02:21	37.3	90	8.0	10.54	10540	1003	3	
03:06	37.4	90	8.0	10.51	10510	1000	0	
21:23	37.4	90	8.0	10.70	10700	1015	15	
21:24	37.2	90	8.0	10.54	10540	1003	3	
23:14	37.2	90	8.0	10.40	10400	992	-8	
23:15	37.6	90	8.0	10.51	10510	1000	0	
01:17	37.6	90	8.0	10.30	10300	984	-16	
01:18	38.0	95	8.0	10.51	10510	1000	0	
02:17	37.9	95	8.0	10.51	10510	1000	0	
21:36	37.9	95	8.0	10.23	10230	979	-21	
21:37	38.3	95	8.0	10.50	10500	1000	0	
23:34	38.3	95	8.0	10.55	10550	1003	3	
00:43	38.7	95	8.0	10.48	10480	998	-2	
02:31	38.2	95	8.0	10.51	10510	1000	0	
03:51	38.3	95	8.0	10.49	10490	999	-1	
21:35	38.3	95	8.0	10.20	10200	977	-23	
21:36	39.0	95	8.0	10.53	10530	1002	2	
22:59	39.0	95	8.0	10.65	10650	1011	11	

23:00	38.7	100	8.0	10.52	10520	1001	1
00:51	38.7	100	8.0	9.96	9960	958	-42
Max positive T deviation:		14.6	Max negative T deviation:				-41.5

Run ID:			TiQ11					
Pressure (GPa):			3					
Temp (C):			1000					
Duration (Total) (s):			349740					
Duration at Run T (s):			348840					
Cumulative Time (hrs)	OP	V	A	mV	uV	T	Deviation from Nominal T	Notes
00:00	10.5	20		0.33	330	55	-945	
00:03	15.0	40		1.67	1670	222	-778	
00:06	20.0	50	5.0	3.12	3120	372	-628	
00:08	25.0	60	6.0	4.75	4750	525	-475	
00:11	30.0	75	6.5	6.83	6830	707	-293	
00:13	35.0	85	7.5	9.54	9540	926	-74	
00:15	37.0	90	8.0	10.51	10510	1000	0	T
00:21	36.8	90	8.0	10.43	10430	994	-6	
00:29	37.0	90	8.0	10.56	10560	1004	4	
00:39	37.0	90	8.0	10.54	10540	1003	3	
01:17	37.0	90	8.0	10.62	10620	1009	9	
01:50	37.0	90	8.0	10.36	10360	989	-11	
02:38	36.8	90	8.0	10.54	10540	1003	3	
04:23	36.9	90	8.0	10.44	10440	995	-5	
08:43	37.4	90	8.0	10.50	10500	1000	0	
22:57	37.4	90	8.0	10.42	10420	993	-7	
22:59	37.7	90	8.0	10.53	10530	1002	2	
02:24	37.7	90	8.0	10.45	10450	996	-4	
05:39	37.8	90	8.5	10.82	10820	1024	24	
05:47	37.7	95	8.5	10.61	10610	1008	8	
21:32	37.7	95	8.5	10.69	10690	1014	14	
03:54	37.7	95	8.5	10.73	10730	1017	17	
04:33	37.7	95	8.5	10.63	10630	1009	9	
10:01	37.7	95	8.5	10.33	10330	987	-13	
00:39	38.9	95	8.5	10.51	10510	1000	0	
08:09	38.5	95	8.5	10.49	10490	999	-1	
23:30	38.5	95	8.5	10.36	10360	989	-11	
01:09	38.5	95	8.5	11.12	11120	1046	46	Q

Max positive T deviation:	46.1	Max negative T deviation:	-13.3

Run ID:			TiQ12					
Pressure (GPa):			3					
Temp (C):			1200					
Duration (Total) (s):			159300					
Duration at Run T (s):			158580					
Cumulative Time (hrs)	OP	V	A	mV	uV	T	Deviation from Nominal T	Notes
00:00	10.5	20		0.30	300	51	-1149	
00:01	15.0	40		1.54	1540	208	-992	
00:03	20.0	50	5.0	2.93	2930	353	-847	
00:05	25.0	60	5.0	4.57	4570	509	-691	
00:07	30.0	75	6.0	6.66	6660	693	-507	
00:09	35.0	85	7.0	9.35	9350	911	-289	
00:12	41.4	100	8.0	13.24	13240	1201	1	T
00:20	41.6	105	8.0	13.21	13210	1199	-1	
00:34	41.6	105	8.0	13.00	13000	1184	-16	
00:35	42.0	105	8.0	13.29	13290	1204	4	
00:58	42.0	105	8.0	13.14	13140	1194	-6	
00:59	42.2	105	8.0	13.22	13220	1199	-1	
01:31	42.2	105	8.0	13.15	13150	1194	-6	
01:32	42.3	105	8.0	13.19	13190	1197	-3	
02:03	42.7	105	8.0	13.05	13050	1187	-13	
02:04	42.7	105	8.0	13.25	13250	1202	2	
02:45	42.7	105	8.0	13.14	13140	1194	-6	
02:46	42.9	105	8.0	13.22	13220	1199	-1	
20:15	42.9	105	8.0	12.38	12380	1139	-61	Q
Max positive T deviation:		4.5	Max negative T deviation:				-61.3	

10.3 Grain Boundary Diffusion of Li Run Parameters

Run ID:			LiGB1					
Pressure (GPa):			3					
Temp:			1000					
Duration (Total) (s):			22320					
Duration at Run T (s):			21720					
Cumulative Time (hh:mm)	OP	V	A	mV	uV	T	Deviation from Nominal T	Notes
00:00	10.5	20		0.22	220	38	-962	
00:02	15.0	40		1.07	1070	154	-846	
00:04	20.0	50		2.00	2000	258	-742	
00:06	30.0	75	5.0	4.57	4570	509	-491	
00:08	35.0	85	6.0	6.96	6960	718	-282	
00:10	40.5	100	7.0	10.70	10700	1015	15	T
00:12	40.2	100	7.0	10.68	10680	1013	13	
00:14	40.1	100	7.0	10.62	10620	1009	9	
00:16	40.0	100	7.0	10.52	10520	1001	1	
00:26	40.0	100	7.0	10.53	10530	1002	2	
00:36	40.0	100	7.0	10.51	10510	1000	0	
00:53	40.2	100	7.0	10.43	10430	994	-6	
00:54	40.2	100	7.0	10.51	10510	1000	0	
01:04	40.3	100	7.0	10.48	10480	998	-2	
01:31	40.7	100	7.0	10.53	10530	1002	2	
02:26	40.7	100	7.0	10.38	10380	990	-10	
02:27	41.0	105	7.0	10.52	10520	1001	1	
03:25	41.0	105	7.0	10.40	10400	992	-8	
03:26	41.2	105	7.0	10.49	10490	999	-1	
04:36	41.2	105	7.0	10.37	10370	990	-10	
04:37	41.6	105	7.0	10.54	10540	1003	3	
06:12	41.6	105	7.0	10.44	10440	995	-5	Q
Max positive T deviation:			14.6	Max negative T deviation:			-10.3	

Run ID:			LiGB2					
Pressure (GPa):			3					
Temp (C):			800					
Duration (Total) (s):			77880					
Duration at Run T (s):			77400					
Cumulative Time	OP	V	A	mV	uV	T	Deviation from Nominal T	Notes
00:00	10.5	20		0.10	100	18	-782	
00:02	20.0	50	5.0	1.53	1530	207	-593	
00:05	30.0	75	5.0	4.17	4170	472	-328	
00:08	38.5	95	7.0	8.03	8030	807	7	T
00:00	38.4	95	7.0	8.16	8160	817	17	
00:12	38.3	95	7.0	8.22	8220	822	22	
00:13	38.2	95	7.0	8.17	8170	818	18	
00:15	38.1	95	7.0	8.21	8210	821	21	
00:17	37.9	95	7.0	8.19	8190	819	19	
00:20	37.8	95	7.0	8.12	8120	814	14	
00:46	37.8	95	7.0	8.33	8330	831	31	
00:48	37.0	95	7.0	7.96	7960	801	1	
01:20	37.0	95	7.0	8.03	8030	807	7	
01:21	36.8	95	7.0	7.96	7960	801	1	
02:06	36.8	95	7.0	8.06	8060	809	9	
02:07	36.5	90	7.0	7.95	7950	800	0	
03:10	36.5	90	7.0	8.03	8030	807	7	
03:11	36.3	90	7.0	7.93	7930	798	-2	
04:18	36.3	90	7.0	7.94	7940	799	-1	
05:06	36.3	90	7.0	7.96	7960	801	1	
05:46	36.3	90	7.0	7.95	7950	800	0	
21:38	36.3	90	7.0	7.90	7900	796	-4	Q
Max positive T deviation:			30.7	Max negative T deviation:			-4.1	

Run ID:			LiGB3					
Pressure (GPa):			3					
Temp (C):			800					
Duration (Total) (s):			78000					
Duration at Run T (s):			77580					
Cumulative Time	OP	V	A	mV	uV	T	Deviation from Nominal T	Notes
00:00	10.5	20		0.22	220	38	-762	
00:02	20.0	45		2.27	2270	287	-513	
00:04	25.0	60	5.0	3.53	3530	412	-388	
00:07	35.2	85	6.5	7.94	7940	799	-1	T
00:09	35.0	85	6.5	8.17	8170	818	18	
00:10	34.8	85	6.5	8.08	8080	811	11	
00:12	34.4	85	6.5	8.01	8010	805	5	
00:33	34.4	85	6.5	7.98	7980	802	2	
01:02	34.0	85	6.5	7.93	7930	798	-2	
01:38	34.0	85	6.5	7.97	7970	802	2	
02:31	33.9	85	6.5	7.95	7950	800	0	
03:42	33.9	85	6.5	7.98	7980	802	2	
04:57	34.0	85	6.5	7.95	7950	800	0	
06:31	34.3	85	6.5	7.95	7950	800	0	
21:40	34.3	85	6.5	8.19	8190	819	19	Q
Max positive T deviation:			19.4	Max negative T deviation:			-1.6	

Run ID:			LiGB5					
Pressure (GPa):			3					
Temp (C):			1100					
Duration (Total) (s):			11820					
Duration at Run T (s):			11040					
Cumulative Time (hrs)	OP	V	A	mV	uV	T	Deviation from Nominal T	Notes
00:00	10.5	20			0	0	-1100	
00:03	20.0	50		1.45	1450	198	-902	
00:10	40.0	100	5.5	5.82	5820	621	-479	
00:13	48.5	120	8.0	11.95	11950	1107	7	T
00:16	47.5	120	8.0	11.97	11970	1109	9	
00:20	46.9	120	8.0	11.91	11910	1104	4	
00:24	46.7	120	8.0	11.84	11840	1099	-1	
00:39	46.7	120	8.0	11.86	11860	1101	1	
01:08	46.7	120	8.0	11.48	11480	1073	-27	
01:09	47.5	120	8.0	11.85	11850	1100	0	
01:55	47.5	120	8.0	11.59	11590	1081	-19	
01:56	48.0	120	8.0	11.86	11860	1101	1	
02:39	48.5	120	8.0	11.86	11860	1101	1	
03:17	48.5	120	8.0	11.86	11860	1101	1	Q
Max positive T deviation:			8.8	Max negative T deviation:			-27.2	